Thermoeconomic optimization studies of the refrigeration systems using metaheuristic techniques

A thesis submitted in fulfilment of the requirements for the degree of

Doctor of Philosophy

by

Makkitaya Swarna Nagraj

(Roll No:176107002)

Department of Chemical Engineering,

Indian Institute of Technology Guwahati,

Guwahati – 781039, Assam, India.

July 2023

TH-3395_176107002

Department of Chemical Engineering,

Indian Institute of Technology Guwahati,

Guwahati – 781039

Assam, India.

STATEMENT

The present thesis entitled, "**Thermoeconomic optimization studies of the refrigeration systems using metaheuristic techniques**" has been carried out by me under the supervision of Dr. R. Anandalakshmi, and Dr. Prakash Kotecha, Department of Chemical Engineering, Indian Institute of Technology Guwahati. This work has not been submitted elsewhere for the award of any degree.

Makkitaya Swarna Nagraj

Department of Chemical Engineering

Indian Institute of Technology Guwahati

Guwahati – 781039

Assam, India.

TH-3395_176107002

Department of Chemical Engineering,

Indian Institute of Technology Guwahati,

Guwahati – 781039

Assam, India.

THESIS CERTIFICATE

It is certified that the work described in this thesis, entitled "**Thermoeconomic optimization studies of the refrigeration systems using metaheuristic techniques**", done by Makkitaya Swarna Nagraj, a Ph.D. student of 'Department of Chemical Engineering', Indian Institute of Technology Guwahati, for the award of the degree of Doctor of Philosophy has been carried out under our supervision. This work has not been submitted elsewhere for the award of any degree.

Signature of Supervisor(s)

Dr. R. Anandalakshmi
Associate Professor,
Thesis Co-supervisor
Department of Chemical Engineering,
Indian Institute of Technology Guwahati,
Guwahati – 781039
Assam, India.

Dr. Prakash Kotecha
Associate Professor,
Thesis Co-supervisor
Department of Chemical Engineering,
Indian Institute of Technology Guwahati,
Guwahati – 781039
Assam, India.

TH-3395_176107002

Dedicated

To

God,

Parents, Husband

&

Parents-in-laws

TH-3395_176107002

Acknowledgment

My sincere gratitude goes out to **Dr. R. Anandalakshmi**, **Associate Professor,** Department of Chemical Engineering, IIT Guwahati, and **Dr. Prakash Kotecha**, **Associate Professor,** Department of Chemical Engineering, IIT Guwahati, for their support and direction in helping to make this project a success. I would like to express my sincere gratitude for your professional guidance and insights, which assisted me in determining the focus and methods of my research. Your prompt comments and helpful critiques have significantly raised the caliber of my work. Your support and inspiration have always given me the drive and inspiration I need to keep moving and accomplish my objectives. This has enhanced my knowledge of the subject and my research abilities for my thesis work. It has been a great opportunity for me to work for them. I am grateful to them for instilling trust and believing in me during my Ph.D. studies. I must express my gratitude for their unequivocal freedom, which allowed me to consider different research avenues, exercise my imagination, and be accepted for straightforward technical talks. I closely worked under their supervision and learned a lot from them that will help me with my future research.

I would like to extend my deepest gratitude to the distinguished members of my PhD committee, **Prof. Pallab Ghosh (Chairperson)**, **Dr. Deepak Sharma**, and **Dr. Raghvendra Gupta**, for their invaluable guidance and encouragement throughout my doctoral journey. Your advice, criticism, and support have been crucial in assisting me in reaching my objectives and significantly advancing the area of optimization. I appreciate everything you have done for me, as well as the knowledge and insights you have shared with me throughout my doctoral pathway.

I would like to extend my sincere gratitude for the help and support **IIT Guwahati** has given me throughout my PhD thesis. As a doctoral student, I encountered many obstacles, but with the direction and support of my alma mater, I was able to surmount them. My college education provided me with the information and abilities I needed to carry out my study job. The professors and advisers who led me through my doctoral studies were crucial in shaping my academic work path. They provided intellectual assistance and constructive comments, which assisted me in improving the content of my study and developing my critical thinking skills.

I sincerely thank the Department head of Chemical engineering and the professors for their assistance and encouragement during my doctoral journey. The administrative team has been

TH-3395_176107002

incredibly helpful and effective in running the department's operations, and for that, I am also appreciative.

I would like to gratefully acknowledge my lab seniors, Ms. Remya Kommadath, Mr. Sandeep Singh Chauhan, Mr. Debasis Maharana, and Dr. K. Dharmalingam, for all of your help and advice while I was working in the lab. I appreciate the chance to collaborate with such a great team, and the knowledge and abilities I have acquired from you will continue to influence my educational career.

I want to sincerely thank my lab colleagues, Mr. Aditya Koneru, Mr. Marungsha Brahma, Mr. Abhishek Roy, Ms. Mili Bang, Mr. Vivek Ramchandani, Mr. Arnab Dutta, Mr. Saheb Singh, Ms. Juri Sonowal, Mr. Rajanikant Baro, Mr. Nikhil Purao, Mr. S. Siddharth, for your companionship and support throughout our time working together in the lab. I am thankful to have had the chance to work with such a great group of individuals because the information and skills I have acquired from our shared experience will continue to influence my study career.

I would like to thank my friends, Ms. Maithilee Patawar, Mr. Deepak Kumar Mishra, Ms. Shweta Kumbhar, Dr. Mahesh Nagargoje, Mr. Ankush Sontakke, Mrs. Priyanka Dixit, Ms. Roushani Kumari, Dr. Deepti Nair, Mr. Naveen Kumar Yaranal, Mr. Nilotpal Biswas, Mr. Rigved Samant, and Mr. Pravin Suryawanshi from the bottom of my heart for your enduring support and companionship throughout my PhD adventure. Pursuing a doctorate degree has been a difficult but rewarding experience, and your existence in my life has provided solace and encouragement throughout this path.

I would like to express sincere gratitude to my Parents (**Mr. Nagraj Chandrashekhar Makkitaya** and **Mrs. Premalata Nagraj Makkitaya)**, my Parent-in Laws (**Mr. Jayaram U Kekuda, Mrs. Sujatha Kekuda)**, my sister (**Mrs. Swati Makkitaya**) and my sister in -law (**Ms. Vaishnavi U Kekuda**), for the unwavering affection, encouragement, and direction you have provided me throughout my life. Your constant support and confidence in me have assisted me in achieving my objectives and overcoming the difficulties I encountered along my journey.

I deeply appreciate my husband, **Mr. Suhas U Kekuda**, for his unwavering love and assistance over the years. Your never-ending support, tolerance, and understanding have been priceless to me and have enabled me to get through the difficulties that come with earning a Ph.D. You have always been a source of comfort and inspiration in my life. Your encouragement has

TH-3395_176107002

helped me endure even when things were difficult, and your confidence in me has enabled me to accomplish my objectives. I am extremely grateful for your ongoing love and support, which have served as my compass in life. Your willingness to sacrifice your time, energy, and money to help me has been a witness to your love and devotion to our relationship.

Finally, I would like to extend my gratitude to Prof. Parameswar K. Iyer, acting director of IIT Guwahati, Prof. T. G. Sitharam, and Prof. Gautam Biswas, the prior directors of the institute, for their unwavering support and inspiration throughout my PhD journey.

I want to say thank you to everyone who has supported me along the way, whether directly or indirectly, for your consistent encouragement, support, and advice. I appreciate all of your contributions—big and small—to my life because they have allowed me to get to where I am now. I cannot possibly thank everyone who has impacted my life and supported me along the journey, but please know that I value every act of kindness, encouraging remark, and supportive moment. Your support in my life has been priceless, whether it has been during the difficult times or the times when you have shared in my victories.

Makkitaya Swarna Nagraj

TH-3395_176107002

Abstract

Refrigeration systems play a crucial role in maintaining thermal comfort by removing excess heat from enclosed spaces. These systems are vital for various applications, from cooling buildings to preserving perishable goods. The primary goal is to provide a cooling load to the evaporator through chilled water to maintain a specific temperature within the enclosed space. Among the various refrigeration systems, the vapor compression refrigeration system (VCRS) stands as the most widespread choice due to its high coefficient of performance (COP). However, VCRS consumes a significant amount of electricity because of its compressor, contributing indirectly to substantial CO_2 emissions. To address the issues of energy consumption and CO_2 emissions, researchers have turned their attention to refrigeration systems driven by alternative low-grade energy sources, such as vapor absorption refrigeration systems (VARS) and vapor adsorption refrigeration systems. Unfortunately, these sorption technologies tend to suffer from lower efficiency compared to conventional VCRS.

In response to these challenges, a solution has been proposed: the cascaded refrigeration system, which integrates conventional VCRS and VARS. This integration aims to reduce energy consumption and enhance overall system efficiency. Optimization techniques have been instrumental in achieving these objectives while ensuring that the system is not overdesigned. Optimization plays a crucial role in system analysis, design, modeling, and performance improvement. A thermoeconomic optimization approach has been developed, combining thermodynamic and economic parameters within a single framework. This approach can be solved using various metaheuristic algorithms, offering flexibility in finding optimal solutions. Both single and multi-objective thermoeconomic optimization studies have been conducted to determine optimal values for objectives such as total annual cost, exergy destruction, exergy efficiency, COP, and other decision variables like temperatures and mass flow rates. Literature shows that the optimization of these systems has been studied using genetic algorithm (GA) and particle swarm optimization (PSO). However, according to the No Free Lunch theorem, no optimization algorithm can determine the optimal solutions for all problems. Therefore, the thermoeconomic optimization of the studied systems is done using the recently proposed metaheuristic techniques. These optimizations have been applied to standalone and cascaded refrigeration systems using recently proposed metaheuristic techniques. The primary objectives of the present work are as follows:

TH-3395_176107002

- Thermoeconomic optimization of conventional vapor absorption refrigeration systems (VARS) and modified vapor absorption refrigeration systems (MVARS)
- Thermoeconomic optimization of vapor compression-absorption cascaded refrigeration systems (CRS) with different absorbent-refrigerant combinations
- Thermoeconomic optimization of subcooler integrated vapor compression-absorption cascaded refrigeration systems (SCRS) with different absorbent-refrigerant combinations
- Thermoeconomic optimization of vapor recompression-absorption refrigeration systems (VRARS) with different absorbent-refrigerant combinations

These studies employ various single and multi-objective metaheuristic algorithms to find optimal solutions. The following sections will delve deeper into the specific aspects of each optimization study.

Optimization of Vapor Absorption Refrigeration Systems (VARS and MVARS): In this research, the governing equations of energy, exergy, mass, and component balance are solved to determine various parameters for the entire system. The thermophysical properties of the refrigerant are obtained from REFPROP 9.0 software, while equations from the literature are used for the absorbent/salt. A modified VARS is proposed to improve its performance, and a multi-objective thermoeconomic optimization study is conducted. This study focuses on minimizing the total annual cost of the systems and reducing the total exergy destruction. Different metaheuristic techniques, including the multi-objective genetic algorithm (MOGA), multi-objective particle swarm optimization (MOPSO), and multi-objective sanitized teaching learning-based optimization (MOsTLBO), are employed. Two models, VARS and MVARS, are studied with MOGA determining the minimum annual cost for both models, MOPSO reporting the minimum exergy destruction. The results yield Pareto points that offer optimal solutions based on specific requirements. MVARS excels from an exergy perspective, while VARS is favored economically. MVARS exhibits approximately 17% less exergy destruction but incurs a 0.9% higher total annual cost compared to conventional VARS.

Optimization of Cascaded Refrigeration Systems (CRS): A single-objective thermoeconomic optimization of CRS with various absorbent-refrigerant combinations is conducted. Metaheuristic techniques, such as sanitized Teaching Learning Based Optimization (sTLBO), Atom Search Optimization (ASO), Coyote Optimization Algorithm (COA), Yin-

TH-3395_176107002

Yang Pair Optimization (YYPO), and Tree Growth Algorithm (TGA), are utilized to optimize the total annual cost. The objective function is based on energy, exergy, economic, and environmental performance criteria. Decision variables include cascade, evaporator, absorber, generator, condenser, overlap temperatures, and the effectiveness of the solution heat exchanger. COA reports the minimum total annual cost for all considered absorbent-refrigerant combinations, with the lowest total annual cost achieved for ($CaCl_2$-LiBr-$LiNO_3$)-H_2O-R290 combination at 13164.76 US $/year.

Optimization of Subcooler Integrated Systems (SCRS): To compare the advantages and disadvantages of subcooler-integrated vapor compression absorption refrigeration systems (SCRS) with standalone CRS, single-objective thermoeconomic optimization of SCRS with various absorbent-refrigerant combinations is performed. The total annual cost of the system is formulated using energy, exergy, and economic performance criteria and minimized using metaheuristic algorithms (sTLBO, ASO, COA, YYPO, TGA). R290 combined with all absorbent solution/solution mixtures-water combinations yields the optimal total annual cost for both standalone and subcooled systems. R290 combined with ($CaCl_2$-LiBr-$LiNO_3$)-H_2O provides the minimum total annual cost at 13164.8 US $/year and 15401.9 US $/year for standalone and subcooled systems, respectively. While the COP of the optimal subcooled system is approximately 250% higher than its standalone counterpart, the higher compressor work results in a penalty cost nearly 190% higher for the subcooled system. Both COA and sTLBO report quick convergence to the optimal fitness function for all refrigerant-absorbent combinations.

Optimization of Vapor Recompression-Absorption Refrigeration Systems (VRARS): The multi-objective thermoeconomic optimization of VRARS with LiBr-H_2O and ($CaCl_2$-LiBr-$LiNO_3$)-H_2O as working fluids is investigated using metaheuristic techniques (MOGA, MOPSO, MOsTLBO). This system utilizes the rejected heat from the condenser to heat the absorbent-refrigerant mixture in the generator and pressurize the superheated refrigerant in the compressor. The optimization aims to achieve maximum exergy efficiency and minimum total annual cost. Two cases are studied with different sets of decision variables, including temperatures, compression ratio, mass flow rate of the absorber coolant, and the effectiveness of the solution heat exchanger. MOPSO determines the minimum total annual cost, while MOsTLBO focuses on maximizing exergy efficiency. The results indicate that LiBr-H_2O exhibits higher exergy efficiency (~8% higher) than ($CaCl_2$-LiBr-$LiNO_3$)-H_2O, while ($CaCl_2$-LiBr-$LiNO_3$)-H_2O incurs a lower total annual cost (~3% less) than LiBr-H_2O for Case 1. For Case 2, the exergy efficiency remains the same for both working pairs, but the total annual cost

TH-3395_176107002

for ($CaCl_2$-LiBr-$LiNO_3$)-H_2O is approximately 5% less than LiBr-H_2O. MOsTLBO outperforms MOGA and MOPSO based on the inverted generational distance for both cases. Moreover, the maximum exergy efficiency and minimum total annual cost are improved by approximately 36% and 41%, respectively, for Case 2 compared to Case 1.

In summary, the optimization of refrigeration systems, whether standalone or cascaded, holds significant promise for minimizing energy consumption, reducing CO_2 emissions, and achieving cost-effective operation. The choice of refrigerant-absorbent combinations and system configurations plays a crucial role in determining the optimal performance. By utilizing advanced metaheuristic algorithms, researchers can uncover Pareto-optimal solutions that balance conflicting objectives and guide the selection of the most suitable refrigeration system for specific requirements.

TH-3395_176107002

Nomenclature

a	Acceleration
a^c	Capital recovery factor
A	Heat transfer area (m^2)
$\dot{B}$	Exergy flow (kW)
$\dot{B}_D$	Exergy destruction (kW)
$\dot{B}_{in}$	Input exergy (kW)
$\dot{B}_{out}$	Output exergy (kW)
b	Specific exergy (kJ/kg)
C_p	Specific heat capacity (kJ/kg K)
C_T	Annual cost ($/year)
C_{exer}	Cost of exergy input ($/kW h)
COP	Coefficient of performance
C_{CO_2}	Cost charged for CO_2 ($/ton)
C_{el}	Electricity cost ($/kW h)
C_{Env}	Penalty cost/Carbon tax ($/year)
CR	Compression ratio
$\dot{E}$	Energy (kW)
f, Fit	Fitness of the solution
F_d^i	Interaction force
G_d^i	Constraint force
h, H	Specific enthalpy (kJ/kg)
i_r	Interest rate (%)
$LMTD$	Logarithmic mean temperature difference
$\dot{m}$	Mass flow rate (kg/s)
m_d^i	Mass of the solution
m_f	Maintenance factor
m_{CO_2}	Mass of CO_2 emitted (kg)
Ny	Period of repayment (years)
P	Pressure (MPa, kPa, bar)

TH-3395_176107002

P_a	Association probability
P_s	Scatter probability
$\dot{Q}$	Heat load (kW)
r, rand	Random number
s	Specific entropy (kJ/kg K)
top	Period of operation (hours)
T	Temperature (˚C, K)
T_C	Crystallization temperature (˚C)
U	Overall heat transfer coefficient (kW/m^2 K)
v,V	Velocity
$\dot{W}$	Work (kW)
x	Decision variables
X, w	Concentration of absorbent in solution (%)
Z	System capital cost ($)
Z_{Comp}	Compressor cost ($)
	Greek symbols
α	Depth weight
β	Multiplier weight
δ	Search radii
$\mathcal{E}$	Effectiveness of solution heat exchanger
η	Efficiency
λ	Emission factor (kg/kW h)
ρ	Density (kg/m^3)
θ	The reduction rate of power
	Subscripts
ci	Cold stream inlet
co	Cold stream outlet
in	Inlet
hi	Hot stream inlet
ho	Hot stream outlet
i	i-th stream
min	Minimum

TH-3395_176107002

Abs	Absorber
Comp	Compressor
Cascade con	Cascade condenser
Cond	Condenser
Env	Environment
Evp	Evaporator
Gen	Generator
Shx	Solution heat exchanger
Subc	Subcooler-evaporator
isen	Isentropic
mix	Mixture
P	Pump
r	real
ref_1	Refrigerant in vapor compression refrigeration system
ref_2	Refrigerant in vapor absorption refrigeration system
salt	Absorbent
	Abbreviations
ASO	Atom search optimization
CCU	Cost of cold utility
CFC	Cholorolfluorocarbon
COA	Coyote optimization algorithm
COP	Coefficient of performance
CRS	Cascaded refrigeration system
GA	Genetic algorithm
GPF	Global Pareto Front
GWP	Global warming potential
HC	Hydrocarbon
HCFC	Hydrochlorofluorocarbon
HFC	Hydrofluorocarbon
HFO	Hydroflouro-olefin
HTL	High temperature loop
HVAC	Heating, ventilation, and air conditioning
IGD	Inverted generational distance

TH-3395_176107002

LB	Lower bound
LiBr	Lithium bromide
LiCl	Lithium chloride
LTL	Lower temperature loop
MOGA	Multi objective genetic algorithm
MOPSO	Multi objective particle swarm optimization
MOsTLBO	Multi objective sanitized teaching learning based optimization
MVARS	Modified vapor absorption refrigeration system
ODP	Ozone depletion potential
ORC	Organic Rankine Cycle
PSO	Particle swarm optimization
SCRS	Subcooler integrated cascaded refrigeration system
sTLBO	Sanitized teaching learning based optimization
TAC	Total annual cost
TEO	Thermoeconomic optimization
TGA	Tree growth algorithm
UB	Upper bound
VARS	Vapor absorption refrigeration system
VAdRS	Vapor adsorption refrigeration system
VCRS	Vapor compression refrigeration system
VRARS	Vapor recompression absorption refrigeration system
YYPO	Yin-yang pair optimization
1,2,3…	State points

TH-3395_176107002

Table of Contents

TH-3395_176107002

TH-3395_176107002

TH-3395_176107002

TH-3395_176107002

List of Figures

TH-3395_176107002

TH-3395_176107002

TH-3395_176107002

List of Tables

TH-3395_176107002

TH-3395_176107002

CHAPTER 1

Introduction

1.1. Energy demand and consumption in residential and commercial buildings

The scientific community agrees that the energy sector is highly sensitive and a significant contributor to climate change. Repercussions of this are associated with a variety of energy system requirements, such as energy demand and supply, as well as energy pricing and transportation. The population of the world has been increasing rapidly over the last few decades, accompanied by economic progress. As a result, energy usage is significantly escalating. Most energy generated is mainly consumed by electric power production, transportation, industrial, residential, and commercial buildings, as shown in Fig. 1.1 (a) [1]. From the survey, it has been observed that only the industrial and residential sector consumes electricity up to 42 % and 27%, respectively, while the commercial sector accounts for 21% of electricity usage, as shown in Fig. 1.1. (b) [2]. A significant portion of the energy in the residential and commercial sectors is utilized for heating, ventilation, and air conditioning (HVAC) systems powered by electricity to provide a comfortable environment by either space cooling or heating. Due to a combination of factors, including the growing global population, rising incomes, growing concern for food safety, expanding industries, and increasing global warming, the demand for air conditioning and refrigeration systems has been rising.

(a)

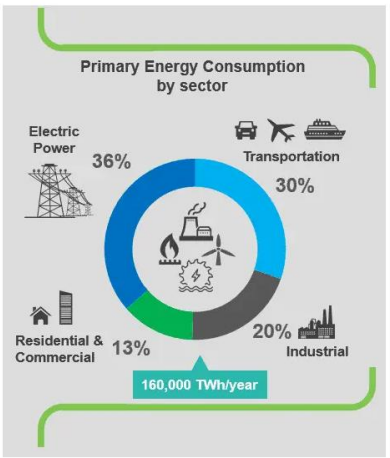

(b)

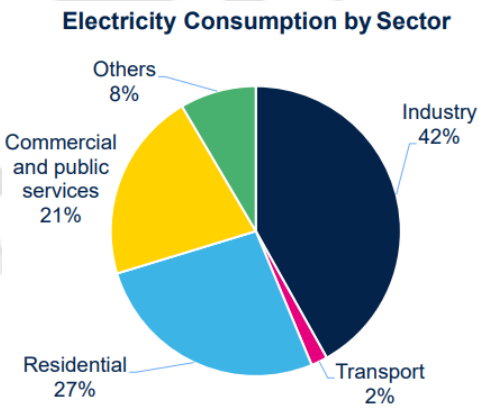

Fig. 1. 1 (a) World energy consumption [1] **(b) Global electricity consumption (Sector wise)** [2]

Fig. 1.2 illustrates the global energy distribution among cooling sectors such as space cooling, mobile cooling, and stationary refrigeration. Space cooling can be defined as comfort cooling through air-conditioning of the buildings (residential, commercial, and industrial premises), which consumes 41% of the total electricity supplied, indicating the largest energy consumer.

TH-3395_176107002

Stationary refrigeration uses any refrigeration system to maintain and/or decrease the temperature of air for process cooling, product storage, and goods that utilize 34% of the electricity provided. Mobile cooling includes providing cooling for vehicle air conditioning and transport refrigeration trucks, which utilizes about 25% [3].

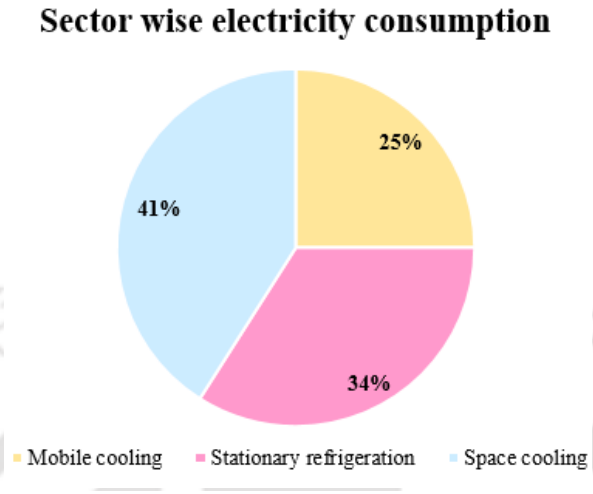

Fig. 1. 2 Global energy consumption (by cooling sector)

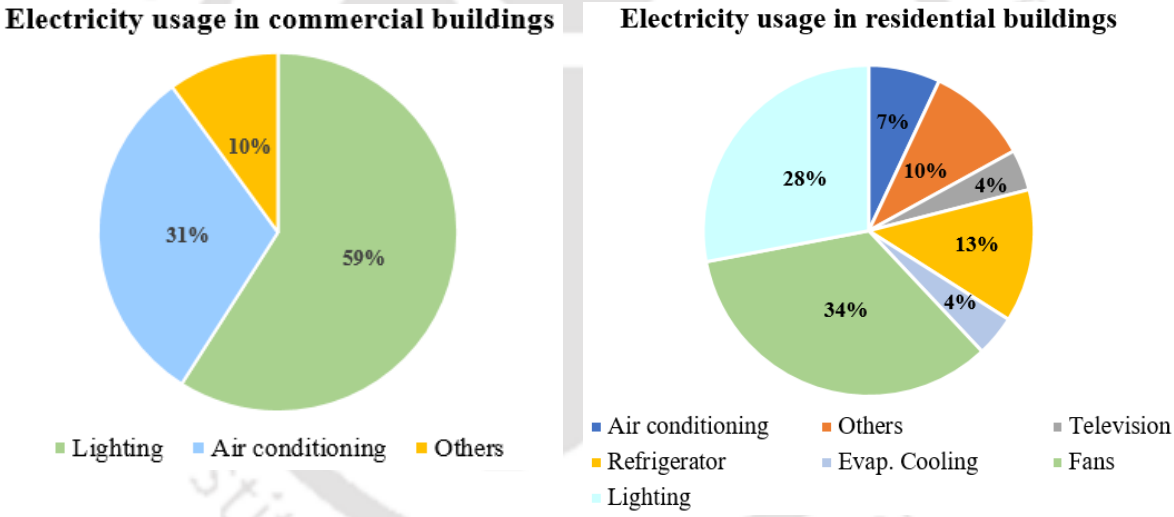

Fig. 1. 3 Consumption of electricity in the residential and commercial sectors [5]

The International Energy Agency (IEA) reports that almost 20% of the electricity used in buildings worldwide is used for cooling [4]. In the commercial building sector, electricity/energy consumption for air conditioning is reported to be 31 %, while in the residential buildings, refrigerator and air-conditioning use 13% and 7% of the total energy supplied, as shown in Fig. 1.3 [5].

Air conditioning and refrigeration units with compression refrigeration systems run on electricity that relies primarily on fossil fuels to generate power. According to the Energy Statistical 2023 report of India, about 14,84,442 GWh of electricity was generated in India during 2021-2022 from thermal, hydro, nuclear, and renewable energy sources (RES).

TH-3395_176107002

However, it can be observed that thermal energy source has the majority of the contribution in electricity generation than other resources (Fig. 1.4)[6]. About 58% of the electricity is generated with fossil fuels/thermal, primarily coal, justifying the larger contribution, while non fossil fuel sources (solar, wind, hydro, nuclear) contribute nearly 42% of the total electricity; however, the nuclear source is the lowest contributor (~2%) in total electricity generation (Fig. 1.5)[7].

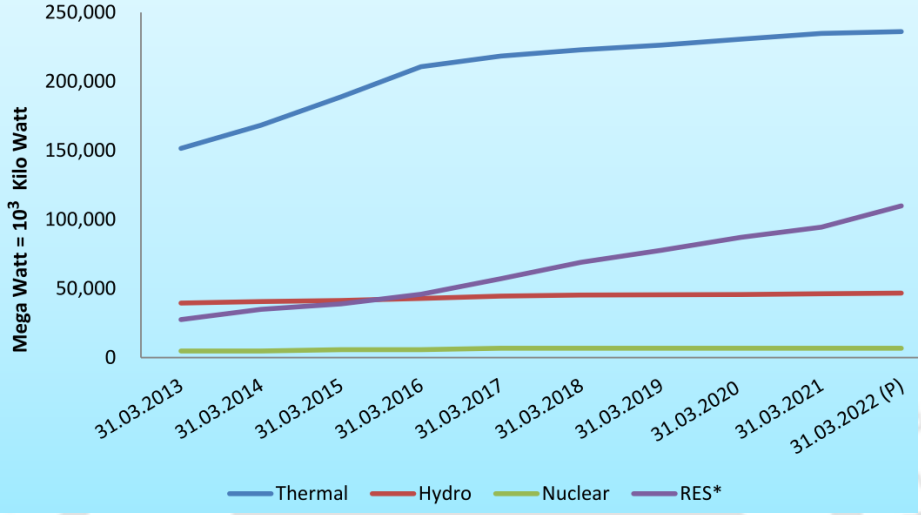

Fig. 1. 4 Electricity generated (MW) from different sources in India during 2021-2022 [6]

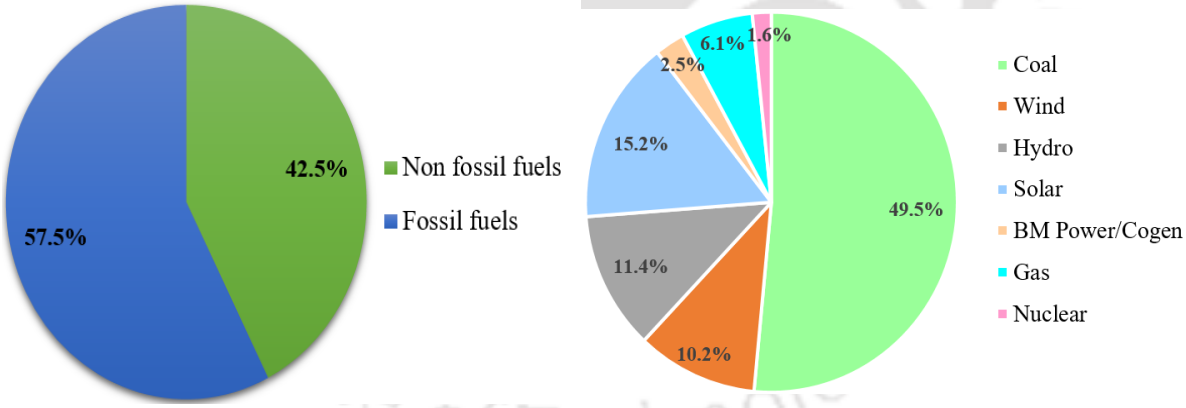

Fig. 1. 5 Electricity production in India using different sectors [7]

About 69% of the coal that is available in India is burned to produce electricity [6]. The burning of fossil fuel emits CO_2 leading to global warming. A surge in climate change is caused by an increase in the volume of greenhouse gases in the atmosphere which will contribute to global warming and negatively impact many fields, including agricultural production, ecology, water resources, and human life. Climate change is also responsible for extreme weather events, such as floods and droughts, that are becoming more frequent and severe. CO_2 is one of the greenhouse gases emitted during various human activities, such as burning fossil fuels,

TH-3395_176107002

industrial processes, deforestation, and many others. A data survey reports that CO_2 emission rose by 51% from 1990 to 2015 [4].

Fig. 1.6 shows that several recent years have had more than 1.2 °C above average temperature from 1850-1900. There has been nearly a 1 °C rise in the global temperature proving 2010-2019 to be the warmest decade so far due to an increase in CO_2 emission. The Paris Agreement on Climate Change urges signatory countries to work towards limiting the rise in global temperature to 1.5 °C (2.7 °F) over pre-industrial levels, with a long-term goal of keeping it well below 2 °C (3.6 °F). The long-term average temperature of the earth is predicted to increase by 1.5 °C (2.7 °F) and 2 °C by 2034 and 2060 respectively. This prediction is reported using ten-year moving average temperature relative to the average temperature recorded between 1850 and 1900 as shown in Fig. 1.6 [8].

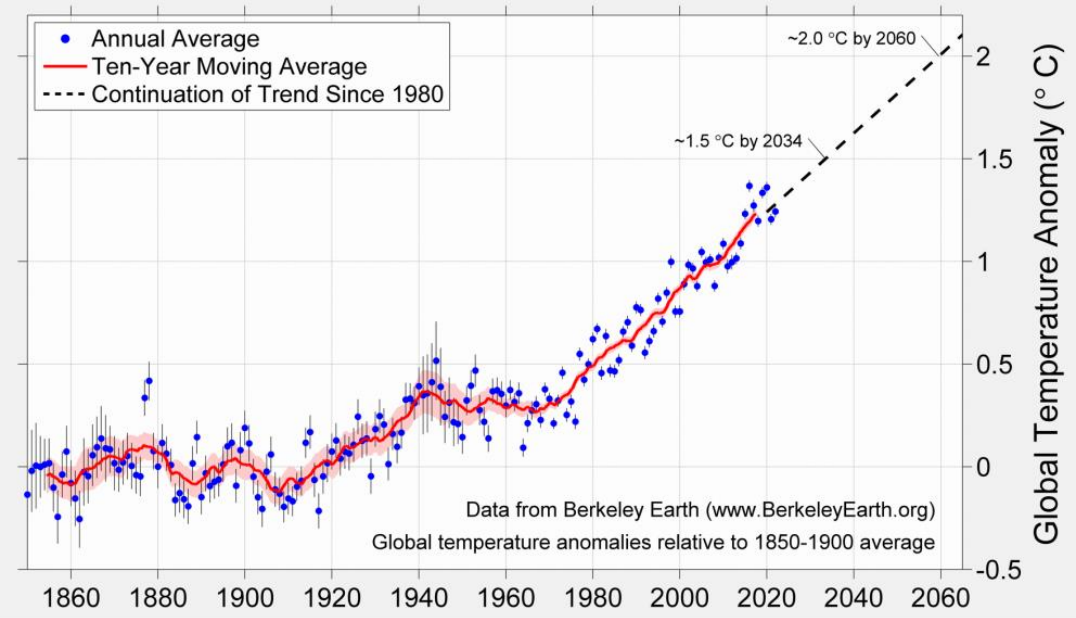

Fig. 1. 6 Rise in the temperature from 1850-2022 due to climate change [8]

This recurrence of warmer temperatures directly impacts the electricity consumption for air conditioning (AC), such as a 1°C increase in temperature, raises the consumption of electricity by around 15% than regular [9]. The Economist Intelligence Unit [10] forecasts that the global sales of new cooling equipment will be a total of 4.8 billion between 2019 and 2030 due to the global temperature rise. Wang et al. [11] predicted that the total annual cooling energy used by the residential building would rise by 30.7% and 80.3% in 2050 and 2080, respectively than, in 2020. From 2022 to 2030, the market for HVAC systems is expected to increase at a compound annual growth rate (CAGR) of 6.3% from a market size of USD 136.3 billion in 2021 [4]. It has been predicted that by 2050, the consumption of air conditioners will rise to 5.5 billion in developing countries which may lead to a 37% growth in electricity demand [12]. According to

TH-3395_176107002

the Director of the IEA, the growing demand for air conditioners is one of the most critical blind spots in today's energy debate, and an essential and relatively simple step is for governments to set higher efficiency standards for cooling. Energy demand due to air conditioning is expected to triple by 2050, reaching 6,205 TWh [13]. Based on the increase in the cooling demand, India cooling action plan (ICAP) provides a 20-year perspective (2017-18 to 2037-38) to address the cooling demand across sectors, as shown in Fig. 1.7. The building sector cooling demand shows the most significant growth at nearly 11 times as compared to the baseline; the cold-chain and refrigeration sectors will grow around 4 times while transport air-conditioning will grow around 5 times the 2017-18 levels (Fig. 1.7).

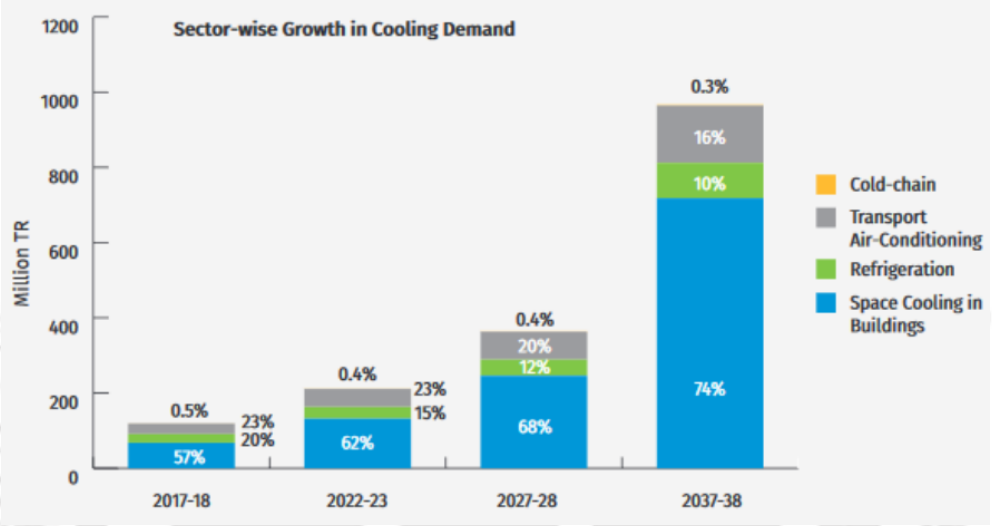

Fig. 1. 7 Cooling demand of India: Sector-wise [14]

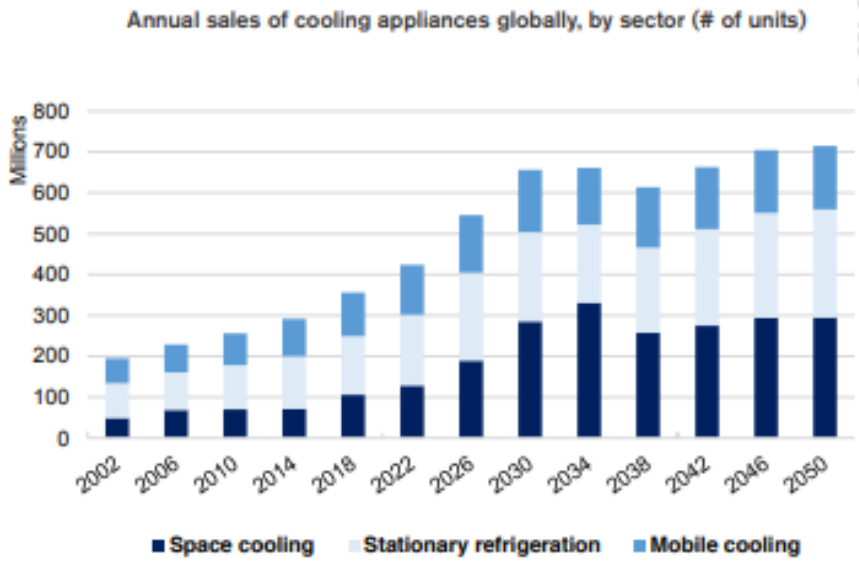

Fig. 1. 8 Increase in the global demand for cooling equipment [3]

TH-3395_176107002

Fig. 1.8 shows that there will be a significant rise in the annual sale of cooling equipment compared to the 2022 year. A higher contribution is observed for space cooling and stationary refrigeration appliances.

1.1.1. Overview of the HVAC system

HVAC (Heating, Ventilation, and Air Conditioning) systems are responsible for maintaining a comfortable indoor environment in buildings, which includes controlling the temperature, humidity, and air quality. However, HVAC systems also consume a significant amount of energy, and their performance has a direct impact on building energy consumption. In general, HVAC systems account for a large portion of building energy consumption, particularly in commercial buildings. This is because HVAC systems have to work continuously to maintain comfortable indoor conditions, and they require a lot of energy to heat or cool the air and distribute it throughout the building. To minimize building energy consumption, it is important to optimize the performance of HVAC systems. This can be achieved through various means, such as selecting energy-efficient HVAC equipment, implementing building automation systems that control the HVAC system based on occupancy and weather conditions, and ensuring that the HVAC system is properly maintained and serviced.

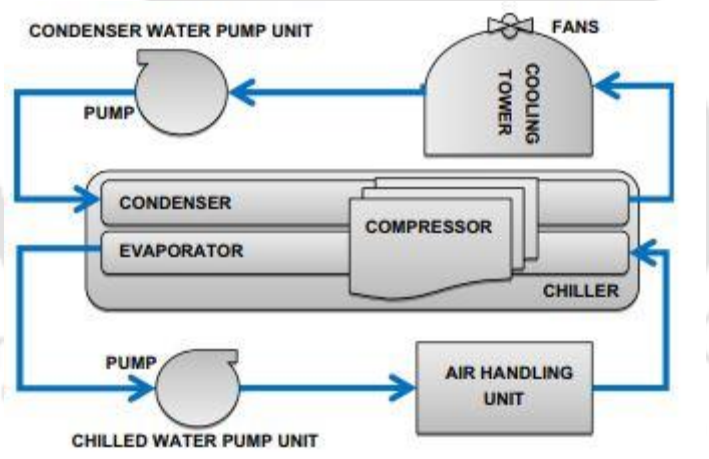

Fig. 1. 9 Air handling section of HVAC [15]

The HVAC system consists of mainly (i) an Air handling unit through which cold air is sent to the ventilated room. (ii) Chiller unit where the main process of refrigeration takes place (iii) Cooling tower where the coolant from the condenser is cooled using air and again sent back to the condenser. The air handling section of the HVAC is shown in Fig. 1.9. It includes an air handling unit, a cooling tower, and a refrigeration system. The refrigeration system consists of a condenser, evaporator, and compressor, i.e., a conventional vapor compression refrigeration system that is driven by high-grade energy such as electricity. The cooling section of an HVAC

TH-3395_176107002

system is responsible for removing heat from indoor air and circulating cool air throughout a building.

In this process, the cooling section works in tandem with the other HVAC system components, such as the air handler, ductwork, and thermostat. The efficiency of the cooling section of an HVAC system can have a significant impact on the overall energy consumption of a building. Using energy-efficient cooling equipment, such as high-efficiency compressors and evaporator coils, can help to reduce energy consumption and lower operating costs. Proper maintenance and regular cleaning of the cooling section can also help to ensure efficient operation and extend the lifespan of the HVAC system.

1.2. Overview of cooling technologies

Refrigeration systems remove heat from a closed space and then reject it in the surrounding environment, where it makes little or no difference. It combines the types of equipment connected sequentially to produce a cooling effect and controls the space temperature. Refrigeration and cooling have become essential aspects of modern life, allowing us to have access to preserve a wider variety of foods, preserving the effectiveness of medical supplies, and facilitating industrial processes to maintain required temperatures for better performance.

To meet the desired demand for fundamental refrigeration study of the chiller is needed to get more efficient air-conditioners and refrigerators. It is necessary to understand thoroughly (i) the multiple cooling needs, (ii) the size and location of the thermal, waste energy resources, and (iii) the optimal combination of the novel/emerging energy sources, thermal storage systems, and efficient technologies to effectively integrate these resources with the required services.

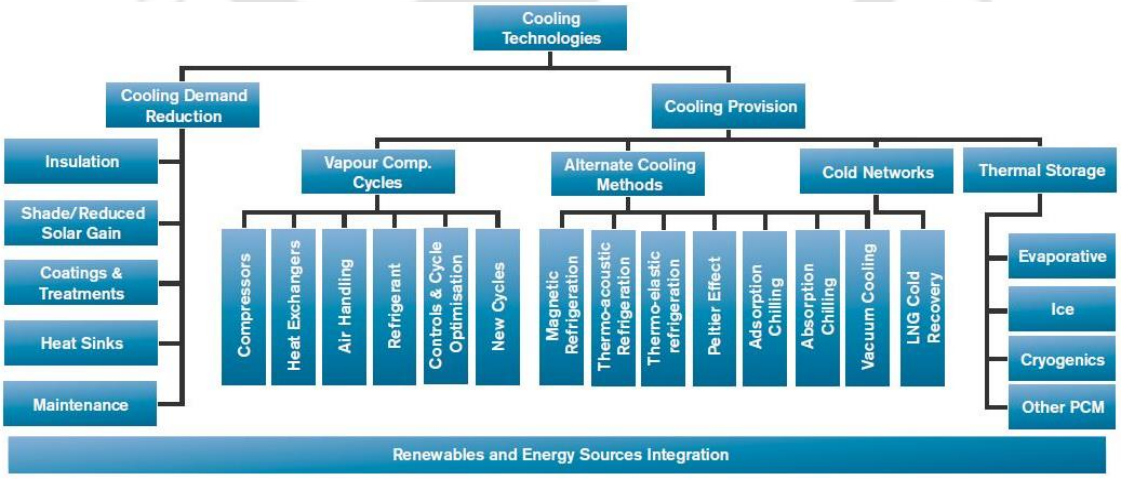

Fig. 1. 10 Overview of cooling technologies [3]

Fig. 1.10 shows the different types of cooling technologies, including traditional cooling technologies and novel cooling technologies, such as thermoelectric cooling, magnetic cooling,

TH-3395_176107002

and adsorption cooling, along with various ways to reduce the cooling demand. The chiller can be operated using any cooling provisions as given in Fig. 1.10. It illustrates various active cooling techniques as well as some passive cooling strategies for lowering cooling demand. Insulating buildings properly can help to reduce heat gain and loss to maintain a comfortable indoor temperature, while the use of shading devices like shutters or blinds can assist in minimizing solar heat gain, which also helps to reduce the requirement for cooling. Utilizing heat sinks made of high thermal mass materials, such as concrete or stone, can assist in absorbing extra heat during the day and release it at night, minimizing the need for mechanical cooling.

Regular maintenance of cooling devices, such as air conditioning units, may ensure that they function efficiently, reducing energy consumption and cooling demand. To provide cooling, the most frequently employed is the vapor compression refrigeration cycle; however, there are alternative cooling methods as well, such as sorption methods (absorption & adsorption), that are becoming popular. Cold networks are centralized cooling systems that deliver chilled water or other cooling fluids to multiple buildings. During off-peak times when power is less expensive, thermal storage devices may be utilized to store cold energy, which can subsequently be used to provide cooling during peak times. Emerging technologies such as magnetic refrigeration, and thermos acoustic refrigeration are not widely accepted yet because of their higher cost, lower efficiency, and limited availability, whereas compression and absorption refrigeration systems show higher efficiency, which is necessary to minimize energy consumption and operating cost. Therefore, the primarily implemented refrigeration systems are:

- Vapor compression refrigeration system (VCRS)
- Vapor absorption refrigeration system (VARS)
- Vapor adsorption refrigeration system (VAdRS)

1.2.1. Vapor compression refrigeration system (VCRS)

The vapor compression refrigeration system is reversed Carnot cycle of the heat engine. Fig. 1.11 (a) depicts the functioning of the VCRS, which is comprised of four principal components: the compressor, the condenser, an expansion valve, and an evaporator. Low-pressure refrigerant enters the evaporator, absorbs latent heat from the surrounding environment (streams 4-1), and transforms into a low-temperature saturated vapor that enters the compressor. The compressor uses high-grade energy such as electricity, to elevate the pressure. As a result, the temperature of the refrigerant also increases (streams 1-2). The superheated refrigerant from the compressor then enters the condenser, where it rejects latent heat and condenses to a high-pressure saturated liquid through phase change (stream 2-3). A reduction in the pressure and temperature of the saturated liquid is caused by an expansion valve, leading

TH-3395_176107002

to the formation of the vapor-liquid mixture (streams 3-4), which then returns to the evaporator to continue the cycle [16].

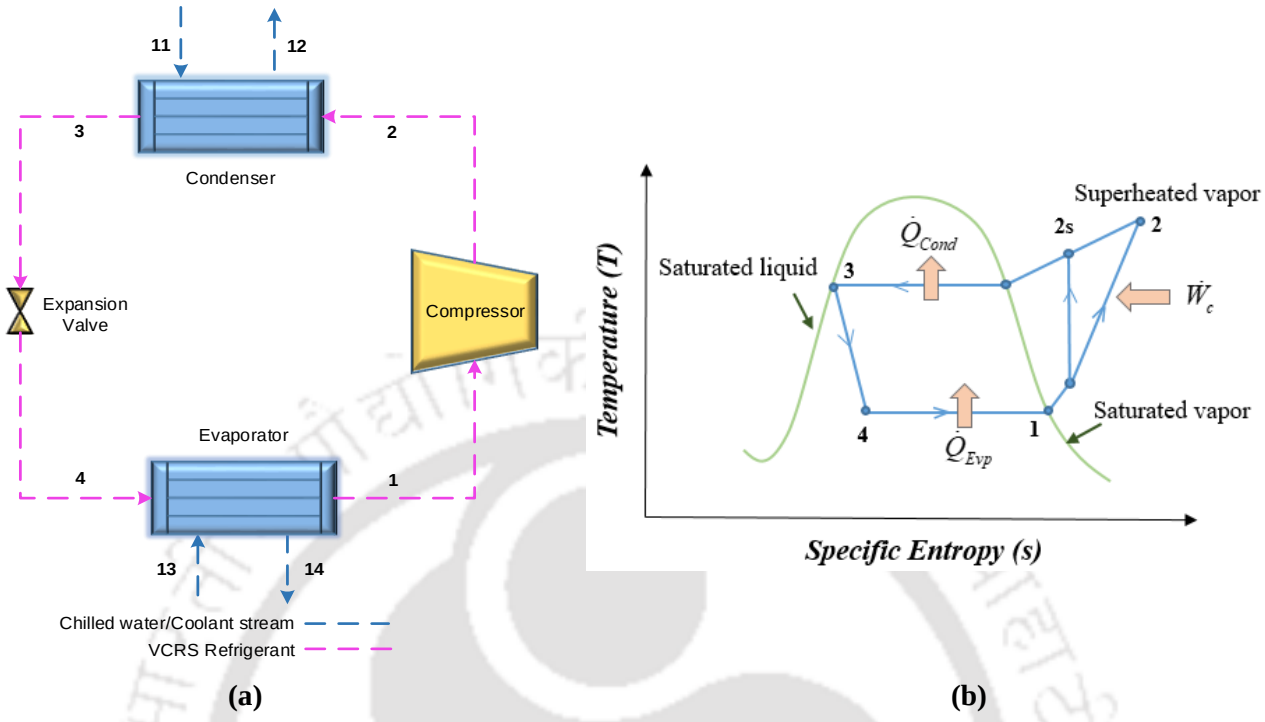

Fig. 1. 11 (a) Schematic of Vapor Compression Refrigeration System (VCRS) [16] **(b) T-S diagram of VCRS**

The Temperature-Entropy (T-S) diagram of VCRS is illustrated in Fig. 1.11 (b), which shows the various states of the refrigerant at each stage of the cycle. The low-pressure liquid refrigerant enters the evaporator, where it absorbs heat from the surroundings and evaporates into a low-pressure vapor (Points 4-1). During this phase change, refrigerant volume increases due to the vaporization process, where the liquid refrigerant absorbs heat from the surroundings and changes into a vapor. On the T-S diagram, this process is represented by a horizontal line, indicating a constant temperature while the entropy increases. The refrigerant enters the compressor as a low-pressure vapor. As it passes through the compressor, its pressure and temperature increase. On the T-S diagram, this process is represented by a steep vertical line, indicating an increase in pressure while the entropy remains relatively constant (Points 1-2s). After compression, the high-pressure and high-temperature vapor enters the condenser. In this stage, heat is transferred from the refrigerant to the surroundings, causing it to condense into a high-pressure liquid (Points 2s-3). The high-pressure liquid refrigerant passes through an expansion valve or throttling device, where its pressure is reduced at Points 3-4.

VCRS shows superior performance compared to other refrigeration systems. Refrigerants such as Chlorofluorocarbons (CFCs), hydrochlorofluorocarbons (HCFCs), hydrofluorocarbons (HFCs), and hydrocarbons (HCs) are generally used for VCRS to produce a cooling effect due

TH-3395_176107002

to their excellent thermodynamic properties. These refrigerants aid in determining the lower refrigeration temperatures required than other systems.

1.2.2. Vapor absorption refrigeration system (VARS)

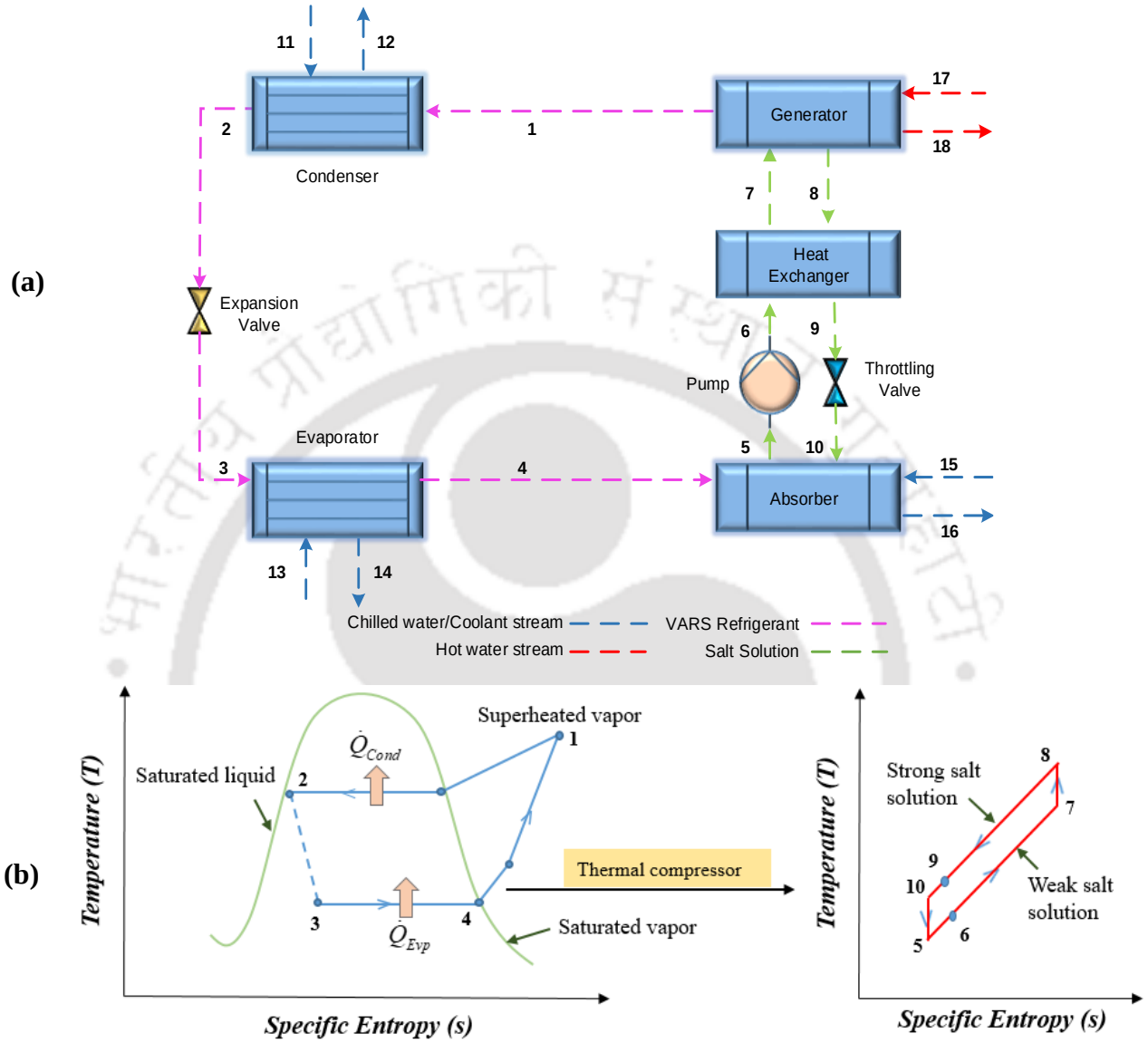

Fig. 1. 12 (a) Schematic of Vapor Absorption Refrigeration System (VARS) [16] **(b) T-S diagram of VARS**

Though VCRS is known for its efficient cooling, it utilizes refrigerants that are phased out due to their high global warming potential (GWP) and ozone depletion potential (ODP). The leakage of these refrigerants has an adverse impact on the environment and contributes to global warming. Additionally, VCRS has a high initial investment cost due to expensive compressors, refrigerant costs, and installation costs. Furthermore, the operating cost of VCRS is also high because of the use of high-grade energy systems obtained from burning fossil fuel, resulting in a significant amount of CO_2 emission into the atmosphere. The power or work required to compress the refrigerant in the VCRS is relatively large as refrigerant undergoes a

TH-3395_176107002

significant change in specific volume. To overcome these problems, a vapor absorption refrigeration system was introduced.

VARS utilizes a thermally driven compressor instead of a power-driven compressor, which simplifies the system and reduces manufacturing costs. This system comprises of generator, absorber, and heat exchanger that acts as a thermal compressor using a refrigerant-absorbent working pair. The schematic for VARS is shown in Fig. 1.12 (a). These systems can be operated on low-grade heat systems such as solar energy**,** waste heat from industrial processes, geothermal energy, and biomass energy, which decreases the need for high-grade energy sources and their associated environmental effects. Moreover, natural substances can be used as working fluid pairs in VARS, mitigating the potential threat of ozone depletion and global warming.

In VARS, the cooling load is provided by the chilled water supplied to the evaporator (streams 14-15). Saturated vapor refrigerant from the evaporator enters the absorber, mixed with absorbent solution (stream 4), forming an exothermic mixture. This heat is rejected using the coolant streams (streams 15-16). The absorber-refrigerant mixture is then directed to the generator through a heat pump and heat exchanger (streams 5-7). In the generator, the refrigerant is vaporized and transformed to a superheated form using heat supplied from hot water streams (streams 17-18). Superheated refrigerant from the generator is sent back to the evaporator via condenser and expansion valve, where the pressure is reduced along with the reduction in temperature (streams 1-3). This low-temperature and low-pressure refrigerant re-enters the evaporator to continue the cycle (Fig. 1.12 (a)) [16]. The strong solution containing less refrigerant is sent back to the absorber through the solution heat exchanger by exchanging its heat with a weak concentration solution (stream 8-10). The heat rejected by the condenser is removed by using coolant streams (streams 11-12).

The entire cycle is presented in a T-S diagram, as shown in Fig. 1.12 (b). The T-S diagram (Fig. 1.12 (b)) explanation for Points (3-4,4-1,1-2,2-3) drawn for the evaporator, thermal compressor, condenser, and expansion valve is similar to VCRS. For thermal compressor in VARS, with temperature variations, the entropy of the solution also varies (Points: 5-10). Within the thermal compressor, temperatures, pressure, and entropies are increased for the weak absorber-refrigerant solution, while the strong absorber-refrigerant solution experiences a decrease in those parameters. Point 8 (absorbent-refrigerant solution stream) and Point 1 (pure refrigerant stream) are at the same temperature since both are the outlet streams of the generator. The volume of the refrigerant throughout the thermal compressor was constant.

TH-3395_176107002

The selection of the absorbent for VARS plays a crucial role in the efficient operation and performance of the VARS. The absorbent used in this cycle should have a good affinity towards the refrigerant circulating in the system, and it should have specific properties such as low air pressure, high heat storage capability, and a large boiling point difference. In addition, the absorbent should be chemically stable and not react with the refrigerant under operating conditions. The absorbent-refrigerant mixture should have a low crystallization temperature and low corrosivity. It should not corrode the materials used in the system, such as pipes, pumps, and heat exchangers. Commonly used absorbents are water (H_2O), lithium bromide (LiBr), lithium chloride (LiCl), and ionic liquids.

1.2.3. Vapor adsorption refrigeration system (VAdRS)

Even though VARS is known for its lower operating costs and ability to be operated using low-grade energy sources; however, these systems are susceptible to problems with absorbent solution corrosivity and crystallization. VCRS uses high-grade energy and refrigerants that directly or indirectly harm the environment. Therefore, to address issues, adsorption refrigeration was put forward. Unlike VARS, the adsorption system does not require any corrosion protection and no crystallization temperature as it does not employ a corrosive absorbent solution whereas compared to VCRS, the adsorption refrigeration system is also thermally driven, works with green refrigerants like water and has no adverse effect on the atmosphere, making it more sustainable system.

A schematic of the vapor adsorption refrigeration system (VAdRS) is given in Fig. 1.13. (a). Instead of an absorption unit, the VAdRS consists adsorption-desorption unit. The system includes an evaporator, an adsorber cum desorber filled with the adsorbent, a condenser, and an expansion valve. The adsorption refrigeration system operates in multiple phases. In the adsorption phase, the refrigerant vapor enters the adsorber, where it is adsorbed onto the surface of the solid adsorbent material. In this phase, the adsorber pressure is constant and maintained at evaporator pressure, while the concentration of the adsorbed refrigerant changes. To reach the condenser pressure where the desorption starts, isosteric heating commences, whereby along with temperature, pressure also increases till condenser pressure is reached; however, the amount of adsorbed refrigerant is constant. In the desorption phase, the adsorbent material is heated to liberate the absorbed refrigerant vapor, due to which the temperature of the refrigerant vapor rises. The refrigerant vapor released by the adsorbent is condensed to a saturated liquid in the condenser. As the maximum desorption temperature is reached, the isosteric cooling starts, where the temperature and pressure of the refrigerant reduce until evaporator pressure is reached. Once the evaporator pressure is reached, the adsorption process starts, and the cycle

TH-3395_176107002

repeats [17]. Depending on variations in the adsorbent temperature and the vapor pressure of the refrigerant, the refrigerant frequently gets adsorbed or desorbed on these beds.

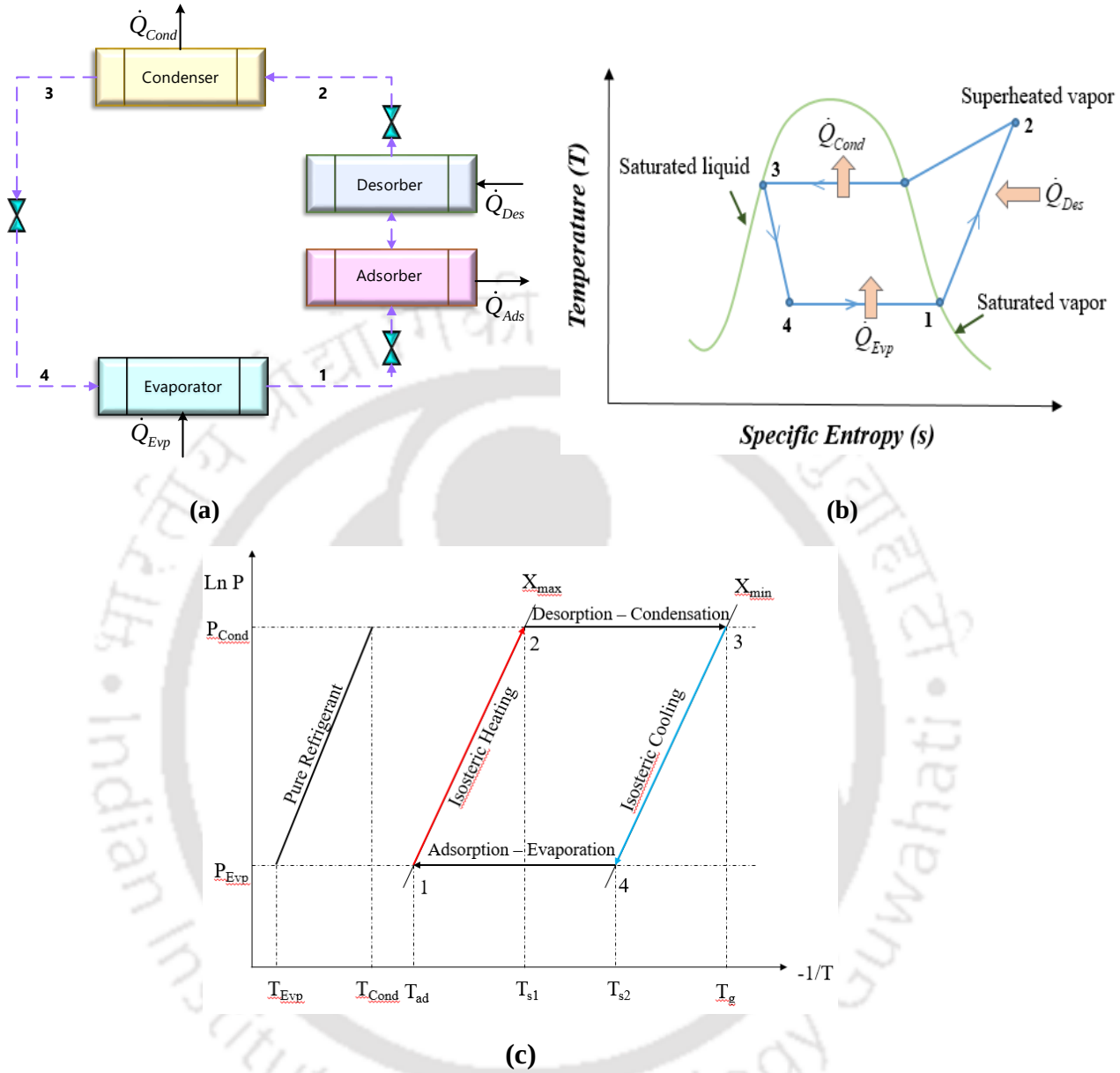

Fig. 1. 13 (a) Schematic of Vapor Adsorption Refrigeration System (VAdRS) (b)T-S diagram of VAdRS (c) Clapeyron diagram [18]

Based on the working of the adsorption refrigeration system, the T-S diagram has been shown in Fig. 1.13 (b). The T-S diagram representation for VAdRS is similar to the VCRS. The Clapeyron diagram for the adsorption refrigeration systems has been illustrated in Fig. 1.13 (c), which represents the thermodynamic properties of the refrigerant during the phase transition process. X_{max} and X_{min} in Fig. 1.13 (c) indicates the maximum and minimum concentration of refrigerant adsorbed. In Fig. 1.13 (c), Points 1-2 depict the isosteric heating process where the temperature and pressure increase at a constant concentration of X_{max} while

TH-3395_176107002

Points 2-3 indicate the desorption-condensation where the concentration of the refrigerant changes from X_{max} to X_{min}. Isosteric cooling at constant X_{min} is shown using Points 3-4, whereas Points 4-1 illustrates the adsorption-evaporation process where refrigerant concentration changes from X_{min} to X_{max}.

The efficiency and performance of the adsorption refrigeration rely on the adsorbents selection. Adsorbents with a wider range of adsorption capacity with temperature variation, higher heat, and mass transfer properties, along with thermal stability and low susceptibility to corrosion are considered good for the adsorption system. In addition, distinctive properties of a refrigerant should be examined, and that includes the heat of vaporization, thermal conductivity, boiling point and working pressures, reactivity and stability, toxicity, environmental impact, and freezing point. The most commonly used adsorbent/refrigerant pairs are silica gel/water, zeolite/water, activated carbon/methanol, activated carbon/ammonia, and calcium chloride/ammonia. If the refrigeration system is below 0˚C, methanol is a good choice as the working pressure of methanol is always less than atmospheric pressure, which avoids the leakage problem.

Besides these, other technologies like magnetic refrigeration, ice slurry refrigeration, and thermoacoustic refrigeration may dominate in the future. Magnetic refrigeration uses the magnetic properties of specific materials to obtain refrigeration. It works on the principles of the magnetocaloric effect. The compression process in the VCRS is replaced by adiabatic magnetization and expansion by adiabatic demagnetization. Initially, magnetocaloric material is surrounded by the applied magnetic field, because of which all moments will become aligned. This alignment causes a decrease in entropy and an increase in the temperature of the material leading to magnetization. The heat generated due to magnetization is removed by water and then, the system is demagnetized, i.e., once the heat is removed, the magnetic field is removed gradually. Due to this, the alignment of all moments (magnetic dipoles) becomes disordered, resulting in a reduction in the temperature. This cooling effect occurs because of the release of thermal energy as the material returns to its original state. The material is kept in thermal contact with the environment. Once the material and refrigerated environment are in thermal equilibrium, the cycle can be repeated. Gadolinium alloys are mostly used to produce strong magnetic fields, while paramagnetic materials are used as magnetocaloric materials [19].

1.3. Scope of optimization in the refrigeration system

Optimizing a refrigeration system is crucial to ensure its efficient operation without unnecessary overdesign. This can be achieved through a comprehensive analysis, design,

TH-3395_176107002

modelling, and performance evaluation using a thermoeconomic optimization approach. This approach combines thermodynamic and economic considerations within a single framework to enhance the performance of the system. For refrigeration systems, energy and energy efficiency are critical performance metrics. Higher system performance is reflected in higher efficiencies, which are characterized by the capacity to convert a larger fraction of input energy into effective cooling output. Finding the correct operating temperatures for the system is essential for achieving maximum efficiency. Operating cost optimization largely depends on the optimal area of the heat exchanger. The system can achieve improved efficiencies and reduce the amount of energy consumed to deliver the desired cooling effect by designing the heat exchanger area in the most optimal manner.

Exergy destruction occurs when energy undergoes irreversible processes or is dissipated as waste heat due to irreversibilities within the system. An exergy destruction assessment of the refrigeration system is necessary to further improve system performance. This study aids in locating systemic areas where energy is being lost or deteriorated. It is possible to obtain important insights into how to create techniques for more effective resource utilization by identifying these causes of exergy destruction. The effects of potential system improvements on energy efficiency can be determined by evaluating the magnitude of exergy destruction. In thermal systems, the fuel that is given to the system normally provides the exergy input. Exergy, which is closely associated with energy quality, is the maximum amount of useful work that can be produced by a system. The fuel undergoes combustion or is subjected to a chemical reaction to produce heat, which powers the thermal system. Increasing the temperature of the heat source (such as combustion gases or a heat reservoir) that is provided to the refrigeration system raises the exergy input. As a result of the larger exergy input, the system is likely capable of converting more useful work potential. To balance maximizing exergy intake and minimizing exergy losses, it is essential to identify the optimal temperatures of the system.

The efficiency of the system can be considerably improved, and exergy destruction may be decreased, by optimizing system-wide variables like temperature. Optimizing the temperature of a refrigeration system can significantly enhance both energy and exergy efficiencies. The temperature differential between the heat source (high temperature) and the heat sink (low temperature) may be improved and brought closer to Carnot efficiency by optimizing the temperature ranges inside the refrigeration system. More heat may be transmitted and transformed into usable work as a result of this optimization, which results in a boost in energy efficiency. The reduction of energy losses inside the system can be assisted by temperature

TH-3395_176107002

optimization. Reduced heat transfer losses are the result of smaller temperature differences between the system and its surroundings. The system may maximize the performance of heat exchange operations by operating at optimal temperature ranges. By optimizing the temperature, it is possible to decrease temperature differences, pressure drops, and other causes of irreversibilities, which will lead to less exergy destruction and improve the exergy efficiency of the system.

The optimization of the refrigeration system not only saves energy but also contributes to cost reduction by considering the interaction of thermodynamic and economic parameters by optimizing resource utilization, sizing and selecting components, operating conditions and system configurations. This ensures the best possible balance between performance and cost-effectiveness.

1.4. Introduction to optimization

Optimization is the process of finding the best possible solution to a problem within a given set of constraints and a specified search space. It involves identifying the decision variables that affect the outcome of a system or process and determining how to employ those variables to achieve the desired result. Generally, this is used for seeking the optimal values of various factors like cost minimization, less energy consumption, or an increase in profit or efficiency of the system. In the case of refrigeration, it can be applied to minimize the cost, area, and exergy destruction of the system and increase the efficiency of the system. A generic representation of the optimization problem can be shown as Eq. (1.1) where *x* is the vector of decision variables, *n* is number of objectives, *h (x)* indicates equality constraints, and *p* is the total number of equality constraints, while *g (x)* denotes inequality constraint and *m* denotes the total number of inequality constraints, which allows all the operations within a safe limit, and *d* is number of decision variables. Decision variables should lie between the range of the given lower bound (*LB*) and upper bound (*UB*).

$$\begin{aligned} &\textit{Minimize / Maximize} \quad F(x) = \{ f_1(x), f_2(x), ..., f_n(x) \} \\ &\textit{Subject to} \\ &\qquad g_i(x) \geq 0, \ i = 1, 2...m \\ &\qquad h_i(x) = 0, \ i = 1, 2...p \\ &\qquad LB_i \leq x_i \leq UB_i, \ i = 1, 2, ...d \end{aligned} \tag{1.1}$$

Various methods, such as direct search and gradient-based methods, are proposed to solve such problems. Direct search methods strongly depend on the starting point of the search, while gradient-based methods like the steepest decent method, conjugate gradient method, etc. need

TH-3395_176107002

information about the gradient of the system to guide search space for determining the optimal solution.

Optimization algorithms are classified as deterministic and stochastic. Deterministic algorithms (mathematical programming methods) are primarily implemented in linear and mixed integer linear programming, while due to the nonlinearity of the problem, stochastic algorithms such as metaheuristic techniques are preferred. Mathematical programming aids to achieve global optimum value for a problem however the timespan to get that is undefined as it will not guarantee the span duration required to solve large-scale problems. Therefore, metaheuristics techniques are often preferred to solve large-scale optimization problems.

Compared to mathematical programming techniques, metaheuristic techniques have several advantages, including the ability to solve black-box optimization problems, accommodate conflicting objectives, handle nonlinearities, not require gradient information, and the problem formulation in the conventional inequality and equality form [20]. Evolutionary algorithms are meta-heuristic and are inspired by natural evolution. These are based on Charles Darwin's law of "survival of the fittest." Metaheuristic techniques such as genetic algorithm (GA), particle swarm optimization (PSO), artificial bee colony (ABC), teaching learning based optimization (TLBO), firefly algorithm (FA), and many others are available. Though several algorithms are available, mostly implementation of GA, direct search method, and NSGA-II were reported for the optimization study of refrigeration systems.

Optimization problems are generally divided into two types: Single-objective and multi-objective optimization. In the case of one objective situation, the problem is a single objective, whereas multi-objective optimization needs to evaluate two or more conflicting objectives simultaneously. As illustrated in Fig. 1.14, solutions in the feasible search space ($\mathbf{S_1}$, $\mathbf{S_2}$) correspond to scalar objective functions ($\boldsymbol{f_1}$, $\boldsymbol{f_2}$) located on the straight line. Selecting an optimal solution based on the required objective is much easier in a single-objective problem, i.e., in the case of objective maximization, $\boldsymbol{f_1}$ is better than $\boldsymbol{f_2}$ and vice versa.

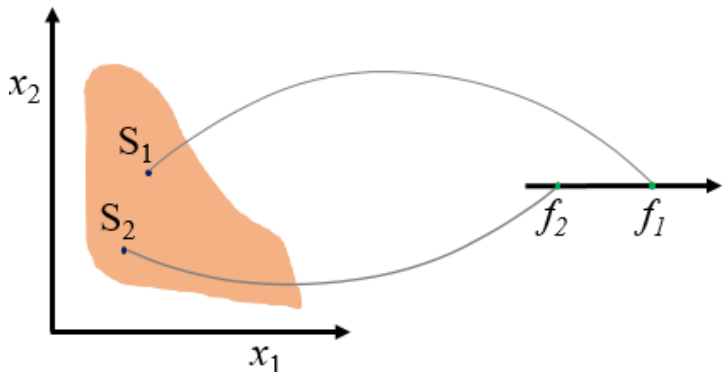

Fig. 1. 14 Single-objective optimization decision variable search space and objective space

TH-3395_176107002

Unlike single-objective optimization, multi-objective optimization will consist of many solutions in the feasible region. The solutions not dominated by any solution (non-dominated solutions) form a Pareto front, as shown in Fig. 1.15. In Fig. 1.15, **T**, **V**, and **P** are the non-dominated solutions forming a Pareto front, while **S**, **U**, and **Q** are the dominant ones. Fig. 1.15 is an example of the minimization of both objective functions, i.e., f_1 & f_2.

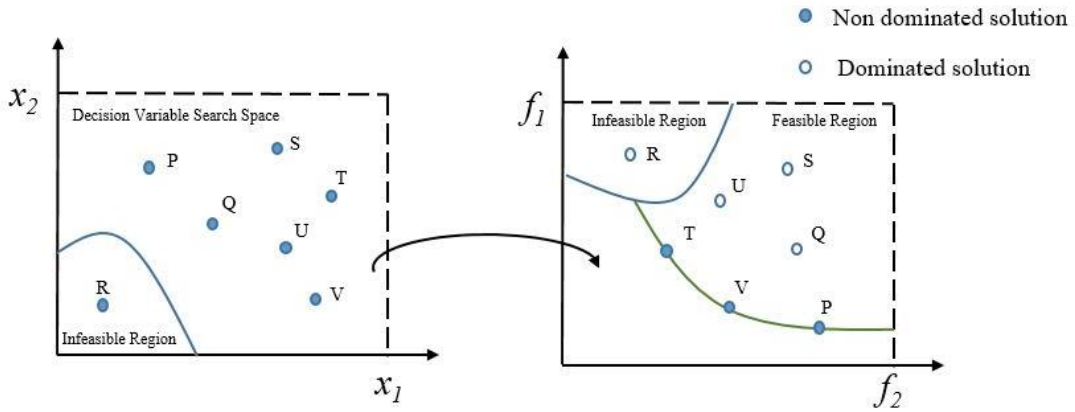

Fig. 1. 15 Multi-objective optimization decision variable search space and objective space [21]

In multi-objective optimization, a random population is generated, and the fitness of each population member is evaluated. Later, based on the fitness, ranks are assigned to each solution. The rank one solutions are the non-dominated solutions and form a Pareto front. The Pareto front solutions are also stated as Pareto optimal solutions. Without deteriorating at least one objective, non-dominated solutions cannot be improved with regard to any objective. To describe the diversification of the solutions in a given Pareto front, the crowding distance is determined. The Pareto fronts are developed using given rankings of solutions and crowding distance. There are several optimum solutions for multi-objective optimization, and users can select the best one based on the importance of their objectives.

1.5. Optimization and metaheuristic algorithms

Optimization can be incorporated in the aspects such as analysis, design, modelling, and operations for better functioning of refrigeration systems. The thorough literature search shows that refrigeration system efficiency can be improved while overall CO_2 emissions can be reduced by choosing the ideal design of equipment, operating conditions, and refrigerant. The nature of optimization problems of the refrigeration system is nonlinear, complex, multimodal, and multi-dimensional [22]. An optimization problem can be solved using mathematical programming techniques as well as metaheuristic techniques; however, if the problem is extremely nonlinear and non-convex and has several local optima, optimizing it using a mathematical programming technique becomes difficult [23]. Mathematical programming

TH-3395_176107002

techniques are time-consuming, and require gradient information while metaheuristic techniques are stochastic and do not require gradient information, initial guesses, or comprehensive information about the optimization problems or systems. Similarly, due to their robustness and ability to handle vast amounts of data and non-linearities, these metaheuristic techniques are applied to refrigeration system optimization. According to the no free lunch theorem [24], no algorithm can determine optimal solutions for all optimization problems and hence there are several metaheuristic techniques to solve an optimization problem. Some of the single-objective and multi-objective metaheuristics techniques employed in the current work are briefly described here.

1.5.1. Sanitized teaching learning based optimization algorithm (sTLBO)

Rao et al. [25] proposed a population-based metaheuristic technique named the teaching-learning based optimization (TLBO) algorithm in 2011, which focuses on the teaching-learning concept in a classroom. The TLBO variation employed in this study is sanitized teaching learning based optimization (sTLBO) [26], which does not use a duplication removal procedure and needs only two functional evaluations per member of the population in each iteration. In sTLBO, the population is denoted as a class, the solution as a learner, and the best solution as a teacher. Each learner (or population member) receives learning from the teacher (Teacher phase) as well as other learners (in the Learner Phase). A new solution (X_{new}) is generated in the teacher phase using the best student (X_{best}) and mean (X_{mean}) of all the students in the class for each generation, as shown in Eq. (1.2).

$$X_{new} = X + r\left(X_{best} - T_f X_{mean}\right) \tag{1.2}$$

where X is the old solution, T_f is the teaching factor which can be either 1 or 2, and r is a random number between 0 to 1. In the student phase, a random student from the class is selected as a partner (X_p) to generate a new solution, as given in Eq. (1.3).

$$\begin{aligned} X_{new} &= X + r\left(X - X_p\right) \quad if \;\; f < f_p \\ X_{new} &= X - r\left(X - X_p\right) \quad if \;\; f \geq f_p \end{aligned} \tag{1.3}$$

In Eq. (1.3), f is the fitness of the old solution (X), and f_p is the fitness of the partner solution (X_p). The fitness of the newly generated solution is compared to that of the learner in the teacher or learner phase. If the new solution has better fitness than the previous one, it replaces the current learner/solution. The user-defined parameters of the algorithm include population size, maximum iteration, and termination criteria.

TH-3395_176107002

1.5.2. Atom search optimization algorithm (ASO)

Atom search optimization (ASO) is a recently proposed population-based meta-heuristic technique by Zhao et al. [27], that mimics the motion of the atomic particles studied in molecular dynamics. In ASO, each solution in the population is called an atom, and a factor termed mass indicates the quality of the solutions and is determined using the objective functions of all solutions. Heavier mass suggests a better solution and vice versa. The user-defined parameters of the algorithm include population size, maximum iteration, termination criteria, depth weight (α), and multiplier weight (β). Every solution in ASO updates its position with the help of two associated parameters: acceleration (a) and velocity (v). The acceleration of the solutions is calculated using the position and mass of that solution ($m_d^i(t)$), interaction force ($F_d^i(t)$), and constraint force $G_d^i(t)$.

$$M_i(t) = e^{-\frac{Fit_i(t) - Fit_{best}(t)}{Fit_{worst}(t) - Fit_{best}(t)}} \tag{1.4}$$

$$m_i(t) = \frac{M_i(t)}{\sum_{j=1}^{N} M_j(t)} \tag{1.5}$$

$$F_i^d(t) = \sum_{j \in Kbest} rand_j F_{ij}^d(t) \tag{1.6}$$

$$G_i^d(t) = \beta e^{-\frac{20t}{T}} \left(x_{best}^d(t) - x_i^d(t) \right) \tag{1.7}$$

$$a_i^d(t) = \frac{F_i^d(t)}{m_i^d(t)} + \frac{G_i^d(t)}{m_i^d(t)} \tag{1.8}$$

Eqs. (1.4)-(1.7) show the calculation of mass, interaction force, and constraint force. Here, the best solution (Fit_{best}) will be the minimum fitness, and the worst solution will be (F_{worst}). In Eq. (1.6), *Kbest* is a subset of an atom population and is made up of the first K atoms with the best fitness functions. Using updated mass, interaction, and constraint force, acceleration is updated, as shown in Eq. (1.8)

$$v_i^d(t+1) = rand_i^d v_i^d(t) + a_i^d(t) \tag{1.9}$$

$$x_i^d(t+1) = x_i^d(t) + v_i^d(t+1) \tag{1.10}$$

In Eq. (1.9), for d^{th} of the i^{th} atom, $x_d^i(t)$ is the position, $v_d^i(t)$ is the velocity, and $a_d^i(t)$ is the acceleration of the t^{th} iteration. The velocity is varied using the corresponding acceleration and its previous velocity as shown in Eq. (1.9), position is updated using updated velocity (Eq.

TH-3395_176107002

(1.10)). It should be noted that in ASO, the solution selection strategy is (μ, λ), i.e., the population of the present iteration updates its position without further comparison with the population of the previous iteration, and the best solution obtained so far is always saved. Every updated atom also updates the best solution, and in case the best solution remains unchanged, the best solution is copied to a randomly selected atom.

1.5.3. Coyote optimization algorithm (COA)

Coyote optimization algorithm (COA) is a nature-inspired population-based metaheuristic technique based on social conditions, experience exchange, and hunting methods of the coyotes proposed by Pierezan and Coelho [28]. Based on the multiple packs, which consist of a specific number of coyotes, the population of COA is determined. Each solution is termed a coyote in COA, and its objective function is considered its social condition. The minimum cost determined is stated as the alpha of the pack. The coyotes share their social condition, and this cultural tendency can be calculated using Eq. (1.11) for each pack. Here, *Nc* indicates the number of coyotes in the packs.

$$cult_j^{p,t} = \begin{cases} O^{p,t}_{\frac{(Nc+1)}{2},j,} & Nc\ is\ odd \\ \dfrac{O^{p,t}_{\frac{(Nc)}{2},j} + O^{p,t}_{\frac{(Nc+1)}{2},j}}{2}, & Otherwise \end{cases} \tag{1.11}$$

where $O^{p,t}$ represents the ranked social conditions of all coyotes of the p^{th} pack in the t^{th} instant of time for every j in the range [1, D]. Here D indicates the no. of decision variables. Each solution in the pack generates a potential new solution using two randomly selected solutions and the median of the same pack, as shown in Eq. (11). To signify the cultural interaction in the packs, alpha influence (δ_1) and pack influence (δ_2) are considered in this algorithm, determined using Eq. (11). Cr_1 and Cr_2 indicate the random coyotes selected from the pack. In Eq. (1.12), r_1, *and* r_2 have been considered as the random numbers between [0,1]. $soc^{p,t}$ is the solution of the p^{th} pack at t^{th} instant of time.

$$\begin{aligned} \delta_1 &= alpha^{p,t} - soc^{p,t}_{cr_1} \\ \delta_2 &= cult^{p,t} - soc^{p,t}_{cr_2} \\ new\_soc^{p,t}_c &= soc^{p,t}_c + r_1\delta_1 + r_2\delta_2 \end{aligned} \tag{1.12}$$

$$pup_j^{p,t} = \begin{cases} soc^{p,t}_{r_1,j}, & rnd_j < P_s\ or\ j = j_1 \\ soc^{p,t}_{r_2,j}, & rnd_j \geq P_s + P_a\ or\ j = j_2 \\ R_j, & Otherwise \end{cases} \tag{1.13}$$

TH-3395_176107002

Additionally, a new solution $pup^{p,t}$ is generated inside a pack for every iteration known as birth inside a pack using Eq. (1.13) and is accepted if it has a better objective function than the worst solution in the pack. In Eq. (1.13), P_s and P_a denote scatter and association probability, respectively, R_j is a random number inside the j^{th} decision variable bounds, rnd_j is a random number between [0,1], and r_1 & r_2 are the random coyotes from the p^{th} pack. After generating all new solutions, transitions between the packs occur based on the probability calculated where two solutions are selected from two randomly chosen packs, and the selected solutions are transferred to another pack. The primary condition under which a newly generated solution is permitted into the pack is if its objective function is better than that of the objective function of the new solution. The user-defined parameters are termination criteria, the number of packs (N_p), and the number of coyotes (N_C).

1.5.4. Tree growth algorithm (TGA)

This algorithm was put forward by Cheraghalipour et al. [29] in 2018 based on the competition of trees in the forest for light and nutrients. Trees can sense the existence of nearest competitors through light sensors called "Phytochrome," which can evaluate the proportionality of red and UV light in sunlight received. In TGA, each population member is called a tree. The algorithm is proposed for the minimization of the objective functions; hence, the best tree will have a minimum fitness and vice versa.

The new members are generated using four groups of size *N1, N2, N3,* and *N4*. A local search on *N1*, better solutions in the population, is performed several times using Eq. (1.14). If the fitness of the new solution (T_i^{j+1}) is better than the old solution (T_i^{j}), then the old solution will be replaced by the new one. In Eq. (1.14), θ is the tree reduction rate of power, and the value of r lies between [0,1]. The next *N2* better solutions generate new solutions using two nearby solutions (x_1 & x_2) with minimal distance d_i calculated using Eq. (1.15) . The value of λ and α lies between [0,1] in Eq. (1.16).

$$T_i^{j+1} = \frac{T_i^j}{\theta} + rT_i^j \tag{1.14}$$

$$d_i = \left(\sum_{i=1}^{N_1+N_2} \left(T_{N_2}^j - T_i^j \right)^2 \right)^{0.5} \quad \& \quad d_i = \begin{cases} d_i \ if \ \ T_{N_2}^j \neq T_i^j \\ \infty \ if \ \ T_{N_2}^j = T_i^j \end{cases} \tag{1.15}$$

$$\begin{aligned} y &= \lambda x_1 + (1-\lambda) x_2 \\ T_{N_2}^j &= T_{N_2}^j + \alpha_i y \end{aligned} \tag{1.16}$$

TH-3395_176107002

Each time a new solution is generated, it replaces its parent solution if its objective function is better than that of the parent solutions. The worst *N3* solutions (*N3 = N - N1 + N2* where *N* is the population size) from the population are replaced by random solutions generated within the bounds. After generating *N* new members, *N4* (*N4 = N1*) solutions are generated from the updated *N1* solutions using the mask operator concerning the best solution of the *N1* population. The mask operator is a vector of binary variables of the same length as the decision variables. It switches the variables among the best solution and newly generated solution based on mask operator value to determine a new modified solution. If the mask operator has a value of 1 for a particular variable, then that variable in the newly generated solution is replaced with the variable from the best solution, else the variables from the newly generated solutions are retained. The *N4* solutions are added to the population, and the best *N* members are allowed into the next iteration. The solution selection strategy for this algorithm is greedy selection, i.e., the old solution is replaced with the new one if the objective function of the new solution is better than the old one. The user-defined parameters in TGA are the group size *N1, N2*, the number of times the local search is to be performed, population size, and the termination criteria.

1.5.5. Yin-Yang pair optimization algorithm (YYPO)

Yin Yang Pair Optimization (YYPO) was introduced by Punnathanam and Kotecha [30], based on the principle of harmony between dualities conflicting and complimenting nature. In YYPO, decision variables are dealt with in their normalized form (value between 0 to 1). Unlike other metaheuristic techniques, it is not population-based and works with two points (P_1 & P_2). Point P_1 focuses on exploitation, and point P_2 concentrates on exploring the variable space. The two solutions update their position by searching a region around their position, which is decided by two search radii (δ_1 & δ_2) of the hypersphere, and these radii are not user-defined. The search radii are self-adaptive and can decrease or increase periodically to reflect the contraction and expansion of the search volumes around points P_1 and P_2.

This algorithm constitutes two stages: the splitting stage and the archive stage, where the splitting stage occurs in every iteration, and the archive stage is performed at every archive updating interval of iterations. P_1 and P_2 and their corresponding radii (δ_1 & δ_2) will enter the splitting stage; however, at a time, a single point (P) along with its search radii (δ) will undergo the splitting stage. In this stage, multiple new solutions within the search radius of the two points, P_1 and P_2, are generated, and the best among them is treated as P_1 and P_2 for the next

TH-3395_176107002

iterations. These newly selected P_1 and P_2 points are stored in an archive till an archive update interval is encountered.

$$\begin{aligned} &if \;\; R < 0.5 \\ &S_j^j = S_j + r\delta \\ &S_{j+D}^j = S_j - r\delta \\ &else \\ &S_k^j = S^j + r\left(\delta/\sqrt{2}\right) \quad if \;\; B_k^j = 1 \\ &S_k^j = S^j - r\left(\delta/\sqrt{2}\right) \quad else \end{aligned} \tag{1.17}$$

In Eq. (1.17), the value of R and r lies between [0,1]. S is the matrix where multiple copies of P are stored. The binary matrix B can be generated by randomly selecting 2D unique integers between 0 and 2D-1 (where D is the number of decision variables) and converting them into binary strings of length D. The subscript indicates the point number, and the superscript denotes the decision variable number. The archive updating interval is decided once after every archive update stage, and its value is between the minimum archive interval (I_{min}) and maximum archive interval (I_{max}). In the archive update stage, the best among all the points stored in the archive is updated as P_1 and the second best as P_2. After every archive update stage, the search radii are updated using Eq. (1.18).

$$\begin{aligned} \delta_1 &= \delta_1 - \left(\delta_1/\alpha\right) \\ \delta_2 &= \delta_2 + \left(\delta_2/\alpha\right) \end{aligned} \tag{1.18}$$

The selection strategy for the YYPO algorithm is (μ + λ), i.e., the objective functions of the solutions in the archive (old solutions) and the objective functions of the new solutions generated in the split function are combined, and the best objective function among all solutions is selected.

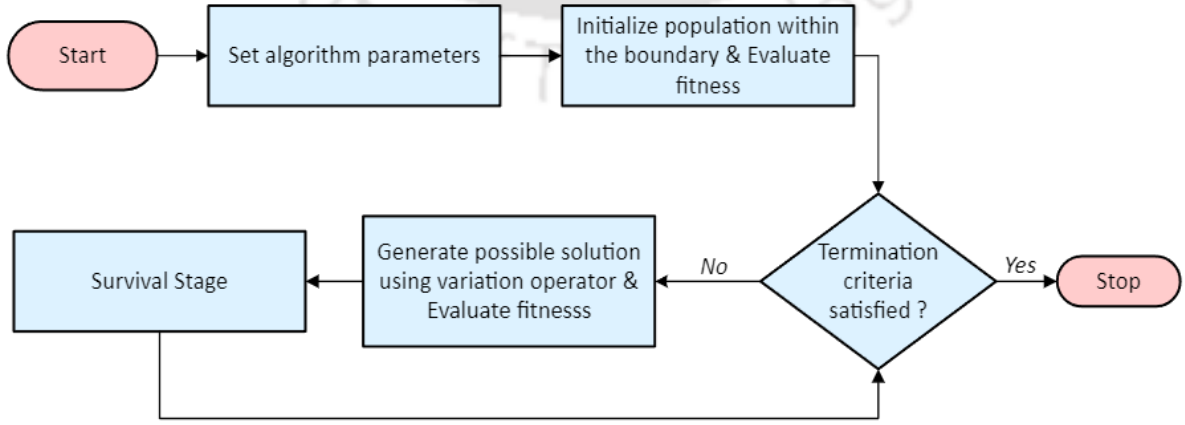

Fig. 1. 16 General framework of single-objective metaheuristic algorithms

TH-3395_176107002

The user-defined parameters of YYPO include the maximum and minimum archive update intervals (between 1 to the maximum number of iterations), expansion or contraction factor (α) for search radii, and the termination criteria. The general implementation of single-objective metaheuristic algorithms is shown in Fig. 1.16.

1.5.6. Multi-objective genetic algorithm (MOGA)

Multi-objective genetic algorithm (MOGA) is the multi-objective variant of GA, a population-based stochastic technique utilizing the principle of genetics and natural selection to generate potential solutions. Moreover, it uses the non-dominated sorting and crowding distance to determine the Pareto front in each iteration. The search process of MOGA begins with an initial population generated within the search space. The chromosomes are categorized into multiple fronts based on their fitness using the non-dominated sorting method, where chromosomes are ranked with respect to their dominance. Generally, the k^{th} front (rank = k) solutions are dominated by all solutions in $(k\text{-}1)^{th}$ and its lower fronts. The crowding distance is calculated to specify the diversity of the solutions in a particular front. MOGA uses an iterative process involving the selection, variation, and survival stages to identify the Pareto optimal solutions. The tournament selection is employed to determine the parents for the mating pool. When playing the tournament between solutions, the least ranked solution is preferred; however, if the solutions have the same rank, the solution with a larger crowding distance is selected. After creating the mating pool, the intermediate crossover and adaptive mutation are employed to generate offspring. The offspring generated using the intermediate crossover is given in Eq.(1.19) .

$$X_C = X_{P1} + rRatio\left(X_{P2} - X_{P1}\right) \tag{1.19}$$

In Eq.(1.19), X_C indicates the newly generated offspring using two parent solutions X_{P1} and X_{P2}. The *Ratio* represents the weighted average of the parents having a size of [1, D], and *r* is the random number between 0 and 1. At the end of the iteration, the non-dominated sorting and crowding distance calculations are used to identify the next iteration population. The highest priority from the last selected front is provided to the least ranked and well-diverse solutions for the next population iteration [31]. The '*gamultiobj*' function provided in Mathworks is utilized for determining the Pareto solutions in this work, and more details regarding this algorithm are available at https://bit.ly/32aEiQ6 and https://bit.ly/34wMsoP.

1.5.7. Multi-objective particle swarm optimization algorithm (MOPSO)

Multi-objective particle swarm optimization (MOPSO) is a multi-objective version of PSO, which follows the principle of bird flocking or fish schooling. MOPSO uses a fixed-size

TH-3395_176107002

external repository to store the non-dominated solutions, and a grid-based approach is employed to ensure a well-distributed Pareto front. The external repository is initialized with the non-dominated solutions present in the initial swarm. Each non-dominated solution is associated with a crowding distance factor as the iteration progresses to eliminate the excess solutions when the repository becomes full.

In PSO, each particle/solution is associated with a velocity (V) and position (X). The position of the particle in the i^{th} iteration is updated as per Eq. (1.20) using the personal best position of each particle (*pbest*), and a global best position (*gbest*) selected from the repository. The inertia weight and acceleration coefficients are indicated using w, C_1, and C_2, respectively. Note that r_1 and r_2 are random numbers between 0 and 1. In each iteration, the personal best position of each particle will get updated if the newly updated position of the particle dominates it. Simultaneously, a roulette wheel selection chooses the global best position from the external repository.

$$\begin{aligned} V_{i+1} &= wV_i + r_1C_1\left(pbest_i - X_i\right) + r_2C_2\left(gbest - X_i\right) \\ X_{i+1} &= X_i + V_i \end{aligned} \tag{1.20}$$

After the position update, a few selected particles are mutated with random solutions generated within the decision variable bounds, as in Eq.(1.21).

$$X_{selected} = lb + r\left(ub - lb\right) \tag{1.21}$$

Note that *lb* and *ub* indicate the lower and upper bounds of the decision variables. The solutions that undergo the mutation are selected based on the iteration number and the mutation percentage. At the end of each iteration, the external repository is updated with non-dominated solutions, and the excess non-dominating solutions are discarded using the crowding distance of the solutions [32]. The solutions in the external repository at the termination criteria are reported as the Pareto front determined by the algorithm.

1.5.8. Multi-objective sanitized teaching learning based optimization algorithm (MOsTLBO)

Multi-objective sanitized teaching learning based optimization (MOsTLBO) is a multi-objective variation of TLBO, which uses the non-dominated sorting method to solve multi-objective optimization problems. This algorithm consists of teacher and learner phases to modify the solutions in every iteration. Each solution performs the teacher and, subsequently, the learner phases. In the teacher phase, a solution generates a new potential solution using the best solution (X_{best}) and mean of the population (X_{mean}) as given in Eq. (1.22)

TH-3395_176107002

$$X_i^{new} = X_i + r\left(X_{best} - T_f X_{mean}\right) \tag{1.22}$$

In Eq.(1.22), T_f is the teaching factor which can be either 1 or 2, and r is the random number between 0 and 1. The teacher solution required for generating a new solution in the teacher phase is randomly selected from the first-front solutions. In the learner phase, a randomly selected solution aids in generating a new solution, as given in Eq.(1.23) .

$$X_i^{new} = \begin{cases} X_i + r\left(X_i - X_p\right) & if \;\; f\left(X_i\right) \le f\left(X_p\right) \\ X_i - r\left(X_i - X_p\right) & if \;\; f\left(X_p\right) \le f\left(X_i\right) \\ X_i + r\left(X_i - X_p\right) & if \;\; \left(f\left(X_i\right) \; and \;\; f\left(X_p\right) \; are \; non\text{-}dominated \; and \; r \le 0.5\right) \\ X_i - r\left(X_i - X_p\right) & if \;\; \left(f\left(X_i\right) \; and \;\; f\left(X_p\right) \; are \; non\text{-}dominated \; and \; r > 0.5\right) \end{cases} \tag{1.23}$$

X_P is the randomly selected partner solution, and r is the random number between 0 and 1. In both phases, the dominant solution among the new and its parent solutions is considered in the population. If both the solutions are non-dominated, then one of the solutions is kept in the population with an equal probability. The non-dominated sorting method is employed by considering the first front solutions of the previous iteration and the updated population of the current iteration to determine the first front solutions for the next iteration. According to the MOsTLBO algorithm, the first front solutions determined after the termination criteria are reported as the Pareto front [33]. The general implementation of multi-objective metaheuristic algorithms is shown in Fig. 1.17 respectively

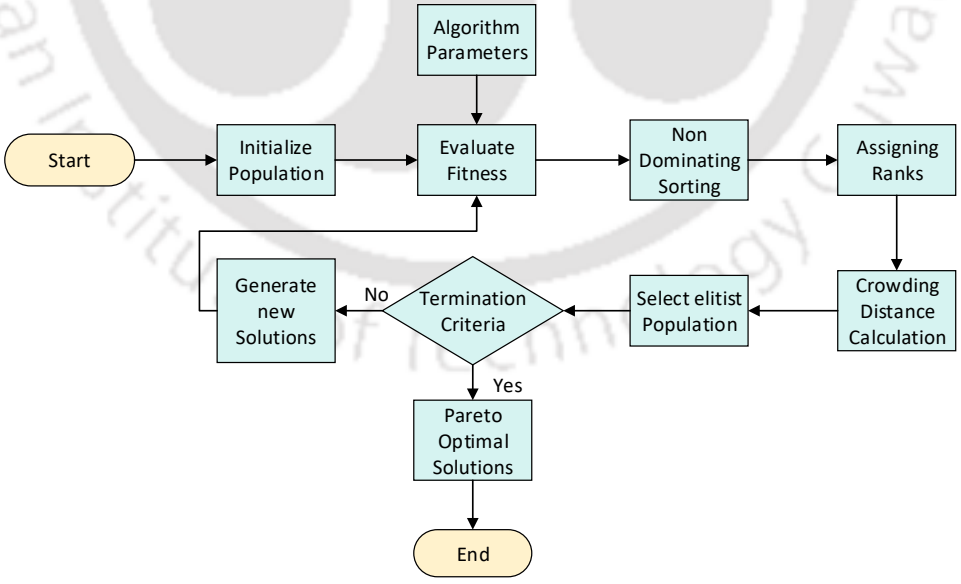

Fig. 1. 17 Overview of implementation of a multi-objective metaheuristic algorithm

TH-3395_176107002

1.6. Thermoeconomic optimization

Optimization of refrigeration systems assists in reducing energy consumption, operating costs, and environmental impact by providing optimal decision variables. Combining thermodynamic parameters with economic parameters, researchers have put forward the thermoeconomic concept. The main objective of thermoeconomic optimization is to minimize the total cost of the system while maintaining a desired level of performance. This entails maximizing both the economic performance, involving capital and running expenses, and the thermodynamic performance, which includes the efficiency of the system. Thermoeconomic optimization is typically performed using mathematical models and optimization algorithms. Optimization algorithms search for the optimal solution based on thermodynamic and economic constraints and objectives. The results of thermoeconomic optimization can be used to identify the most cost-effective design or operating conditions for the energy system. This can help reduce operating costs, improve system efficiency, and increase profitability. Thermoeconomic optimization is beneficial for complex energy systems, such as combined heat and power plants or refrigeration systems, where many interacting components and trade-offs between thermodynamic performance and economic performance. By taking a holistic approach that considers both thermodynamic and economic factors, thermoeconomic optimization can help identify solutions that achieve optimal performance and cost-effectiveness.

1.7. Motivation of the work

The need for refrigeration systems is increasing due to changes in population, food habits, urbanization, industrialization, and climate change. Refrigeration systems are essential for keeping food fresh, supporting several businesses, and providing comfort in various applications. Improvements and optimization in refrigeration systems are required to address issues like energy efficiency, economic effectiveness, environmental impact, and increase the performance and sustainability of refrigeration systems in diverse applications. It is crucial to continuously look for new methods to enhance refrigeration systems and make them more productive and efficient due to constant technology improvements and shifting regulatory requirements. Here are some potential areas for improvement of refrigeration systems in the near future:

- Energy efficiency: Energy efficiency is one of the primary challenges confronting refrigeration systems. The majority of refrigeration systems consume significant energy to maintain the cool temperature of food and other items, which may be expensive for

TH-3395_176107002

businesses. By increasing the energy efficiency of refrigeration systems, less power is required to accomplish an equivalent amount of cooling or freezing, resulting in less electricity consumed and lower greenhouse gas emissions from power generation. The environmental footprint of refrigeration systems may be mitigated by increasing energy efficiency. Optimizing refrigeration systems can help to reduce energy consumption, lower operating costs, and improve overall energy efficiency.

- Refrigerant gases: The refrigerant gases used in conventional refrigeration systems, such as hydrofluorocarbons (HFCs), can contribute to global warming and ozone depletion. Alternative refrigerants, such as hydrocarbons and natural refrigerants, have lower global warming potential and can be employed to boost the environmental sustainability of refrigeration systems.
- System design: Considerations like load estimations, appropriate component size, and the choice of energy-efficient equipment may all be taken into account when beginning the optimization process at the design stage. Design optimization guarantees that the refrigeration system is customized to the specific requirements and operational conditions, maximizing efficiency from the start.
- Maintenance and repairs: Regular maintenance and repairs are essential for ensuring the optimal performance and longevity of refrigeration systems. Optimizing refrigeration systems can help to reduce downtime and maintenance costs. This can improve system reliability, reduce the risk of equipment failure, and extend the lifespan of refrigeration systems.
- Operational efficiency: Refrigeration systems optimization can enhance operational efficiency by reducing energy waste, improving system performance, and increasing productivity/product shelf life. Efficient and well-maintained refrigeration systems ensure that products are stored at the appropriate temperature and humidity levels, preventing spoilage and extending product shelf life. This can result in cost savings and improved overall business performance.
- Integration with other systems: Refrigeration systems can be integrated with other systems, such as energy storage or renewable energy systems, to improve overall energy efficiency and reduce costs of the systems.

Overall, refrigeration system optimization is essential for improving energy efficiency, food safety, maintenance and reliability, operational efficiency, and sustainability in various applications.

TH-3395_176107002

1.8. Organization of the thesis

The thesis has been presented in seven chapters with the following outline:

Chapter 1 starts with a brief introduction to energy consumption and its relation with the HVAC system. A concise overview of conventional refrigeration systems along with their pro and cons is given. A general introduction to the single-objective, multi-objective, and thermoeconomic optimization of refrigeration systems is presented.

Chapter 2 discusses the state of art of different aspects of VCRS, VARS, and cascaded refrigeration systems (CRS). A comprehensive literature review of the thermoeconomic optimization study and the metaheuristic techniques employed to optimize refrigeration systems are described. Based on the research scope observed, the objectives of the current work are provided.

Chapter 3 covers the thermoeconomic optimization study of the VARS and modified VARS (MVARS). The performance of the different metaheuristic techniques on these systems is discussed here.

Chapter 4 includes the thermoeconomic optimization analysis of the CRS with different absorbent-refrigerant combinations using various metaheuristic algorithms. The impacts of the decision variables on the various parameters of the system are also addressed.

Chapter 5 outlines a comparative thermoeconomic optimization study of CRS and subcooled CRS (SCRS) with different absorbent-refrigerant combinations to find an efficient system based on energy, exergy, economic, and environmental analyses.

Chapter 6 discusses the thermoeconomic optimization analysis of vapor recompression absorption refrigeration system (VRARS) with different absorbent-refrigerant combinations and two cases based on different sets of decision variables.

Chapter 7 covers the significant conclusions from the thermoeconomic optimization study of the different cascaded refrigeration systems considering various absorbent-refrigerant combinations. Further, the future scope of the current study is addressed in detail.

1.9. Closure

The present chapter focuses on the rising energy consumption and demand of the HVAC sector due to various issues such as growing urbanization, climate change, and many others. The conventional refrigeration systems that can be employed in the cooling section of the

TH-3395_176107002

HVAC are discussed briefly, along with their advantages and drawbacks. A general overview of single and multi-objective optimization and the role of optimization for refrigeration systems is explained here. The next chapter (Chapter 2) covers state-of-art related to various analyses and optimization of refrigeration systems.

भारतीय प्रौद्योगिकी संस्थान गुवाहाटी • Indian Institute of Technology Guwahati •

TH-3395_176107002

CHAPTER 2

State of the art

2.1. Introduction

The first artificial refrigeration technique was presented by a Scottish physician and professor William Cullen in 1756. In 1834, Jacob Perkins put forward the vapor compression refrigeration system, while John Gorrie, an American physician, designed the first refrigeration system to produce ice [34]. The first gas absorption refrigeration system using NH_3 dissolved in water was put forward by Ferdinand Carre in 1859; however, this system was only used for manufacturing ice in industries. Using halogen compound refrigerants, compression systems were developed for home applications, operated with high-grade energy, but it was observed that these refrigerants have adverse effects on the environment. With the rising concern over global warming, the demand for refrigeration systems is growing rapidly; hence, it has become imperative to enhance the efficiency of refrigeration systems and reduce the harmful impact on enviornment. Therefore, a comprehensive literature survey on the vapor compression, absorption, and cascaded refrigeration systems with various refrigerants and absorption-refrigerant as working pairs has been thoroughly reviewed based on energy, exergy, economic analysis, and optimization. This chapter provides a quick summary of many key study findings. The key objectives are set at the end of this chapter based on the research gaps identified. Fig. 2.1 depicts the flow chart for the current chapter.

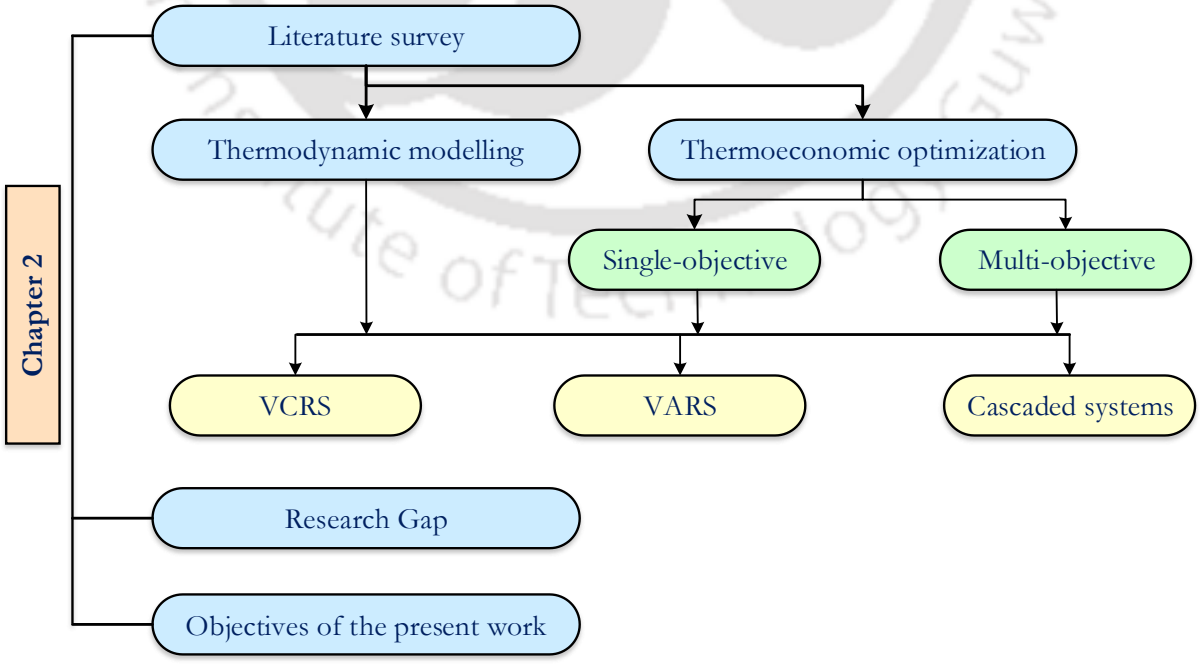

Fig. 2. 1 Flowchart for the state-of-the-art chapter

TH-3395_176107002

2.2. State of art on vapor compression refrigeration system

2.2.1. Working fluids in VCRS

Chlorofluorocarbons (CFCs) have been widely used in refrigeration applications since the 1930s due to their outstanding thermodynamic properties, such as low freezing point, non-flammability, and chemically inert behavior with other metals. CFC-11/R-11, CFC-12/R-12, CFC-13/R-13, CFC-113/R-113, CFC-114/R-114, and CFC-115/R-115 are some of the examples of common CFC refrigerants. A mixture including a CFC and any other chemical is also classified as a CFC refrigerant. In particular, CFCs were frequently used in home refrigerators and small refrigeration systems, with R-12/Freon-12 (Dichlorodifluoromethane) being the refrigerant of preference, while R-11 (Trichlorofluoromethane) was utilized for blowing polyurethane foam for insulating refrigerators [35]. To measure the impact of refrigerants on the environment, generally, two parameters are considered: ozone depletion potential (ODP) and global warming potential (GWP). ODP is a numerical depiction of the stratospheric ozone depletion induced due to the substance molecules emitted in the atmosphere and computed by comparing the ozone depletion potential of the refrigerant/chemical to an equal mass of R-11; hence, ODP of R-11 has been assigned as 1.0. Most CFCs have ODPs of 1.0 [36], whereas GWP indicates the capacity of chemical/refrigerant to trap heat in the atmosphere over a specific period. It is measured relative to the CO_2, thus assigning the GWP of CO_2 as 1, considered for 100 years. R-12 and R-11 have GWP of 8500 and 5000, respectively, which is quite a large number [36].

Higher ODP and GWP signify greater potential to deplete the ozone layer and heat-trapping capacity of the substance. CFCs are combinations of halogens, and the chlorine released from the CFC destroys the ozone layer, seriously impacting human health and the environment. Therefore, several international agreements have been developed to stop the utilization of chemicals with high ODP, beginning with the Vienna Convention on the Protection of the Ozone Layer in 1985, the Montreal Protocol for substances that deplete the Ozone Layer in 1987 in the industrial sector and the London Amendments of 1990 to eradicate the CFC consumption [37]. Higher ODP chemicals containing chlorine and bromine, which are used as refrigerants, solvents, and foam-blowing agents, have been phased out of production and use as a result of the Montreal Protocol and its subsequent amendments.

To reduce CFC usage, another kind of refrigerant is hydrochlorofluorocarbons (HCFCs), a combination of the elements hydrogen, chlorine, fluorine, and carbon was proposed as an alternative since they have lower GWP compared to CFCs [38]–[41]. HCFC-22/R-22, HCFC-

TH-3395_176107002

123/R-123, HCFC-124/R-124, and HCFC-142b/R-142b are some of the typical HCFC refrigerants. Jung et al. [42] reported that HCFC123 and HFC134a were the better alternatives for CFC-11 and CFC-12, respectively. A parametric study was done by Arora et al. [43] based on coefficient of performance (COP), exergy destruction, and exergy efficiency for refrigerants R-22, R407C, and R410A. The results indicated that the COP and exergy efficiency for R-22 were higher than R-407C and R-410A. HCFCs can nevertheless be regarded as dangerous despite having a lower ODP and lower chlorine atoms than CFCs. HCFCs are likewise being monitored and abolished from the refrigeration industry, along with CFCs. The GWPs of both CFCs and HFCs lie in the higher range than hydrofluorocarbons (HFCs) leading to the global warming problem. Many countries, including India, Brazil, USA, have agreed to completely phase out HCFC refrigerants by 2030 due to the Montreal Protocol [44]–[46]. Therefore, the adoption of HFCs and natural refrigerants as a replacement for CFCs and HCFCs has been increased as they have zero ODP due to the absence of chlorine [47]–[49].

HFC refrigerants contain hydrogen, fluorine, and carbon elements. Some of the common HFC refrigerants are R-32, R-125, R-134a, R-143a, R413a, and R-152a. Spauschus [50] reported the knowledge gaps for R134a implementation as an alternative for R12 by reviewing some of the properties, such as stability, solubility, and lubricity of R134a and also discussed the compressor and refrigeration system requirements. Padilla et al. [51] tested R413a as a direct replacement for R-12 and concluded that the system operating with R413a performed better in terms of overall energy and exergy efficiency than R-12. Kilicarslan and Hosoz [52] analyzed the energy and exergy of the cascaded VCRS with various refrigerant couples such as R152a–R23, R290–R23, R507–R23, R234a–R23, R717–R23 and R404a–R23. Amid all cases, the highest COP and lowest irreversibility were obtained for the refrigerant couple R717–R23, whereas R507–R23 showed the lowest COP and highest irreversibility. Though the HFC shows good performance when operated in the refrigeration system, HFCs are much more potent greenhouse gases with higher GWP than CO_2 such as the GWP of R-125 is 3500, R-134a is 1430, R-143a is 4470 [53]. The adoption of the 2016 Kigali Amendment to the Montreal Protocol will phase down the production and consumption of some HFCs and avoid much of the projected global increase and associated climate change. Also, these refrigerants (CFCs, HCFCs & HFCs) can be leaked anywhere from manufacturing air conditioning equipment to installing and disposing of old units aiding in to rise of the global warming issue. Therefore, refrigeration systems with low ODP and GWP refrigerants are preferred over CFCs, HCFCs & HFCs.

TH-3395_176107002

Pure hydrocarbon (HCs) refrigerants have zero ODP and negligible GWP, such as CO_2 has a GWP of 1, R290 (Propane) of 0.02, R600 (butane) of 0.006, and R717(NH_3) of 0 [54], [55]. Kabul et al. [56] with R600a (isobutane), and it was concluded that R600a could be used as a replacement refrigerant in domestic refrigerators working with HCFCs and HFCs. Bayrakc and Ozgur [57] compared the energy and exergy performance of VCRS using pure HCs such as R290, R600, R600a and R1270 (isopentane) as refrigerants with R22 and R134a. Based on the energy and exergy efficiency, the best replacement refrigerant for R22 and R134a was R1270. Higher energy and exergy efficiencies were obtained for R1270 and R600 than for R290 and R600a. Rasti et al. [58] tested R436A (mixture of 46% R600a and 54% R290) and R600a as an alternative refrigerant to R134a for the energy efficiency improvement of the domestic refrigerator. R436a and R600 determined reduced energy consumption than R134a. A comparative energy and exergy analysis of transcritical R744, R404a, and R290 in VCRS was done by Shilliday et al. [59]. For the single stage, R404 and R290 exhibited higher COPs when compared with R744. R744 showed the highest total cycle exergy ratio. Yu and Teng [60] used different proportions R290 and R600 to replace R134a and observed that all of the HC refrigerant combinations produced results that were better than R134a in terms of energy factors (EFs), on-time ratios, and power usage. Fig. 2.2 illustrates a summary of the history of refrigerants and the corresponding amendments.

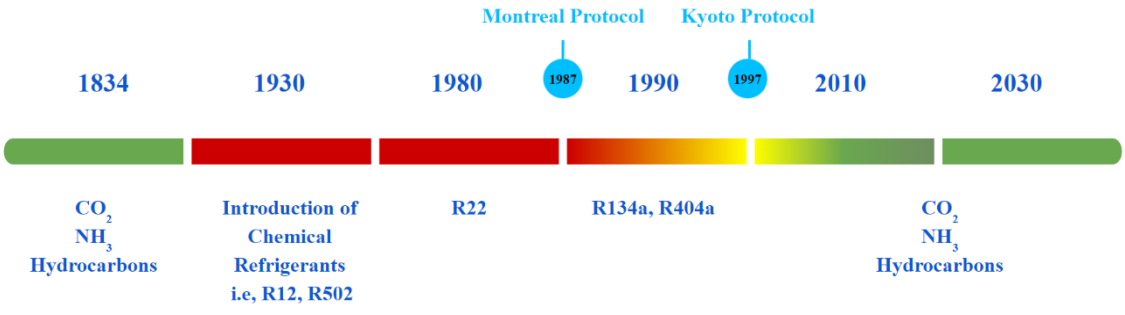

Fig. 2. 2 History of refrigerant and amendments since 1834 [61]

Hydroflouro-olefins (HFO) are also one of the type of refrigerants that also has zero ODP and negligible GWP compared to CFCs, HCFCs, and HFCs. They are composed of hydrogen, fluorine, and carbon atoms but contain at least one double bond between the carbon atoms. The frequently utilized HFO refrigerants are R1234yf and R1234ze, which have zero ODP and GWP of 4 and 7, respectively. Yataganbaba et al. [62] studied the exergy analysis of a two-evaporator VCRS with R1234yf, R1234ze, and R134a as refrigerants and reported that R1234yf and R1234ze could be utilized as a better alternative to R134a. Jemaa et al. [63] investigated the energy and exergy analysis of the R1234ze as a replacement for R134a in

TH-3395_176107002

VCRS with an internal heat exchanger. It was observed that exergy destruction obtained for R1234ze was lower than for R134a. Energy and exergy analysis of a cascaded VCRS with low GWP refrigerants such as R23, R41, and R170 in the low-temperature cycle (LTC) while R32, R1234yf, R1234ze, R161, R1270, R290 and R717 in the high-temperature cycle (HTC) was done by Sun et al.[64]. R41/R161 and R170/R161 were recommended for use in cascaded VCRS, R161 was recommended for use in HTC, and R41 and R170 were recommended for use in LTC. Fig. 2.3. shows the development in the utilization of the refrigerant.

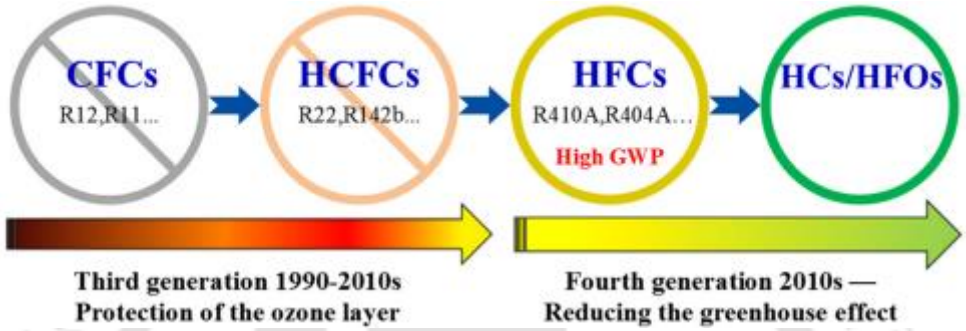

Fig. 2. 3 Development of refrigerant usage since the 1990s [65]

2.2.2. Performance augmentation in VCRS

Adding a subcooler to the refrigeration system lowers the temperature of the refrigerant below its saturation point (condensing temperature) before it enters the expansion valve. This helps to increase the efficiency and capacity of the system by allowing the refrigerant to absorb more heat from the evaporator. Llopis et al. [66] theoretically analyzed the possibilities of the energy performance of CO_2 transcritical refrigeration systems using a dedicated mechanical subcooling cycle. The mechanical subcooling (MS) cycle was used to subcool the refrigerant of a main cycle at the exit of the condenser through their thermal coupling in the subcooler. Adding such MS improved the COP by 20% and the cooling capacity by 28.8% more than conventional VCRS. Yang and Yeh [67] performed a study to determine the optimal degrees of subcooling for the initial cost saving and minimal total exergy destruction of the VCRS due to the addition of a subcooler using two approaches. The optimal degrees of subcooling for a VCRS were between 2 °C and 6 °C for initial cost saving and from 4 °C to 7 °C for the minimal total exergy destruction for R134a, R22, R410A, and R717.

Chen et al. [68] compared modified VCRS (MVRC) and traditional VCRS (TVRC) results based on the energy and exergy analysis with R290/R600 zeotropic mixture as a working fluid. An internal subcooler with an additional bypass tube was added to MVRC. Under the same operating conditions, COP, volumetric cooling capacity, and exergy efficiency of MVRC were enhanced by up to an average of 8.9%, 12.4%, and 10.4% over TVRC. Li et al. [69] proposed

TH-3395_176107002

a detailed study of the thermodynamic relationship between subcooling power and the rise of the cooling capacity of VCRS based on the parameter RICOSP (the ratio of the rise in the cooling output to the subcooling power). The impact of the compressor speed, inlet temperature, and flow rates of cooling water and chilled water on RICOSP was studied. RICOSP was increased by 17.4% and 8% when the speed of the compressor and flow rate of cooling water were reduced by 80%, respectively. Mogaji et al. [70] conducted experiments by employing a dedicated mechanical subcooler in a VCRS and noticed that the COP of a traditional VCRS was improved by 18% to 33.5% for an evaporator range of -10 °C to 35 °C after the addition of a subcooler. Roy et al. [71] combined a dedicated subcooler with VCRS for high-temperature lift between the evaporator and condenser. R134a was used in the VCRS, while low GWP refrigerants (R152a, R1234ze, and R290) were used in the subcooler cycle. The proposed system reported a ~27% improvement in energy and exergy efficiency, while cost was reduced by ~2% compared to a conventional VCRS with R152a in the subcooler cycle.

To attain a low temperature, such as -40 °C to -50 °C for food storage, VCRS requires a larger compression ratio and a greater temperature differential, leading to low volumetric efficiency and lower COP of the system [72]. Bhattacharyya et al. [73] optimized the cascaded VCRS for simultaneous refrigeration and heating applications with working pair C_3H_8 in low-temperature and CO_2 in high-temperature cycles to determine the maximum COP. Lee et al. [74] conducted a thermodynamic analysis of a two-stage cascaded VCRS with CO_2 and NH_3 as refrigerants to determine the optimal condensing temperature of the cascade condenser. The study aimed to maximize COP and minimize the exergy destruction of the system considering various design parameters. Da Silva et al. [75] carried out a comparative study of the CO_2 cascade system and the direct expansion conventional system using R404A and R22 based on energy efficiency and cost analysis. Due to various advantages of CO_2 over R404A and R22, such as reduction in electric energy, low compression ratio, reduction of CO_2 refrigerant charge, low GWP, higher enthalpy, higher degree of liquid subcooling and cooling capacity, and many others, it was concluded that new installations of refrigeration systems with CO_2 refrigerant can be done. Sun et al. [76] presented a comparative analysis of cascaded VCRS for refrigerant pairs refrigerant couples R41/R404A and R23/R404 based on the thermodynamic performance. Under the same operation condition, it was reported that the input power of R41/R404A was less and COP was higher than that of R23/R404A. The theoretical analysis indicated that R41/R404A was a more potential refrigerant couple than R23/R404A. Faruque et al. [77] studied the thermodynamic performance of the two staged

TH-3395_176107002

VCRS using HC as refrigerants. Trans-2-butane (T2BUTENE) was used in the lower temperature circuit (LTC) and Toluene (toluene), Cyclopentane (CYCLOPEN), and Cis-2-butane (C2BUTENE) were used in high-temperature circuit (HTC). It was reported that using HC refrigerants on cascade refrigeration systems determined a minimum 7.21 % higher COP than the recently employed refrigerants in previously established works.

2.3. State of art for vapor absorption refrigeration system

2.3.1. Working fluids in VARS

For VARS, the working fluid is a combination of two substances: a refrigerant and an absorbent. A refrigerant is typically a volatile liquid that evaporates at a low temperature and pressure to provide cooling, whereas as absorbent is a liquid or solid material that absorbs the refrigerant vapor. Generally, NH_3-H_2O [78]–[83] and H_2O-LiBr [84]–[89] are used as refrigerant-absorbent pairs in the VARS. NH_3 is used as a refrigerant for large industries where low temperature is required for process cooling; however, NH_3-H_2O have difficulty in separation leading to the addition of an extra distillation column in the system due to the small boiling point difference between NH_3 and H_2O and also NH_3 is toxic. LiBr- H_2O crystallizes and corrodes metals, necessitating thicker metallic components that would be in contact with LiBr- H_2O. Researchers have been focusing their studies on the new absorbent-refrigerant pairs to overcome these drawbacks. Arivazhagan et al. [90] studied the half-effect VARS with R134a-DMAC (N, N dimethylacetamide) as a refrigerant-absorbent pair for the cold storage application. It was reported that R134a-DMAC showed better results regarding COP and exergy efficiency than NH_3-H_2O for low heat source temperatures. However, there was a limitation in using this pair. Due to the smaller boiling point difference (191 °C) between R134a and DMAC, some amount of absorbent can boil along with the refrigerant, which may reduce the cooling capacity and damage the evaporator. Hence, Roy and Maiya [91] proposed two add-on components, i.e., rectifier and liquid vapor heat exchanger (LVHX), to avoid the boiling point difference issue in the half-effect VARS with R134a-DMAC and observed that the system performed better when the efficiencies of the rectifier and LVHX were high.

Farshi et al. [92] put forward a detailed study based on the first and second law of thermodynamics using ammonia lithium nitrate (NH_3/$LiNO_3$) and ammonia sodium thiocyanate (NH_3/NaSCN) as working fluids. They reported that for low generator temperatures, NH_3/LiNO3 cycles performed better, while for high generator temperatures, NH_3/NaSCN cycles showed superior performance in terms of COP and exergy efficiency. Patel et al. [93] compared the exergy analysis of VARS with LiCl-H_2O and LiBr-H_2O as an

TH-3395_176107002

absorber-refrigeration pairs and concluded that LiCl-H_2O performance was better than the LiBr-H_2O absorption system. Li et al. [94] studied VARS with a mixture of $CaCl_2$, LiBr, and $LiNO_3$ in the ratio (8.72:1:1) with H_2O as a refrigerant. Higher COP was observed than in the conventional LiBr- H_2O system. Farshi and Asadi [95] compared the performance of single and double-effect VARS using NH_3/$LiNO_3$ and NH_3/NaSCN as refrigerant-absorbent pairs. For double-effect VARS, the COP determined was enhanced by 60%, while exergy efficiency was reduced by 16% than single-effect VARS. Zhang et al. [96] proposed a novel absorption refrigeration, heating, and Organic Rankine Cycle (ORC) power system operated on a low-grade heat system with NaOH-H_2O as a working fluid. The proposed system was observed to be better than the independent electrical refrigeration, heating, and power system.

An ionic liquid is a green solvent obtained in a liquid state, which is non-volatile, thermally stable, non-flammable, and environmentally benign. These liquids have negligible vapor pressure, which leads to easier separation of absorbent and refrigerant fluids [97]. Martín and Bermejo [97] investigated thermodynamic analysis of VARS using ionic liquid as absorbent and supercritical CO_2 as a refrigerant. However, the COP of this cycle was less than the NH_3-H_2O system due to the necessity of operating with a higher solution flow rate. A thermodynamic evaluation of VARS with imidazolium-based ionic liquids as absorbent was done by Kim et al. [98]. The maximum COP was reported for H_2O-[emim][BF4] (1-ethyl-3-methylimidazolium tetrafluoroborate) pair. Takalkar et al. [99] employed a novel ionic liquid 1 Ethyl-3-methylimidazolium ethyl sulphate (EMISE) as absorbent and H_2O as a green refrigerant for single effect VARS and it was noted that the COP obtained for the proposed pair was slightly higher than NH_3-H_2O but lower than LiBr-H_2O under same operating condition.

Asensio-Delgado et al. [100] proposed a thermodynamic model and analysis of the compressor-integrated absorption refrigeration system with 16 pairs of HFC and HFO refrigerants with low GWP and low viscosity ionic liquids. HFCs performed superior to HFOs because of their higher solubility in ionic liquids. The combination R32/[C2mim][Tf2N] determined better COP and exergy efficiency than others. Chen et al. [101] used a hydrophilic dual amino-functionalized ionic liquid 3-aminopropyl tributyl phosphonium glycinate ([aP4443][Gly]) as absorbent and H_2O as a refrigerant in the single effect VARS. Based on the results, it was observed that COP obtained for this pair was higher than NH_3-H_2O and slightly lower than LiBr-H_2O under the same operating conditions. Qian et al. [102] conducted a thermal analysis of novel single-effect VARS combined with compressors between absorber-evaporator and generator-condenser. Ionic liquids, i.e., 1-butyl-3-methylimidazolium dibutylphosphate [BMIM][DBP], 1-methyl-3-methylimidazolium dimethylphosphate

TH-3395_176107002

[MMIM][DMP],1-ethyl-3-methylimidazolium dimethylphosphate [EMIM] [DMP], and 1-ethyl-3-methylimidazolium acetate [EMIM][AC] were absorbents and H_2O was used as refrigerant. The proposed system showed better performance than the traditional VARS. Based on COP, [EMIM] [DMP] was selected as the best absorbent.

2.3.2. VARS driven by renewable energy sources

One of the advantages of VARS over VCRS is that it can be operated on low-grade heat systems such as waste heat by exhaust gas, solar energy, geothermal energy, and many others. Kalinowski et al. [103] used a single-effect absorption refrigeration system with NH_3-H_2O. The system was operated using high-temperature exhaust gas from the gas turbine producing electric power. This combination contributed to the saving of 1.9 MW of electricity usage. Salmi et al. [104] utilized the waste heat of ships as an energy resource for operating VARS with H_2O-LiBr and NH_3-H_2O as working pairs. Estimated energy savings were 47 and 95 tons of fuel every year for ISO and tropical conditions, respectively. An experimental study of VARS driven by automotive exhaust gas heat with NH_3-H_2O as a working fluid was put forward by Rêgo et al. [105]. The exhaust system of an automotive internal combustion engine was connected to the VARS generator. It was reported that by monitoring exhaust gas flow, VARS was able to operate within a wide range of engine speeds. Stalin et al. [106] discussed the theoretical design of VARS operated using solar energy and waste heat produced in a plant for heat generation with phase-changing materials for storage.

Cao et al. [107] used waste heat to operate VARS for shipboard application and compared the obtained results with VCRS. Fuel combustion and CO_2 emission of this system were lowered by 62% than the VCRS under specified conditions. Ebrahimi et al. [108] reported a thermoeconomic study and exergy balance of VARS operated by waste heat from data centers, while Lu et al. [109] studied VARS driven by industry waste heat using technoeconomic analysis. Chaboki et al. [110] testified the use of exhaust gases (High-pressure steam) of auxiliary engines to run the VARS in a ship with LiBr-H_2O as an absorbent-refrigerant pair. The proposed system had 31% lower total irreversibility than the conventional VCRS. Zhou et al. [111] experimentally investigated exhaust gas-operated (150°C-350°C) VARS with NH_3-NaSCN. The proposed system showed satisfactory performance under wide operating conditions, indicating that the system is appropriate for both air-conditioning and freezing applications.

VARS uses almost zero global warming potential and ozone depletion potential refrigerants and it is the most viable cogeneration option to recover waste heat from existing industrial

TH-3395_176107002

processes to produce the cooling effect. However, VARS is costlier and less effective than VCRS. Therefore, VARS must be improved in design and operation to be on par with VCRS. Several modifications were proposed in the basic design and operation of VARS to improve its drawbacks against VCRS. In the recent past, improvements in the VARS were suggested through the influence of operating and control parameters, the number of stages involved and modifications in the components of the VARS. Gebreslassie et al. [112] studied exergy analysis of the half-effect to triple-effect VARS. They concluded that COP and exergy efficiency were enhanced significantly from half to triple effect. Kaynakli et al. [113] reported the double effect series flow VARS performance with LiBr-H_2O as a working fluid based on energy and exergy analysis, parametric and comparative study considering exergy destruction and mass flow rate of heat sources. The proposed system was operated on low-grade energy sources such as hot water, hot air, and steam via a high-pressure generator. It was observed that exergy destruction was maximized when hot air was used as a heat source and minimized with utilization of the hot water. Abed et al.[114] presented a detailed study on various options in the subcomponents, internal energy recovery, and the working fluids of single-stage VARS to improve its performance.

Kholghi et al. [115] compared a branched generator-absorber heat exchanger (branched GAX) and the GAX cycle, revealing that the branched GAX cycle was more advantageous over GAX based on the COP and the exergy efficiency. It was reported that a 14% improvement in COP and a 10.6% decrease in exergy destruction was observed for branched GAX than those for the GAX cycle. Bagheri et al. [116] performed a comprehensive advanced exergy analysis of the parallel flow double-effect VARS to improve system knowledge and decide the priority of the various system components for the overall performance improvement of VARS. A novel hybrid dual evaporator absorption refrigeration system with NH_3-H_2O as a working pair was put forward by Mohammadi et al. [117]. In the proposed system, two compressors were employed between the evaporators and absorbers to raise the absorber pressure to a higher level. Based on energy, exergy, and economic analysis, it was noted that only employing a compressor between the higher temperature evaporator and absorber was beneficial in improving the COP significantly than the without compressor system.

2.4. State of art on cascaded refrigeration systems

Although VARS can be operated on low-grade heat systems and utilizes refrigerant with very low GWP and ODP, it has the drawback of lower thermal efficiency than VCRS, while VCRS operates on high-grade energy sources such as electricity. VCRS requires larger power

TH-3395_176107002

compared to VARS, which leads to higher electricity consumption [118], obtained from burning fossil fuels that emit a significant amount of CO_2 in the atmosphere [119] and uses refrigerants with high ODP and GWP, contributing to global warming issues. The cascaded refrigeration system (CRS), i.e., integration of VARS and VCRS, reduces the compressor work by a considerable amount than conventional VCRS due to the reduction in condenser temperature, and also it can be operated at a lower evaporator temperature than VARS. This CRS was coupled with a heat exchanger that serves as a condenser in the VCRS and an evaporator in the VARS.

Garimella et al.[120] coupled a subcritical CO_2 VCRS with LiBr-H_2O operated VARS, driven by turbine exhaust stream waste, and reported that electricity consumption was lowered by 31% compared to VCRS. Wang et al.[121] analyzed CRS with LiBr-H_2O and R134a using solar energy. The COP of CRS was observed to be 6.1, and there was a 50% reduction in power consumption compared to VCRS. Anand et al. [122] put forward a comparative study of VARS, VCRS, and cascaded VARS & VCRS (CRS) based on the energy and exergy analysis. It was reported that compressor work and exergy loss for CRS was lower than conventional VCRS and the obtained COP of the CRS was better than VARS. Mohammadi and Ameri [123] studied different configurations (depending on the cooling system of the chiller, i.e., air-cooled or water-cooled) of the CRS to determine the best configuration based on energy and exergy approaches. The CRS was operated using a micro-turbine. It was observed that a system with water-cooled chillers determined the highest second-law efficiency and water consumption among all configurations. Most researchers have reported that implementation of the CRS aided in reducing electricity consumption compared to conventional VCRS and also improved the energy and exergy efficiency of the system, as shown in Table 2.1.

2.4.1. Performance augmentation in CRS (VCRS + VARS)

Xu et al. [143] studied the energy performance of the absorption-compression refrigeration system with both evaporator-condenser (EC) and evaporator-subcooler (ES) systems in detail. It was noted that the ES system showed good performance at the higher evaporator and lower generator temperatures, while the EC system saved more energy than the ES system at the lower evaporator and higher generator temperatures. Wang et al. [144] proposed a novel absorption system that can recover all condensation heat. This was done by improving the grade of condensation heat through the inclusion of vapor compressors, intercoolers, and subcooler in place of condenser in the VARS. NH_3-H_2O was the working fluid. In this system, the heat

TH-3395_176107002

Table 2. 1 Literature on cascade refrigeration systems (VCRS+VARS)

Author(s)	Working fluids		Highlights
	Compression	Absorption	
Kairouani and Nehdi [124]	R717, R22, R134a	NH_3-H_2O	The proposed CRS was driven by geothermal energy. COP was increased by 37-54% in CRS compared to a single compression and absorption refrigeration system under the same operating condition.
Sun and Guo [125]	R22	LiBr-H_2O	The reported CRS saved more than 25% of primary energy compared to a conventional electrically driven VCRS.
Seyfouri and Ameri [126]	R22	LiBr–H_2O	Four configurations of a system that consists of a compression and an absorption chiller powered by a micro-turbine were studied. The configuration with an intercooler and subcooler. (Configuration 4) was observed to be most efficient in terms of energy saving, while for Configuration 1, COP was improved by 440% than the base case for the compression section. Here, the base case included only the compression section and micro-turbine.
Cimsit and Ozturk [127]	R134a, R-410A, NH_3	LiBr-H_2O, NH_3-H_2O	The electrical energy consumption was reduced by 48-51% in the CRS than conventional VCRS for the same refrigerants. For the absorption section of CRS, COP determined by LiBr-H_2O was improved by 33% than NH_3-H_2O under the same operating conditions.
Colorado and Velázquez [128]	R134a, CO_2, NH_3	LiBr-H_2O	It was reported that R134a/LiBr-H_2O showed higher COP in CRS, while higher irreversibilities in the cascade heat exchanger were observed for CO_2 and NH_3.
Jain et al. [129]	R410A, R407C, R134A, R22	LiBr-H_2O	Compared to conventional VCRS, a 155% improvement in the COP of the compression section was observed, and electricity consumption was reduced by 61% in CRS under specified operating conditions.

TH-3395_176107002

Cimsit et al.[130]	NH_3, R134a, R410A	LiBr-H_2O, NH_3-H_2O	For LiBr-H_2O in the absorption section of CRS, the COP was improved by 27%, while the total exergy destruction rate was reduced by 20% than NH_3-H_2O. NH_3/LiBr-H_2O pair showed substantially better thermodynamic performance than CO_2/LiBr-H_2O when employed in the CRS.
Colorado and Rivera [131]	CO_2, R134a	LiBr-H_2O	A comparative study was done on the compression-absorption single-stage (CASS) and compression-absorption double-stage (CADS) systems. The electrical energy consumption in the refrigeration cycles was about 45% lower than in conventional VCRS under the same operating conditions. COP obtained in the CADS was 50% higher than in CASS. Systems operated with R134a gave higher COP than the system operated with CO_2 for both CASS and CADS.
Jain et al. [132]	CO_2	NH_3-H_2O	For the proposed CRS, primary energy consumption was reduced by 60.6%, and electrical COP was improved by 153.6% compared to conventional two-stage VCRS under specified operating conditions.
Dixit et al. [133]	CO_2, NH_3, R134a	LiBr-H_2O	For the reported CRS, R134a-LiBr/H_2O showed better performance based on the first and second laws of thermodynamics than other pairs. For NH_3-LiBr/H_2O, the cascade condenser showed the highest irreversibilities. For the CO_2-LiBr/H_2O system, it was the refrigerant throttle valve of VCRS, and in the case of the R134a-LiBr/H_2O system, it was the compressor.
Chen et al. [134]	NH_3	NH_3-H_2O	An absorption/absorption–compression refrigeration system was studied to recover more energy from a variable-temperature heat source. The exergy efficiency of the proposed system was as high as 25.94%. The cooling energy output of the proposed system was increased by 28.21% compared to the conventional VARS.

TH-3395_176107002

Patel et al. [135]	NH_3	LiBr-H_2O	A system that combines two-stage VCRS integrated with a single-stage VARS was put forward. This system reduced compressor work by 28% compared two-stage VCRS.
Salhi et al. [136]	R1234yf, R1234ze (E), R1233zd (E)	LiBr-H_2O, LiCl-H_2O	The proposed CRS was driven by geothermal energy. The electricity consumption was reduced by 51.36–54.16% compared to conventional VCRS. Enhanced performance was noted for LiBr-H_2O-R1234yf among all pairs.
Lijuan et al. [137]	R22	LiBr-H_2O	An evaporative subcooler was introduced to improve the performance of CRS. COP was observed to be 2.56 times higher than the traditional VARS.
He et al. [138]	R134a	LiBr-H_2O	A cascade system solar-driven absorption cycle coupled with an air-cooled electricity-powered parallel-type dual-source VCRS was reported. Compared with the conventional VCRS, the COP of the proposed cycle was higher by 133.33%, power consumption was reduced by 20.80%, and the energy-saving rate was 26.70 % for the whole system on a typical day.
Chen et al. [139]	R134a	[bmim]Zn2Cl5/NH_3 & NH_3/H_2O (steam power)	A combination of steam power, VCRS, and the compression-absorption refrigeration system was studied here. Using the mid-temperature heat source, the heat-driven turbine assisted the system at low temperatures. The proposed system reported better thermal performance than the two-stage absorption system and conventional CRS.
Jianbo et al. [140]	HFC or HCFC (such as R134a, R124, R125, R152a, and R32)	Organic working fluids (such as DMAC, NMP, and DMF)	A novel system was proposed, which was the combination of the absorption-compression cascade refrigeration driven by waste heat and a VCRS. Theoretical calculation results show that the proposed combined cycle had a higher performance coefficient compared to conventional VCRS.
Agarwal et al. [141]	R1234yf	LiBr-H_2O	An integration of VCRS with a triple-effect VARS driven by waste heat by a gas turbine or steam turbine was reported. This system reduces electricity consumption by 45.84% compared to the conventional VCRS. The COP and exergy

TH-3395_176107002

			efficiency of the compression section in the cascade system were improved by 85.26% and 85.28%, respectively, than conventional VCRS.
Jain and Colorado [142]	Transcritical CO_2	LiBr-H_2O	A comparative study of transcritical VCRS (TVCRS) and a novel structure of transcritical vapor compression-absorption integrated refrigeration system (TVCAIRS) was conducted. COP and exergy efficiency of the proposed system were 28.6% and 26.9 %, respectively, higher than the TVCRS. The total annualized cost of TVCAIRS was 17.8% less than the equivalent TVCRS at the base case.

TH-3395_176107002

rejected by the condenser was used for the generator using a compressor, which reduced the input energy by 70%-80% than traditional VARS. Xu et al.[145] investigated two refrigeration systems, i.e., VARS and VCRS, integrated using evaporator-condenser (EC) and evaporator-subcooler (ES) heat exchanger. It was reported that EC saved 22.5% more electric energy than ES by consuming 4.6 times more low-grade heat energy than ES at the optimized condition. The exergy efficiencies obtained for EC and ES were 20.5% and 31.6%, respectively, indicating that ES showed lower exergy destruction than EC.

Jing et al. [146] studied the exergoeconomics of solar absorption-subcooled compression hybrid cooling system (SASCHCS) used in low-rise buildings to determine the cost-effective configuration of SASCHCS. It was concluded that the minimum product flow rate should be used to determine the optimal size of the VARS subsystem, and the collector area should be utilized to obtain the optimal cooling capacity of the VARS. Jain et al. [147] reported a comparative study of vapor compression-absorption integrated refrigeration system (VCAIRS) and vapor compression-absorption cascaded refrigeration system (VCACRS) based on energy and exergy efficiencies. The electrical energy requirement for VCAIRS was higher by 21.4% as compared to VCACRS; however, it was 63% less than equivalent VCRS. The exergy efficiencies obtained by VCAIRS, VCACRS, and equivalent VCRS were 27.9%, 32.7%, and 18.8 %, respectively.

Ye et al. [148] performed an energy analysis of a solar-assisted VARS integrated with a subcooled VCRS using an evaporator-subcooler heat exchanger and observed that the compressor work was reduced substantially while the overall COP of the system was improved. Liu et al. [149] reported a comparative study of VARS integrated with compressor. Based on the position of the compressor, two systems were studied, i.e., system 1 included a compressor between absorber and evaporator while system 2 had a compressor between generator and condenser. R1234yf/[HMIM][TfO], R1234yf/[HMIM][PF6], R1234yf/[HMIM][BF4] were employed as working fluids. It was observed that the COP of system 1 and system 2 were 4 and 1.5 times the conventional VARS at the same conditions. Carvalho and Barbieri [150] carried out a comparative study of a cascaded compression system (VCCRS) and a cascaded compression/absorption system (VCACRS) based on thermoeconomic performances. It was concluded that VCCRS showed better exergy efficiency with 38.46% reduced exergy destruction than VCACRS, while VCACRS showed a 10.26% lower value of total annual cost than VCCRS.

Chen et al. [151] conducted a performance comparison between cascade mode and subcooling mode air-cooled solar-assisted absorption-compression hybrid systems. $COP_{electric}$

TH-3395_176107002

of the cascade and subcooling mode increased by 63.9% ~ 166.7% and 15.9% ~ 29.8%, respectively, compared to the vapor compression subsystem. Herrera-Romero and Colorado-Garrido [152] presented a compression–absorption cascade refrigeration system with the inclusion of three more heat exchangers, i.e., a solution refrigerant heat exchanger (SRHE): placed between the generator & condenser, a refrigerant heat exchanger (RHE): placed between condenser and cascade heat exchanger and internal heat exchanger (IHE): in between evaporator and compressor. NH_3-$LiNO_3$, NH_3-NaSCN, and NH_3-H_2O in the VARS and R134a in the VCRS were used as working fluids. Almost 50% of the compressor work was reduced in the present system with NH_3-NaSCN and R134a as working fluids, compared to a conventional VCRS.

Despite all these advantages, cascaded refrigeration systems are more expensive and more complicated to build when compared to a single refrigeration system. Riffat and Wong [153] introduced a gas-driven absorption-compression model that will be driven by waste heat by the engine. The bulky condenser in the VARS was eliminated, and a compacted generator-condenser and compressor were introduced. It was concluded that the COP was observed to be better than VARS. LiBr-H_2O and CH_3OH/LiBr–$ZnBr_2$ were the working fluids in this study. This configuration utilizes the heat rejected by the refrigerant to separate the refrigerant from the absorbent solution in the generator instead of using an additional external heat source. An experimental study of a compression/absorption hybrid heat pump operated on waste heat was done by Kim et al. [154] using NH_3-H_2O as a working fluid. This research aimed to examine the impact of refrigerant mixture composition on the operational parameters of a hybrid heat pump. Razmi et al. [155] proposed a novel system modelled using an absorption/recompression refrigeration system, compressed air energy storage, and wind turbines. The analysis of the proposed system was done based on a thermodynamic and economic approach. It was shown that the proposed system obtained a total COP of 2.431 and an exergy efficiency of 17.05%. Razmi et al. [156] conducted an energy and exergy analysis of the hybrid combination of absorption and recompression refrigeration systems. A compressor was introduced between the generator and the condenser coil. The maximum COP of the proposed system determined was 4.4 at a generator temperature of 60 °C. Some recent studies done on cascaded refrigeration systems are shown in Table 2.2.

TH-3395_176107002

Table 2. 2 Recent literature on cascaded refrigeration systems

Author(s)	Working pairs		Highlights
	Compression	Absorption	
Mousavi and Mehrpooya [157]	CO_2	NH_3-H_2O	The exergy, exergoeconomic, and exergoenviornmental analysis of the new cascaded absorption compression hybrid system was carried out. The overall exergy efficiency and irreversibility rate of this system were reported as 69% and 83.4 kW, respectively.
Ustaoglu [158]	R134a, R152a, R717, R290, R407c, R507a	NH_3-H_2O	Advanced exergy analysis was conducted for the absorption-compression cascaded refrigeration system. The largest exergy destruction, 53.8% of total destruction, occurred in the generator. The largest and lowest irreversibility was found for R507a and R152a, respectively. More than 50% of all energy losses fall into the category of avoidable losses that can be shunned by maintenance, replacement, or arrangement of the operating conditions in the components.
Askari et al. [159]	R1234yf	LiBr–H_2O	Integrated organic Rankine cycle (ORC, toluene)/ejector-cascade compression (R1234yf)–absorption (LiBr–H_2O) refrigeration system/thermo-electric generator (TEG) powered by the linear Fresnel solar collectors were studied. COPs of the ejector (EJR)-vapor compression (VCR), ejector (EJR)-vapor absorption (VAR), and cascade cycles were reported as 5.49, 0.95, and 0.74, respectively. Application of EJR in the system increased the exergy efficiency, COP of VCRS, COP of VARS, and COP of cascade system by 51.19%, 19.67%, 21.05%, and 27.02%, respectively, over the system without ejector.
Gado et al. [160]	R134a	Adsorption pair: Silica gel/water	PVT-powered cascade adsorption-compression refrigeration system has been developed and analyzed. A comparative study of the proposed system with sorption compression refrigeration systems was reported. The proposed system achieved an annual energy saving of 24.8% than the conventional VCRS.
Higa et al. [161]	NH_3	NH_3-H_2O	A hybrid compression-assisted absorption refrigeration system using condensation in a heat recovery ammonia generator was put

TH-3395_176107002

			forward. The study was done based on energy and exergy efficiency. It was reported that external heat source and power demand for the proposed system was decreased by 57.4% compared to traditional VARS and 34.2% compared to traditional VCRS, respectively.
Kadam et al. [162]	R134a	NH_3-H_2O, Acetaldehyde-N/ N-dimethylformamide	Double effect VARS was integrated with VCRS for district cooling purposes. A comparative study of parallel and cascaded combinations of the VARS and VCRS was carried out. The COP of the compression unit in the cascaded systems was higher by 252% than conventional VCRS. The electrical energy utilization factor was 30.5% less for acetaldehyde-N, N-dimethylformamide working fluid compared to ammonia/water in the cascade configuration.

2.5. State of art on single-objective thermoeconomic optimization of the refrigeration systems

Optimization for a refrigeration system is required to guarantee that the system will operate efficiently and is not overdesigned. It can be implemented for better system analysis, design, modelling, and performance. Researchers put forward a thermoeconomic optimization approach that helps to improve the performance of the system by combining thermodynamic and economic considerations on a single platform. An optimization problem for a refrigeration system can be formulated to obtain minimum system capital cost, total area, and exergy destruction or maximization of coefficient of performance and exergy efficiency. Such problems can be handled using mathematical programming or metaheuristic techniques. Many research articles have successfully implemented thermoeconomic optimization in refrigeration systems using various mathematical programming.

The thermo-economic analysis studied on thermal systems achieves a minimum total annual cost of the plant by employing the second law of thermodynamics and economic factors, which has been used extensively to optimize refrigeration systems. Brendeng and Aflekt [163] discussed the economic optimization of the refrigeration plant using the mathematical expressions developed by Backstrom. d'Accadia and Rossi [164] applied the theory of exergy cost to get the optimal cost for a refrigeration plant. Usta and Ileri [165] studied thermoeconomic optimization to obtain minimum lifetime system cost for different cases of

TH-3395_176107002

VCRS using the modified Hooke and Jeeves method with refrigerants R12, R134A, R22, 502, and R717. Amongst all refrigerants, maximum COP and minimum lifetime cost were determined for R717 under optimized conditions. Grosu et al. [166] proposed the technoeconomic optimization study of VCRS using Generalized Reduced Gradient (GRG) Methods to minimize the total annual cost with R22 as a refrigerant. Sanaye and Malekmohammadi [167] studied the thermal and economic optimization of the VCRS using the Lagrange multiplier method. The objective of the study was to minimize the total cost of the system.

Al-Otaibi et al. [168] performed thermoeconomic optimization of the VCRS to determine the optimal cost of the system using R134a as a refrigerant. The efficiencies of the compressor, condenser, evaporator, and electric motor were considered as decision variables. Hosoz and Ertunc [169] employed an artificial neural network to model and determine optimal performance parameters for a cascaded VCRS with R134a as a refrigerant. The artificial neural network (ANN) model was trained using the data obtained from the experimental data. This model was used for predicting parameters of the system, such as evaporating temperature in the lower circuit, compressor power in both circuits, and the COP for the overall system. Selbaş et al. [170] reported the exergy-based thermoeconomic optimization of the subcooled and superheated compression cycle to minimize the cost with the refrigerants R22, R134a, and R407c. The optimization study was carried out using the coefficient structural bonds method. O¨zkaymak et al. [171] conducted a thermoeconomic optimization study of superheating and sub-cooling heat exchangers in VCRS using the coefficient structural bond method. The objective was to determine the minimum cost using optimal temperatures and corresponding areas with R22, R134a, R404a, and R502 as refrigerants. It was observed that the VCRS performance was enhanced with superheating and subcooling.

Zhao et al. [172] studied VCRS optimization to minimize the total cost of the system and solved using a modified genetic algorithm. Constraints were mechanical limitations, environmental conditions, and cooling effects. Baakeem et al. [173] conducted an optimization study of the multistage VCRS with the help of exergy, energy, and economic analysis with different refrigerants. The conjugate directions method was used to maximize the COP. R717, R22, R134a, R1234yf, R1234ze (E), R410A, R404A, and R407C were used as refrigerants. An optimization study of VCRS using R290, R1234yf, R744, and R134a was put forward by Paula et al. [174] to determine a minimal geometric structure and efficient system from the environmental point of view using the most suitable low GWP alternative refrigerant. The Nelder Mead Simplex method was used to perform the optimization. Rezayan and

TH-3395_176107002

Behbahaninia [72] conducted a thermoeconomic analysis of a cascaded/double-effect VCRS with CO_2/NH_3 as refrigerants. The objective function was to minimize the total annual cost of the system, which included costs of input exergy to the system and annualized capital cost of the system. The formulated objective function was solved by the direct search method.

Misra et al. [175] used the theory of exergy cost to determine the optimal cost for a VARS. Misra et al. [176], [177] studied the thermoeconomic optimization of single-effect VARS using LiBr-H_2O and aqua-ammonia as working fluids using simplified cost minimization methodology by formulating exergoeconomic cost equations for all components. Double-effect VARS was analyzed using LiBr-H_2O to find optimal operating temperatures for estimating the minimum cost of the system. The optimization study was carried out using a simplified cost minimization methodology [178]. Misra et al. [179] implemented the structural coefficient method to obtain the minimum product cost. The coefficient structural bond removes the need for complicated numerical techniques, and the optimization was achieved by successive local optimization of subsystems of the main system. Zebbar et al. [180] analyzed a single effect LiBr absorption heat transformer based on first and second law analysis using a coefficient structural bond method to determine optimal operating parameters. Kizilkan et al. [181] optimized a VARS using the coefficient structural bond method to determine the optimal heat exchanger area and operating temperatures.

Single-stage VARS optimization using sequential quadratic programming (SQP) in the Generalized Algebraic Modeling System (GAMS) was reported by Rubio-Maya et al. [182] to minimize the total annual cost. Mazzei et al. [183] proposed optimization of the VARS to maximum COP and the minimum total heat transfer area. CONOPT solver in GAMS, based on the generalized reduced gradient method, was used to solve this optimization problem. Mussati et al. [184] employed a CONOPT solver in GAMS which is based on the generalized gradient search method to minimize exergy destruction, total area, and total annual cost for a specific cooling capacity. Azhar and Siddiqui [185] studied the optimization of single to triple-effect VARS driven by CNG and LPG to maximize COP and minimize the supplied gas requirement. COP achieved for triple-effect VARS was ~132% higher, and the gas requirement was ~122% lower than the single effect at the optimal conditions. Zhao et al. [186] optimized the single-effect LiBr-H_2O absorption chiller modeled using the heat current method to maximize the cooling capacity of the system. MATLAB inbuilt function *fmincon* was used to solve this constrained problem. *fmincon* uses the sequential quadratic programming method. Mussati et al. [187] extended series flow double effect VARS to a superstructure based optimization model combined with VCRS. The objective of the proposed problem was to

TH-3395_176107002

minimize the total heat transfer area and to find the optimal configuration of the CRS using mathematical programming using the CONOPT solver in GAMS (generalized reduced gradient algorithm). It was observed that the total heat transfer area of the obtained optimal configuration was ~7.3% smaller than the reference case. R134a with LiBr-H_2O was the working fluid pair.

Metaheuristic algorithms have several advantages over mathematical programming such as solving black-box optimization problems, accommodating conflicting objectives, not requiring gradient information, handling nonlinearities, and not necessitating the problem formulation in the standard inequality and equality form [20]. Therefore, researchers employed population-based metaheuristic algorithms to solve the refrigeration system optimization problem. The second law analysis of an absorption chiller was conducted by Myat et al. [188] to minimize the specific entropy using GA. It was observed that a reduction in the entropy generation led to the maximization of the COP of VARS. The generator had the largest exergy destruction due to its higher contribution to the total entropy generation of the system. After optimization of VARS, the specific entropy generation was reduced from 37 W/K Rton to 33 W/K Rton, i.e., ~11% reduction than the base case.

Mohammadi et al. [189] studied thermoeconomic optimization of the hybrid triple effect parallel flow VARS integrated with a compressor in between the evaporator and absorber. PSO algorithm was used to conduct an optimization study to minimize the unit production cost (UPC). These results showed that the higher evaporator and condenser temperature affected the COP and UPC of the system. Under optimal conditions of evaporator temperature at 6 °C and condenser temperature at 40 °C, the COP was improved by 200%, and UPC was decreased by 57% than the base case. Xu et al. [190] studied the optimization of solar absorption-subcooled compression hybrid cooling for cold storage using a genetic algorithm. The main objectives were to find the minimum annual energy saving (AES), payback period (PBP), maximum net present value (NPV), and internal rate of return (IRR). The AES per collector area obtained and minimum PBP were reported as 68.8 kWh m^{-2} and 4.96 years, respectively. The maximum NPV and IRR were reported as 0.2 million dollars and 15.40%, respectively. Table 2.3 shows the literature survey on the different optimization methods employed to determine the optimal decision variables and objective function for VARS and CRS.

TH-3395_176107002

Table 2. 3 Literature on thermoeconomic single-objective optimization of refrigeration systems

Author(s)	Optimization Algorithm	System	Highlights
Cha´vez-Islas et al. [191]	Branch and bound	VARS	The combined synthesis and optimization of processes for VARS with NH_3-H_2O as a working fluid was solved to minimize the capital and operating costs. For Case 1, air-cooled heat exchangers (HEs) yielded ~7% lower cost than water cooling, while for Case 2, water-cooling HEs reported ~10% minimized cost than air-cooling HEs.
Beghi et al. [192]	PSO	mixed multi-scroll/multi-screw chiller system	The objectives were to reduce power consumption and operating costs. The proposed PSO showed 13.81% and 7.05% seasonal electric energy savings with respect to the Sequential strategy (MS) and Symmetric strategy (SS).
Ghorbani et al. [193]	PSO, Pattern search method, Enumerative method	Mixed refrigerant refrigeration cycle	PSO was observed to be superior to the direct search method in finding the decision variables. PSO minimized energy consumption by ~9% & ~12% for configuration A and ~0.6% & 3% for configuration B than the pattern search method & enumerative method, respectively, under optimal conditions.
Cimsit et al.[194]	Simplex direct search method	Compression - Absorption CRS	The minimum cost was reduced by 3.3%, while COP and exergy efficiency were enhanced by 7% and 3.1%, respectively, compared to the base case under optimal conditions.
Jain et al. [195]	Direct search method	Compression - Absorption CRS	The total annual cost was minimized by 11.9% compared to the base case, with a 22.4% reduction in investment cost by system optimization.
Jain et al. [196]	Direct search method	Series, parallel, and combined series-parallel Compression - Absorption CRS	The power consumption in the compressor of parallel, series, and combined series-parallel was reduced by 60%, 78.1%, and 89.5%, respectively, while the annual total cost was decreased by 21.9%, 29.4%, and 29.4%, respectively, as compared to equivalent VCRS base case under optimal conditions.

TH-3395_176107002

Ghani et al. [197]	Interior point method (default fmincon algorithm)	Double effect VARS	Under optimal operating conditions, it was reported that COP and exergy efficiency were enhanced by 10.25% and 38.5%, respectively, than the base case.
Li et al. [198]	Direct search method	Absorption-subcooled compression cycle	The product cost flow rate, compressor work, and exergy destruction of the optimal design were reduced by 22.33%, 33.44%, and 11.58%, respectively, compared to the base case.
Dixit et al. [199]	Direct search method	Two-stage absorption–compression combined refrigeration system	The proposed system reduced electricity consumption by 89.3% and CO_2 emission from 112.6 to 12.1 tons/year as compared to equivalent VCRS. The annual cost of its operation was 21.6% less than the equivalent VCRS, which was further reduced by 18.2% through system optimization.
Mohtaram et al. [200]	GA	Combined Rankine power and Absorption refrigeration system	An optimization study was conducted to maximize exergy and thermal efficiencies. The maximum thermal efficiency was 22.92% when the inlet temperature and pressure of the turbine and the concentration of ammonia base solution were 16.03 bar, 557.9 K, and 0.38, respectively. The maximum exergy efficiency was 43.12% when the inlet temperature and pressure of the turbine and the concentration of ammonia base solution were 16.03 bar, 558.1 K, and 0.28, respectively.
Patel et al. [201]	Conjugated directions method	ORC-powered compression-absorption CRS	The annualized cost of the present system was decreased by about 12% compared to the base case and the simple payback period was reduced from 5.26 years (base case) to 4.5 years under optimal conditions.
Mussati et al. [202]	Generalized gradient search method	Series double effect VARS	Compared to the conventional double-effect VARS, the total annual cost for the proposed configuration was reduced by 9.5% under optimal conditions.
Jing et al. [203]	NA	Solar/Natural gas driven-VARS, Solar Compression - Absorption integrated refrigeration, Solar	The solar absorption-subcooled compression hybrid cooling system showed the best cost-effectiveness for all types of buildings, owing to its lowest total fuel and product cost flow rate and the least exergy destruction.

TH-3395_176107002

		Absorption-subcooled hybrid cooling system	
Ren and Peng [204]	PSO-GA	VARS	A hybrid optimization strategy by integrating PSO and GA was employed with maximization of the COP as an objective function to determine the corresponding optimal configuration of VARS. COP of the optimal configuration was improved by 30% than the initial one.
Shirmohammadi et al. [205]	GA	Post-combustion CO_2 Recovery Unit with VARS	The amount of power used for the blowers was saved by 14.85 kW, while for compressors (C1 and C2), it was reduced by 23.03 and 22.91 kW, respectively, than the base case under optimal conditions.
Arshad et al. [206]	GA	Series and parallel double effect VARS	Exergy efficiency was improved by 11.6% and 20.81%, while COP was enhanced by 13.73% and 5.71% for series & parallel flow configurations, respectively, than the base case at the optimal operating conditions.
Tavakoli et al. [207]	GA	Double effect VARS	Exhaust gases from the Tehran refinery crude oil furnace were used in a heat recovery steam generator coupled with a double effect VARS. The optimal solution determined showed a 7% reduction in the total annual cost and a 33% improvement in the exergy efficiency than the base case.
Kong et al. [208]	Self-Adaptive Differential Evolution	VCRS	The global optimization strategy for minimizing the system energy consumption was proposed. The total energy saving for the system was observed to be 15.57% for a typical day compared to conventional VCRS at the same conditions.
Arshad et al. [209]	GA	Series and parallel double effect VARS	The total annual cost was reduced by 33.48% and 26.26% for series and parallel configuration than the reference case under optimal conditions.

TH-3395_176107002

2.6. State of art on multi-objective thermoeconomic optimization of the refrigeration systems

Since most of real-world problems inherently involve multiple objectives, the single-objective optimization approach fails to obtain the trade-off between different objectives, providing flexibility in accommodating the preferences of the decision maker. Different solutions may produce trade-offs (conflicting scenarios) among different objectives. A solution that is extreme (in a better sense) with respect to one objective requires a compromise on other objectives. Between these two extreme solutions, there are many other solutions, where a trade-off between the objectives exists.

A multi-objective optimization needs to evaluate two or more conflicting objectives simultaneously. In multi-objective optimization, a set of optimal solutions is given, known as the Pareto optimal set; other solutions do not dominate that and cannot be improved concerning any objective without worsening at least one objective. There are several optimum solutions for multi-objective optimization, and users can select the best one based on the importance of their objectives. Optimization of any process can be stated as finding an alternative that will be economic or will give the highest performance/profit, satisfying all the constraints of that process. This can be done by either maximizing desired factors or minimizing undesired factors. There are classical optimization algorithms such as the weighted sum method, and an ε-constraint method to solve these problems; however, these algorithms suffer from issues like the weighted sum method does not support non-convex problems and heavily depends on the weight coefficients while the ε-constraint method is a time-consuming process, it is difficult to formulate the problem with too many objectives and it has the critical impact of ε on solutions [210]. Therefore, population-based metaheuristic algorithms are preferred to solve multi-objective optimization problems.

Sayyaadi and Nejatolahi [211] studied single and multi-objective optimization analysis using GA for minimum total exergy destruction and total annual cost as objectives for VCRS assisted with cooling tower. They observed that multi-objective optimization was better for the system than single-objective optimization, resulting in 22.51% higher total exergy degradation and 10.37% more total yearly cost than minimum possible. Compared to the minimum values obtained for a single objective, the solution for minimum exergy destruction resulted in an 82.46% increase in cost, while the minimum total yearly cost solution led to a 40.09% increase from the minimum possible reported by a single objective under optimal conditions. Aminyavari et al. [212] conducted an optimization study of a cascaded VCRS with CO_2/NH_3

TH-3395_176107002

as a working pair based on an exergy-economic-environmental approach. Maximum exergy efficiency and minimum annual cost rate of the system were considered as the objectives and solved using multi-objective GA. The Pareto optimal solution reported a maximum exergy efficiency of 45.89% and a total cost rate of 0.01099 US$/s for a cooling capacity of 50 kW. Eini et al. [213] performed multi-objective optimization of a cascaded VCRS based on exergy, economic, environmental, and safety analysis with CO_2/NH_3 and CO_2/C_3H_8 as working fluids. Total exergy efficiency, risk level, and cost rate were the three objective functions and NSGA-II was employed for optimization. The optimal values for the exergy and economic function did not change significantly for both cases. Risk level analysis reported that the CO_2/NH_3 system was found to be a safer one based on risk function, and the cost related to risk function for CO_2/NH_3 was ~135% lesser than $CO_2/C3H_8$ at optimal conditions.

Keshtkar and Talebizadeh [214] studied a multi-objective optimization of a VCRS of cooling water package in the South Pars refinery of Iran based on exergy, economic, and environmental analysis using NSGA-II. Minimization of total irreversibility, total annual cost, and total product of NO_x, CO, and CO_2 by electricity consumption were the objective functions. Compared to the base case, the exergy destruction was reduced by 51.81%, which resulted in the increment of the COP by 87.41% at optimal conditions. Asgari et al. [215] investigated exergy, exergoeconomic, and multi-objective optimization studies of an auto cascade refrigeration cycle using NSGA-II. The objective of this study was to minimize the total avoidable exergy destruction rate, total avoidable investment cost rate, and total avoidable exergy destruction cost rate. The multi-objective optimization study showed 76.78%, 38.66%, and 103.38% enhancements in total avoidable exergy destruction rate, total avoidable investment, and total avoidable exergy destruction cost rates, respectively, compared to the base case. Roy and Mandal [216] analyzed the thermoeconomic multi-objective optimization study of VCRS with low GWP refrigerants (R125a, R600a, R1234ze) using MOGA. Minimization of annual plant cost and maximization of exergy efficiency were the objectives. Based on TOPSIS decision-making analysis, it was reported that R152a was proved as the best refrigerant from the thermodynamic and economic point of view for the studied system.

Zendehboudi et al. [217] optimized VCRS using the hybrid optimization model by coupling the response surface method (RSM) with NSGA-II with R450a as a refrigerant. The objective was to determine the minimum motor-compressor electrical power consumption and discharge temperature and simultaneously maximize the refrigerant mass flow rate in the first scenario, while the second scenario included maximizing cooling capacity as an objective in addition to the first one and excludes minimizing motor-compressor electrical power consumption. It was

TH-3395_176107002

observed that the motor-compressor electrical power consumption and discharge temperature decreased by 18.39% and 53.31%, respectively, in the first scenario optimal results. Roy et al. [218] considered maximum exergy efficiency, minimum plant cost rate, and two compressor discharge temperatures as objectives for optimizing two-stage VCRS and solved the problem using MOGA. From the optimization results, it was noted that R32 showed better thermoeconomic performance over R410a when the compressor discharge of R32 was higher.

A comparative multi-objective thermoeconomic optimization study of a cascaded VCRS with NH_3/CO_2 and C_3H_8/CO_2 as working pairs using a multi-objective heat transfer search algorithm was done by Patel et al. [219]. The objective of the optimization problem was to minimize the total annual cost and exergy destruction. Based on the optimization results, it was reported that the C_3H_8/CO_2 pair offered 5.33% lower cost and 6.42% higher exergy destruction compared to the NH_3/CO_2 pair. Roy and Mandal [220] proposed the thermodynamic analysis and multi-objective optimization study of the cascaded VCRS with different refrigerant pairs (R41–R404A, R170–R404A, R41–R161, and R170–R161) using GA to minimize the total annual cost rate and maximize the exergy efficiency of the system. Considering the TOPSIS method results, it was observed that the R41–R161 and R170–R161 refrigerant pair exhibited a better performance in terms of optimum exergy efficiency and total annual cost rate.

Iranmanesh and Mehrabian [221] performed a multi-objective optimization study of a double-effect absorption refrigeration system with LiBr-H_2O as a working fluid based on solar-driven energy to minimize auxiliary energy and maximize the net profit using NSGA-II. From the results, it was observed that the optimum mass flow rates of hot water passing through the generator and collector played a significant role in reducing the auxiliary energy. Gebreslassie et al. [222] conducted a multi-objective optimization study for an optimized absorption chiller area and the environmental impact of the operation using the ε-constraint method. Jain and Sachdeva [223] reported a multi-objective study of absorption heat transformers using NSGA-II with objectives such as minimization of exergy destruction and total annual cost. The optimal solutions obtained from multi-objective optimization were only 1.0% and 0.8%, respectively, higher than their minimum possible values obtained from single-objective optimization. Panahizadeh et al. [224] put forward the multi-objective optimization of the Iranian Marun Petrochemical Company absorption chiller network was performed using the particle swarm optimization (PSO) algorithm. It was reported that energy and exergy performance coefficients were increased by 5.3% and 6.2%, respectively. The annual cost was reduced by $70,000.00 when the inlet cooling water temperature of the network was decreased from 35 °C to 25 °C.

TH-3395_176107002

Ahmadi and Ahmadi [225] carried out a multi-objective optimization study of an irreversible VARS with a specific entropy generation rate and the ecological coefficient of performance (ECOP) as objectives. Multi-objective evolutionary algorithm (MOEA) improved by the NSGA-II algorithm was employed to solve the problem. Rao and Patel [226] proposed a multi-objective optimization study of a two-stage thermoelectric cooler using a modified teaching learning-based optimization algorithm to maximize the cooling capacity and COP. Cui et al. [227] investigated energy, exergy, economic analysis, and multi-objective optimization using NSGA-II on the integrated absorption refrigeration cycles. The aim was to minimize the total exergy destruction and the total annual cost of the proposed system. It was noted that optimal results obtained from multi-objective optimization that total annual cost and total exergy destruction were only higher by 5.9% and 4.5%, respectively, than the minimum possible values determined from the single-objective optimization. Ahmadi et al. [228] implemented NSGA-II for the multi-objective optimization of the irreversible four-temperature-level absorption refrigeration system. The objectives of the proposed study were maximizing the coefficient of performance, ecological function, and thermoeconomic criteria. Shirazi et al. [229] conducted a multi-objective optimization study of single, double, and triple-effect absorption refrigeration systems driven by evacuated tube collectors (ETCs), evacuated flat plate collectors (EFPCs), and concentrating parabolic trough collectors (PTCs), respectively, using GA. Primary energy consumption and total annual cost were considered as the objectives. From the optimization results, it was noted that the double-effect chiller performed better.

An optimization and exergoeconomic analysis of the cascaded system (VCRS+VARS) driven by solar energy using water/Cuo nanofluid in the flat collector system with refrigerants R134a, R1234ze, R1234yf, R407C, and R22 in compression subsystem and LiBr-H_2O in absorption subsystem as working fluid was put forward by Boyaghchi et al. [230]. NSGA-II was implemented to optimize thermal and exergy coefficients of performance and total product cost rate. R134a was the best fluid for energy and exergy, while R1234ze was the best working fluid from a total product cost rate point of view. Turgut and Turgut [231] studied the multi-objective optimization of cascaded vapor compression absorption refrigeration system (CVCARS) with R1234yf, R134a, R717, and R290 as refrigerants in the compression subsystem and LiBr-H_2O as a working pair in absorption subsystem using Artificial Cooperative Search (ACS) algorithm. Minimization of the total annual cost considering costs related to carbon emission and maximization of the exergy efficiency were the objectives. R290 reported the minimum cost, while R717 determined the maximum exergy efficiency

TH-3395_176107002

among all pairs. Jain et al. [232] performed the comparative single and multi-objective optimization study of a cascaded vapor compression-absorption refrigeration system (CRS) and a hybrid vapor compression-absorption refrigeration system (HRS) integrated with the cooling tower using NSGA-II. COP and second law efficiency of the CRS was 82.1% and 25% higher than HRS, and the yearly operational cost and investment cost for CRS were lowered by 46.1% and 10% at optimal operating conditions due to better energy usage and reduced CO_2 emissions. A single and multi-objective optimization study was done on the system using NSGA-II by Jain et al. [233]. The total irreversibility rate and the total product cost were objectives with R410a and LiBr-H_2O as a working fluid. The multi-objective design satisfies the thermodynamic and total product cost criteria better than two single-objective thermodynamic and total product cost-optimized designs.

A multi-objective optimization study for cooling and power cogeneration system using a combination of cascaded refrigeration system (VCRS+VARS) along with an organic Rankine cycle and heat exchanger network was proposed by Sun et al. [234]. The objectives were to minimize annual cost and exergy destruction and the problem was solved using the ε-constraint method. The proposed system was compared with cascaded refrigeration without ORC integration, and it was reported that the proposed system reduced the optimal minimum annual cost and maximum total exergy destruction by 1.6% and 31.5%, respectively. Salim and Kim [235] optimized a combined ORC and VCRS with R245fa, R245ca, and R236ea in ORC and R410a in VCRS as refrigerants using NSGA-II. The objectives were to minimize the total annual cost and maximize thermal efficiency. The multi-objective optimization results showed that R236ea determined the lowest cost and the lowest system efficiency, R245ca obtained the highest cost and the highest system efficiency, while R245fa provided an optimized system between the two extremes. Wu et al. [236] proposed an optimization study of the novel system, which combines supercritical Brayton and VARS to recover engine waste heat. Multi-objective optimization was performed using NSGA-II on the system to obtain maximum exergy efficiency and minimum total product unit cost. Compared with the single supercritical CO_2 Brayton cycle, the proposed integrated system reported 2.29–2.54% higher exergy efficiency and 8.16–18.93% higher thermal efficiency; however, the total product unit cost increased by at least 29.56% at different evaporator temperatures (−10 to 10 °C).

Razmi et al. [237] analyzed thermoeconomic and multi-objective optimization studies of an absorption/recompression refrigeration system with an ANN and NSGA-II. The system obtained a COP of 4.88 and an exergy efficiency of 37.43% under optimal operating conditions. Ghaebi et al. [238] conducted a single and multi-objective optimization study of a

TH-3395_176107002

novel combined power and ejector refrigeration cycle using GA. The outcomes of multi-objective optimization reported that the thermal efficiency of the system and the sum of the unit cost of the product were enhanced by 8.16% and 4.7%, respectively, than the base case. Rashidi and Khorshidi [239] optimized a multi-generation system that combined a reverse osmosis desalination unit, water heater, organic Rankine cycle, photovoltaic solar collectors, and a single effect VARS to determine minimum total cost rate and maximum exergy efficiency as two objective functions using multi-objective differential evolution algorithm.

Some of the recent thermoeconomic optimization studies on the different cascaded refrigeration systems combined with a power cycle (may include integration of VARS, VCRS, and ORC) are presented in Table 2.4.

2.7. Research gap

From the literature, it has been noted that various studies were conducted on the thermoeconomic optimization of refrigeration systems. However, some of the research gaps have been observed, as given below:

- Though researchers have been using single absorbents such as LiBr-H_2O in the VARS; however, the system may suffer from crystallization and corrosiveness issues. This problem can be addressed using a mixture of absorbent solutions. From the literature survey, it has been found that ($CaCl_2$-LiBr-$LiNO_3$)-H_2O has lower crystallization temperature and is less corrosive than LiBr-H_2O; but, no thermoeconomic optimization study has been conducted using ($CaCl_2$-LiBr-$LiNO_3$)-H_2O as an absorbent-refrigerant working pair in the absorption section of the cascaded refrigeration system (VCRS+VARS), subcooler integrated cascaded refrigeration system and vapor recompression absorption refrigeration system (VRARS).
- The addition of a subcooler improves the cooling capacity and efficiency of the refrigeration systems. A comparative study of thermoeconomic optimization of the standalone cascaded refrigeration system (VCRS+VARS) and subcooler integrated refrigeration systems employing metaheuristic techniques with low ODP and GWP refrigerants such as R290, R123, R1234yf, and R1234ze in the compression section and various absorbent solutions such as LiBr-H_2O, LiCl-H_2O, and $CaCl_2$-LiBr-$LiNO_3$-H_2O in the absorption section to identify the most efficient refrigeration system based on energy, exergy, and cost has not been performed.

TH-3395_176107002

Table 2. 4 Recent literature on refrigeration systems combined with the power cycle

Author(s)	Working pairs		Highlights
	Compression/ORC	Absorption	
Azizimehr et al. [240]	ORC: R123, R245fa, R134a	-	Both single and multi-objective optimization analysis was reported using TLBO. From the multi-objective optimization results, it was observed that for R123, thermal efficiency, exergy efficiency, and were improved by 27.85%, 27.66%, while the system cost rate was lowered by 9.90%, respectively. For R245fa, thermal efficiency and exergy efficiency were enhanced by 32.78%, and the cost rate was decreased by 17.31%. These values for R134a were 65.89%, 65.40%, and 20.10%, respectively. All improvements and reductions were presented compared to the base case under optimal conditions.
Wang et al. [241]	ORC: R1336mzz(Z)	NH_3-H_2O	A combined cooling, heating, and power system was proposed to recover the waste heat from the gas turbine. A techno-economic environmental performance and a multi-objective optimization of the proposed system were done. The proposed system, under primary design conditions, showed a thermal efficiency of 52.95%, exergy efficiency of 40.20%, total cost rate of 13.75 $/h, and total GHG emissions of 926.69 kt CO_2, while under multi-objective optimization conditions, the system determined thermal efficiency of 67.88%, exergy efficiency of 42.62%, total cost rate of 10.60 $/h, and total GHG emissions of 923.55 kt CO_2.
Yang et al. [242]	VCRS: NA ORC: Transcritical CO_2	LiBr-H_2O &	A multi-objective optimization of a combined system of VARS and power cycle was carried out for waste heat recovery. Thermal efficiency, annual total cost, and Eco-indicator 16 (EI16) were the objectives and were solved using NSGA-II. The final optimal solution reported that an increase of 13.17% in thermal efficiency and a decrease of 13.49% in Eco-indicator 16 determined an 8.94% increment in annual total cost.

TH-3395_176107002

Musharavati et al. [243]	ORC: NH_3	NH_3-H_2O	A comparative exergy, multi-objective optimization, and an extended environmental analysis of three different configurations of ORC, VARS, and the thermoelectric generator were carried out using NSGA-II. Configuration 3 determined the maximum exergy efficiency as 19.42% compared to the other two. It had been reported that for configuration 3, multi-objective optimization determined higher turbine work by 33.3% than the base case.
Mahmoudan et al. [244]	VCRS: Toluene ORC: Toluene	-	A novel multi-generation energy system driven by geothermal energy and an LNG heat sink was optimized here using NSGA-II. The cascade system incorporates a flash-binary geothermal system, a regenerative ORC, a simple ORC, a VCRS, a regasification unit, and a reverse osmosis desalination system. The analysis was done regarding energy, exergy, and exergoeconomic. Heating load, cooling load, power, and freshwater are the main products of the proposed system. It was reported that the proposed system achieved maximum exergy efficiency of 29.15% and a total product cost per exergy unit of 1.512 $/GJ at optimal operating conditions.
Davoodi et al. [245]	VCRS: R134a ORC: NH_3	NH_3-H_2O	Optimization of a multi-generation system consisting of the solar cycle, ammonia-water power cycle, VCRS, and VARS using a genetic algorithm was reported. From the results obtained for all cooling loads, the maximum exergy efficiency was determined as 65.66% when the optimal generator temperature, turbine inlet temperature, average boiler pressure, and average ammonia concentration were determined as 110.5 °C, 210 °C, 58.56 bar, and 81.16%, respectively.

TH-3395_176107002

- In the optimization study of the refrigeration system, exergy destruction plays an important role. Higher exergy destruction lowers the performance of the system and hence will consume more energy to achieve a given cooling effect. This will lead to higher operating costs for the system. Exergy destruction is determined using the specific enthalpy, entropy, and mass flow rate of the specific stream. Hence considering utility mass flow rate as the decision variable will have a significant impact on the exergy destruction; however, the typical decision variables considered are outlet temperatures and the effectiveness of the heat exchangers. The optimization study with utility mass flow rate has not been addressed.
- The cost of cold utility is directly related to the thermodynamic efficiency of a system. In general, the higher the efficiency of a system, the lower the cost of cold utility. In refrigeration systems, the cost of the cold utility is a significant factor to consider. The total cost of the refrigeration system consists of operating and investment costs. Operating cost includes electricity cost, utility cost, and labor cost. Most of the literature have considered electricity cost but not the utility cost.
- Most researchers have employed genetic algorithm (GA) or particle swarm optimization (PSO) to optimize the model. However, the no-free lunch theorem [24] suggests implementing multiple metaheuristic techniques because a single algorithm cannot effectively handle all optimization problems. The present work aims to optimize different refrigeration systems using various metaheuristic techniques and compare these systems for effective system determination.

2.8. Objectives

Motivated by the observed research gap, this thesis aims to study thermoeconomic optimization of the standalone and combined refrigeration systems using metaheuristic techniques to determine efficient refrigeration systems. Single and multi-objective thermoeconomic optimization study has been conducted with objectives such as minimizing total annual cost, minimizing total area, minimizing exergy destruction, maximizing exergy efficiency, maximizing COP, and many other optimal decision variables such as temperatures and mass flow rates while satisfying all the constraints. The performance of various metaheuristic techniques on refrigeration systems and the impact of decision variables on determining the efficient system using various analyses have been addressed. The specific objectives are as follows:

TH-3395_176107002

- Thermoeconomic optimization of conventional vapor absorption refrigeration systems (VARS) and modified vapor absorption refrigeration systems (MVARS)
- Thermoeconomic optimization of vapor compression-absorption cascaded refrigeration system (CRS) with different absorbent-refrigerant combinations
- Thermoeconomic optimization of subcooler integrated vapor compression-absorption cascaded refrigeration system (SCRS) with different absorbent-refrigerant combinations
- Thermoeconomic optimization of vapor recompression-absorption refrigeration system (VRARS) with different absorbent-refrigerant combinations

The above studies are conducted with various single and multi-objective metaheuristic algorithms.

2.9. Closure

This chapter discusses the basic equations required for the thermodynamic modelling of refrigeration systems. A brief description of the single and multi-objective metaheuristic algorithms employed in the current work is provided. A comprehensive literature survey on the energy, exergy, economic, and environmental analyses and the theromoeconomic optimization studies of the refrigeration system has been covered. Furthermore, the research gap observed, along with the objectives of the present work, are presented. The next chapter (Chapter 3) describes the detailed investigation of the multi-objective thermoeconomic optimization study of the VARS and modified VARS.

TH-3395_176107002

CHAPTER 3

Multi-objective thermoeconomic optimization study of VARS and modified VARS

3.1. Introduction

VARS can be considered a better alternative to conventional VCRS in various cooling and refrigeration applications. VCRS uses mechanical compressors, which need power input for its operation. On the other hand, VARS utilizes various low-temperature heat sources as an energy input to the thermal compressor. VARS is the most viable cogeneration option to recover waste heat from existing industrial processes to produce the cooling effect. However, VARS is costlier and less effective than VCRS. Hence, improving its design and operation is unavoidable to be comparable with VCRS. Recently, considerable optimization studies have been conducted on the VARS using various approaches. It benefitted the VARS in terms of energy conservation and exergy augmentation. For better efficiency of the refrigeration systems, thermo-economic analysis on thermal systems can be performed to achieve a minimum total annual cost of the plant by employing the second law of thermodynamics and economic factors simultaneously, which has been employed extensively to optimize VARS.

It is well known that inefficient use of energy resources leads to exergy destruction. However, exergy destruction is inversely proportional to the total annual cost of the system. Multi-objective optimization can be implemented to optimize these conflicting objectives. Unlike single-objective optimization, it is impossible to determine a single optimal solution that would benefit all the conflicting objectives in the multi-objective model. Hence, Pareto optimal solutions, which are better in at least one objective function in the objective space, are obtained in multi-objective. In the classical optimization techniques such as the weighted sum method, ε-constraint method, etc., only one Pareto solution might be obtained with a single run, and these methods have to be simulated multiple times with different parameter settings to obtain multiple Pareto optimal solutions. On the other hand, metaheuristic techniques are population-based techniques, and hence they can provide more than one Pareto optimal solution in a single run. In addition, the 'No Free Lunch theorem for optimization'[24] states that it is impossible to determine a universal solver for any optimization problem. Hence in this work, three multi-objective metaheuristic techniques, namely MOGA, MOPSO, and MOsTLBO, are used to determine the Pareto optimal solutions for the minimal exergy destruction and minimum annual cost.

TH-3395_176107002

In this chapter, a reduction in the total annual cost of the VARS through thermo-economic optimization is discussed. Further improvements on the VARS have been suggested by adopting multi-objective thermoeconomic optimization. A single-stage VARS is formulated as a multi-objective optimization problem considering minimizing exergy destruction and total annual cost as conflicting objective functions. The performance of three metaheuristic evolutionary algorithms, MOGA, MOPSO, and MOsTLBO, are compared to achieve these objectives. The performance of these algorithms in achieving Pareto solutions, the convergence of Pareto solutions, computational time to converge towards global optima, and an inverted generational distance over the iteration of the Pareto fronts are also analyzed. The secondary aim is to check whether all the algorithms mentioned above perform better in all the aspects of optimization of the ARS system. Decision variables for VARS are generator temperature T_1 (°C), condenser temperature T_2 (°C), evaporator temperature T_4 (°C), absorber temperature T_5 (°C), and effectiveness of heat exchanger (ε). Along with T_1 (°C), T_2 (°C), T_4 (°C), T_5 (°C), and ε, temperatures of absorber coolant inlet stream, T_{15} (°C), condenser coolant outlet stream, T_{12} (°C), hot and cold streams of the generator, T_{17} and T_{18} (°C) and mass flow rate of coolant, $\dot{m}_{11}$ (kg/s) are also considered as decision variables in the modified VARS (MVARS) system for improving the basic VARS. MVARS is also solved as a multi-objective optimization problem using MOGA, MOPSO, and MOsTLBO algorithms to minimize total annual cost and exergy destruction.

3.2. Mathematical formulation and simulation

3.2.1. System description

The main difference between absorption and compression cooling systems is a thermally driven compressor in the former in place of a power-driven compressor in the latter. Thermo-chemical compressor employs two primary chemical unit operations of absorption and desorption using a refrigerant-absorbent working pair. In the current work, the system and economic models were adopted from Rubio-Maya et al. [182] with certain modifications. The schematic representation of MVARS is depicted in Fig. 3.1. The system provides a cooling effect to chilled water $\dot{Q}_4$ for cooling applications and uses waste heat $\dot{Q}_1$ from various sources. MVARS is a representative case for efficient utilization of available energy resources, which further aids in reducing the cost of coolant utilized. The system operates steadily with low-grade steam as the heat source. The working of MVARS is similar to the VARS; however, the difference between modified VARS (MVARS) and VARS is that in MVARS, the coolant streams (Fig. 3.1: stream 11-14) used for the absorber and condenser are the same, while in

TH-3395_176107002

VARS, two different coolant streams are considered. Here, water is considered as a hot utility and cold utility/coolant for both systems.

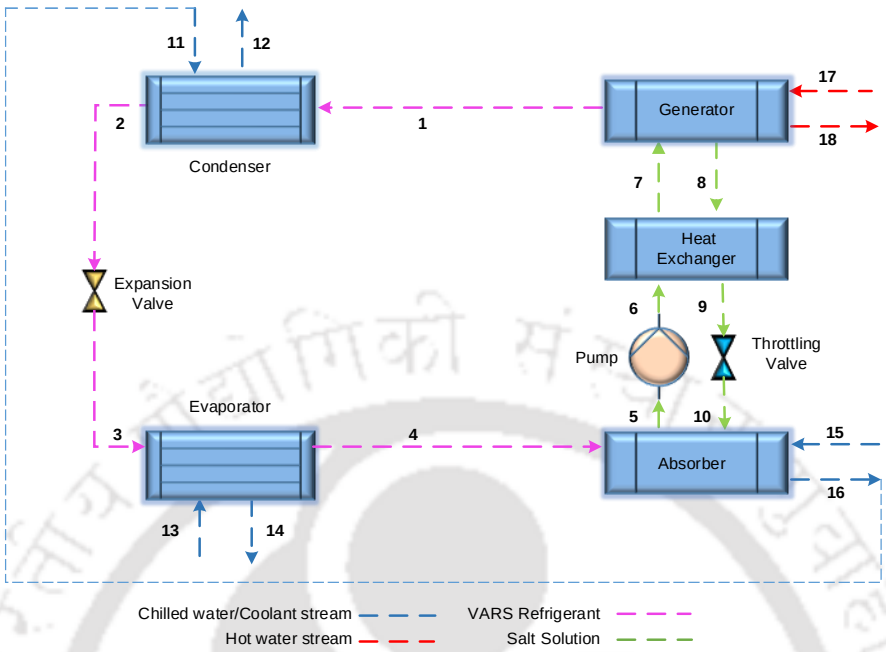

Fig. 3. 1 Schematic of modified vapor absorption refrigeration system (MVARS)

- **Model Assumptions**

The assumptions considered in this study are as follows: heat exchange between the system and surroundings occurs only in the evaporator, and the cooling capacity of the evaporator to produce chilled water is 201 kW. Other ancillary equipment needed for refrigeration and air-conditioning are not considered in this analysis. Temperature variation within the generator, condenser, evaporator, and absorber is neglected. It is ensured that the temperature of the strong solution entering the solution expansion valve is 5°C above the crystallization temperature of LiBr. The refrigerant and the solution expansion valves are treated as adiabatic. Pump work and pressure losses are neglected. LiBr solutions in the generator and the absorber are in equilibrium, and thermodynamic properties are calculated as the equilibrium values at their respective temperatures, pressures, and concentrations. The refrigerant exiting the condenser and evaporator and the LiBr solutions exiting the absorber and generator is considered to be at their saturated state.

3.2.2. Thermodynamic model of VARS and MVARS

The enthalpies and entropies of the refrigerant and coolant are calculated using REFPROP 9.0 software. The concentrations, enthalpies, and specific heat capacities for absorbent-

TH-3395_176107002

refrigerant mixture are determined using Eqs. (A.1-A.3, A.5), given in Appendix-A. The mass flow rate of the refrigerant, strong and weak solution are calculated using Eqs.(3.1)-(3.3).

$$\dot{Q}_4 = \dot{m}_4 \left(H_4 - H_2 \right) \tag{3.1}$$

$$\dot{m}_8 \left(X_8 - X_5 \right) = \dot{m}_4 X_5 \tag{3.2}$$

$$\dot{m}_5 \left(X_8 - X_5 \right) = \dot{m}_4 X_8 \tag{3.3}$$

The effectiveness of the solution heat exchanger based on strong and weak solutions can be expressed using Eqs.(3.4) and (3.5), respectively.

$$\varepsilon = \frac{\left(\dot{m} C_p \right)_8}{\left(\dot{m} C_p \right)_{\min}} \frac{T_1 - T_9}{T_1 - T_5} \tag{3.4}$$

$$\varepsilon = \frac{\left(\dot{m} C_p \right)_5}{\left(\dot{m} C_p \right)_{\min}} \frac{T_7 - T_5}{T_1 - T_5} \tag{3.5}$$

Heat loads on the generator, condenser, absorber, and solution heat exchanger, as well as the mass flow rates of chilled water in the evaporator, steam in the generator, and cooling water in the condenser and the absorber can be calculated using Eqs.(3.6)-(3.10).

$$\dot{Q}_{Gen} = \dot{m}_8 H_8 + \dot{m}_4 H_1 - \dot{m}_5 H_7 = \dot{m}_{17} \left(H_{17} - H_{18} \right) \tag{3.6}$$

$$\dot{Q}_{Cond} = \dot{m}_4 \left(H_1 - H_2 \right) = \dot{m}_{11} \left(H_{12} - H_{11} \right) \tag{3.7}$$

$$\dot{Q}_{Evp} = \dot{m}_4 \left(H_4 - H_2 \right) = \dot{m}_{13} \left(H_{13} - H_{14} \right) \tag{3.8}$$

$$\dot{Q}_{Abs} = \dot{m}_4 H_4 + \dot{m}_8 H_9 - \dot{m}_5 H_5 = \dot{m}_{15} \left(H_{16} - H_{15} \right) \tag{3.9}$$

$$\dot{Q}_{SHX} = \dot{m}_8 \left(H_8 - H_9 \right) = \dot{m}_5 \left(H_7 - H_5 \right) \tag{3.10}$$

In Eqs. (3.6-3.10), *Gen* denotes Generator, *Cond* denotes Condenser, *Evp* denotes Evaporator, *Abs* denotes Absorber and *SHX* denotes solution heat exchanger.

$$r = \frac{Q_5}{Q_2} \tag{3.11}$$

$$T_{11} = T_{16} = \frac{r T_{12} + T_{15}}{1 + r} \tag{3.12}$$

In MVARS, the temperature of the coolant stream (T_{11}) is calculated using Eqs.(3.11)-(3.12). Exergy input ($\dot{B}_{in}$) to the system can be calculated using Eq.(3.13).

TH-3395_176107002

$$\dot{B}_{D,Total} = \sum_{\substack{All\ heat \\ exchangers}} \dot{B}_D$$
$$\dot{B}_{in} = \dot{B}_{D,Total} + \left(\dot{B}_{13} - \dot{B}_{14}\right) \tag{3.13}$$

3.2.3. Economic model of VARS and MVARS

The economic analysis is performed based on operating parameters obtained from the thermodynamic analysis to calculate the total operating cost of the plant. The economic model developed by Rubio-Maya et al.[182] was coded and solved in MATLAB for the set of input data given in Eq.(3.14).

$$C_T = top\, C_{exer} \dot{B}_{in} + a^c Z_T \tag{3.14}$$

In the above expression, the first term represents the input exergy ($\dot{B}_{in}$) cost of the fuel supplied (C_{exer}) to the system for the specific period of operations (*top*). The second term indicates the product of the payback period of the system (a^c) and the annual cost recovery factor (Z_T).

$$Z_T = \sum_{\substack{All\ heat \\ exchangers}} Z \ \ where\ \ Z = Z_0 \left(\frac{A}{A_0}\right)^{0.6} \tag{3.15}$$

In Eq.(3.15), Z_0 and A_0 represent reference values and are taken as 7900 \$/kW and 100 m^2, respectively. The recovery factor (a^c) can be calculated using Eq.(3.16).

$$a^c = \left(\frac{i_r \left(1 + i_r\right)^{Ny}}{\left(1 + i_r\right)^{Ny} - 1}\right) \tag{3.16}$$

The multi-objective optimization problem constitutes two or more conflicting objectives to be minimized or maximized subject to certain constraints. Unlike a single-objective optimization problem, the quality of a potential solution in a multi-objective optimization problem cannot be indicated by its objective functions. In multi-objective optimization, there would be *M* conflicting objective functions associated with a single solution. Therefore, selecting a solution compared to multiple other solutions is not a straightforward procedure in multi-objective optimization. A solution X_1 is said to dominate a solution X_2, if and only if it satisfies the condition of (i) X_1 should not be worse than X_2 in every objective, and (ii) X_1 should be better than X_2 in at least one objective.

In multi-objective optimization, Inverted Generational Distance (IGD) is one of the most commonly used performance metrics for identifying the convergence and diversity of the Pareto set reported by an algorithm to the true Pareto. The IGD corresponding to the reported Pareto front can be determined as Eq. (3.17).

TH-3395_176107002

$$IGD = \frac{\left(\sum_{k=1}^{|P|} d_k^2\right)^{1/2}}{|P|} \qquad (3.17)$$

$$where\ d_k = \min_{i=1}^{|Q|} \sqrt{\sum_{m=1}^{M} \left(f_m^k - f_m^i\right)^2}$$

Here, P is the true Pareto, Q is the Pareto reported by the algorithm for an M objective problem, and d_k is the minimum Euclidean distance between the k^{th} point in true Pareto to all the points in the obtained Pareto. IGD provides a better indication of convergence and diversity of the obtained Pareto with respect to true Pareto compared to generational distance (average distance between obtained Pareto point and its closest global Pareto point). It is noted that generational distance provides a lesser even if the number of points on the obtained Pareto is less.

3.2.4. Objective function formulation and optimization

The formulation of objective function from thermodynamic analysis and the application of multi-objective optimization algorithms to achieve the objective (minimization of objective functions) under various constraints are demonstrated in Fig. 3.2. Eq. (3.18) represents the formulation of an optimization problem and constraint to minimize the total annual operating cost and exergy destruction of VARS and MVARS as a multi-objective optimization problem.

$$Objective\ Function: min\ C_T = top\ C_{exer}\dot{B}_{in} + a^c Z_T$$
$$min\ \dot{B}_{D,Total} = \sum_{\substack{All\ heat \\ exchangers}} \dot{B}_D \qquad (3.18)$$
$$Constraint: T_9 - T_c > 5$$

3.3. Model validation

To assess the accuracy of our numerical procedure, the system model was tested for calculating the total annual operating cost using the decision variables reported by Rubio-Maya et al. [182], and the results are in good agreement, as shown in the third column of Table 3.1. It is noted that the total exergy destruction obtained is slightly different compared to the literature [182], and this variation may be due to the calculation of entropy (s) of the refrigerant stream in the saturated vapor region in Rubio-Maya et al. [182]. Hence, minimizing total exergy destruction can be formulated as one of the objective functions for the multi-objective problem, where the minimization of total annual operating cost is the other conflicting

TH-3395_176107002

objective. The multi-objective model is solved using MOGA, MOPSO, and MOsTLBO, and the number of iterations for each algorithm is kept the same to compare the results.

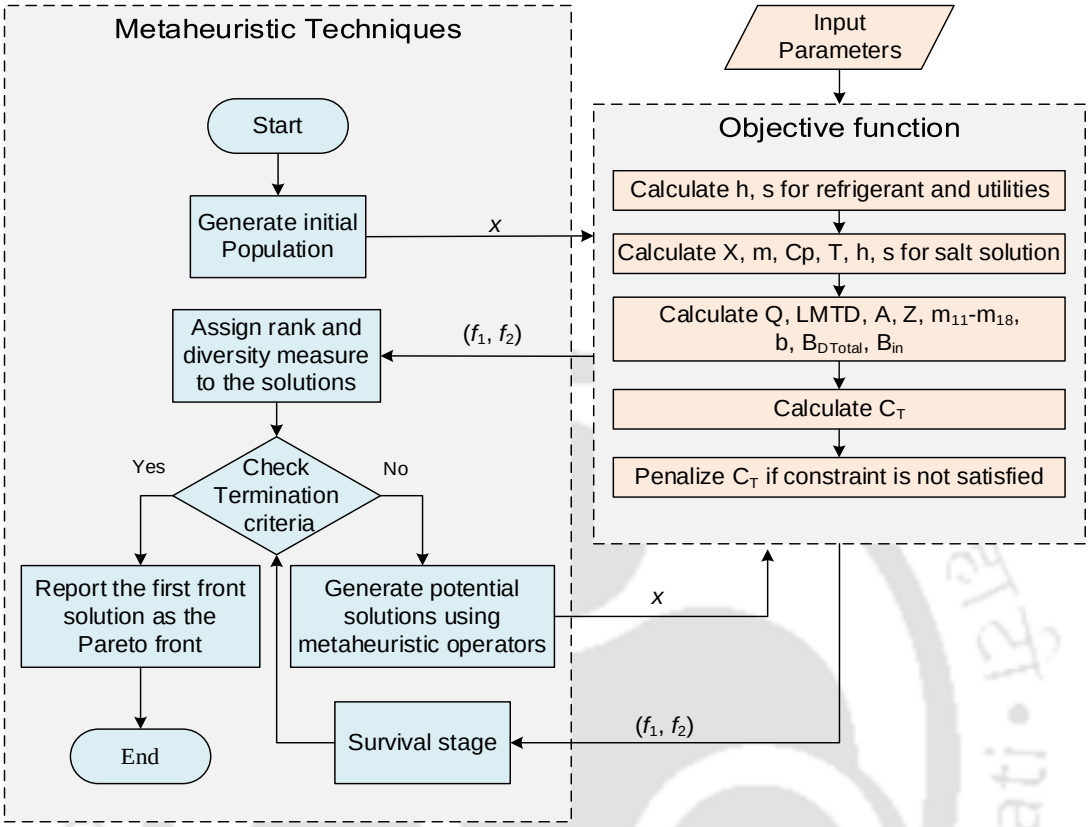

Fig. 3. 2 Flow chart for optimization methodology

The fourth and fifth columns of Table 3.1 show the optimal solution obtained by solving the current problem as a single objective optimization problem (minimization of total annual operating cost) using s-TLBO for both VARS and MVARS. There are no differences in the optimal decision variables obtained using s-TLBO and NLP technique [24] for VARS. It is noted that the exergy destruction decreased from 36.59 kW to 30.10 kW for MVARS. The mass flow rate of the condenser and absorber coolant is primarily responsible for reducing the exergy destruction in MVARS.

In VARS, the mass flow rate of the condenser and absorber coolant is calculated as 19.42 kg/s and 16.54 kg/s, respectively. At the same time, the mass flow rate of the coolant is considered a decision variable, and its optimal value determined using s-TLBO is 10 kg/s, which had a significant impact on exergy destruction in MVARS. It is also reflected in the augmentation of solution heat exchanger effectiveness (0.73 in VARS to 0.77 in MVARS). An increase in temperature of the generator (84.86 to 88.19 ℃), condenser (39.99 to 44.22 ℃), evaporator (8.55 to 9.46 ℃), and absorber (35.59 to 36.94 ℃) is observed in MVARS. These

TH-3395_176107002

higher heat exchanger operating temperatures are obtained as the optimal values from the algorithm (s-TLBO) for the minimum annual cost of plant operation (14481.31 $/year), and it is comparatively higher than VARS (14435.57 $/year). A larger total exchanger area in MVARS [550.99 m^2 in VARS to 696.41 m^2 in MVARS] due to increased operating temperatures of exchangers leads to an increase in the total annual plant operation cost. Exergy destruction can be reduced with well-maintained equipment, which will again increase the total annual cost of the plant operation. For the current problem, the input values of hot stream, coolant, and economic parameters are given in Appendix –B (Table B1).

Table 3. 1 Model validation and single objective optimization of VARS and MVARS

Decision Variables/Parameters	**Rubio-Maya et al.** [182]	**Present work**	**VARS**	**MVARS**
	GAMS	**Model validation**	**sTLBO**	**sTLBO**
Generator temperature (T_1, °C)	84.8	84.8	84.86	88.19
Condenser temperature (T_2, °C)	39.8	39.8	39.99	44.22
Evaporator temperature (T_4, °C)	8.6	8.6	8.55	9.46
Absorber temperature (T_5, °C)	35.5	35.5	35.59	36.94
Effectiveness (ε)	0.707	0.707	0.73	0.77
Absorber coolant inlet temperature (T_{15}, °C)	NA	NA	NA	27
Generator hot stream inlet (T_{17}, °C)	NA	NA	NA	100
Generator hot stream outlet (T_{18}, °C)	NA	NA	NA	99
Condenser coolant outlet temperature (T_{12}, °C)	NA	NA	NA	40
Mass flowrate of absorber coolant (m_{11}, kg/s)	NA	NA	NA	10
Total Exergy destruction (B_D, kW)	39.171	36.70	36.59	30.10
Minimum total annual cost (C_T, $/year)	14,993.9	14,439	14435.57	14481.31
Total area of heat exchanger (m^2)	558.81	551.15	550.99	696.41
System capital cost ($/year)	41, 718	41, 273	41,365.09	47,762.15
Coefficient of performance (COP)	0.7376	0.7774	0.7793	0.7757
Number of population	NA	NA	100	100
Number of generations	NA	NA	200	200

3.4. Results and discussions

3.4.1. Multi-objective optimization of VARS

The detailed procedure and conditions followed for the multi-objective optimization of the VARS model are shown in Fig. 3.3. Table 3.2 displays the total annual cost of plant operation and exergy destruction obtained from three different multi-objective algorithms (MOGA, MOPSO, and MOsTLBO). The corner points of a Pareto front (CP_1 and CP_2) provide the best

TH-3395_176107002

objective functions in at least one of the multiple objectives (Table 3.3). It is shown that CP_1 provides maximum annual operating cost and minimum exergy destruction (desired objective function), whereas CP_2 provides minimum annual operating cost (desired objective function) and maximum exergy destruction. Decision variables are generator temperature T_1 (°C), condenser temperature T_2 (°C), evaporator temperature T_4 (°C), absorber temperature T_5 (°C), and effectiveness of heat exchanger (ε). The optimal values of decision variables for a multi-objective optimization problem obtained using MOsTLBO are discussed here as a representative case. It is noted that the minimum and maximum exergy destruction obtained from the Pareto front is 34.29 kW (CP_1) and 36.47 kW (CP_2), respectively.

The total annual cost corresponding to the minimum and maximum exergy destruction is 15269.66 $/year ($CP_1$) and 14437.42 $/year ($CP_2$), respectively. The generator temperature and the condenser temperature are increased from 80.06 (CP_1) to 84.47°C (CP_2) and 35.68 (CP_1) to 39.96 °C (CP_2), respectively. However, evaporator and absorber temperatures decrease from 9.98 (CP_1) to 8.55 °C (CP_2) and 36.69 (CP_1) to 35.37 °C (CP_2), respectively with a decrease in total annual cost. Similarly, the effectiveness of the heat exchanger increases from 0.73 (CP_2) to 0.85 (CP_1) with a decrease in exergy destruction. This higher cost of 832 $/year has to be paid for a reduction in exergy destruction from 36.47 kW to 34.29 kW. An increase in generator and condenser temperature increases the mass flow rate of refrigerant strong and weak solutions leading to a higher heat load on the absorber and generator. The increased mass flow rates of hot and cold utilities result in higher exergy destruction. On the other hand, higher effectiveness leads to lower LMTD and heat exchanger area, which causes lower heat load. Exergy destruction indicates the non-availability of useful energy to the system and it can be reduced with well-maintained equipment.

Reduction in exergy destruction decreases the cost due to the fuel supply of the system as the exergy input to the plant is decreased. On the other hand, a reduction in exergy destruction increases the system capital cost of plant operation (41494.08 to 47736.89 $/year) due to the larger size of the exchangers (552.79 to 719.69 m^2). The tradeoff between the cost due to the fuel supply of the system and the system capital cost determines the total annual cost of the system. MOGA determines the minimum annual cost, whereas minimum exergy destruction is reported by MOPSO. However, MOsTLBO reports the minimum total annual cost of plant operation 15269.7 $/year for the given minimum exergy destruction of 34.29 kW by effectively capturing the lesser operating temperature of the absorber (36.69 °C), when compared to other algorithms (MOGA and MOPSO).

TH-3395_176107002

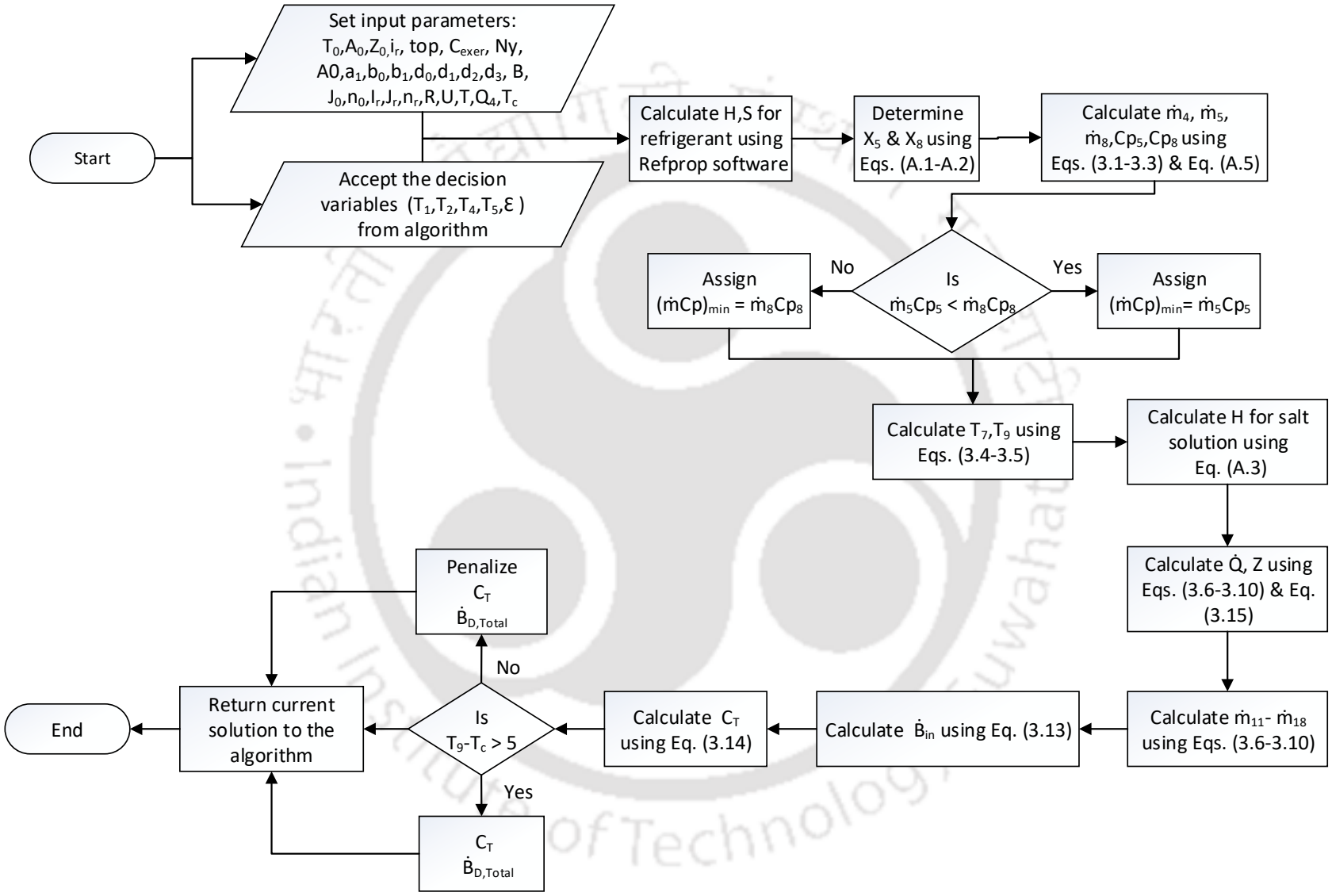

Fig. 3. 3 Flow chart for basic single-stage vapor absorption refrigeration system (VARS)

TH-3395_176107002

Table 3. 2 Multi-objective optimization of VARS

Decision Variables and Parameters	MOGA	MOPSO	MOsTLBO
Generator temperature (T_1, °C)	80.85	80	80.06
Condenser temperature (T_2, °C)	35.04	35	35.68
Evaporator temperature (T_4, °C)	9.98	10	9.98
Absorber temperature (T_5, °C)	37.61	38.89	36.69
Effectiveness (ε)	0.88	0.9	0.85
Minimum total exergy destruction ($B_{D,\,min}$, kW)	34.19	34.04	34.29
Total annual cost corresponding to $B_{D,\,min}$ (C_T, $/year)	15628.25	15910.93	15269.66
System capital cost corresponding to $B_{D,\,min}$ ($/year)	49635.62	51189.91	47736.89
Total area of heat exchanger corresponds to $B_{D,\,min}$ (m^2)	780.00	819.92	719.69
Maximum total exergy destruction ($B_{D,\,max}$, kW)	36.59	36.57	36.47
Total annual cost corresponding to $B_{D,\,max}$ (C_T, $/year)	14435.57	14437.13	14437.42
System capital cost corresponding to $B_{D,\,max}$ ($/year)	41367.57	41394.97	41494.08
Total area of heat exchanger corresponds to $B_{D,\,max}$ (m^2)	551.05	551.78	552.79
Coefficient of performance (COP)	0.8231	0.8258	0.8211
Weak solution concentration (X_5 in %)	53.41	54.13	52.88
Strong solution concentration (X_8 in %)	60.67	60.40	60
Population size	100	100	100
Maximum generations	200	200	200

Boldface fonts in Table 3.3 show the minimum total annual cost of plant operation and minimum exergy destruction obtained by each algorithm, while the **Boldface red fonts** represent the maximum total annual cost of plant operation obtained for minimum exergy destruction in each case (Table 3.3).

TH-3395_176107002

Table 3. 3 Corner points of Pareto front for VARS

Decision variables and parameters	MOGA		MOPSO		MOsTLBO	
	CP_1	CP_2	CP_1	CP_2	CP_1	CP_2
Generator temperature (°C)	80.85	84.85	80	84.95	80.06	84.47
Condenser temperature (°C)	35.04	39.99	35	40.26	35.68	39.96
Evaporator temperature (°C)	9.98	8.55	10	8.68	9.98	8.55
Absorber temperature (°C)	37.61	35.59	38.89	35.57	36.69	35.37
Effectiveness (ε)	0.88	0.73	0.9	0.73	0.85	0.73
Min. total annual Cost ($/year)	**15628.3**	**14435.6**	**15910.9**	**14437.1**	**15269.7**	**14437.4**
Min. Exergy destruction (kW)	**34.19**	36.59	**34.04**	36.57	**34.29**	36.47

3.4.1.1. Convergence of Pareto fronts

Fig. 3.4 shows the convergence of the Pareto front obtained by all the algorithms at specified iterations (50^{th}, 100^{th}, 150^{th}, and 200^{th} iterations) of their best run. An evident improvement in the convergence of the non-dominated solutions is observed in Fig. 3.4. The number of non-dominated points in the region of minimum exergy destruction (and maximum annual cost) is lesser than the region of minimum annual cost (and maximum exergy destruction). Hence the number of choices for interested users in solutions with minimum exergy destruction is less. Moreover, MOsTLBO determined fewer points in the region of minimum exergy destruction. Among all the considered algorithms, MOGA has provided more points in its Pareto front, followed by MOPSO. However, the lack of points in the Pareto front does not infer the quality of the points, while the quality of the Pareto front can be analyzed only with the help of various performance metrics.

(a)

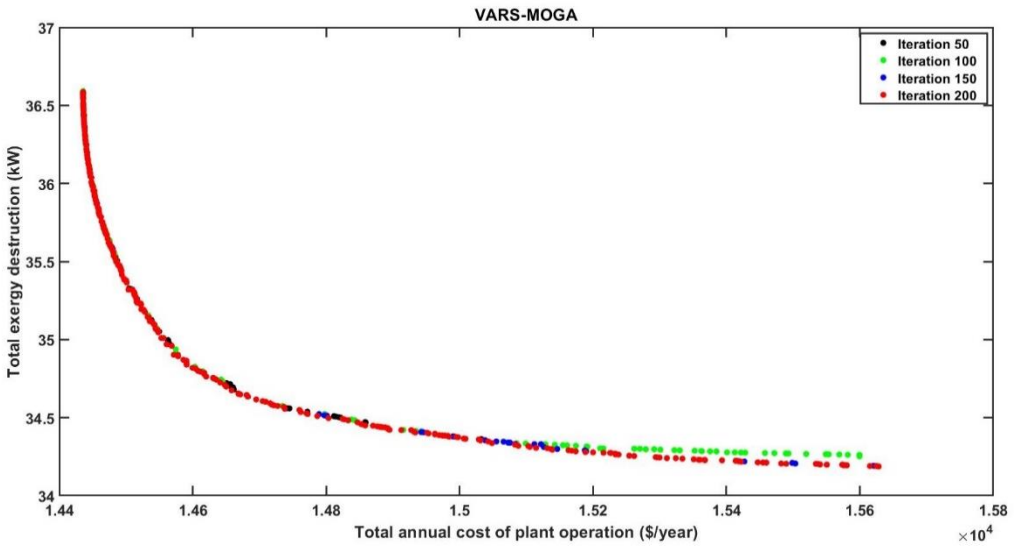

TH-3395_176107002

(b)

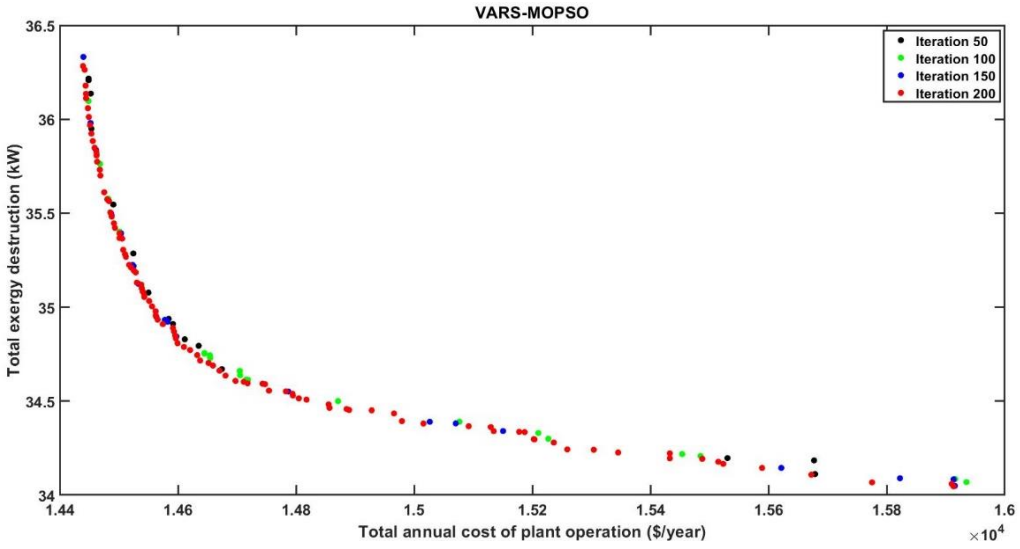

(c)

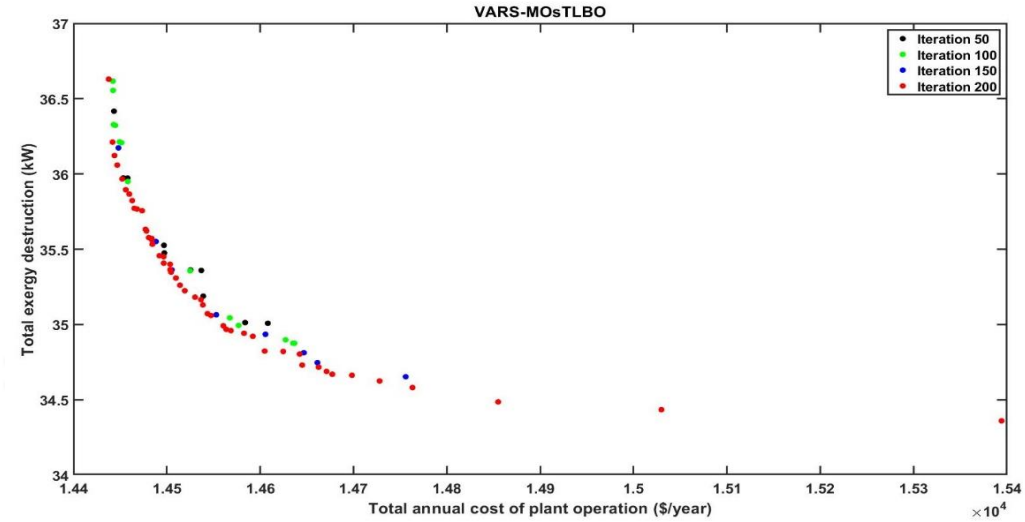

Fig. 3. 4 Convergence of Pareto front obtained by (a) MOGA (b) MOPSO and (c) MOsTLBO on the best run

3.4.1.2. Pareto and Global Pareto fronts

Fig. 3.5 (a, c, and e) show the Pareto front obtained in all five runs, and the plots of Fig. 3.5 (b, d, and f) show the global Pareto front obtained by each algorithm. The global Pareto corresponding to each algorithm is identified by performing the non-dominated sorting method on the set of non-dominated points determined in all the runs. It is found that each run of all the algorithms is converged to its global Pareto front in the region representing minimum total annual cost (and maximum exergy destruction). At the same time, such a trend is not observed in the other region, indicating the minimum exergy destruction (and maximum total annual cost). The number of non-dominated solutions determined by MOsTLBO in all the runs is lesser than MOGA and MOPSO.

TH-3395_176107002

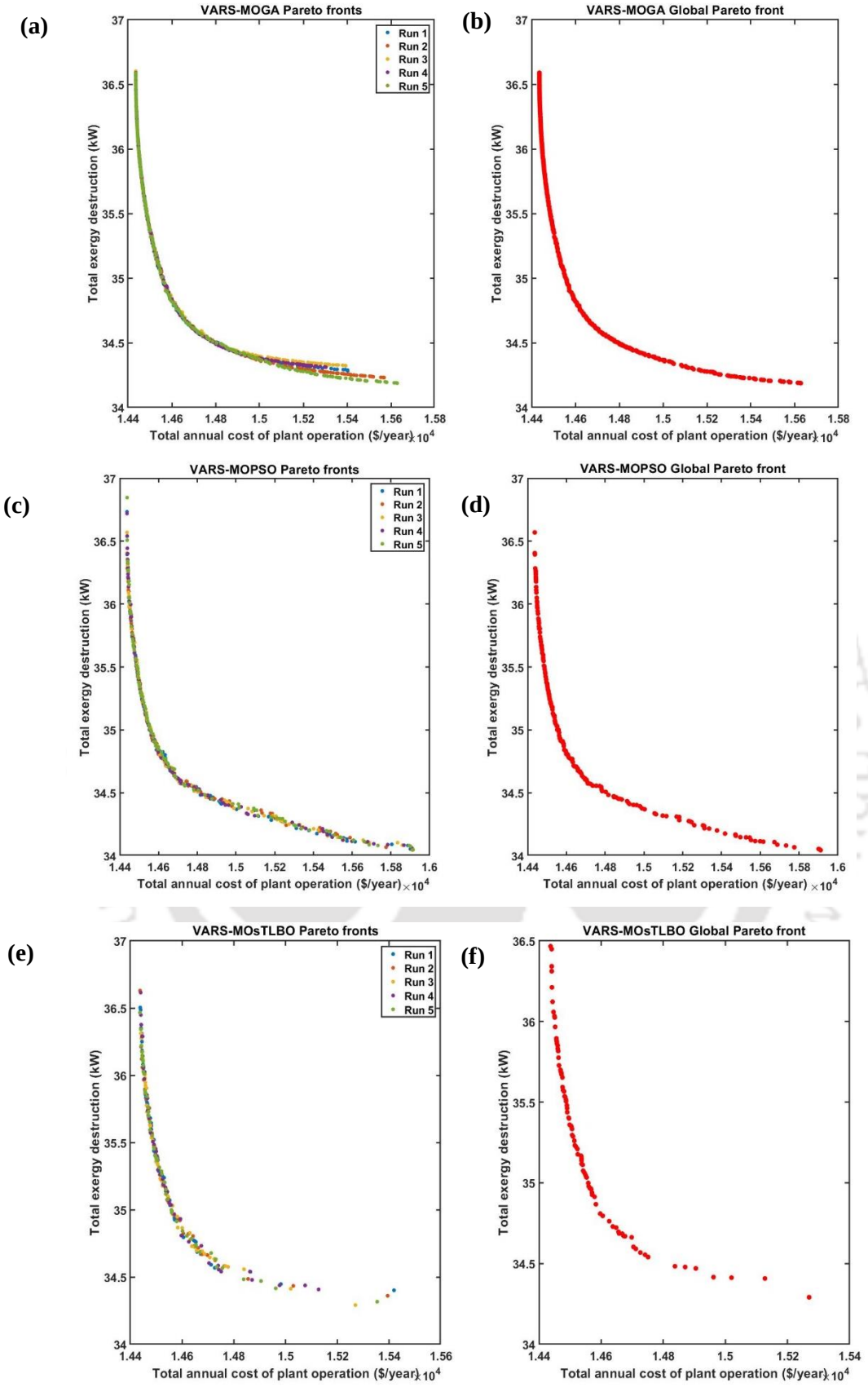

Fig. 3. 5 Pareto front (a, c and e) and the corresponding global Pareto front (b, d and f) obtained by MOGA, MOPSO and MOsTLBO

TH-3395_176107002

It is noticed from Fig. 3.5 (a) that run 5 of MOGA is dominating a few points of other runs in the region with minimum exergy destruction. In contrast, such a conclusion could not be depicted from MOPSO and MOsTLBO. All the runs of MOPSO explored the complete Pareto front, while in the case of MOGA and MOsTLBO, it was found that a few runs could not identify any single point in the extreme region with minimum exergy destruction. Moreover, the Pareto front determined by MOsTLBO lacks evenness as well as the spread in all the runs.

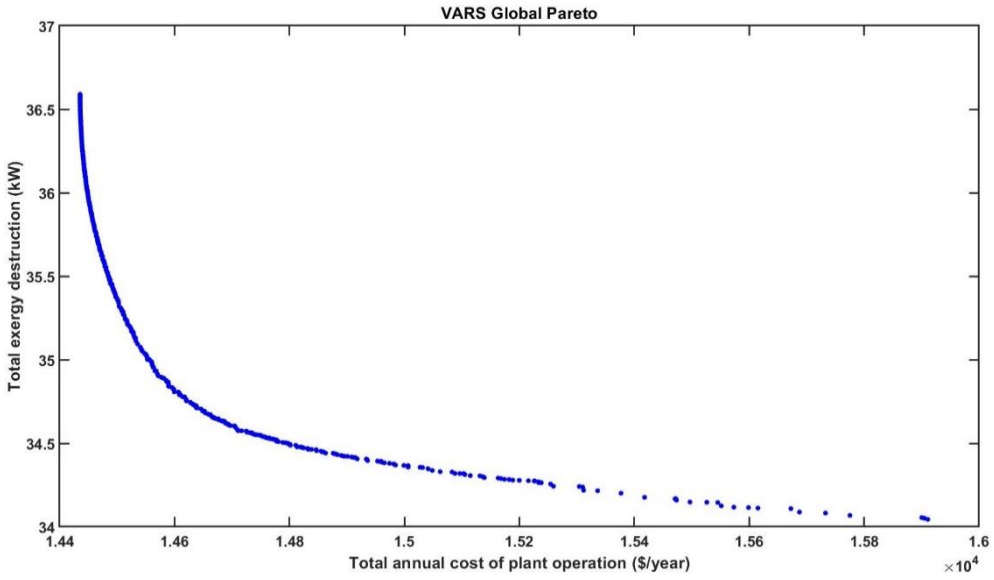

Fig. 3. 6 Global Pareto front obtained by all the algorithms (MOGA, MOPSO and MOsTLBO)

The global Pareto front determined using the non-dominated sorting method performed on all the non-dominated points obtained by every algorithm in all the runs is shown in Fig. 3.6. It is found that the number of Pareto points is decreasing from the region with a minimum annual cost to minimum exergy destruction. The same trend is also evident in Fig. 3.4 and Fig 3.5, which depict that all the considered algorithms could find very few non-dominated solutions in the minimum exergy destruction (maximum total annual cost) region.

3.4.1.3. Inverted generation distance

The global Pareto determined by considering the non-dominated solutions obtained by all the algorithms in each run is treated as the reference points (true Pareto) for calculating the IGD. The IGD of the final Pareto reported by an algorithm in all runs is determined, and the run corresponding to the minimum IGD is considered as the best run. The IGD versus iteration of an algorithm in its best run is depicted in Fig. 3.7. This plot helps in identifying the closeness and diversity of the Pareto points determined by an algorithm in each iteration to the true Pareto front. It is noted that a well-distributed set of non-dominated solutions is not guaranteed as the

TH-3395_176107002

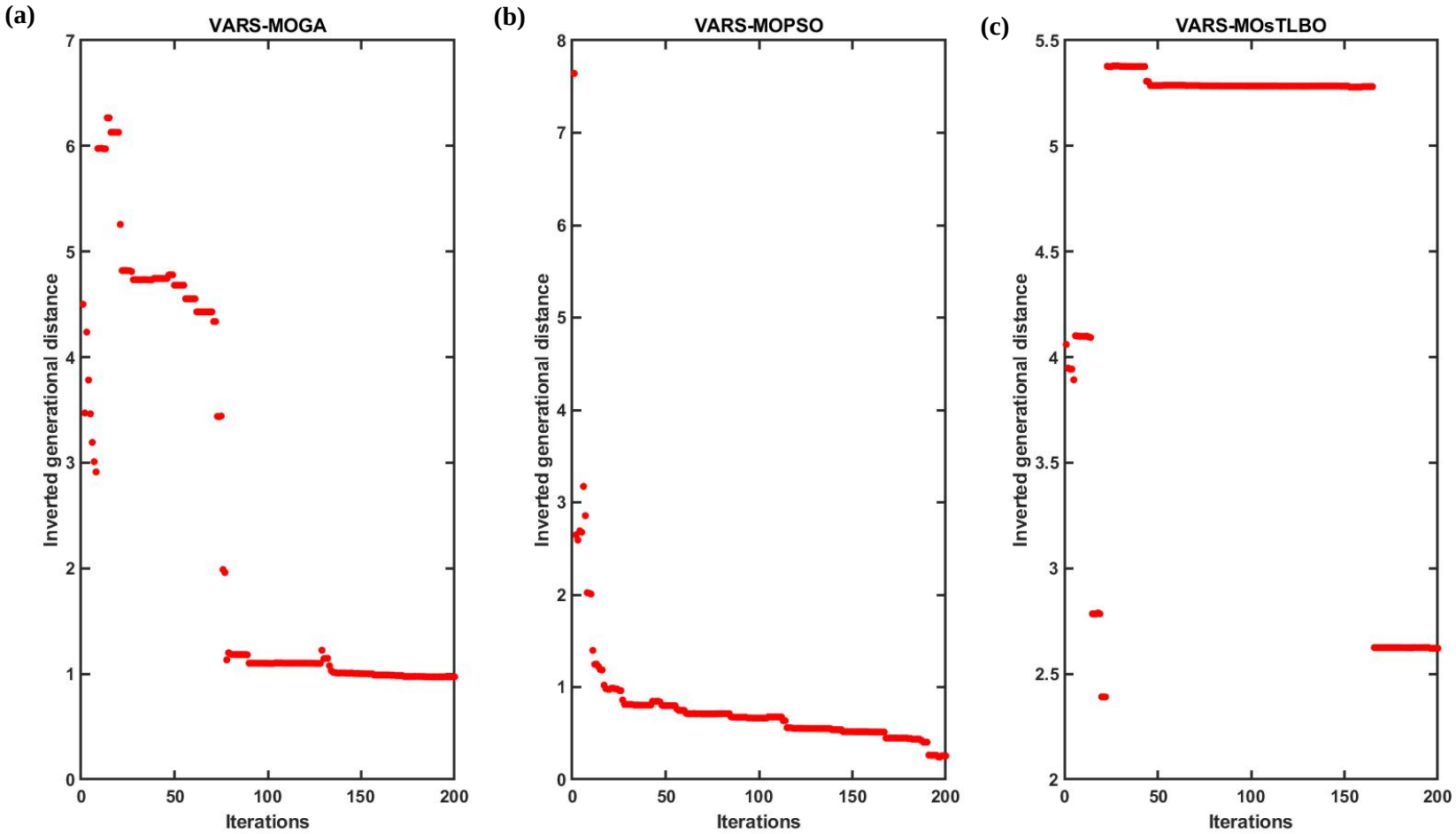

Fig. 3. 7 IGD obtained in the best run of (a) MOGA (b) MOPSO and (c) MOsTLBO

TH-3395_176107002

iteration proceeds. There may arise a situation such that a single point in the Pareto front of the current iteration can dominate multiple points in a region of the Pareto front of the previous iteration. Due to this scenario, there would not exist a monotonic convergence of IGD over iterations. It is found that the IGD obtained by all algorithms is not monotonically decreasing with iterations. MOPSO has determined the least IGD compared to MOGA and MOsTLBO at the end of 200 iterations. It implies that the Pareto front obtained in the best run of MOPSO contains better-converged solutions.

3.4.2. Multi-objective optimization of MVARS

The flowsheet representing the various steps and conditions employed for the multi-objective optimization of the MVARS model is provided in Fig. 3.8. Table 3.4 displays the total annual cost of plant operation and exergy destruction obtained from three different multi-objective algorithms (MOGA, MOPSO, and MOsTLBO). The corner points of a Pareto front (CP_1 and CP_2) provide the best objective functions in at least one of the multiple objectives (Table 3.5). It should be noted that CP_1 provides maximum annual operating cost and minimum exergy destruction (desired objective function), whereas CP_2 provides minimum annual operating cost (desired objective function) and maximum exergy destruction. In contrast to VARS, MVARS uses the outlet coolant stream of absorber ($\dot{m}_{16}$) as an inlet coolant stream to the condenser ($\dot{m}_{11}$) which is a representative case for effective utilization of available energy resources. Decision variables for MVARS are generator temperature, T_1 (°C), condenser temperature, T_2 (°C), evaporator temperature, T_4 (°C), absorber temperature, T_5 (°C), the temperature of absorber coolant inlet stream, T_{15} (°C), condenser coolant outlet stream, T_{12} (°C), hot and cold streams of the generator, T_{17} and T_{18} °C), mass flow rate of coolant, $\dot{m}_{11}$ (kg/s), and effectiveness of heat exchanger (ε).

The optimal decision variables using MOGA, MOPSO, and MOsTLBO for minimizing the exergy destruction and total annual cost of MVARS are shown in Table 3.4. Similar to VARS, the optimal values obtained using s-TLBO are discussed here as a representative case. It is noted that the minimum and maximum exergy destruction obtained from the Pareto front is reported as 28.44 kW (CP_1) and 30.31 kW (CP_2), respectively, and the corresponding total annual cost is 15163.43 $/year ($CP_1$) and 14578.58 $/year ($CP_2$), respectively. The concentration, as well as mass flow rate of the strong, weak solution and the refrigerant, are affected by changes in the evaporator, absorber, generator, and condenser temperatures. This further increases the heat load of the absorber and generator. Heat load determined for absorber and generator are lower for 28.44 kW (CP_1) than in the case of 30.31 kW (CP_2). The change in

TH-3395_176107002

heat load impacts the area of the heat exchangers and the mass flow rate of hot utilities used for the generator, which further leads to a change in exergy destruction. A decrease in exergy destruction increases the effectiveness of the solution heat exchanger, thereby reducing its size and investment cost.

Table 3. 4 Multi-objective optimization of MVARS

Decision Variables and Parameters	MVARS		
	MOGA	MOPSO	MOsTLBO
Generator temperature (T_1,°C)	87.15	88.26	87.76
Condenser temperature (T_2,°C)	41.20	41.07	41.78
Evaporator temperature (T_4,°C)	9.99	10	10
Absorber temperature (T_5, °C)	36.30	38.04	35.50
Effectiveness (ε)	0.87	0.9	0.86
Absorber coolant inlet temperature (T_{15}, °C)	27.01	27	27.00
Generator hot stream inlet (T_{17}, °C)	100.01	100	100
Generator hot stream outlet (T_{18},°C)	98.91	97.84	99
Condenser coolant outlet temperature (T_{12}, °C)	40.00	40	40
Mass flowrate of absorber coolant ($m_{11,}$ kg/s)	10.00	10	10
Minimum total exergy destruction ($B_{D,min}$, kW)	28.39	28.35	28.44
Maximum total annual cost corresponding to $B_{D,min}$ (C_T, $/year)	15301.13	15532.05	15163.43
System capital cost corresponding to $B_{D,min}$ ($/year)	53501.01	54697.08	52759.24
Total area of heat exchanger corresponds to $B_{D,min}$ (m^2)	859.17	894.66	832.02
Maximum total exergy destruction ($B_{D,max}$, kW)	30.43	30.58	30.31
Miniimum total annual cost corresponding to $B_{D,max}$ (C_T, $/year)	14561.14	14562.65	14578.58
System capital cost corresponding to $B_{D,max}$ ($/year)	47851.35	47715.12	48053.22
Total area of heat exchanger corresponds to $B_{D,max}$ (m^2)	699.19	695.31	704.14
Coefficient of performance (COP)	0.8037	0.8041	0.8025
Weak solution concentration (X_5 in %)	52.65	53.65	52.18
Strong solution concentration (X_8 in %)	60.29	60.89	60.25
Population size	100	100	100
Maximum generations	200	200	200

TH-3395_176107002

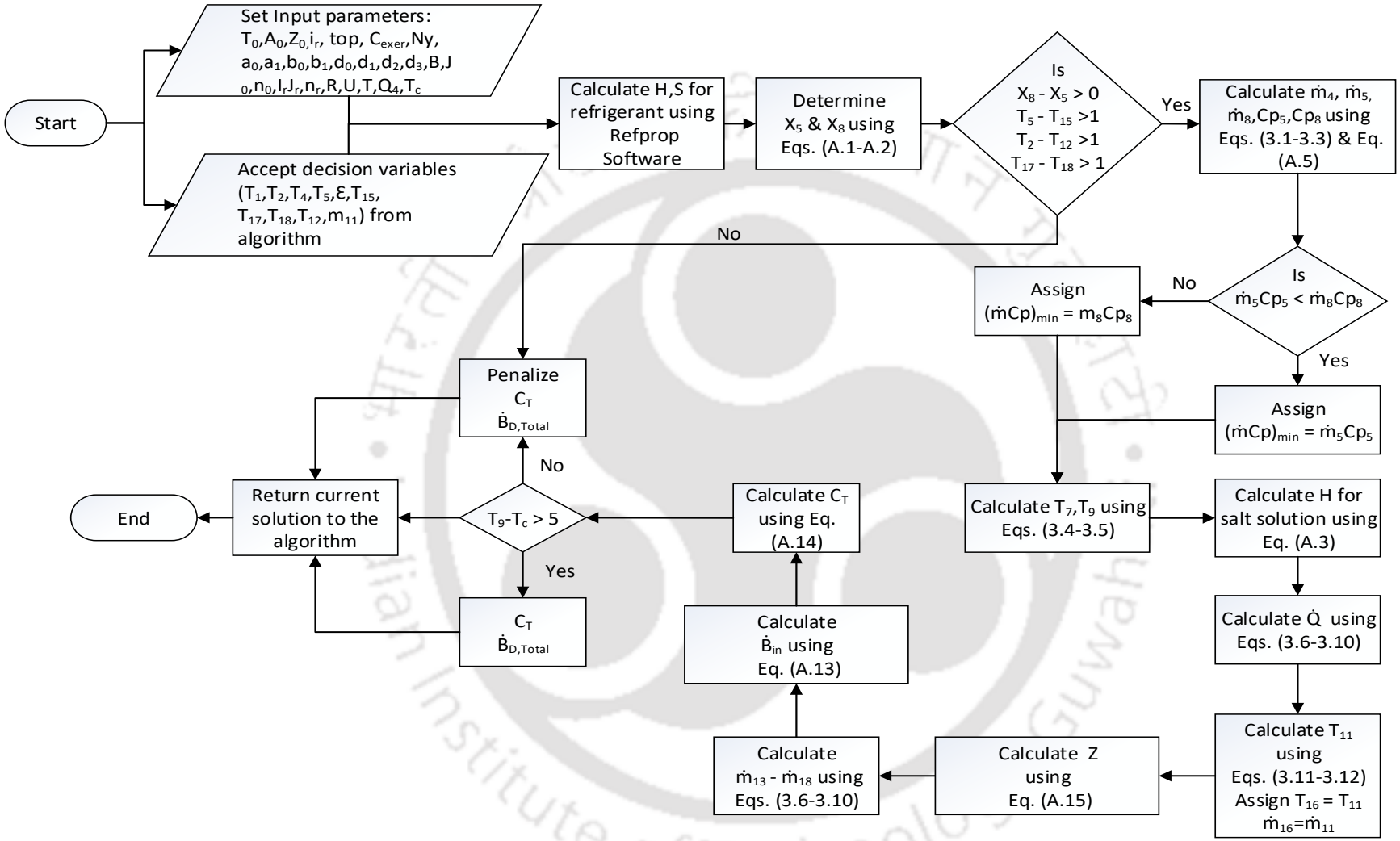

Fig. 3. 8 Flow chart for modified single-stage vapor absorption refrigeration system (MVARS)

TH-3395_176107002

It is noted that the optimal exergy destruction is decreased from 34.29 kW (CP_1) to 28.44 kW (CP_1) for MVARS when compared to VARS (Tables 3.3 and 3.5). It also decreases the optimal value of the total annual cost of plant operation to 15163.43 $/year (CP1) for MVARS (Table 3.5) compared to 15269.66 $/year ($CP_1$) for VARS (Table 3.3). Despite the increase in the capital cost of plant operation (47736.89 $/year (Table 3.2) to 52759.24 $/year (Table 3.4)) due to the larger size of the exchangers (719.69 m^2 (Table 3.2) to 832.02 m^2 (Table 3.4)), MVARS reports the lesser total annual cost of plant operation.

Table 3. 5 Corner points of Pareto fronts for MVARS

Decision variables and Parameters	MOGA		MOPSO		MOsTLBO	
	CP_1	**CP_2**	**CP_1**	**CP_2**	**CP_1**	**CP_2**
Generator temperature (°C)	87.15	88.04	88.26	87.94	87.76	87.89
Condenser temperature (°C)	41.2	44.12	41.07	44.24	41.78	43.81
Evaporator temperature (°C)	9.99	9.55	10	9.5	10	9.39
Absorber temperature (°C)	36.3	36.89	38.04	36.83	35.5	36.44
Effectiveness (ε)	0.87	0.78	0.9	0.78	0.86	0.78
Absorber coolant inlet temperature (°C)	27.01	27.01	27	27	27	27
Generator hot stream inlet (°C)	100.01	100.01	100	100.02	100	100.1
Generator hot stream outlet (°C)	98.91	98.99	97.84	99	99	99
Condenser coolant outlet temperature (°C)	40	40	40	39.99	40	40
Mass flow rate of absorber coolant (kg/s)	10	10	10	10	10	10
Min Cost ($/year)	**15301.1**	**14561.1**	**15532.1**	**14562.7**	**15163.4**	**14578.6**
Min Exergy Destruction (kW)	**28.39**	30.43	**28.35**	30.58	**28.44**	30.31

The corner points (CP_1 and CP_2) reported by all the algorithms are non-dominated solutions except CP_2 of MOPSO, which is dominated by CP_2 of MOGA. This implies that the Pareto front reported by MOGA is more converged to the global Pareto front than MOPSO for MVARS (Table 3.5). Boldface fonts show the minimum total annual cost of plant operation and minimum exergy destruction obtained by each algorithm, whereas the Boldface red fonts indicate the maximum total annual cost of plant operation obtained for minimum exergy destruction in each case (Table 3.5). This lower cost is attributed to effective cold water utilization in the condenser and absorber, which decreased the coolant mass flow rate in the condenser and absorber from 19.37 kg/s and 16.54 kg/s, respectively to 10 kg/s (Tables 3.2 and 3.4). However, MOsTLBO reports the minimum total annual cost of plant operation of 15163.43 $/year ($CP_1$) for the given minimum exergy destruction of 28.44 kW (CP_1) by

TH-3395_176107002

effectively capturing the lesser operating temperature of the absorber (35.50 °C) when compared to MOGA and MOPSO (Tables 3.4 and 3.5)

3.4.2.1. Convergence of Pareto fronts

Fig. 3.9 shows the convergence of the Pareto front obtained by all the considered algorithms at the specified iterations (50th, 100th, 150^{th,} and 200th iterations) of their best run for MVARS. It has been observed that till the 25th iteration, the algorithms have not explored the whole region of the Pareto front. As the iteration proceeds, all the algorithms follow the structure of the global Pareto.

(a)

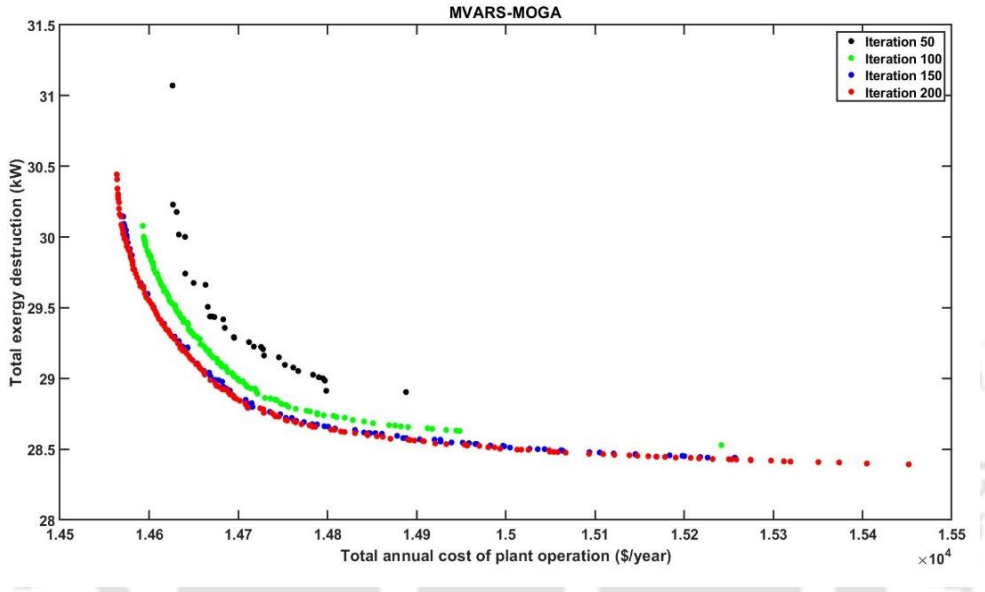

(b)

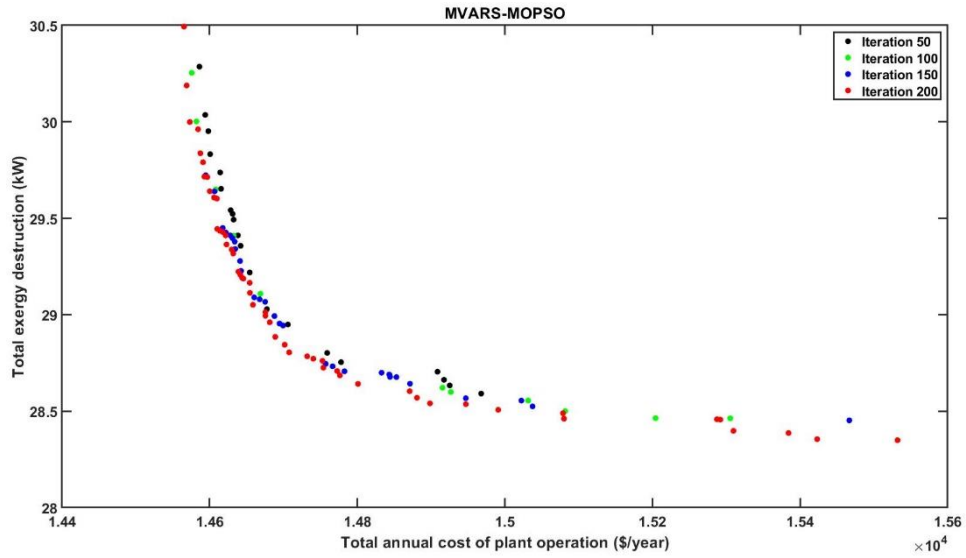

TH-3395_176107002

(c)

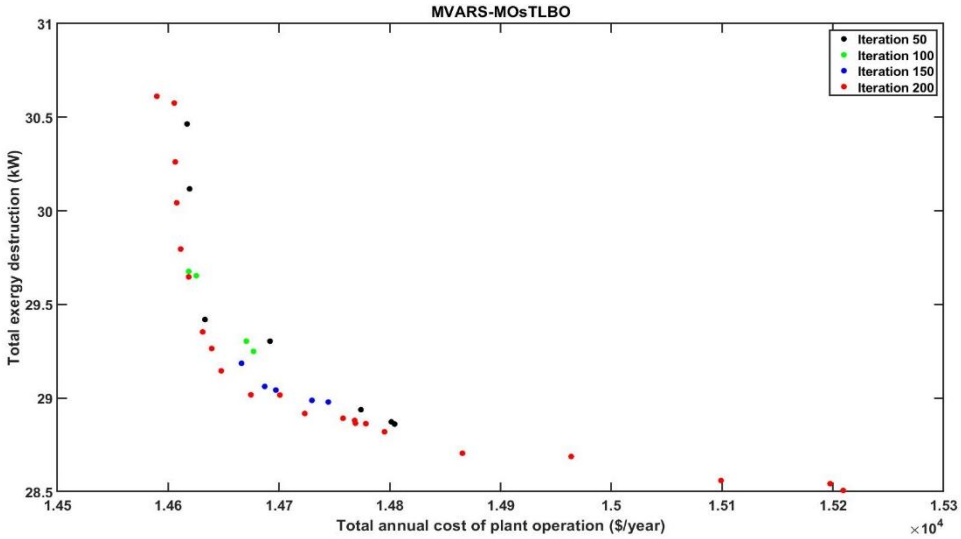

Fig. 3. 9 Convergence of Pareto front obtained by (a) MOGA (b) MOPSO and (c) MOsTLBO on the best run

3.4.2.2. Pareto and Global Pareto fronts

Similar to VARS, the number of non-dominated points in the region indicating minimum exergy destruction (and maximum annual cost) is lesser than the region representing the minimum annual cost (and maximum exergy destruction) for MVARS. It is also evident that there is no single run of all algorithms that obtained all the non-dominated points of its global Pareto. Fig. 3.10 provides the Pareto front obtained in all five runs and the global Pareto front corresponding to each algorithm for MVARS. In contrast to VARS, each run of all the algorithms is not converged to its global Pareto front in the region representing minimum total annual cost (and maximum exergy destruction).

At the same time, such a trend is not observed in annual cost (and maximum exergy destruction). the other region, indicating the minimum exergy destruction (and maximum total annual cost). The global Pareto front of all non-dominated points obtained by every algorithm in all the runs is shown in Fig. 3.11. The diversity of the points at the two extreme regions of the global Pareto is lesser than the interior part. The global Pareto presented in Fig. 3.11 shows a smaller number of points than the Pareto front reported by MOGA in Fig. 3.9, which indicates that only a few points in the Pareto front are determined by MOPSO or MOsTLBO that dominates the Pareto points of MOGA.

TH-3395_176107002

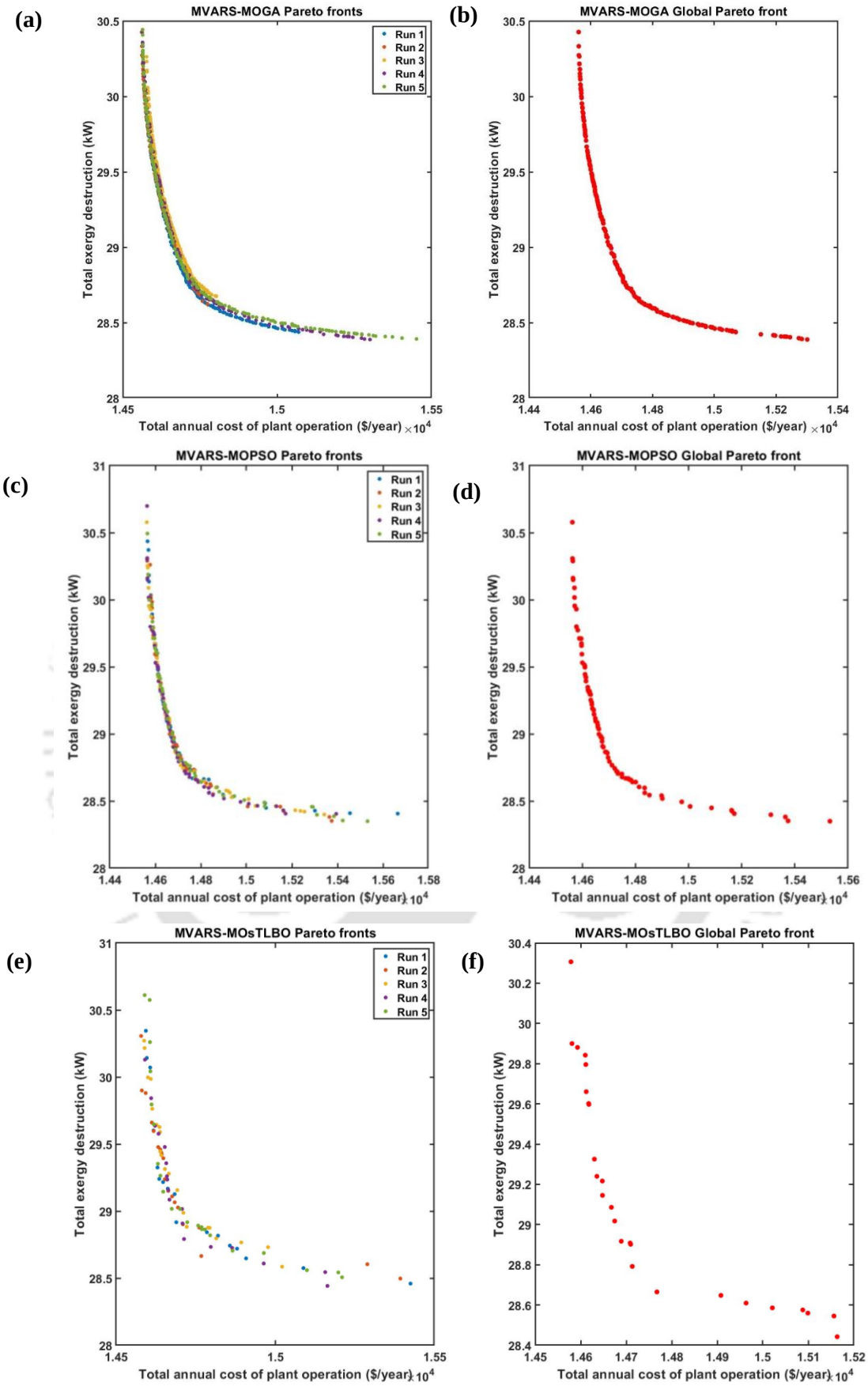

Fig. 3. 10 Pareto front (a, c and e) and the corresponding global Pareto front (b, d, and f) obtained by MOGA, MOPSO, and MOsTLBO

TH-3395_176107002

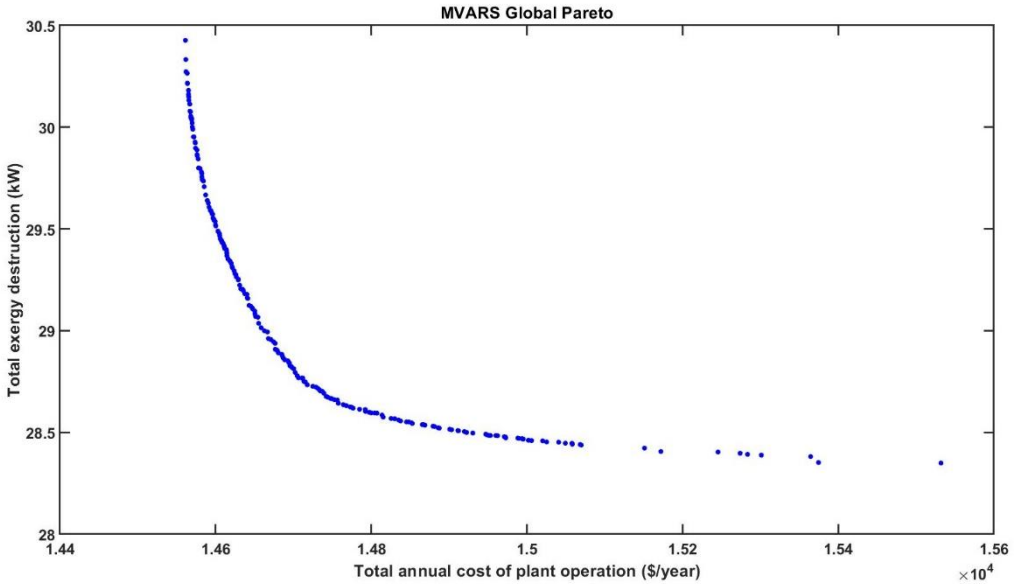

Fig. 3. 11 Global Pareto front obtained by all the algorithms (MOGA, MOPSO, and MOsTLBO)

3.4.2.3. Inverted generational distance

The inverted generational distance over the iteration of the Pareto front determined by all algorithms corresponding to their best run is provided in Fig. 3.12. Similar to VARS, IGD are not monotonically decreasing with the iterations. However, the final IGD reported by all the algorithms is the least value among all iterations indicating that the final Pareto of all algorithms constitutes more diversified solutions than other iterations. The IGD reported in the initial iteration of MOGA is much larger than the IGD of MOPSO and MOsTLBO, which indicates that the non-dominated solutions determined by MOGA in the initial iteration are poor in convergence as well as in diversity. However, as the iteration increases, MOGA also reported an IGD comparable to the final IGD reported by MOPSO.

3.5. Closure

In the present work, multi-objective optimization of single effect LiBr-H_2O Vapor Absorption Refrigeration System (VARS) and Modified VARS (MVARS) were addressed using multi-objective genetic algorithm (MOGA), multi-objective particle swarm optimization (MOPSO), and multi-objective sanitized teaching learning-based optimization (MOsTLBO) techniques. Two separate coolant streams are used for the absorber and condenser in VARS, while MVARS uses the outlet coolant stream of the absorber as an inlet coolant stream to the condenser. Minimization of total annual operating cost and exergy destruction was considered as multi-objective functions. In order to optimize the total annual cost and exergy destruction of the system, the system and economic model proposed by Rubio-Maya [182] were used with certain

TH-3395_176107002

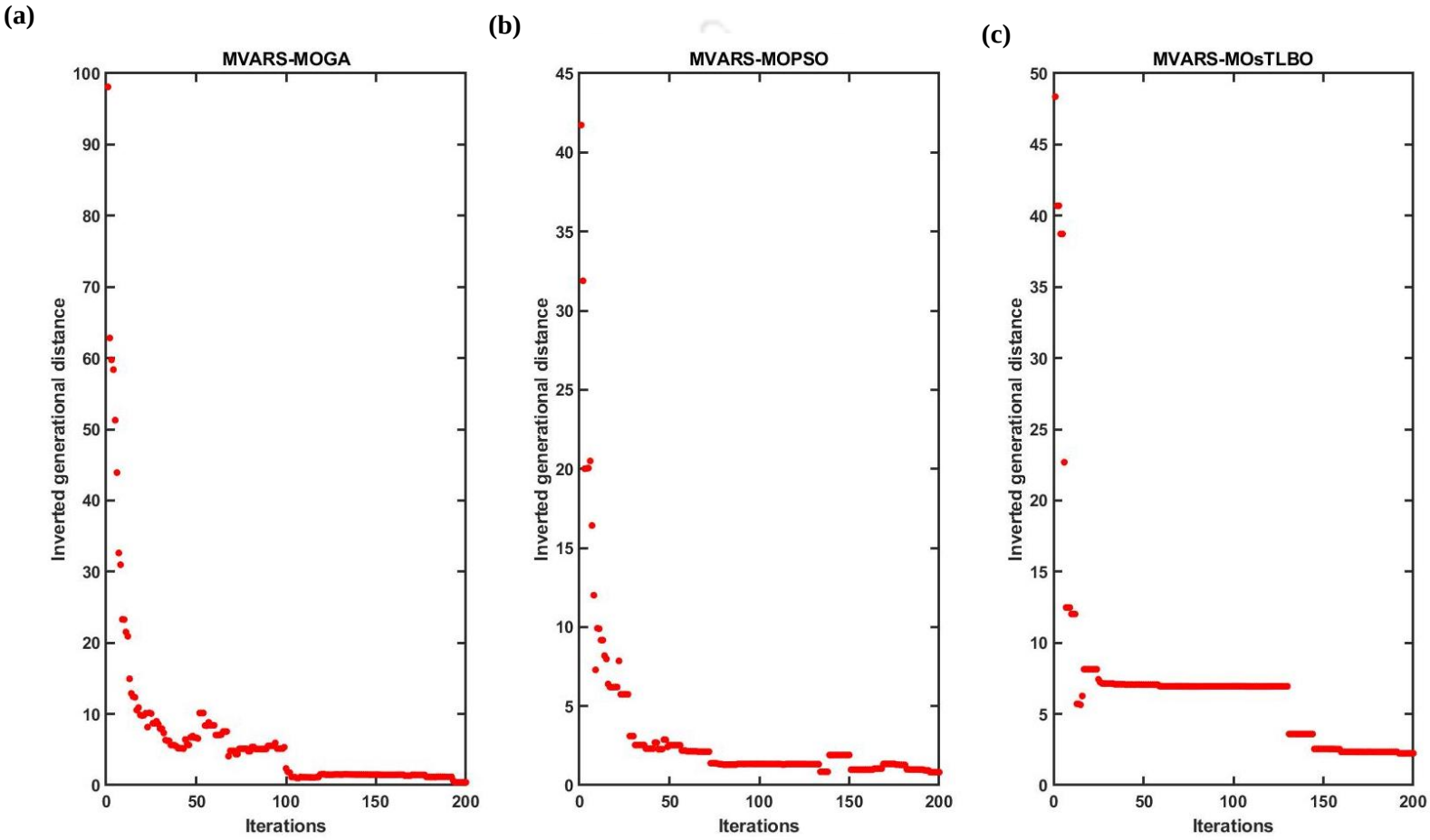

Fig. 3. 12 IGD obtained in the best run of (a) MOGA (b) MOPSO and (c) MOsTLBO for MVARS

TH-3395_176107002

modifications. The results of Rubio-Maya [182] were compared with a single objective sTLBO metaheuristic technique. The following major conclusions obtained from multi-objective optimization of VARS and MVARS are stated as follows:

- The optimization of single-effect LiBr-H_2O ARS using the annual operating cost and exergy destruction to be minimized under the multi-objective optimization methods based on metaheuristic techniques is feasible. Hence, it can be expressed that the ARS model is naturally flexible in solving a multi-objective optimization problem, an alternative approach to single-objective optimization.
- Minimizing exergy destruction is a useful tool in the design and optimization of ARS, from which the design and operating parameters can be identified to have highly efficient system components in terms of exergy destruction.
- It is concluded that the tradeoff between cost due to the fuel supply of the system in terms of minimum exergy destruction and the system capital cost in terms of total heat exchanger area determines the total annual cost of the system.
- For VARS & MVARS, MOGA reports the lowest total annual cost for both cases, while MOPSO determines the lowest exergy destruction. Among VARS & MVARS, exergy destruction determined for MVARS is ~17% lesser, and the total annual cost is ~0.9% higher than conventional VARS.
- MOsTLBO reports the minimum total annual cost of plant operation for the given minimum exergy destruction by effectively tuning the operating temperature of the system components compared to other algorithms (MOGA and MOPSO) for both VARS and MVARS.
- The Pareto points obtained from multi-objective algorithms revealed that the number of non-dominated points in the region of minimum exergy destruction (and maximum annual cost) is lesser than in the region of minimum annual cost (and maximum exergy destruction).
- It is observed that IGDs are not monotonically decreasing with the iterations. IGD of MOPSO is lesser than MOGA and MOs-TLBO, implying that the Pareto front solutions obtained by MOPSO are better-convergence.

TH-3395_176107002

CHAPTER 4

Thermoeconomic optimization of cascade refrigeration system using metaheuristic techniques

4.1. Introduction

The literature survey shows that the compression absorption cascaded refrigeration system (CRS) produces more cooling using less electric energy consumption than classical VCRS for low-temperature cooling applications. CRS can be operated at lower evaporation temperatures, lower compression ratios, and higher volumetric compressor effectiveness, which are difficult to achieve in a single refrigeration system. It is also equally important to select a suitable refrigerant for CRS. An acceptable refrigerant pair would help for a considerable temperature elevation, thereby increasing system efficiency. Despite advantages such as lower electricity consumption and higher COP, CRS is more expensive and more complicated to build when compared to a single refrigeration system (VCRS or VARS). Moreover, the overlapping temperature between the condensing temperature of VCRS and the evaporating temperature of VARS, which is based on the heat transfer between two refrigeration cycles, affects the efficiency of CRS. Though CRS performs better than VCRS and VARS, its capital investment cost is higher, and the operating cost is lower when compared to conventional systems.

This chapter addresses the thermoeconomic optimization study of CRS using metaheuristic techniques and detailed thermodynamic and economic analysis. It is observed from the literature that thermoeconomic optimization of CRS with the salt mixture absorption pair ($CaCl_2$-LiBr-$LiNO_3$-H_2O) as a potential absorbent in VARS as other salts such as LiBr-H_2O suffers from the issue of crystallization [246] and its comparative study with other conventional absorbent pairs have not been addressed. Most of the optimization of the refrigeration systems includes the implementation of metaheuristic techniques such as GA or PSO. However, the current study considers five recent computational intelligence techniques to optimize the CRS.

The current study also considers the cost of cold utility consumed for absorber and condenser. The condenser and absorber temperatures have a significant impact on their respective heat load and corresponding mass flow rate of the cold utilities. Considering these two temperatures as decision variables for the system optimization also have an influence on the heat loads which also affects the utilities required to remove the heat load from the absorber and condenser to maintain the desired temperature. The coolant cost is an essential component in thermoeconomic analysis since it influences the operating cost of a system and may assist in

TH-3395_176107002

finding the potential for cost reductions; however, according to a literature survey, the coolant cost has not been considered yet for the CRS.

Hence, in the current chapter, the thermoeconomic optimization of LiBr-H_2O, LiCl-H_2O, $CaCl_2$-LiBr-$LiNO_3$-H_2O with R290 (Propane), R123 (2,2-Dichloro-1,1,1-Trifluoroethane), R1234yf (2,3,3,3-Tetrafluoropropene), and R1234ze (1,3,3,3-Tetrafluoropropene) in CRS is performed. Detailed energy, exergy, and economic analysis of all CRS components are reported. A nonlinear objective function is formulated for the minimization of the total annual cost (combination of electricity, input exergy, penalty, cold utility, and system capital costs) of CRS. Several metaheuristic techniques such as sanitized Teaching Learning Based Optimization (sTLBO) [26], Atom Search Optimization (ASO) [27], Coyote Optimization Algorithm (COA) [28], Yin-Yang Pair Optimization (YYPO) [30], and Tree Growth Algorithm (TGA) [29] are used to optimize CRS with various absorbent-refrigerant pairs. Optimum operating variables for minimum operating fuel, cold utility, and penalty cost (for CO_2 emission) using metaheuristic techniques and the effect of decision variables on the COP, total area, total annual cost, and exergy destruction are reported.

4.2. Thermoeconomic modelling and optimization of CRS

4.2.1. System description

The schematic of the CRS is shown in Fig. 4.1. In VCRS, R290/R123/R1234yf/ R1234ze were used as refrigerants, while in VARS, absorbent-refrigerant pairs of LiBr/LiCl/($CaCl_2$-LiBr-$LiNO_3$)-H_2O were used. The refrigerant in LTL (VCRS) enters the compressor (point 3) as a saturated vapor after extracting heat from the chilled water (points 21 and 22) in the evaporator (points 2-3). Compressed refrigerant (points 3-4) with high temperature and pressure is cooled in a cascade condenser, where heat is transferred to the evaporator of HTL (VARS), with a particular temperature of approach and sent back to the evaporator (point 2) through a pressure-reducing valve and the cycle repeats itself. Heat load released in cascade condenser is utilized in HTL (VARS) to heat the refrigerant to provide the cooling effect to LTL. The refrigerant in HTL gets evaporated (points 14-5) in the cascade condenser and passes through the HTL thermal compressor (points 5-12). The refrigerant then passes through the HTL condenser (points 12-13), where heat is released, causing the refrigerant to cool. The refrigerant then passes through the HTL throttling valve (points 13-14), where the fluid expands. The refrigerating effect is created only in the LTL evaporator, and the cascade refrigeration operates similarly to any regular refrigeration unit except for the second stage of operation (HTL: VARS). Hence, it is possible to operate CRS at a lower compression ratio and

TH-3395_176107002

higher volumetric efficiency in the compressor. In the thermal compressor, saturated refrigerant vapor from the evaporator mixes with the absorbent solution in the absorber, forming a weak absorbent solution (point 6). The solution is sent to the generator through the solution pump (point 7) and the heat exchanger (point 8) to increase the pressure and temperature. An external low-grade heat source (point 17) is provided to the generator for separating the refrigerant from the weak absorbent solution, and the strong absorbent solution from the generator (point 9) returns to the absorber through the solution heat exchanger (point 10) and pressure reducing valve (point 11). Separated refrigerant gets condensed (point 12) and leaves the condenser as a saturated liquid (point 13).

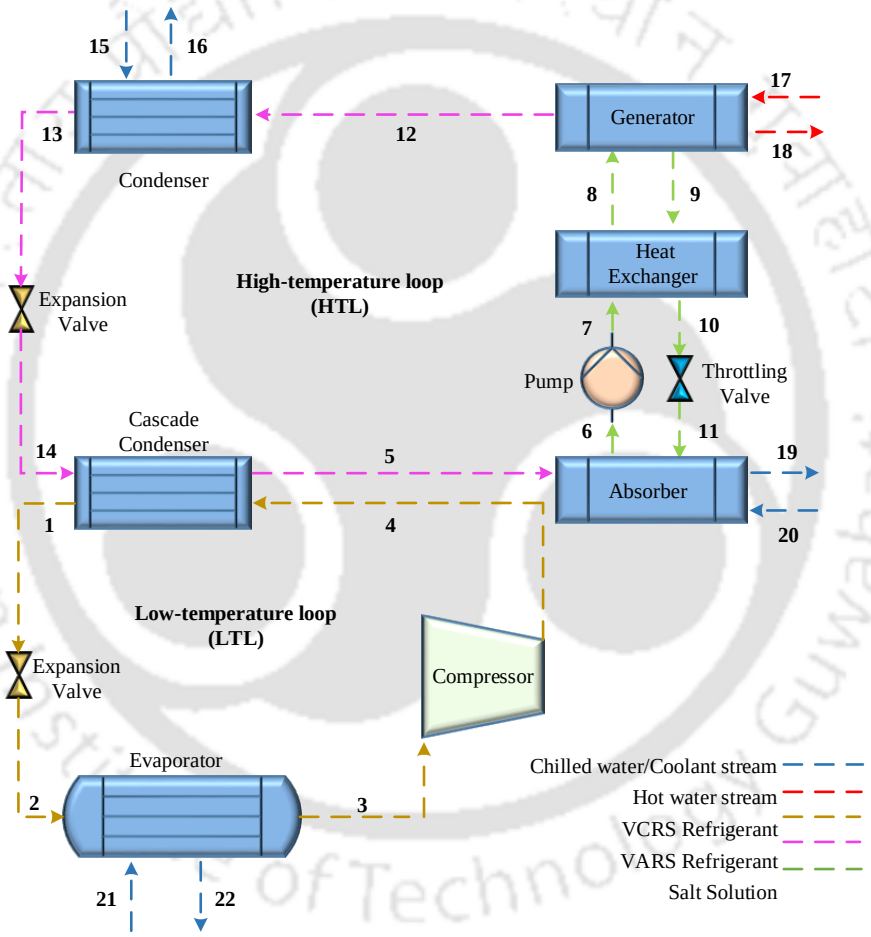

Fig. 4. 1 Schematic of Compression-absorption cascaded refrigeration system [195]

- **Model assumptions**

The energy and exergy analyses, which do not include kinetic and potential energies, are performed at a steady state. The refrigeration load given to the evaporator is 80.7 kW. Reference temperature and pressure are 298 K and 101.3 kPa, respectively. No heat exchange occurs between the system and surroundings other than whatever is mentioned in the analysis.

TH-3395_176107002

The heat source is low-grade steam. Temperature variation within the generator, condenser, cascade condenser, evaporator, and absorber are neglected. The temperature of the strong solution entering the solution expansion valve is always ensured at 5˚C above the crystallization temperature of the absorbent. Expansion valves are adiabatic. Pressure and heat losses in the components of CRS are neglected. Absorbent solutions in the generator and the absorber are in equilibrium, and thermodynamic properties are calculated as equilibrium values at their respective temperatures, pressures, and concentrations. The refrigerant exits the condenser and evaporator, and absorbent solutions exit the absorber, and the generator are at their saturated state. The energy required for other ancillary components of CRS is not considered in the analysis.

4.2.2. Thermodynamic model of CRS

Governing equations of mass, material, and energy balance for all components of CRS are shown below. Refrigerant properties are calculated using REFPROP 9.0. Thermo-physical properties of absorbent-refrigerant pairs are calculated using correlation equations (Eqs. A.1-A.15) given in Appendix A. The mass flow rate of refrigerant in VCRS ($\dot{m}_{ref_1}$), VARS ($\dot{m}_{ref_2}$), weak ($\dot{m}_6$), and strong solution ($\dot{m}_9$) is given in Eqs.(4.1)-(4.4).

$$\dot{Q}_{Evp} = \dot{m}_{ref_1}\left(H_3 - H_2\right) \tag{4.1}$$

$$\dot{Q}_{Cascade\ con} = \dot{m}_{ref_2}\left(H_5 - H_{14}\right) \tag{4.2}$$

$$\dot{m}_6\left(X_9 - X_6\right) = \dot{m}_{ref_2} X_9 \tag{4.3}$$

$$\dot{m}_9\left(X_9 - X_6\right) = \dot{m}_{ref_2} X_6 \tag{4.4}$$

The temperature of absorbent solution streams (8, 9, 10, and 11) can be calculated using the effectiveness of the heat exchanger (ε) as shown in Eqs. (4.5)-(4.6).

$$\varepsilon = \frac{\left(\dot{m}C_p\right)_9}{\left(\dot{m}C_p\right)_{min}} \frac{T_{12} - T_{10}}{T_{12} - T_6} \tag{4.5}$$

$$\varepsilon = \frac{\left(\dot{m}C_p\right)_6}{\left(\dot{m}C_p\right)_{min}} \frac{T_8 - T_6}{T_{12} - T_6} \tag{4.6}$$

Heat load calculation for all heat changers of CRS is shown in Eqs. (4.7-4.11). The calculations of the mass flow rate of chilled water (streams 21-22), cooling water (streams 15-16, 19-20), and hot streams (streams 17-18) are also mentioned in Eqs. (4.8)-(4.12).

TH-3395_176107002

$$\dot{Q}_{Cascade\ con} = \dot{m}_{ref_1}\left(H_4 - H_1\right) \tag{4.7}$$

$$\dot{Q}_{Abs} = \dot{m}_{ref\,2}H_5 + \dot{m}_{11}H_{11} - \dot{m}_6 H_6 = \dot{m}_{20}\left(H_{20} - H_{19}\right) \tag{4.8}$$

$$\dot{Q}_{Shx} = \dot{m}_{11}\left(H_9 - H_{10}\right) = \dot{m}_6\left(H_8 - H_7\right) \tag{4.9}$$

$$\dot{Q}_{Gen} = \dot{m}_{ref_2}H_{12} + \dot{m}_{11}H_9 - \dot{m}_6 H_8 = \dot{m}_{17}\left(H_{17} - H_{18}\right) \tag{4.10}$$

$$\dot{Q}_{Cond} = \dot{m}_5\left(H_{12} - H_{13}\right) = \dot{m}_{15}\left(H_{16} - H_{15}\right) \tag{4.11}$$

$$\dot{Q}_{Evp} = \dot{m}_{21}\left(H_{21} - H_{22}\right) \tag{4.12}$$

The mass balance and actual enthalpy of the compressor outlet stream and the work done by the compressor and pump are given in Eqs.(4.13)-(4.16).

$$H_{4r} = H_3 + \frac{\left(H_{4isen} - H_3\right)}{\eta_C} \tag{4.13}$$

$$\dot{W}_C = m_{ref_1}\left(H_{4r} - H_3\right) \tag{4.14}$$

$$\rho_{mix} = X_6\rho_{salt} + \left(1 - X_6\right)\rho_{water} \tag{4.15}$$

$$\dot{W}_P = \frac{\dot{m}_6\left(P_{13} - P_5\right)}{\rho_{mix}\eta_P} \tag{4.16}$$

The COP of the CRS (VCRS, VARS, and total system) is given as follows:

$$COP_{VCRS} = \frac{\dot{Q}_{Evp}}{\dot{W}_C} \tag{4.17}$$

$$COP_{VARS} = \frac{\dot{Q}_{Cascade\ con}}{\dot{Q}_{Gen} + \dot{W}_P} \tag{4.18}$$

$$COP_{CRS} = \frac{\dot{Q}_{Evp}}{\dot{Q}_{Gen} + \dot{W}_T} \quad where\ \ \dot{W}_T = \dot{W}_C + \dot{W}_P \tag{4.19}$$

In this work, only physical exergy associated with enthalpy and entropy of the stream is taken into consideration. Exergy destruction for all streams and components of CRS and total exergy destruction are given in Eqs. (4.20)-(4.21).

$$\dot{B}_{D,T} = \sum_{\substack{All\ heat \\ Exchangers}} \dot{B}_D + \dot{W}_T \tag{4.20}$$

$$\dot{B}_{in} = \dot{B}_{D,T} + \left(\dot{B}_{21} - \dot{B}_{22}\right) \tag{4.21}$$

TH-3395_176107002

Overall heat transfer coefficient (U) is varied in the range of 0.05-5 kW/m^2 K [195]. Logarithmic mean temperature difference (LMTD) T_m for all heat exchangers is calculated using Eqs. (4.22)-(4.27).

$$T_{m,Evp}=\frac{(T_{21}-T_2)-(T_{22}-T_3)}{log\left(\frac{T_{21}-T_2}{T_{22}-T_3}\right)} \tag{4.22}$$

$$T_{m,Cascade\ con}=(T_1-T_5) \tag{4.23}$$

$$T_{m,Abs}=\frac{(T_{11}-T_{20})-(T_6-T_{19})}{log\left(\frac{T_{11}-T_{20}}{T_6-T_{19}}\right)} \tag{4.24}$$

$$T_{m,Shx}=\frac{(T_9-T_8)-(T_{10}-T_7)}{log\left(\frac{T_9-T_8}{T_{10}-T_7}\right)} \tag{4.25}$$

$$T_{m,Gen}=\frac{(T_{17}-T_9)-(T_{18}-T_{12})}{log\left(\frac{T_{17}-T_9}{T_{18}-T_{12}}\right)} \tag{4.26}$$

$$T_{m,Cond}=\frac{(T_{13}-T_{15})-(T_{13}-T_{16})}{log\left(\frac{T_{13}-T_{15}}{T_{13}-T_{16}}\right)} \tag{4.27}$$

Economic model for CRS

The total cost of the system includes investment and operating costs. As given in Eq. (4.28), investment cost depends on the area of the heat exchangers. This work does not consider the investment cost for valves, pumps, refrigerants, absorbents, and connecting pipes. The cost of the compressor is calculated using Eqs.(4.29)-(4.31). The value of the maintenance factor (m_f) is considered as 1.06 [195].

$$Z=516.6211\ A+268.45 \tag{4.28}$$

$$\eta_{isen}=0.85-0.046667\left(\frac{P_1}{P_3}\right) \tag{4.29}$$

$$Z_C=\left(\frac{573\dot{m}_{ref_1}}{0.8996-\eta_{isen}}\right)\left(\frac{P_1}{P_3}\right)log\left(\frac{P_1}{P_3}\right) \tag{4.30}$$

TH-3395_176107002

$$Z_T = \left(\sum_{\substack{All\ heat \\ Exchangers}} Z + Z_C \right) m_f \tag{4.31}$$

Due to growing environmental concerns, penalty cost is also considered in this work. Penalty cost, known as a carbon tax, is charged for the emission of CO_2 in the atmosphere during the production of steam and electricity from fossil fuels. It is assessed as,

$$C_{Env} = m_{CO_2} C_{CO_2} \tag{4.32}$$

where C_{CO_2} is the cost charged for CO_2 per ton and is considered as 90 US $/ton in this study as per Iran standard. The emission amount of CO_2 (m_{CO_2}) is given as,

$$m_{CO_2} = \lambda \dot{W}_T \, top \tag{4.33}$$

where λ is the emission conversion factor (amount of CO2 emitted for producing 1/kW h) and is considered as 0.968 kg/kW h [196].

The thermoeconomic model relates exergy to the cost of the system. The objective function is to minimize the total annual cost of the CRS and is given as,

$$min\ C_T(x) = top\ C_{exer} \dot{B}_{in} + top\ C_{el}\ \dot{W}_T + a^c\ Z_T + CCU\left(\dot{Q}_{Cond} + \dot{Q}_{Abs}\right) + C_{Env} \tag{4.34}$$

The capital recovery factor (a^c) is determined using Eq. (3.16) in Chapter 3. The first, second, and third term in Eq.(4.34) represents the cost of fuel exergy input, the cost of electricity consumption by compressor and pump and the investment cost of heat exchangers and payback period, respectively. The cost for cold utility (*CCU*) of the refrigeration system is considered as 10 $/ kW h [247].

4.2.3. Optimization model and solution strategy

An optimization problem is formulated based on the CRS thermoeconomic model, derived in Section 2. The objective function of the model and the associated constraints are provided in Eq.(4.35). The decision variables and their bounds are given in the following sections. The mathematical formulation of the constraints is given as:

$$\begin{aligned} &Minimize && C_T(x) \\ &s.t. && X_9 - X_6 > 0 \\ & && T_{10} - T_C \geq 5 \end{aligned} \tag{4.35}$$

The optimization model incorporates two constraints with respect to the stability of the system. The first constraint is related to the relation between the strong and weak solution

TH-3395_176107002

concentration. A positive difference between the weak and strong solution concentration leads to crystallization issues and can be avoided using the constraint given in Eq.(4.35). The second constraint ensures a minimum temperature differential of 5 degrees is maintained between the strong solution passing through the heat exchanger and the absorbent solution crystallization temperature. The optimization model to minimize the total annual cost of CRS is solved for twelve different combinations of absorbent-refrigerant-refrigerant of CRS, constituting three different absorbent-refrigerant pairs in VARS and four different refrigerants in VCRS. The objective function is optimized using five recently proposed metaheuristic techniques, namely sTLBO, ASO, COA, YYPO, and TGA. In the optimization process, upper bounds, lower bounds, and constraints are selected based on absorbent-refrigerant combinations and are transferred to the metaheuristic techniques. the CRS model accepts a potential solution from the algorithm and appropriately calculates the necessary parameters required for the determination of total annual cost. A detailed flow chart of the solution procedure is given in Fig. 4.2.

Metaheuristic techniques are stochastic and require multiple runs to evaluate their effectiveness in determining an optimal solution. In this work, 25 independent runs are considered for the five metaheuristic techniques. The number of new solutions generated in the metaheuristic techniques varies significantly per algorithm; hence, selecting common termination criteria is important in evaluating their performance. Accordingly, maximum function evaluations are fixed as termination criteria with a limit of 3000 functional evaluations to provide a fair chance for all the selected metaheuristic techniques. The population size is set at 30 for all metaheuristic techniques except YYPO, as it works with two potential solutions. The other algorithm parameters are used as provided in the literature of the respective algorithm. The simulations are performed on the MATLAB 2019a platform.

4.3. Problem specification and model validation

Thermodynamic and economic models of CRS are validated for optimal decision variables reported by Jain et al. [195] and are given in Table 4.1. The results of the thermodynamic model are in good agreement with the reported results [195], as shown in the first two columns of Table 4.1. TEO of CRS using sTLBO are also shown in Table 4.1 and are compared against the literature values [195] tabulated in the 3rd and 4th columns. It is observed that sTLBO reported lower condenser, absorber, overlap, and cascade condenser temperatures compared to the literature (Table 4.1). Due to this, the exergy destruction is decreased from 21.87 kW to 17.37 kW.

TH-3395_176107002

Table 4. 1 Model Validation of CRS

Decision variables and other derived parameters	Energy, exergy, and economic model validation of CRS using LiBr-H_2O/R410a		Optimization of the total annual cost of CRS using LiBr-H_2O/R410a	
	Jain et al. [195]	Present work	Jain et al. [195] (Direct search)	Present work (sTLBO)
Cascade condenser temperature (°C)	21	21	21	15
Evaporator temperature (°C)	1.8	1.8	1.8	4
Absorber temperature (°C)	37	37	37	36
Generator temperature (°C)	83.3	83.3	83.3	83.8
Condenser temperature (°C)	39.3	39.3	39.3	38.9
Effectiveness (ε)	0.5	0.5	0.5	0.6
Overlap temperature (°C)	10.3	10.3	10.3	7
Total exergy destruction (kW)	21.87	22.08	**21.87**	**17.37**
Total area of heat exchanger (m^2)	49.04	48.97	**49.04**	**64.64**
System capital cost ($/year)	28782	30493.21	**28782**	**38092.39**
COP_{VCRS}	9.698	9.58	9.698	17.95
COP_{VARS}	0.747	0.751	0.747	0.751
COP_{CRS}	0.633	0.636	0.633	0.68
W_T/kW	8.15	8.42	**8.15**	**4.49**
Investment cost ($/year)	11885	11837	**11885**	**11288**
Penalty cost for CO_2 emission ($/year)	-	-	-	**2159.37**
Cost of cold utility ($/year)	-	-	-	**1,990.3**
Minimum total annual cost ($/year)	11885	11837	-	**15429.77**

Lower cascade condenser temperature required lesser compressor work, and thus exergy destruction was decreased. Differences among the optimum decision variables between the present work and the literature [195] lead to an increase in the overall size (49.04 m^2 to 64.64 m^2) of CRS heat exchangers, and eventually, the system capital cost also increases. Also, the present work has reported higher COP for LTL (VCRS), HTL (VARS), and CRS due to lower compressor work and heat load on the generator. However, the total investment cost (equipment, fuel exergy, and electricity) is lower due to lesser compressor work and total exergy destruction (Table 4.1). For the current problem, the input data of hot stream, coolant, and economic parameters are given in Appendix –B (Table B2).

TH-3395_176107002

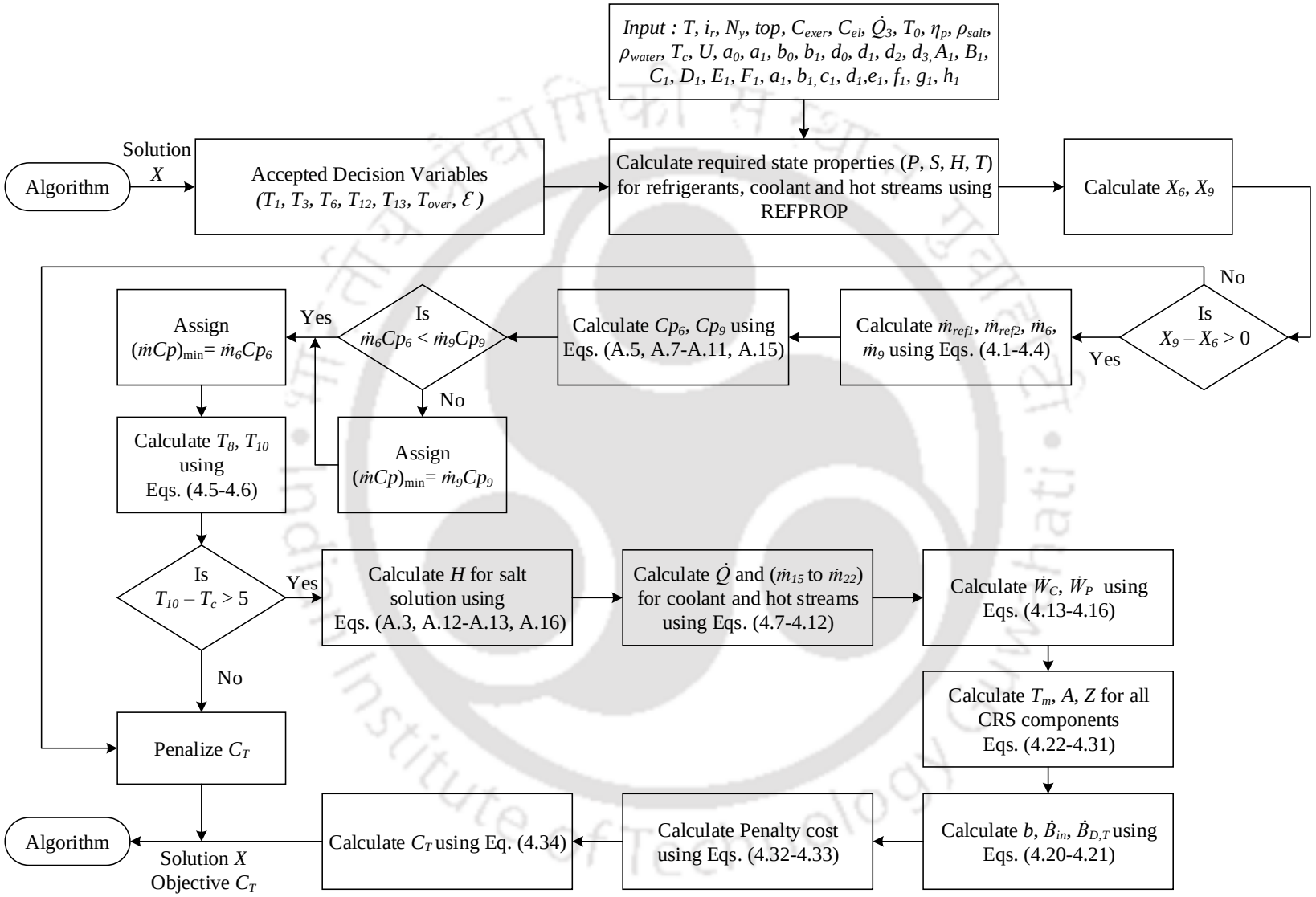

Fig. 4. 2 Flowchart for the solution procedure

TH-3395_176107002

4.4. Results and discussions

4.4.1. Effect of optimum decision variables and derived parameters on the minimum total annual cost of CRS

The optimal decision variables corresponding to all twelve different combinations of absorbent-refrigerant-refrigerant of CRS are given in Table 4.2. The cascade condenser temperature (T_1 in ˚C), evaporator temperature (T_3 in ˚C), absorber temperature (T_6 in ˚C), generator temperature (T_{12} in ˚C), condenser temperature (T_{13} in ˚C), overlap temperature (T_{over} in ˚C), and the effectiveness of solution heat exchanger (ε) are considered as decision variables. Refrigerants such as R290, R123, R1234yf, and R1234ze are used in VCRS, whereas LiBr-H_2O, LiCl-H_2O, ($CaCl_2$-LiBr-$LiNO_3$)-H_2O are used as absorbent-refrigerant pairs in VARS. The evaporator heat load considered here is 80.7 kW. These optimal solutions represent the best among all algorithms over all the runs. The objective was to find the minimum total annual cost of CRS among twelve different combinations, as shown in Table 4.2. The lowest and highest total annual cost (13164.76 $/year and 15406.65 $/year) was found for ($CaCl_2$-LiBr-$LiNO_3$)-$H_2O$-R290 and LiBr-$H_2O$- R1234yf, respectively, in CRS (Table 4.2). It was also found that R290 gives the lowest total annual cost irrespective of absorbent-refrigerant pairs in CRS.

Table 4.3a provides COP and heat exchanger area corresponding to optimal annual cost, and Table 4.3b presents the heat load, costs, and other important thermodynamic parameters related to the optimal annual cost. As a reference case, the thermodynamic analysis of ($CaCl_2$-LiBr-$LiNO_3$)-H_2O-R290 and LiBr-H_2O-R1234yf provide the lowest and highest total annual cost and is considered for discussion. A significant difference is observed between COP_{VARS} and COP_{CRS} of these absorbent-refrigerant-refrigerant pairs, as shown in Table 4.3a. The higher value of COP_{VARS} and COP_{CRS} results from the lower heat load on the generator for ($CaCl_2$-LiBr-$LiNO_3$)-H_2O-R290. Approximately 1˚C reduction in T_{12} of ($CaCl_2$-LiBr-$LiNO_3$)-H_2O-R290 is observed as compared to LiBr-H_2O-R1234yf, which depends on the concentration of the strong solution, leading to 2.23 m^2 and 21.79 kW reduction in area and heat load on the generator, respectively for the given heat source (Table 4.3a-b). Similarly, a 1.4˚C reduction in T_{13} leads to a reduction in the concentration of the strong solution and mass flow rate of a weak and strong solution, which further caused a 1.29 m^2 reduction in the area of the condenser for the given coolant conditions for ($CaCl_2$-LiBr-$LiNO_3$)-H_2O-R290. However, there is no significant reduction in the heat load on the condenser. Though the T_6 remains the same for both the pairs, 2.34 m^2 and 22.85 kW reduction in area and heat load on

TH-3395_176107002

the absorber, respectively, were observed for the given coolant conditions for ($CaCl_2$-LiBr-$LiNO_3$)-H_2O-R290.

A decrease in the heat load on the thermal compressor decreases the area of the solution exchanger (1.89 m^2) for the same ε, and therefore COP_{VARS} and COP_{CRS} increase for ($CaCl_2$-LiBr-$LiNO_3$)-H_2O-R290, as reported in Table 4.3a-b. The increment of 1˚C in T_{over} reduced the temperature and area of the evaporator in HTL (VARS) for (($CaCl_2$-LiBr-$LiNO_3$)-H_2O-R290). It leads to a 2.3 m^2 reduction in the area of the cascade condenser. The investment cost, penalty cost, and cold utility cost are 11312.86 $/year, 2106.85 $/year, and 1986.95 $/year, for LiBr-$H_2O$-R1234yf and 9309.79 $/year, 2096.72 $/year, and 1758.24 $/year, for ($CaCl_2$-LiBr-$LiNO_3$)-$H_2O$-R290, respectively (Table 4.3b). Reduction in the heat load on the absorber reduced the cost of the cold utility for ($CaCl_2$-LiBr-$LiNO_3$)-H_2O-R290 (Table 4.3b). A reduction in total work done by CRS resulted in lesser electricity usage (penalty cost). Exergy destruction, which depends on the mass flow rate of coolants, hot streams, and compressor operation, is reduced for ($CaCl_2$-LiBr-$LiNO_3$)-H_2O-R290 (Table 4.3b).

As mentioned earlier, R290 gives the lowest total annual cost for all absorbent-refrigerant pairs in CRS (Table 4.3a). It is noted that T_{12} is higher and T_{13} and T_{over} are lower for minimum total annual cost, that was obtained for ($CaCl_2$-LiBr-$LiNO_3$)-H_2O-R290 than those obtained for LiCl- H_2O-R290 (Table 4.3a). On the other hand, T_{12} is lower, and T_{13} and T_{over} are higher for minimum total annual cost, which was obtained for ($CaCl_2$-LiBr-$LiNO_3$)-H_2O-R290 than those obtained for LiBr- H_2O-R290. It may be concluded that these three temperatures (T_{12}, T_{13}, and T_{over}) influence the concentration and mass flow rate of weak and strong solutions and thermal compression in the VARS component of CRS (Table 4.3a-b), leading to changes in the heat load, area, exergy destruction, total annual cost for each combination (Table 4.3a-b). The thermodynamic properties obtained at the optimum decision variables of $CaCl_2$-LiBr-$LiNO_3$-H_2O have been shown in Table 4.4.

Effect of operational parameters for LiBr-H_2O-R290

The effect of decision variables on the COP, exergy destruction, total area of heat exchangers, and the total annual cost is shown in Fig. 4.3, as these parameters are mainly considered for the performance study of the refrigeration system. The COP of the system demonstrates the energy performance of the system, while exergy destruction is calculated to check the amount of available energy that has not been utilized. The area of heat exchangers predominantly decides the investment cost of the refrigeration system. Therefore, it becomes necessary to study the effect of decision variables on these parameters. The COP_{CRS}, BDT, total area, and TAC were obtained in the range of 15 - 21 ˚C of T_1 by keeping other optimal

TH-3395_176107002

decision variables constant. The COP_{CRS} increases with cascade condenser temperature (T_1) till 19.5 ˚C and then decreases. An increase in T_1 increases the work of the compression compressor and electric power consumption, resulting in a decrease in the refrigerating effect. As a result, the COP_{VCRS} decreases (Fig. 4.3). On the other hand, an increase in T_1 increases T_5 and the heat load on the cascade condenser, reducing the generator heat load. This further leads to an increase in COP_{VARS}, COP_{CRS}, BDT, and TAC (Fig. 4.3). However, the total heat exchanger area decreases due to a decrease in the overall heat load of CRS components. It is also noted that the curve of BDT and TAC becomes steeper with T_1 whereas the area gets plateau with T_1 (Fig. 4.3). Though an increase in T_1 can improve the performance of VARS and reduce the power consumption of VCRS, it also has increasing exergy destruction and TAC, which may not be feasible for refrigeration systems.

The COP_{CRS}, BDT, total exchanger area of CRS, and TAC were obtained for T_3 in the range of -10 - 4 ˚C with other constant optimum decision variables (Fig. 4.3). An increase in evaporator temperature (T_3) reduces the compressor work and increases COP_{VCRS}. However, reducing cascade condenser heat load and augmenting generator heat load brings no substantial improvement in COP_{VARS}. Thus, it is clear that the increase in COP_{CRS} is due to increased COP_{VCRS} (Fig. 4.3). As a result, the mass flow rate of coolant decreases considerably, resulting in a substantial reduction of BDT, as seen in Fig. 4.3. It is noted that the area of all exchangers except evaporator decreases with T_3. The increase in evaporator area dominates the reduction in the area of other exchangers beyond -1 ˚C, and hence the total area of CRS increases with T_3 at $T_3 > -1$ ˚C. The TAC decreases with the increase in T_3 because of the reduction in the compressor cost, carbon tax, and cold utility cost (Fig. 4.3). Higher evaporator temperature increases the COP of CRS and reduces the BDT and TAC. The TAC decreases with the increase in T_3 because of the reduction in the compressor cost, carbon tax, and cold utility cost (Fig. 4.3). Higher evaporator temperature increases the COP of CRS and reduces the BDT and TAC.

In order to infer the effect of T_6 on COP_{CRS}, BDT, total exchanger area of CRS, and TAC, T_6 is varied in the range of 32 - 46 ˚C with other constant optimum decision variables. An increase in T_6 increases the concentration of the weak solution and the mass flow rate of the strong and the weak solution. This further increases the heat load on the absorber and generator associated with the thermal compressor, thereby decreasing the COP_{VARS} and COP_{CRS} (Fig. 4.3). An increase in the coolant and hot stream flow rate increases BDT with T_6.

TH-3395_176107002

Table 4. 2 Optimal total annual cost and corresponding decision variables of CRS

VARS	VCRS	Cascade condenser temperature (˚C)	Evaporator temperature (˚C)	Absorber temperature (˚C)	Generator temperature (˚C)	Condenser temperature (˚C)	Overlap temperature (˚C)	Effectiveness of solution heat exchanger	Total annual cost/ $/year
Absorbent	Refrigerant								
$LiBr-H_2O$	R290	15	4	36	83.82	38.91	7.01	0.6	15208.27
	R123				83.81	38.90	6.99		15344.17
	R1234yf				83.82	38.91	7.01		15406.65
	R1234ze				83.78	38.88	6.99		15341.52
$LiCl- H_2O$	R290	15	4	36	80.82	41.67	10	0.6	13286.51
	R123				80.82	41.68	10		13424.51
	R1234yf				80.82	41.68	10		13484.45
	R1234ze				80.82	41.68	10		13420.41
$CaCl_2$-LiBr-$LiNO_3$- H_2O	R290	15	4	36	82.57	40.33	8.07	0.6	**13164.76**
	R123				82.52	40.28	8.10		13302.82
	R1234yf				82.50	40.26	8.09		13362.6
	R1234ze				82.54	40.30	8.09		13298.63
Lower bound (LiBr / LiCl / $CaCl_2$-LiBr-$LiNO_3$)		15	-10	36	70	36	5	0.6	
Upper bound (LiBr / LiCl / $CaCl_2$-LiBr-$LiNO_3$)		21	4	42	87	48	10	0.9	

TH-3395_176107002

Table 4. 3 (a) COP and heat exchanger area corresponding to an optimal annual cost of CRS

VARS	VCRS	COP			Area (m^2)					
Absorbent-Refrigerant	Refrigerant	VCRS	VARS	CRS	Cascade condenser	Evaporator	Absorber	Solution heat exchanger	Generator	Condenser
$LiBr-H_2O$	R290	18.48	0.75	0.69	17.33	9.54	11.76	11.61	7.85	6.54
	R123	18.88			17.37		11.75	11.57	7.83	6.55
	R1234yf	18.40			17.35		11.77	11.60	7.85	6.55
	R1234ze	18.60			17.37		11.76	11.58	7.81	6.58
$LiCl-H_2O$	R290	18.48	0.79	0.72	12.15	9.54	11.64	5.96	5.68	4.44
	R123	18.88			12.14		11.63			
	R1234yf	18.40			12.16		11.64			
	R1234ze	18.60			12.15		11.64			
$CaCl_2$-LiBr-$LiNO_3$-H_2O	R290	18.48	0.93	0.84	15.05	9.54	9.43	9.71	5.62	5.26
	R123	18.88			14.99		9.42	9.73	5.59	5.29
	R1234yf	18.40			15.02		9.44	9.74	5.58	5.31
	R1234ze	18.60			15.02		9.43	9.73	5.60	5.28

TH-3395_176107002

Table 4. 3 (b) Heat load and other thermodynamic parameters corresponding to the optimal annual cost of CRS

VARS	VCRS	Heat load (kW)			Thermodynamic Parameters				Annual Cost ($/year)			
Absorbent-Refrigerant	Refrigerant	Absorber	Generator	Condenser	Cascade condenser	Total exergy destruction (kW)	Compressor work (kW)	VCRS Refrigerant mass flow rate (kg/s)	Investment	Penalty	CCU	Total
$LiBr-H_2O$	R290	108.47	113.37	90.18	85.07	17.22	4.37	0.24	11124.96	2096.72	1986.59	15208.27
	R123	108.32	113.20	90.09	84.97	17.10	4.27	0.48	11307.02	2053.12	1984.04	15344.17
	R1234yf	108.49	113.38	90.21	85.09	17.24	4.39	0.55	11312.86	2106.85	1986.95	15406.65
	R1234ze	108.39	113.28	90.15	85.04	17.17	4.34	0.48	11272.72	2083.37	1985.42	15341.52
$LiCl\ H_2O$	R290	103.47	107.20	90.21	85.07	16.10	4.37	0.24	9252.99	2096.72	1936.79	13286.51
	R123	103.36	107.08	90.11	84.97	15.99	4.27	0.48	9436.65	2053.12	1934.75	13424.51
	R1234yf	103.50	107.23	90.23	85.09	16.13	4.39	0.55	9440.30	2106.85	1937.30	13484.45
	R1234ze	103.44	107.16	90.18	85.04	16.07	4.34	0.48	9400.86	2083.37	1936.18	13420.41
$CaCl_2$-LiBr-$LiNO_3$ H_2O	R290	85.64	91.59	90.18	85.07	13.41	4.37	0.24	9309.79	2096.72	1758.24	13164.76
	R123	85.56	91.50	90.08	84.97	13.30	4.27	0.48	9493.28	2053.12	1756.42	13302.82
	R1234yf	85.66	91.60	90.20	85.09	13.43	4.39	0.55	9497.17	2106.85	1758.58	13362.60
	R1234ze	85.62	91.57	90.15	85.04	13.37	4.34	0.48	9457.52	2083.37	1757.73	13298.63

TH-3395_176107002

Table 4. 4 Thermodynamic properties for CRS at the optimum case for ($CaCl_2$-LiBr-$LiNO_3$-H_2O)-R290

State Point	T (˚C)	P (kPa)	$\dot{m}$ (R290/ kg/s)	$\dot{m}$ (H_2O /kg/s)	$\dot{m}$ (Salt solution /kg/s)	X (%)	H (kJ/kg)	S (kJ /kg K)
1	15	731.51	0.24	-	-	-	238.41	1.14
2	4	535.10	0.24	-	-	-	238.41	1.14
3	4	535.10	0.24	-	-	-	579.24	2.37
4	18.60	731.51	0.24	-	-	-	597.68	2.38
5	6.88	0.99	-	0.0363	-	-	2513.5	8.98
6	36	0.99	-	-	0.2693	56.24	324.41	-
7	36	7.50	-	-	0.2693	56.24	324.41	-
8	57.78	7.50	-	-	0.2693	56.24	376.01	-
9	82.54	7.50	-	-	0.2330	64.99	414.48	-
10	54.62	7.50	-	-	0.2330	64.99	351.27	-
11	54.62	0.99	-	-	0.2330	64.99	351.27	-
12	82.54	7.50	-	0.0363	-	-	2654.6	8.49
13	40.30	7.50	-	0.0363	-	-	168.77	0.58
14	6.88	0.99	-	0.0363	-	-	168.77	0.60
15	30	101.32	-	4.3156	-	-	125.82	0.44
16	35	101.32	-	4.3156	-	-	146.72	0.51
17	100	101.32	-	0.0399	-	-	2675.6	7.35
18	90	101.32	-	0.0399	-	-	377.04	1.19
19	30	101.32	-	4.099	-	-	125.82	0.44
20	35	101.32	-	4.099	-	-	146.72	0.51
21	10	101.32	-	3.8431	-	-	42.11	0.15
22	5	101.32	-	3.8431	-	-	21.12	0.076

TH-3395_176107002

As shown in Fig. 4.3, an increase in the heat load on the VARS components further increases the total exchanger area and TAC with T_6. It can be observed that low absorber temperature will aid in improving the performance of the absorption refrigeration system as well as CRS by obtaining higher COP and lower BDT and TAC.

It is noted that T_{12} is varied in the range of 70 - 87 ˚C for determining the effect of T_{12} on COP_{CRS}, BDT, total exchanger area of CRS, and TAC with other constant optimum decision variables as shown in Fig. 4.3. The increase in T_{12} reduces the heat load on VARS exchangers, and hence, COP_{VARS} and COP_{CRS} increase with T_{12}. The decreasing trend of BDT is attributed to heat load reduction on the absorber and solution heat exchanger, reduction in the mass flow rate of coolant, hot streams, and strong and weak solutions with T_{12}. As heat load decreases, the area of exchangers also reduces, and thus the overall area and TAC of CRS decreases (Fig. 4.3). Maintaining a higher generator temperature will reduce the BDT, TAC of CRS and improve COP, which means in the view of energy, exergy, and economically CRS performs better.

The COP_{CRS}, BDT, the total area of CRS, and TAC were obtained in the range of 36 - 48 ˚C for T_{13} by maintaining other optimal decision variables constant. The increase in T_{13} adversely affects the COP of the system as the refrigerating effect of COP_{VARS} decreases. As a result, COP_{CRS} decreases with T_{13}. As T_{13} increases, the concentration of the strong solution decreases, and the mass flow rate of strong and weak solutions increases. This further leads to an increase in the heat load of the absorber and solution heat exchanger. Hence, BDT increases due to the increase in mass flow rate of coolant and hot streams (Fig. 4.3). The increase in heat load increases the total area of CRS components and TAC, as observed in Fig. 4.3. Lower condenser temperature in VARS demonstrates satisfactory performance by all means for both CRS and VARS.

The effect of T_{over} in the range of 5 - 10 ˚C is shown on COP_{CRS}, BDT, the total area of CRS, and TAC for other constant optimal decision variables (Fig. 4.3). Heat load on absorber and generator in VARS increases with T_{over}, due to which cascade condenser area reduces, and the area of the absorber, solution heat exchanger, generator, and condenser increases. As a result, the total area of CRS components and TAC reaches a minimum point, where an increase in the area of all VARS exchangers is equal to the decrease in the area of the cascade condenser, and then TAC increases with T_{over} due to an increase in the area of VARS exchangers. The increase in T_{over} increases the concentration of the weak solution and the mass flow rate of strong and weak solution, coolant, and hot streams, which increases BDT (Fig. 4.3). Overlap temperature decides the evaporator temperature of VARS. A smaller value of overlap temperature will have

TH-3395_176107002

higher COP and lower BDT, as required for a refrigeration system. Minimum area and TAC can be obtained by keeping a temperature near 8 ºC.

The COP_{CRS}, BDT, the total area of CRS, and TAC were displayed in the range of ε = 0.6 to 0.9 when other optimal decision variables are constant. It is noted that the COP_{CRS} increases with ε due to improvement in COP_{VARS}. The increase in ε decreases the heat load, and the reduced thermal compressor heat load results in lower mass flow rates of coolant and hot streams, resulting in lower BDT at higher ε. Improved ε increases the area of the absorber, solution heat exchanger, and generator, and hence the total area increases (Fig. 4.3). Crystallization occurs beyond ε = 0.75, and hence the operating CRS beyond ε = 0.75 is not feasible. Therefore, the TAC is infeasible, as shown in Fig. 4.3.

The effect of decision variables on COP_{CRS}, BDT, the total area of CRS heat exchangers, and TAC are illustrated within their upper and lower bounds for LiCl-H_2O-R290 and ($CaCl_2$-LiBr-$LiNO_3$)-H_2O-R290 in Fig. 4.4 and Fig. 4.5. The same trends like LiBr-H_2O-R290 has been observed for LiCl and $CaCl_2$-LiBr-$LiNO_3$ except for COP. It is observed that COP_{VCRS} decreases with T_1 due to the increase in compression work for LiCl-H_2O-R290 and ($CaCl_2$-LiBr-$LiNO_3$)-H_2O-R290 (Figs. 4.4 and 4.5), which further decreases COP_{VCRS} and COP_{CRS} with T_1.

4.4.2. Convergence and statistical analysis

This section discusses the convergence of all algorithms for all combinations of absorbent-refrigerant-refrigerant of CRS as given in Fig. 4.6-4.9. The convergence is determined by considering the best run values over the maximum function evaluations corresponding to each studied algorithm. Fig. 4.6 discusses the convergence curve for R290. A quick convergence to the optimal value is observed by TGA, sTLBO, and COA for LiBr-H_2O, LiCl-H_2O, and ($CaCl_2$-LiBr-$LiNO_3$)-H_2O, respectively. Although TGA and sTLBO showed quick convergence, the best value is determined by COA among three absorbent-refrigerant pairs with R290. The initial solution determined by sTLBO showed a higher total annual cost than other algorithms except by ASO for LiCl-H_2O with R290. However, sTLBO was able to identify better solutions than ASO, TGA, and YYPO for all three absorbent-refrigerant pairs with R290. TGA showed lesser improvement in the convergence by utilizing a higher number of function evaluations. As an example, TGA achieved a 4.1 % improvement to the final objective value using 18.5-100 % of the function evaluations for LiBr-water. A similar trend is shown for ($CaCl_2$-LiBr-$LiNO_3$)-H_2O using sTLBO, where 55 % of the function evaluations were used for an improvement of 0.01% in achieving the final objective value.

TH-3395_176107002

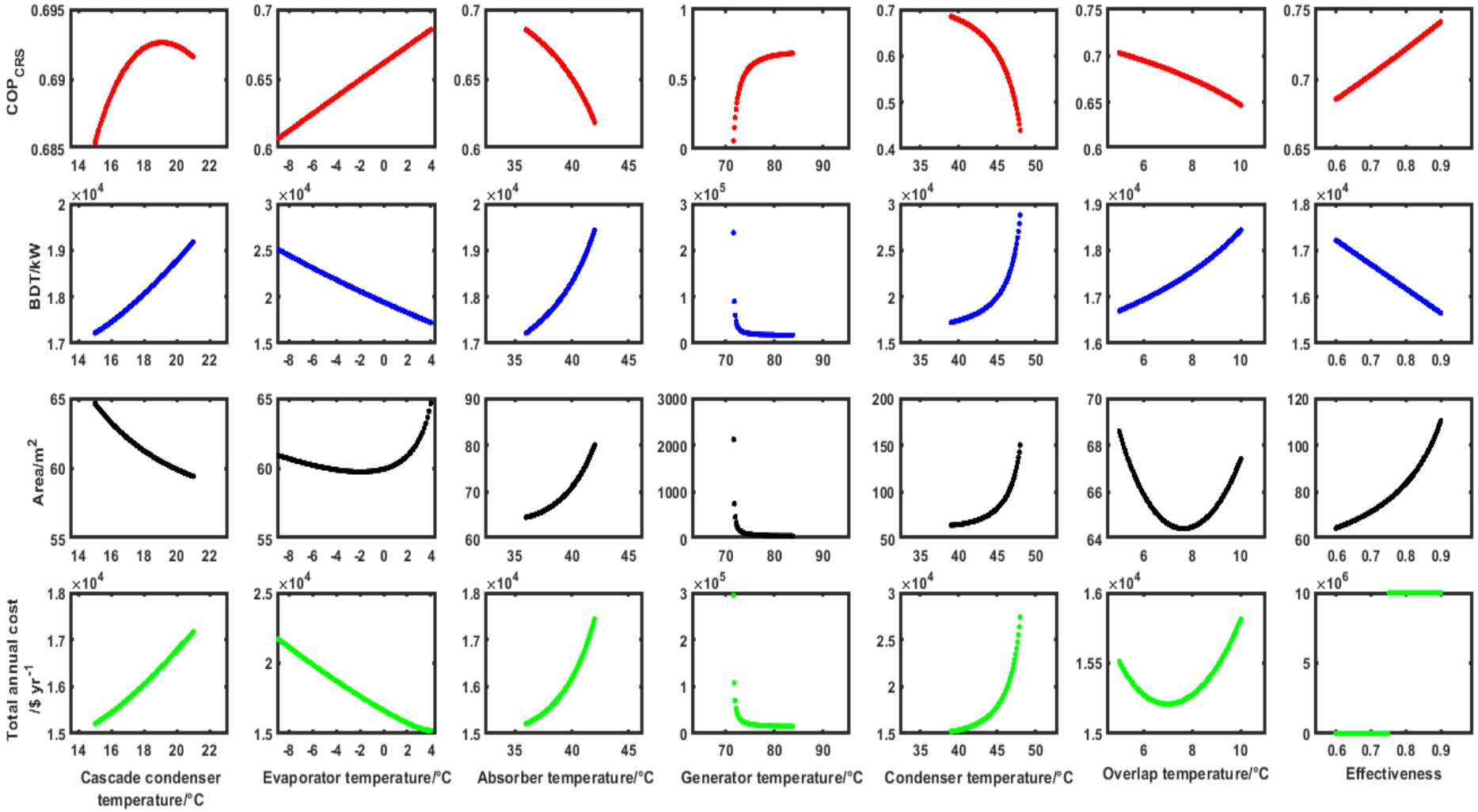

Fig. 4. 3 Effect of operational parameters for LiBr-H_2O-R290

TH-3395_176107002

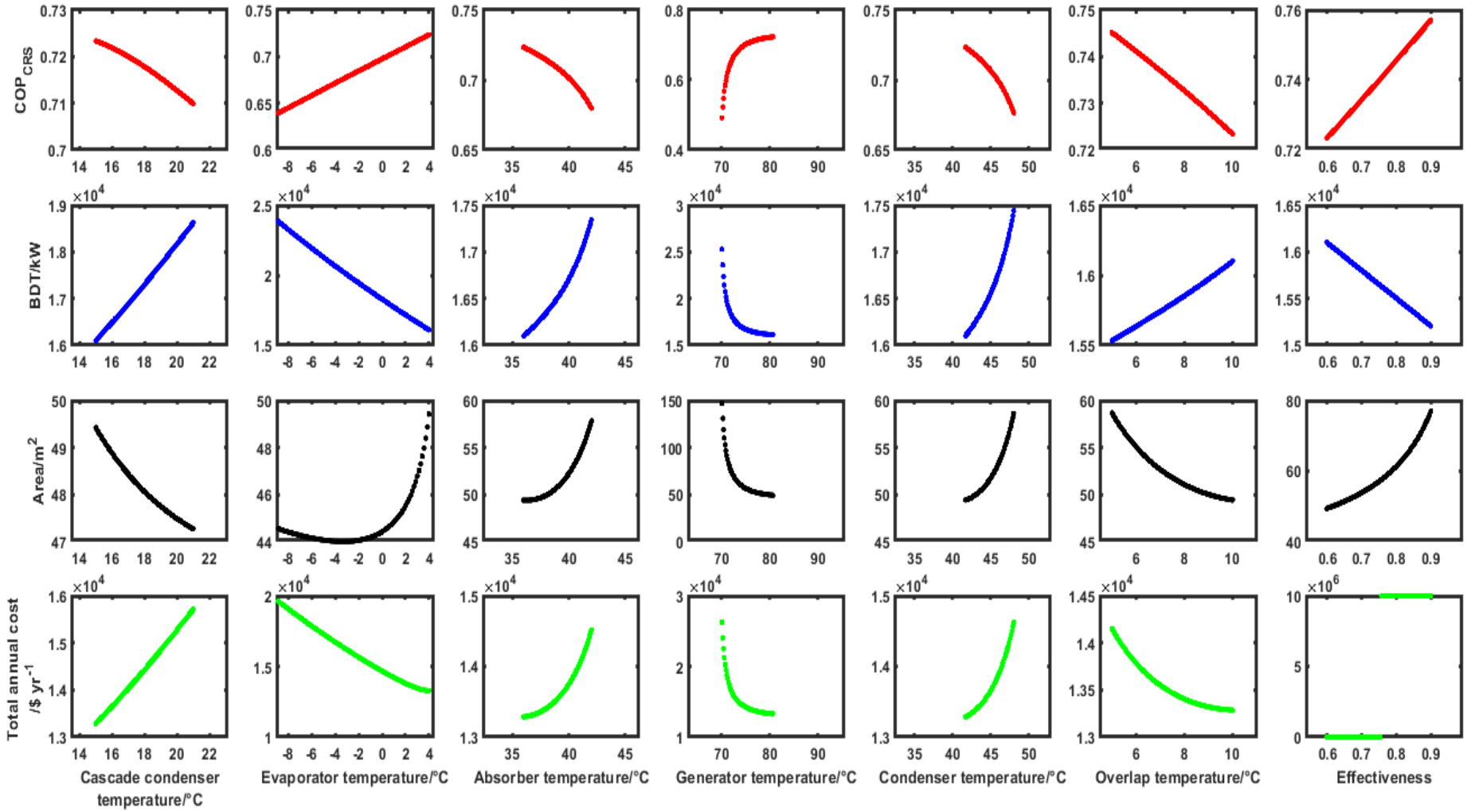

Fig. 4. 4 Effect of operational parameters for LiCl-H_2O-R290

TH-3395_176107002

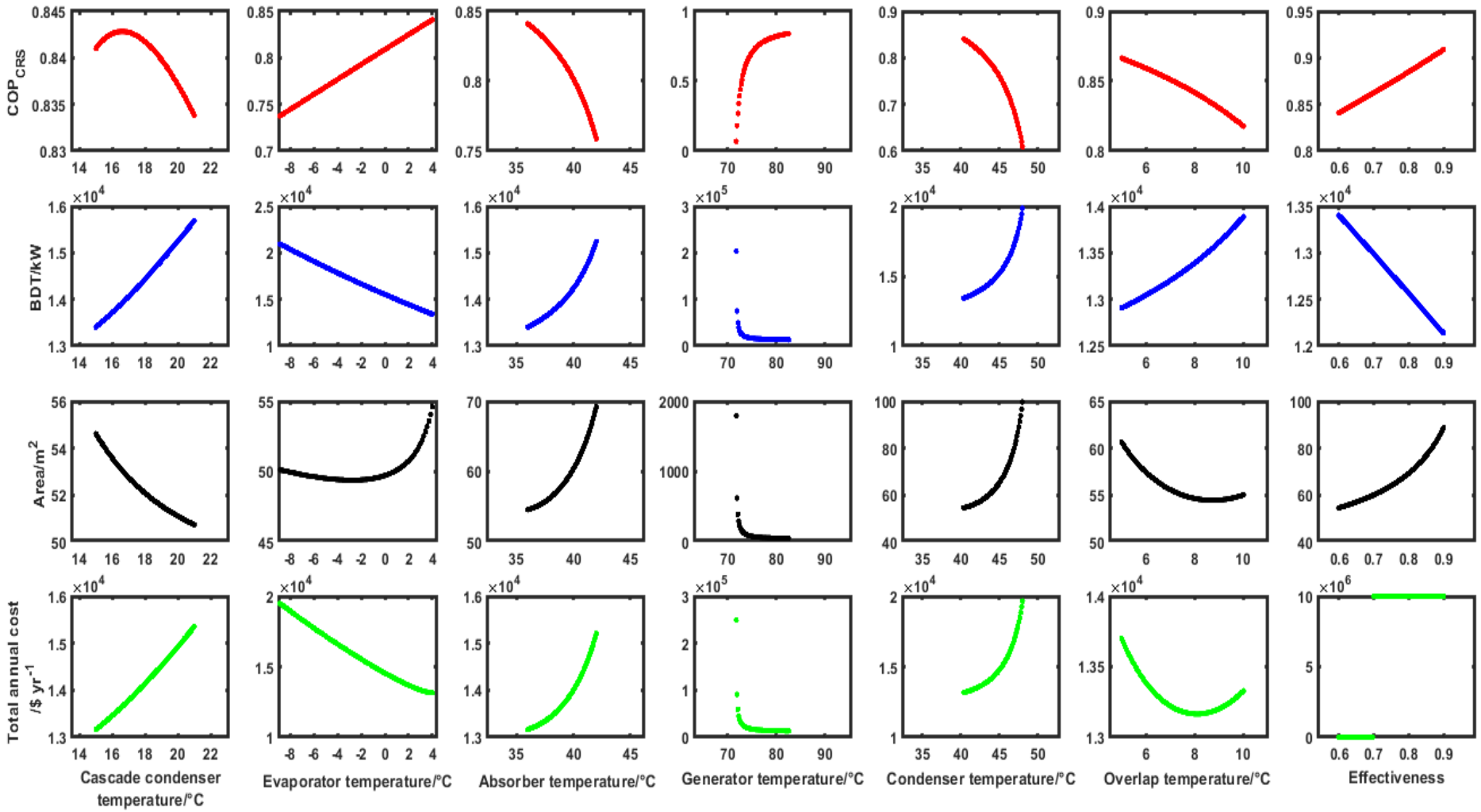

Fig. 4. 5 Effect of operational parameters for $CaCl_2$-LiBr-$LiNO_3$-H_2O-R290

TH-3395_176107002

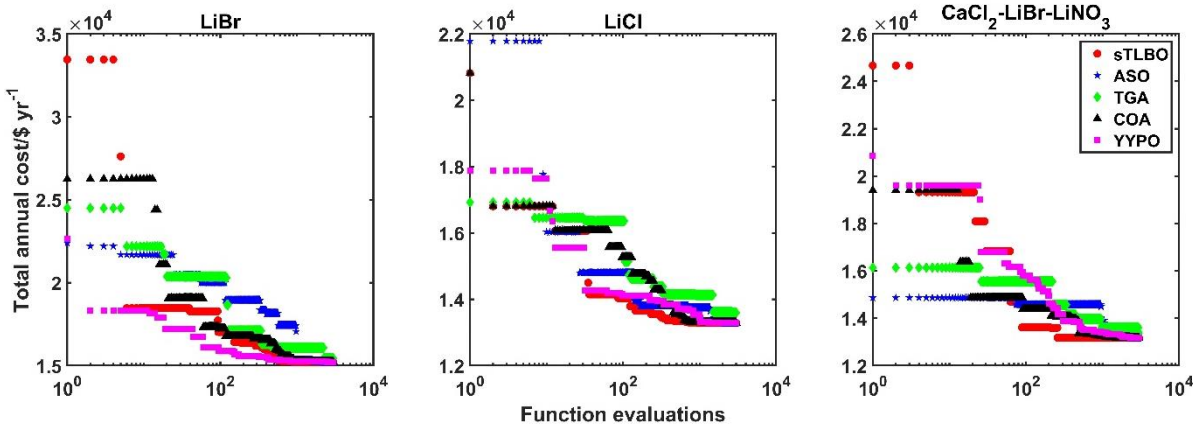

Fig. 4. 6 Convergence curve for R290

While using R123 as the refrigerant in VCRS, a quick convergence to the final solution is observed for LiBr-H_2O and LiCl-H_2O using TGA, as shown in Fig. 4.7. On the other hand, sTLBO converged quickly to the final objective value for ($CaCl_2$-LiBr-$LiNO_3$)-H_2O. The best value is reported by COA even though it consumed higher function evaluations for LiBr-H_2O and LiCl-H_2O. TGA utilized only 60% of function evaluations for LiBr-H_2O and reported a worse solution among reported solutions.

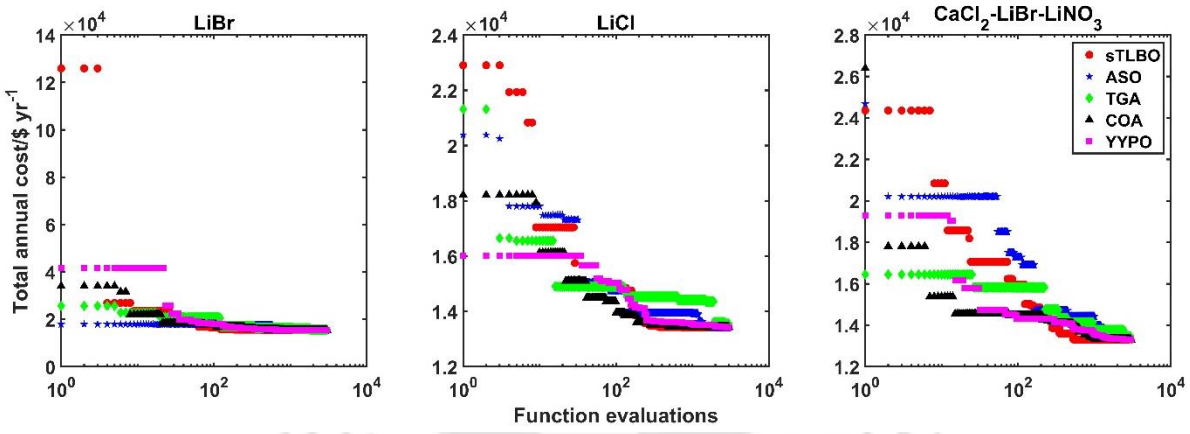

Fig. 4. 7 Convergence curve for R123

Apart from worse solutions (second worse solution with ($CaCl_2$-$LiNO_3$-LiBr)-H_2O), TGA showed smaller improvement in the convergence for a large number of function evaluations for all absorbent-refrigerant pairs with R290. TGA used 65 %, 37 %, and 68 % of function evaluations and improved 3.2 %, 0.4 %, and 3 % in the final objective value for LiBr-H_2O, LiCl-H_2O, and ($CaCl_2$-LiBr-$LiNO_3$)-H_2O, respectively. The initial value reported by YYPO for LiCl-H_2O and ($CaCl_2$-LiBr-$LiNO_3$)-H_2O is the lowest; however, it was not converged to a better solution, which COA determined. (Fig. 4.7)

TH-3395_176107002

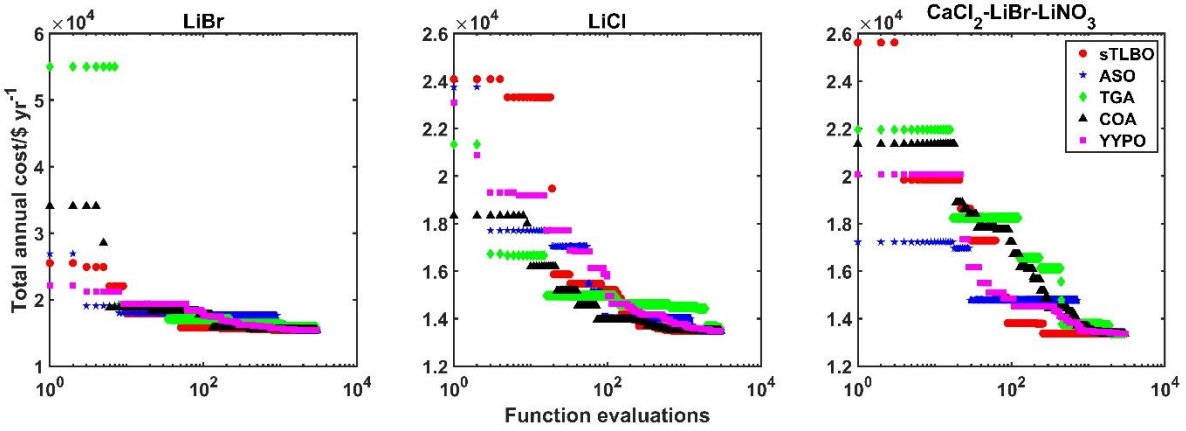

Fig. 4. 8 Convergence curve for R1234yf

The use of R1234yf as a refrigerant with all three absorbent-refrigerant pairs is given in Fig. 4.8. TGA and sTLBO showed quick convergence in achieving the final objective value for LiBr-H_2O, ($CaCl_2$-LiBr-$LiNO_3$)-H_2O, and LiCl-H_2O, respectively. TGA showed better improvement in the objective functions during the initial convergence phase; however, it could not improve the objective function in the later phase even after using a higher number of function evaluations. TGA utilized 64 %, 36 %, and 85 % of the total function evaluations in achieving 0.03 %, 0.04%, and 2.8 % of improvement in reaching the final objective function for LiBr-H_2O, LiCl-H_2O, and ($CaCl_2$-LiBr-$LiNO_3$)-H_2O, respectively (Fig. 4.8).

In Fig. 4.9, TGA achieved quick convergence for the absorbents LiBr-H_2O and ($CaCl_2$-LiBr-$LiNO_3$)-H_2O by utilizing 67 % and 63.8 % of the maximum function evaluations, respectively. It is noted that sTLBO showed swift convergence by utilizing 88 % of the function evaluations in reaching its final value for LiCl-H_2O.

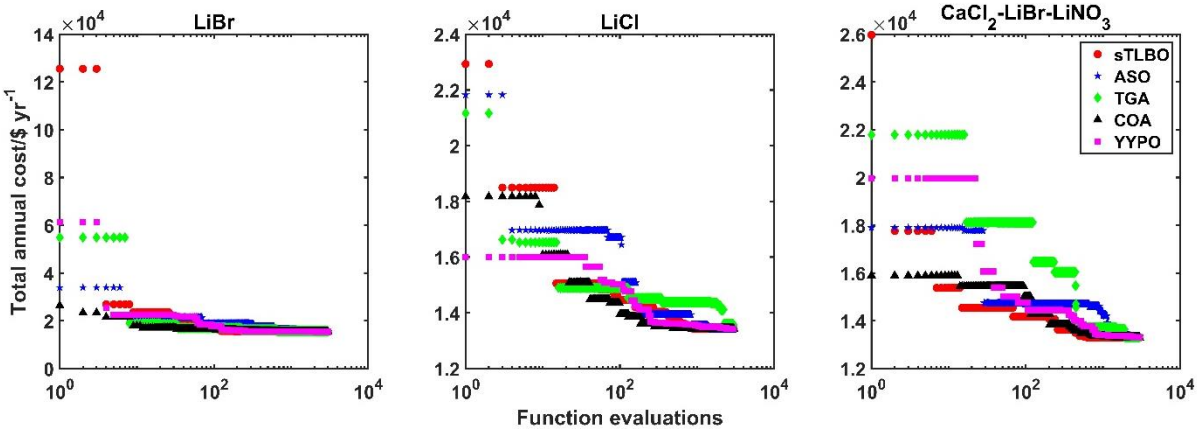

Fig. 4. 9 Convergence curve for R1234ze

TH-3395_176107002

Table 4. 5 Best, Mean, and standard deviation values for 12 Absorbent-Refrigerant-Refrigerant pairs for CRS

VARS	VCRS	Best					Mean					Standard Deviation				
Absorbent	Refrigerant	sTLBO	ASO	TGA	COA	YYPO	sTLBO	ASO	TGA	COA	YYPO	sTLBO	ASO	TGA	COA	YYPO
$LiBr-H_2O$	R290	15208.29	15208.82	15422.46	**15208.27**	15215.40	15209.03	15645.07	15843.79	**15208.53**	15271.43	1.09	678.42	170.79	**0.25**	46.11
	R123	15344.19	15344.49	15632.94	**15344.17**	15352.12	15344.74	15500.89	16025.12	**15344.48**	15400.79	0.50	159.96	165.28	**0.44**	35.84
	R1234yf	15406.71	15407.35	15841.68	**15406.65**	15416.47	15407.23	15591.99	16118.27	**15406.93**	15474.50	0.54	151.65	156.28	**0.26**	38.58
	R1234ze	**15341.52**	15341.53	15592.17	**15341.52**	15348.31	15342.32	15484.97	16036.39	**15341.71**	15400.04	1.24	138.10	189.05	**0.15**	40.11
$LiCl-H_2O$	R290	13286.53	13286.56	13594.14	**13286.51**	13293.72	13286.77	13570.17	13980.36	**13286.52**	13342.55	0.32	209.02	211.00	**0.01**	42.55
	R123	13424.51	13424.85	13546.35	**13424.51**	13436.05	13425.00	13705.27	14068.64	**13424.53**	13482.67	0.59	204.74	252.41	**0.02**	28.33
	R1234yf	13484.45	13484.68	13607.93	**13484.45**	13491.79	13484.83	13824.62	14096.52	**13484.47**	13542.64	0.50	184.40	253.16	**0.03**	30.97
	R1234ze	13420.43	13420.95	13520.85	**13420.41**	13431.65	13420.93	13729.82	14075.58	**13420.43**	13477.11	0.74	221.40	230.61	**0.03**	25.41
$CaCl_2$-LiBr-$LiNO_3$-H_2O	R290	13164.80	13180.17	13378.37	**13164.76**	13175.60	13165.60	13965.98	13880.37	**13165.17**	13254.30	0.67	1238.33	305.76	**0.51**	63.27
	R123	13302.97	13350.24	13349.72	**13302.82**	13320.32	13304.60	13900.62	13968.71	**13303.11**	13414.24	1.56	870.29	305.63	**0.23**	71.77
	R1234yf	13362.85	13400.55	13384.74	**13362.60**	13375.94	13364.30	13887.32	13950.42	**13362.89**	13469.33	1.14	866.01	310.51	**0.23**	72.49
	R1234ze	13298.77	13357.25	13320.10	**13298.63**	13311.51	13300.55	13936.03	13927.09	**13299.09**	13400.08	1.55	852.43	355.78	**0.46**	68.81

TH-3395_176107002

The initial solution determined by sTLBO was worse than other algorithms; however, it improved the solutions and reported the best solution for LiBr-H_2O and the second-best solution for LiCl-H_2O and ($CaCl_2$-LiBr-$LiNO_3$)-H_2O. The convergence observed by YYPO is devoid of any abrupt changes, as observed for TGA and sTLBO.

The best, mean, and standard deviation of the objective functions reported by each algorithm over the independent runs for the twelve combinations of absorbent-refrigerant-refrigerant are given in Table 4.5. The best value for each of the absorbent-refrigerant-refrigerant combinations of each of the algorithms represents the minimum total annual cost determined over all the runs by the corresponding algorithm. For example, the best annual cost determined by sTLBO for the LiBr-H_2O-R290 combination is 15208.29 $/year. Similarly, the mean value for the absorbent-refrigerant-refrigerant combination represents the mean of the total annual cost reported for all the runs by the corresponding algorithm. The standard deviation for each algorithm represents the total annual cost variance determined from the mean in all the runs (Table 4.5).

Among all the algorithms, COA determined solutions with the least total cost for all combinations of absorbent-refrigerant-refrigerant except LiBr-H_2O-R1234ze. It may be noted that sTLBO identified the best solution for LiBr-H_2O-R1234ze. However, the deviation in the best cost determined by COA with sTLBO is in the range of 10^{-3}. It needs to be mentioned that COA reported the best mean value in all combinations of absorbent-refrigerant-refrigerant. This further shows that COA determined better solutions in most of the runs compared to other reported algorithms. The least standard deviation of COA and the closeness of the mean value with the best value emphasize the ability of COA to determine solutions closer to the best solution in most of the runs. The standard deviations reported by ASO and TGA are comparatively higher than other algorithms. This shows their inefficiency in determining better solutions consistently.

4.5. Closure

The current study investigates the thermoeconomic optimization of a compression-absorption cascaded refrigeration system (CRS). Refrigerants with low ODP and GWP such as R290, R123, R1234yf, and R1234ze in VCRS and suitable absorbent-refrigerant pairs of LiBr-H_2O, LiCl-H_2O, and ($CaCl_2$-LiBr-$LiNO_3$)-H_2O in VARS are used as working pairs. A nonlinear objective function was considered for minimizing the total annual cost of the system. Total annual cost includes investment, maintenance, carbon tax/penalty, and cold utility costs. The optimization analysis is performed with five computational intelligence techniques: sTLBO, ASO, TGA, COA, and YYPO. The effect of decision variables on system efficiency

TH-3395_176107002

in terms of energy, exergy, and economics is studied. The important conclusions obtained from the analysis of CRS are stated below:

- The lowest and highest total annual cost (13164.76 $/year and 15406.65 $/year) is reported for ($CaCl_2$-LiBr-$LiNO_3$)-$H_2O$-R290 and LiBr-$H_2O$- R1234yf, respectively, in CRS. It is also to be mentioned that R290 in VCRS offers the lowest total annual cost irrespective of absorbent-refrigerant pairs in VARS. The minimum total annual cost provided by LiCl- H_2O-R290 is higher than ($CaCl_2$-LiBr-$LiNO_3$)-H_2O-R290 and lower than LiBr- H_2O-R290.
- The effect of decision variables on COP_{CRS}, BDT, total heat exchanger area of CRS, and TAC are reported within their upper and lower bounds for all absorbent-refrigerant-refrigerant combinations. It may be concluded that generator temperature, condenser temperature, and overlap temperature (T_{12}, T_{13}, and T_{over}) predominantly influence the operation of CRS.
- A quick convergence to the respective optimal objective function is observed by TGA, sTLBO, and COA for the most number combinations of absorbent-refrigerant-refrigerant. TGA showed lesser improvement in the convergence while utilizing a higher number of function evaluations for most combinations of absorbent-refrigerant-refrigerant.
- Among all the algorithms, COA was able to determine solutions with the least total cost for all combinations of absorbent-refrigerant-refrigerant except LiBr-H_2O-R1234ze. COA reported the lowest standard deviation, and ASO and TGA reported the highest standard deviations. The higher standard deviation shows the inefficiency of ASO and TGA in determining better solutions consistently.

TH-3395_176107002

CHAPTER 5

Comparative thermoeconomic and environmental analyses of CRS and subcooled CRS

5.1. Introduction

A literature survey shows that adding a subcooler to the refrigeration system enhances efficiency and cooling capacity performance and the cascade refrigeration system reduces electric energy utilization and performs better from an energy point of view. However, exergy, economic, and environmental performances also have to be accounted for in the overall behavior of the system. The literature shows that no thermoeconomic optimization study has been conducted using ($CaCl_2$-LiBr-$LiNO_3$)-H_2O as an absorbent-refrigerant working pair in the absorption section of the subcooled cascaded refrigeration system (SCRS), as well as the comparative study of SCRS and CRS. Furthermore, while calculating the total annual cost of the system, most literature does not consider the cost of cold utility.

Therefore, this study presents thermoeconomic optimization of the subcooled cascaded refrigeration system (SCRS) employing metaheuristic techniques with low ODP and GWP refrigerants in the compression section and different absorbent solutions in the absorption section. Environmental issues such as global warming are associated with higher ODP and GWP refrigerants; therefore, low ODP and GWP refrigerants are selected for the compression section. A comparison between the SCRS and CRS is also performed in order to identify the most efficient refrigeration system in terms of energy, exergy, and cost (with the inclusion of the cost of cold utility). The no-free lunch theorem [24] suggests implementing multiple metaheuristic techniques because a single algorithm cannot handle all sorts of optimization problems effectively.

Hence, this work comprises of a comparative study of thermoeconomic optimization of SCRS and CRS with low ODP and GWP refrigerants in the compression section and different absorbent solutions in the absorption section, including the cost of cold utility while determining the total annual cost. A comparative study of SCRS and CRS that includes detailed thermodynamics and economic analysis. Both systems use LiBr-H_2O, LiCl-H_2O, $CaCl_2$-LiBr-$LiNO_3$-H_2O in VARS and low GWP and ODP refrigerants R290, R123, R1234yf, and R1234ze in VCRS. A nonlinear objective function primarily consisting of energy, exergy, and economic parameters is developed to minimize the total annual cost of the system. Various metaheuristic algorithms such as sTLBO [26], ASO [27], COA [28], TGA[29], and YYPO [30] are tested to

TH-3395_176107002

optimize CRS and SCRS. The effect of decision variables, i.e., outlet temperatures of heat exchangers such as the evaporator, condenser, subcooler, generator, and absorber on total annual cost along with total exergy destruction, COP of the system.

5.2. Thermoeconomic modelling and optimization of SCRS

5.2.1. System description

The schematic of SCRS is illustrated in Fig. 5.1. It mainly consists of the compression refrigeration subsystem (VCRS) and absorption refrigeration subsystem (VARS). In the VCRS, refrigerant R290/R123/R1234yf/R1234ze is utilized while LiBr/LiCl/(CaC_{l2}-LiBr-$LiNO_3$)-H_2O absorbent solution/solution mixtures-water pair is used in VARS.

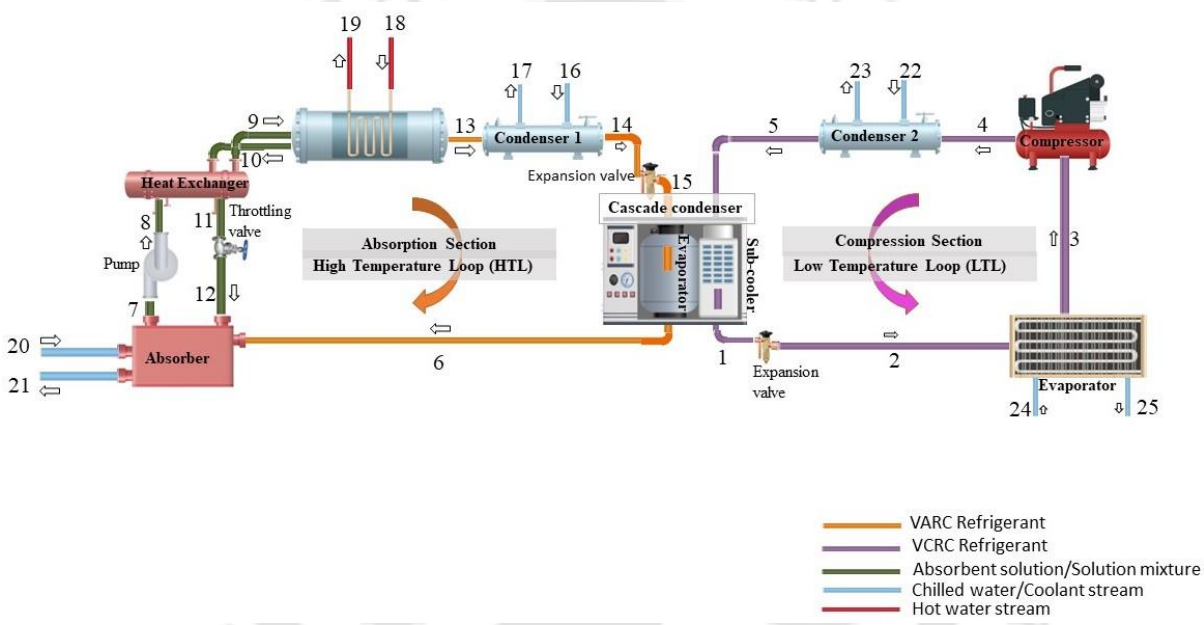

Fig. 5. 1 Schematic of Subcooled Cascaded Refrigeration System (SCRS)

The only difference between CRS (evaporator-condenser) and SCRS is the addition of a subcooler between the condenser and expansion valve in the compression subsystem, which acts as an evaporator for VARS. Chilled water (streams 24-25) heat load is transferred to the VCRS. Saturated vapor refrigerant (stream 3) is pressurized using a compressor and sent to condenser 2 (stream 4). In condenser 2, the heat load is removed by the coolant stream (stream 22-23) by condensing a saturated liquid refrigerant (stream 5). Subcooled refrigerant (stream 1) is returned to the evaporator via an expansion valve (stream 2). The heat load removed from the subcooler is supplied to VARS, and the refrigerant in VARS (stream 6) is converted into saturated vapor. In the absorber, the absorbent solution/solution mixture is mixed with saturated vapor refrigerant forming a weak solution (stream 7). The coolant (stream 20-21) removes the heat released in the absorber. The weak solution is pumped (stream 8) through the

TH-3395_176107002

solution heat exchanger resulting in a high temperature-high pressure absorbent solution/solution mixture-water mixture (stream 9) that is sent to the generator. The generator separates the refrigerant (stream 13) and absorbent solution/solution mixture (stream 10) using low-grade heat supplied (stream 18-19). A strong absorbent solution/solution mixture (stream 10) is sent back to the absorber through a solution heat exchanger (stream 11) and throttling valve (stream 12). Superheated refrigerant (stream 13) is condensed in condenser 1 (stream 14) by removing its heat using coolant (stream 16-17) and sent to the evaporator-subcooler through an isenthalpic expansion valve (stream 15).

- **Model assumptions**

Kinetic and potential energies are not considered in the energy and exergy study, which is carried out at a steady state. The evaporator is subjected to an 80.7 kW refrigeration load. 298 K and 101.3 kPa are used as the reference temperatures and pressures. It is low-grade steam that provides the heat. The evaporator, absorber, condenser, cascade condenser, and generator all have temperature variations that are disregarded. In order to prevent crystallization of the absorbent, the temperature of the strong solution entering the solution expansion valve is always kept at 5 °C higher. An adiabatic device is an expansion valve. In the component parts of SCRS, pressure and heat losses are disregarded. The thermodynamic characteristics at the corresponding temperatures, pressures, and concentrations are estimated as equilibrium values for the absorbent solutions in the generator and absorber, which are in equilibrium. The refrigerant exits the condenser and evaporator, and absorbent solutions exit the absorber, and the generator are in their saturated state. The energy required for other ancillary components of SCRS is not considered in the analysis.

5.2.2. Thermodynamic model of SCRS

Thermodynamic model equations are formulated based on the mass, component, and energy balance equations. Refrigerant properties are calculated using REFPROP 9.0. Thermo-physical properties of absorbent-refrigerant pairs are calculated using correlation equations (Eqs. A.1-A.15) given in Appendix A. For the evaporator, the Eqs.(5.1)-(5.3) aid in determining the mass flow rate of refrigerant in VCRS ($\dot{m}_{ref_1}$), the mass flow rate of chilled water ($\dot{m}_{24}$), and Logarithmic mean temperature difference (LMTD) $T_{m,\,Evp.}$

$$\dot{Q}_{Evp} = \dot{m}_{ref_1}\left(H_3 - H_2\right) \tag{5.1}$$

$$\dot{Q}_{Evp} = \dot{m}_{24}\left(H_{24} - H_{25}\right) \tag{5.2}$$

TH-3395_176107002

$$T_{m,Evp} = \frac{(T_{24} - T_2) - (T_{25} - T_3)}{log\left(\frac{T_{24} - T_2}{T_{25} - T_3}\right)} \tag{5.3}$$

The compressor in VCRS is assumed to be isentropic. Using the isentropic efficiency of the compressor, the actual enthalpy of the superheated refrigerant stream can be calculated, which can assist in computing the work done by the compressor, as shown in Eqs.(5.4)-(5.5).

$$H_{4r} = H_3 + \frac{(H_{4isen} - H_3)}{\eta_{isen}} \tag{5.4}$$

$$\dot{W}_C = \dot{m}_{ref_1}(H_{4r} - H_3) \tag{5.5}$$

One of the differences in the configuration of CRS and SCRS is the inclusion of an additional condenser in SCRS (condenser 2), due to which the VCRS is operated at a higher pressure than CRS. The heat load ($\dot{Q}_{Cond\,2}$), and ($\dot{m}_{22}$) are calculated using the heat balance equation given in Eqs.(5.6)-(5.7) while the LMTD of condenser 2 is calculated in Eq. (5.8).

$$\dot{Q}_{Cond\,2} = \dot{m}_{ref_1}(H_4 - H_5) \tag{5.6}$$

$$\dot{Q}_{Cond\,2} = \dot{m}_{22}(H_{23} - H_{22}) \tag{5.7}$$

$$T_{m,Cond\,2} = \frac{(T_5 - T_{22}) - (T_5 - T_{23})}{log\left(\frac{T_5 - T_{22}}{T_5 - T_{23}}\right)} \tag{5.8}$$

In SCRS, VARS and VCRS are integrated with a heat exchanger that acts as an evaporator in VARS and as a subcooler. The heat rejected from the subcooler (Eq.(5.9)) is supplied as a cooling load to VARS (Eq. (5.10)). The mass flow rate refrigerant in VARS ($\dot{m}_{ref_2}$) is also calculated using Eq.(5.10). The LMTD of this evaporator-subcooler ($T_{m,Subc}$) is the overlapping temperature, i.e., the temperature difference maintained between the evaporating refrigerant stream in VARS and the subcooling refrigerant in VCRS.

$$\dot{Q}_{Subc} = \dot{m}_{ref_1}(H_5 - H_1) \tag{5.9}$$

$$\dot{Q}_{Subc} = \dot{m}_{ref_2}(H_6 - H_{15}) \tag{5.10}$$

$$T_{m,Subc} = (T_1 - T_6) \tag{5.11}$$

TH-3395_176107002

Absorber in VARS deals with the absorbent as well as refrigerant streams. Therefore, the mass flow rate of the strong and weak solution is determined using component balance equations, as shown in Eqs.(5.12)-(5.13).

$$\dot{m}_7\left(X_{10}-X_7\right)=\dot{m}_{ref_2}X_{10} \tag{5.12}$$

$$\dot{m}_{10}\left(X_{10}-X_7\right)=\dot{m}_{ref_2}X_7 \tag{5.13}$$

The absorber heat load ($\dot{Q}_{Abs}$), coolant mass flow rate ($\dot{m}_{20}$), and LMTD ($T_{m,\ Abs}$) are determined using Eqs. (5.14)-(5.16).

$$\dot{Q}_{Abs}=\dot{m}_{ref\,2}H_6+\dot{m}_{12}H_{12}-\dot{m}_7H_7 \tag{5.14}$$

$$\dot{Q}_{Abs}=\dot{m}_{20}\left(H_{21}-H_{20}\right) \tag{5.15}$$

$$T_{m,\,Abs}=\frac{\left(T_{12}-T_{21}\right)-\left(T_7-T_{20}\right)}{log\left(\frac{T_{12}-T_{21}}{T_7-T_{20}}\right)} \tag{5.16}$$

The work done by pump ($\dot{W}_P$) is computed using the density of the absorbent-refrigerant mixture (ρ_{mix}) and pump efficiency (Eqs.(5.17)-(5.18) . The total work done by the compressor and pump is shown in Eq.(5.19) .

$$\rho_{mix}=X_7\rho_{salt}+\left(1-X_7\right)\rho_{water} \tag{5.17}$$

$$\dot{W}_P=\frac{\dot{m}_7\left(P_{14}-P_6\right)}{\rho_{mix}\eta_P} \tag{5.18}$$

$$\dot{W}_T=\dot{W}_C+\dot{W}_P \tag{5.19}$$

The temperature of the inlet and outlet streams of the solution heat exchanger in a thermal compressor is determined using the effectiveness of the exchanger (Eqs.(5.20)-(5.21)).

$$\varepsilon=\frac{\left(\dot{m}C_p\right)_{10}}{\left(\dot{m}C_p\right)_{min}}\frac{T_{13}-T_{11}}{T_{13}-T_7} \tag{5.20}$$

$$\varepsilon=\frac{\left(\dot{m}C_p\right)_{7}}{\left(\dot{m}C_p\right)_{min}}\frac{T_{9}-T_{7}}{T_{13}-T_7} \tag{5.21}$$

Later, based on the temperatures and enthalpies of the inlet and outlet streams, the heat load ($\dot{Q}_{Shx}$) and LMTD ($T_{m,\ Shx}$) are calculated using Eqs. (5.22)-(5.24).

TH-3395_176107002

$$\dot{Q}_{Shx} = \dot{m}_{12}\left(H_{10} - H_{11}\right) \tag{5.22}$$

$$\dot{Q}_{Shx} = \dot{m}_{7}\left(H_{9} - H_{8}\right) \tag{5.23}$$

$$T_{m,Shx} = \frac{\left(T_{10} - T_{9}\right) - \left(T_{11} - T_{8}\right)}{log\left(\frac{T_{10} - T_{9}}{T_{11} - T_{8}}\right)} \tag{5.24}$$

Equations for generator heat load ($\dot{Q}_{Gen}$), the mass flow rate of the hot utility stream ($\dot{m}_{18}$), and LMTD ($T_{m,\,Gen}$) calculation are given below (Eqs. (5.25)-(5.27)).

$$\dot{Q}_{Gen} = \dot{m}_{ref_2} H_{13} + \dot{m}_{12} H_{10} - \dot{m}_{7} H_{9} \tag{5.25}$$

$$\dot{Q}_{Gen} = \dot{m}_{18}\left(H_{19} - H_{18}\right) \tag{5.26}$$

$$T_{m,Gen} = \frac{\left(T_{18} - T_{10}\right) - \left(T_{19} - T_{13}\right)}{log\left(\frac{T_{18} - T_{10}}{T_{19} - T_{13}}\right)} \tag{5.27}$$

The rejected heat by the condenser after converting superheated refrigerant to saturated liquid refrigerant is assessed using Eq.(5.28). The mass flow rate of the coolant used for removing condenser heat load is calculated with Eq.(5.29) while the LMTD ($T_{m,\,Cond1}$) of the condenser in VARS is obtained using Eq.(5.30).

$$\dot{Q}_{Cond\,1} = \dot{m}_{6}\left(H_{13} - H_{14}\right) \tag{5.28}$$

$$\dot{Q}_{Cond\,1} = \dot{m}_{16}\left(H_{17} - H_{16}\right) \tag{5.29}$$

$$T_{m,Cond1} = \frac{\left(T_{14} - T_{16}\right) - \left(T_{14} - T_{17}\right)}{log\left(\frac{T_{14} - T_{16}}{T_{14} - T_{17}}\right)} \tag{5.30}$$

The coefficient of performance (COP) of the individual VCRS, VARS, and total system are calculated using Eqs.(5.31)-(5.33) based on the heat load supplied to the evaporator, subcooler, and work done by the compressor and pump.

$$COP_{VCRS} = \frac{\dot{Q}_{Evp}}{\dot{W}_{C}} \tag{5.31}$$

$$COP_{VARS} = \frac{\dot{Q}_{Subc}}{\dot{Q}_{Gen} + \dot{W}_{P}} \tag{5.32}$$

$$COP_{SCRS} = \frac{\dot{Q}_{Evp}}{\dot{Q}_{Gen} + \dot{W}_{T}} \tag{5.33}$$

TH-3395_176107002

Based on the second law of thermodynamics, the total exergy destruction of the SCRS is determined (Eqs.(5.34)-(5.35)).

$$\dot{B}_{D,T} = \sum_{\substack{All\ heat \\ Exchangers}} \dot{B}_D + \dot{W}_T \tag{5.34}$$

$$\dot{B}_{in} = \dot{B}_{D,T} + \left(\dot{B}_{24} - \dot{B}_{25}\right) \tag{5.35}$$

$$\dot{B}_D = \sum_{in} \dot{m}b - \sum_{out} \dot{m}b \tag{5.36}$$

Total exergy destruction is the difference between exergy input ($\dot{B}_{in}$) and output ($\dot{B}_{out}$). Exergy destruction of the component is calculated using Eq.(5.36). Refrigeration is performed on the secondary fluid stream (chilled water) supplied to the evaporator. Therefore, the exergy output of chilled water is considered.

5.2.3. Economic model of SCRS

The thermoeconomic optimization connects the exergy and costs in a single framework. The total annual cost for the proposed system is considered as Eq.(5.37).

$$C_T = input\ exergy\ cost + investment\ cost + maintenance\ cost + penalty\ cost \tag{5.37}$$

The objective function to minimize the total annual cost of SCRS and CRS is solved for twelve different combinations of absorbent solution/solution mixture-water-refrigerant of SCRS constituting three different absorbent solution/solution mixture-water pairs in VARS and four different refrigerants in VCRS and is given as Eq. (5.38),

$$min\ C_T(x) = top\ C_{exer}\dot{B}_{in} + top\ C_{el}\ \dot{W}_T + a^c\ Z_T + C_{Env} + CCU\left(\dot{Q}_{Cond\ 2} + \dot{Q}_{Abs} + \dot{Q}_{Cond\ 1}\right) \tag{5.38}$$

Capital recovery factor (a^c) is calculated using Eq. (3.16) in Chapter 3. The total hours of operations, interest rate, and period of payment are considered the same as the CRS study case (Chapter 4). The cold utility (CCU) cost is 10 US \$/kW [247] for the water-cooled heat exchangers considered in this work. The input exergy cost (C_{exer}) is considered as 0.03785 US \$/kW h, whereas the electricity cost is (C_{el}) 0.0610 US \$/kW h. The investment cost for the SCRS is determined using the equations given in Eqs. (4.28-4.31) in Chapter 4. The penalty cost (carbon tax) is computed based on the CO_2 emission in the atmosphere due to compressor work. The amount of CO_2 emitted and penalty cost imposed are calculated using Eqs. (4.32-4.33) in Chapter 4.

TH-3395_176107002

5.2.4. Optimization model and solution strategy

An optimization model generally consists of an objective function, equality constraint, and inequality constraints. The thermodynamic modelling component of this work includes the derivation and formulation of the objective function, as well as two constraints: (i) the concentration of the weak solution (X_7), should always be lower than the concentration of the strong solution (X_{10}) and (ii) the temperature of the solution, before entering the throttling valve, does not reach the crystallization temperature (T_C). These constraints are given as follows:

$$X_{10} - X_7 > 0 \ \ and \ \ T_{11} - T_C \geq 5 \tag{5.39}$$

Subcooler temperature (T_1, ˚C), evaporator temperature (T_3, ˚C), condenser 2 temperature (T_5, ˚C), absorber temperature (T_7, ˚C), generator temperature (T_{13}, ˚C), condenser 1 temperature (T_{14}, ˚C), overlap temperature ($T_{overlap}$, ˚C), and effectiveness of solution heat exchanger (ε) are considered as decision variables SCRS. The decision variables for CRS are the same as in Chapter 4. The bounds of decision variables for SCRS are given as follows,

$$\begin{aligned} &15 \leq T_1 \leq 21;\ -10 \leq T_3 \leq 4;\ 36 \leq T_5 \leq 48;\ 36 \leq T_7 \leq 42;\ 70 \leq T_{13} \leq 87;\ 36 \leq T_{14} \leq 48 \\ &5 \leq T_{overlap} \leq 10;\ 0.6 \leq \varepsilon \leq 0.9; \end{aligned} \tag{5.40}$$

The bounds of decision variables for CRS are given as follows,

$$\begin{aligned} &15 \leq T_1 \leq 21;\ -10 \leq T_3 \leq 4;\ 36 \leq T_6 \leq 42;\ \ 70 \leq T_{12} \leq 87;\ 36 \leq T_{13} \leq 48 \\ &5 \leq T_{overlap} \leq 10;\ 0.6 \leq \varepsilon \leq 0.9; \end{aligned} \tag{5.41}$$

The objective function is optimized using five recently proposed metaheuristic techniques: sTLBO, ASO, TGA, COA, and YYPO. In the optimization process, upper bounds, lower bounds, and constraints are selected based on thermodynamic characteristics of absorbent solution/solution mixture-water-refrigerant combinations, and the information is incorporated into the metaheuristic techniques. The SCRS and CRS model acquires a possible solution from the metaheuristic techniques and suitably calculates the required parameters for determining the total annual cost for CRS and SCRS. Metaheuristic techniques are stochastic and must be performed in multiple runs to determine their efficiency in evaluating an optimal solution. The current work considers 25 independent runs for all five metaheuristic techniques (sTLBO, ASO, TGA, COA, and YYPO) considered in the present work. The number of new solutions generated is not the same for all the metaheuristic techniques considered in this work and varies considerably for different metaheuristic techniques. Therefore, choosing general termination criteria is important in assessing their potential. Correspondingly, the maximum number of function evaluations (3000) is chosen as termination criteria by considering all the selected

TH-3395_176107002

metaheuristic techniques. The population size is chosen as 30 for all metaheuristic techniques. However, this does not apply to YYPO as it functions with two possible solutions. The other parameters of each metaheuristic technique are considered as provided in the literature of the respective metaheuristic technique. The simulations are performed on the MATLAB 2019a platform. A brief description of the metaheuristic techniques used in this work is given below.

5.3. Model validation of the thermodynamic model

Table 5. 1 Model Validation of SCRS

Parameters	Thermodynamic model validation		
	Xu et al. [145]	**Present work**	**Error (%)**
Subcooler Temperature (T_1, °C)	18	18	-
Evaporator temperature (T_3, °C)	0	0	-
Condenser 2 temperature (T_5, °C)	40	40	-
Absorber temperature (T_7, °C)	40	40	-
Generator temperature (T_{13}, °C)	90	90	-
Condenser 1 temperature (T_{14}, °C)	40	40	-
Effectiveness (ε)	0.68	0.68	-
Overlap temperature ($T_{overlap}$, °C)	8	8	-
$\dot{Q}_{Subc}$ (kW)	19.83	19.83	0
$\dot{Q}_{Evp}$ (kW)	100	100	0
$\dot{Q}_{Abs}$ (kW)	25.19	24.68	1.31
$\dot{Q}_{Gen}$ (kW)	26.01	25.89	0.46
$\dot{Q}_{Cond1}$ (kW)	21.14	21.10	0.19
$\dot{W}_C$ (kW)	23.65	23.75	0.42
COP_{SCRS}	0.4148	0.4135	0.31
$\dot{m}_{ref_2}$ (Refrigerant mass flow rate in VARS)	0.0085	0.0084	1.18
$\dot{m}_{ref_1}$ (Refrigerant mass flow rate in VCRS)	0.5173	0.5173	0

The research findings of Xu et al.[145] for the cooling capacity of 100 kW cooling capacity was considered to validate the thermodynamic model. Table 5.1 shows the comparison of heat load and other associated parameters of SCRS between the present work and Xu et al.[145].

TH-3395_176107002

The current thermodynamic model of SCRS simulated for the decision variables (condenser 2 temperature (T_5, °C), evaporator temperature (T_3, °C), absorber temperature (T_7, °C), generator temperature (T_{13}, °C), condenser 1 temperature (T_{14}, °C), effectiveness (ε), overlap temperature ($T_{overlap}$, °C), subcooler temperature (T_1, °C) given by Xu et al.[145]. The calculated parameters from the present work ($\dot{Q}_{Evp}$ (kW), $\dot{Q}_{Abs}$ (kW), $\dot{Q}_{Gen}$ (kW), $\dot{Q}_{Cond1}$ (kW), $\dot{W}_C$ (kW), $\dot{Q}_{Subc}$ (kW), COP_{SCRS}, $\dot{m}_{ref_2}$ (refrigerant mass flow rate in VARS, kg/s), $\dot{m}_{ref_1}$ (refrigerant mass flow rate in VCRS, kg/s)) are in good agreement with the findings of Xu et al.[145], as shown in Table 5.1. Therefore, the proposed thermodynamic and economic model can be considered valid and expressed as a mathematical programming model for the optimization of SCRS.

5.4. Results and discussions

The objective function is solved using recently proposed metaheuristic techniques, namely sTLBO, ASO, COA, YYPO, and TGA, for an evaporator load of 80.7 kW. A comparative study of CRS and SCRS based on energy, exergy, and economic performance is discussed to understand the effect of subcooling on the cascaded refrigeration system (CRS). For the current problem, the input data of hot stream, coolant, and economic parameters are given in Appendix –B (Table B2).

5.4.1. Analysis of optimum decision variables and derived parameters on the minimum total annual cost of SCRS and CRS

The best solutions among all algorithms over all the runs are reported as the optimal solutions. The objective function was to identify the minimum total annual cost of SCRS and CRS from the twelve different absorbent solution/solution mixture-water-refrigerant combinations, as shown in Table 5.2. The lowest and highest total annual cost (15401.91 US $/year and 16785.10 US $ year) was found for ($CaCl_2$-LiBr-$LiNO_3$)-H_2O-R290 and LiBr-H_2O-R123, respectively, for SCRS whereas the lowest and highest total annual cost (13164.80 US $/year and 15406.71 US $/year) was found for ($CaCl_2$-LiBr-$LiNO_3$)-$H_2O$-R290 and LiBr-$H_2O$-R1234yf, respectively, for CRS (Table 5.2).

Input exergy cost is predominantly dependent on the exergy destruction of the system, while penalty cost is determined based on the work done by the compressor. The LiBr-H_2O-R123 pair has higher exergy destruction and compressor work, which results in higher input exergy and penalty cost raising the total annual cost of the pair. In the case of $CaCl_2$-LiBr-$LiNO_3$-R290, the exergy destruction and compressor work are lower, resulting in a reduced cost than

TH-3395_176107002

LiBr-H_2O-R123. The same justification applies to the total annual cost obtained for ($CaCl_2$-LiBr-$LiNO_3$)-H_2O-R290 and LiBr-H_2O-R1234yf in CRS. It was also noted that R290 gives the lowest total annual cost regardless of absorbent solution/solution mixture-water pairs in both CRS and SCRS.

Table 5. 2 The minimum total annual cost for SCRS and CRS

VARS Absorbent Refrigerant mixture	VCRS Refrigerant	Investment Cost	Penalty Cost	CCU Cost	Total Cost
SCRS (US $/year)					
LiBr-H_2O	R290	8486.90	6129.34	1114.87	15731.11
	R123	**9326.68**	**6380.87**	**1077.55**	**16785.10**
	R1234yf	9369.63	6086.01	1151.03	16606.67
	R1234ze	9168.82	6134.06	1124.19	16427.08
LiCl-H_2O	R290	8191.02	6120.71	1109.78	15421.52
	R123	9095.82	6384.60	1071.66	16552.08
	R1234yf	9003.43	6092.67	1142.20	16238.29
	R1234ze	8849.01	6140.86	1116.39	16106.26
$CaCl_2$-LiBr-$LiNO_3$-H_2O	**R290**	**8198.94**	**6121.86**	**1081.11**	**15401.91**
	R123	9103.91	6383.44	1049.97	16537.33
	R1234yf	9014.40	6092.58	1107.96	16214.93
	R1234ze	8859.10	6140.52	1086.38	16086.00
CRS (US $/year)					
LiBr-H_2O	R290	11126.04	2096.73	1985.53	15208.29
	R123	11307.13	2053.12	1983.95	15344.19
	R1234yf	**11312.67**	**2106.85**	**1987.19**	**15406.71**
	R1234ze	11272.72	2083.37	1985.42	15341.52
LiCl-H_2O	R290	9253.03	2096.73	1936.77	13286.53
	R123	9436.66	2053.12	1934.74	13424.51
	R1234yf	9440.29	2106.85	1937.32	13484.45
	R1234ze	9400.87	2083.37	1936.19	13420.43
$CaCl_2$-LiBr-$LiNO_3$-H_2O	**R290**	**9309.46**	**2096.72**	**1758.61**	**13164.80**
	R123	9493.97	2053.12	1755.88	13302.97
	R1234yf	9497.36	2106.88	1758.60	13362.85
	R1234ze	9458.19	2083.37	1757.21	13298.77

Figs. 5.2 (a-b) show the minimum total annual cost reported by various metaheuristic techniques (sTLBO, ASO, COA, YYPO, and TGA) for SCRS and CRS using three different absorbent solution/solution mixture-water combinations (LiBr-H_2O (S1), LiCl-H_2O (S2),

TH-3395_176107002

$CaCl_2$-LiBr-$LiNO_3$-H_2O (S3)) in VARS and four low GWP and ODP refrigerants (R290 (R1), R123 (R2), R1234yf (R3), and R1234ze (R4)) in VCRS. As stated earlier, no single algorithm can solve all the optimization problems efficiently; because of this, five recent metaheuristic techniques have been implemented to determine which algorithm performs better.

In this case, COA and sTLBO obtain the minimum cost for both the absorbent solutions for SCRS (Fig. 5.2 (a)) and CRS (Fig. 5.2 (b)). Table 5.6 shows that the standard deviation for ASO, TGA, and YYPO are significantly higher than for COA and sTLBO. A higher standard deviation indicates the poor performance of the algorithm, indicating that these algorithms provide no better value for optimizing the total annual cost.

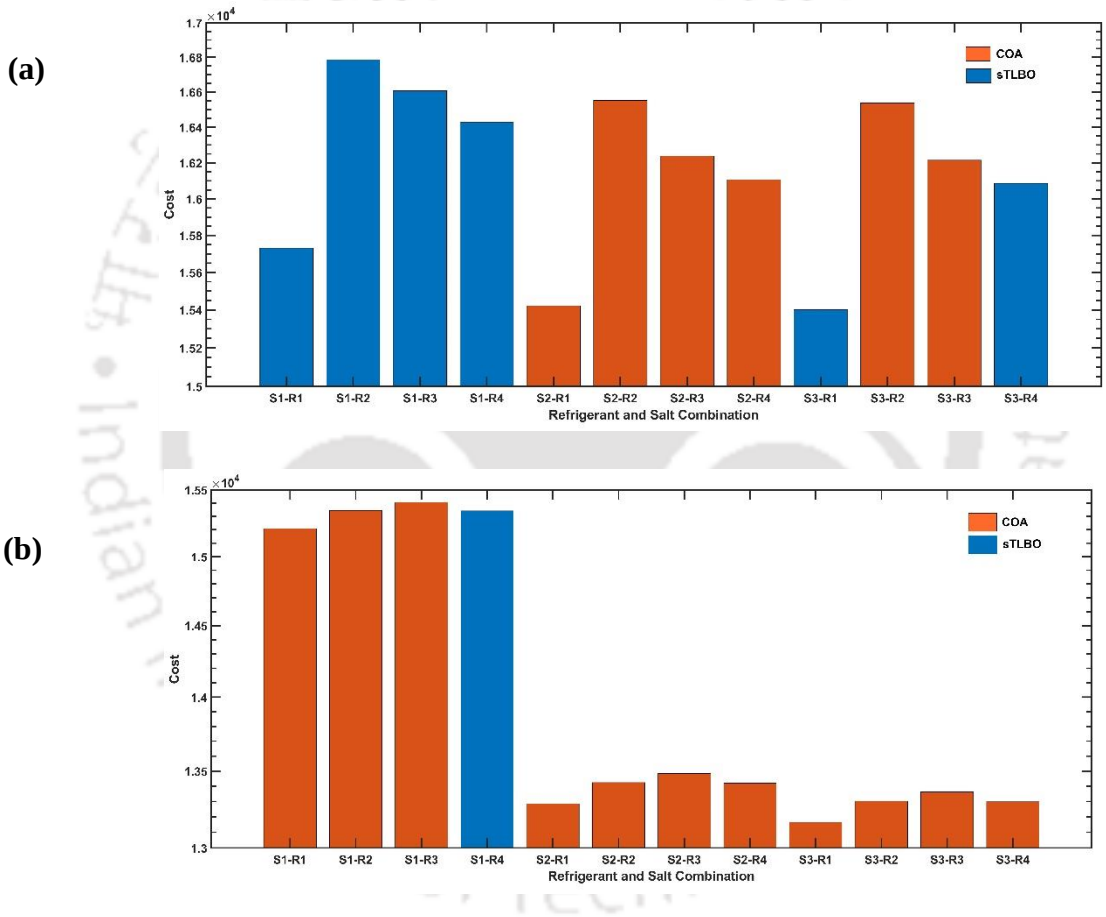

Fig. 5. 2 Minimum total annual cost corresponding to each absorbent solution/solution mixture-water-refrigerant pair for (a) SCRS (b) CRS

COA and sTLBO behave equally better for SCRS (Fig. 5.2 (a)), whereas COA alone is able to perform with almost all combinations for CRS consistently (Fig. 5.2 (b)). It is noted that sTLBO determines the minimum total annual cost (15401.91 US $/year) for SCRS, whereas COA finds out the minimum total annual cost (13164.80 US $ year) for CRS for the same S3-R1 combination (Table 5.2 and Figs. 5.2 (a-b)). Compared to SCRS, CRS is operated at a lower

TH-3395_176107002

pressure, resulting in lower compressor work and hence lesser penalty cost. SCRS is operated at higher pressure, determining the higher penalty cost and, hence, the higher total annual cost. For all the cases, SCRS has a higher cost than CRS, as shown in Figs. 5.2 (a-b). Further analysis on minimum total annual cost, optimum decision variables, and derived parameters are as follows.

5.4.2. Energy analysis

Table 5. 3 Comparison between SCRS, CRS, and reference paper

Parameters	SCRS	CRS	Jain et al. [195]
COP	2.93	0.84	0.63
COP_{VCRS}	6.33	18.48	9.70
COP_{VARS}	0.93	0.93	0.75
$B_{D,T}$ (kW)	8.03	13.41	21.87
W_C (kW)	12.75	4.37	8.51
Q_{Subc} (kW)	13.74	-	-
$Q_{Cond\ 2}$ (kW)	79.71	-	-
Q_{Abs} (kW)	13.84	85.68	113.96
Q_{Gen} (kW)	14.80	91.63	119.08
$Q_{Cond\ 1}$ (kW)	14.56	90.18	94.15
$Q_{Cascade}$ (kW)	-	85.07	89.02
A_{Subc} (m^2)	2.41	-	-
A_{Evp} (m^2)	9.54	9.54	4.99
$A_{Cond\ 2}$ (m^2)	11.06	-	-
A_{Abs} (m^2)	1.52	9.44	10.08
A_{shx} (m^2)	1.58	9.77	7.62
A_{Gen} (m^2)	0.9	5.6	7.84
$A_{Cond\ 1}$ (m^2)	0.86	5.28	6.30
$A_{Cascade}$ (m^2)	-	14.97	12.19

Table 5.3 displays a comparison between the thermodynamic and geometric parameters for the optimal absorbent solution/solution mixture-water-refrigerant combination ($CaCl_2$-LiBr-$LiNO_3$-H_2O-R290) for CRS, SCRS, and Jain et al. [195] which is considered as a reference paper in the present study. Table 5.4 and Table 5.5 show the optimal values of decision variables and thermodynamic properties at the optimum case for SCRS respectively.

TH-3395_176107002

Table 5. 4 Optimal decision variables for SCRS

VARS Absorbent refrigerant	VCRS Refrigerants	Condenser 2 (VCRS) temperature (˚C)	Evaporator temperature (˚C)	Absorber temperature (˚C)	Generator temperature (˚C)	Condenser 1 (VARS) Temperature (˚C)	Overlap temperature (˚C)	Effectiveness of solution heat exchanger	Subcooler temperature (˚C)
$LiBr-H_2O$	R290	36.27	4	36	83.79	38.89	7.12	0.6	15.32
	R123	36.14			83.85	38.93	7.01		
	R1234yf	36.16			83.77	38.87	6.96		15
	R1234ze	36.18			83.84	38.93	7.00		
$LiCl-H_2O$	R290	36.30	4	36	80.83	41.69	10	0.6	15
	R123	36.16			80.74	41.60			
	R1234yf	36.19			80.82	41.68			
	R1234ze	36.22			80.89	41.74			
$CaCl_2$-LiBr-$LiNO_3$-H_2O	**R290**	**36.30**	**4**	**36**	**82.52**	**40.28**	**8.14**	**0.6**	**15**
	R123	36.15			82.50	40.26	8.09		
	R1234yf	36.19			82.55	40.31	8.09		
	R1234ze	36.21			82.41	40.18	8.07		

TH-3395_176107002

Table 5. 5 Thermodynamic properties for SCRS at the optimum case for ($CaCl_2$-LiBr-$LiNO_3$-H_2O)-R290

State Point	T (˚C)	P (kPa)	$\dot{m}$ (R290/ kg/s)	$\dot{m}$ (H_2O /kg/s)	$\dot{m}$ (Salt solution /kg/s)	X (%)	H (kJ/kg)	S (kJ/kg K)
1	15	1256.2	0.24	-	-	-	238.56	1.13
2	4	535.1	0.24	-	-	-	238.56	1.14
3	4	535.1	0.24	-	-	-	579.24	2.37
4	46.46	1256.2	0.24	-	-	-	633.1	2.41
5	36.31	1256.2	0.24	-	-	-	296.54	1.33
6	6.86	0.99	-	0.0059	-	-	2513.5	8.98
7	36	0.99	-	-	0.0436	56.26	324.38	-
8	36	7.50	-	-	0.0436	56.26	324.38	-
9	57.78	7.50	-	-	0.0436	56.26	375.98	-
10	82.51	7.50	-	-	0.0377	64.99	414.43	-
11	54.61	7.50	-	-	0.0377	64.99	351.25	-
12	54.61	0.99	-	-	0.0377	64.99	351.25	-
13	82.51	7.50	-	0.0059	-	-	2654.5	8.49
14	40.28	7.50	-	0.0059	-	-	168.70	0.58
15	6.86	0.99	-	0.0059	-	-	168.70	0.60
16	30	101.32	-	0.6968	-	-	125.82	0.44
17	35	101.32	-	0.6968	-	-	146.72	0.51
18	100	101.32	-	0.0064	-	-	2675.6	7.35
19	90	101.32	-	0.0064	-	-	377.04	1.19
20	30	101.32	-	0.6622	-	-	125.82	0.44
21	35	101.32	-	0.6622	-	-	146.72	0.51
22	30	101.32	-	3.8144	-	-	125.82	0.44
23	35	101.32	-	3.8144	-	-	146.72	0.51
24	10	101.32	-	3.8431	-	-	42.11	0.15
25	5	101.32	-	3.8431	-	-	21.12	0.076

TH-3395_176107002

Jain et al. [194] have done a study on the CRS with a working pair as R410a in VCRC and LiBr-H_2O in the VARS section different than the presented results and an evaporator load of 80.7 kW. The COP_{SCRS} is higher than the COP_{CRS}, and the Jain et al. [194], as shown in Table 5.3. Adding a subcooler in the system improves COP_{SCRS} by ~250% compared to CRS for $CaCl_2$-LiBr-$LiNO_3$-H_2O-R290 and ~365 % for the reference paper [195]. In SCRS, the subcooler considerably decreases the cooling load supplied to the VARS, due to which the mass flow rate, heat load, area, and exergy destruction of all system components tend to decrease. SCRS subcooler is maintained at higher pressure due to higher condenser temperature. This further increases the compressor pressure and work for SCRS, which reduces COP_{VCRS} compared to CRS. Lower compressor pressure results in lower work done and a higher value of COP_{VCRS} in CRS (Tables 5.3 and 5.4).

The lesser heat load of the generator significantly impacts VARS and COP_{SCRS}. This results in a higher value of COP_{SCRS} despite having higher compressor work, as observed in Tables 5.3 and 5.4. The heat load supplied to the VARS is 91.63 kW in CRS and 14.80 kW in SCRS for ($CaCl_2$-LiBr-$LiNO_3$)-H_2O-R290 (Table 5.3), while for reference paper [195], it is determined as 119.08 kW which is higher than both cases. However, COP_{VARS} is the same for both SCRS and CRS, whereas the reference paper [195] has obtained a 24 % lower value than both CRS and SCRS (Table 5.3) due to the difference in the heat load supplied. The variation in the heat load obtained for the thermal compressor of the current study (SCRS and CRS) and reference paper [195] is due to the enthalpy difference of the absorbent-refrigerant mixture solution. The amount of energy transferred to VARS is lesser in SCRS compared to CRS. This is due to the lesser enthalpy difference between the inlet and outlet streams of the subcooler. CRS handles high enthalpy difference that varies significantly depending on absorbent solution/solution mixture-water-refrigerant combinations. The heat load of the absorber, generator, and solution heat exchanger varies significantly for all combinations in the case of CRS (results not shown), whereas there are no significant changes observed for SCRS (Table 5.3). This is primarily due to differences in the sensible and latent heat load of the streams involved in each heat exchanger of CRS and SCRS. Based on the energy analysis, SCRS can be considered more efficient than CRS.

5.4.3. Exergy analysis

The total exergy destruction (BDT) of the system is calculated by the amount of input and output exergy as shown in Eq. (11). As seen in Table 5.3, the heat load of the thermal compressor in the SCRS is much lesser for the CRS and reference paper [195]. This is because

TH-3395_176107002

of less refrigeration load received by VARS, which reduces the mass flow rate of the refrigerant, absorbent-refrigerant mixture, and the utilities provided. As an example, the mass flow rate of cold utilities decreases from 4 kg/s to 0.66 kg/s, 4.32 kg/s to 0.7 kg/s, and 0.04 to 0.006 kg/s for the absorber, condenser, and generator, respectively, after the addition of subcooler in SCRS for the case of $CaCl_2$-LiBr-$LiNO_3$-H_2O (results not shown). In the case of the reference paper, mass flow rates of utilities for the absorber, condenser, and generator are 5.46 kg/s, 4.51 kg/s, and 0.052 kg/s, respectively, which seems to be higher than CRS and SCRS. Compressor work (W_c) also contributes to exergy destruction in the system (Table 5.3). Even with a high W_c, a significant reduction (40%) in exergy destruction is observed for SCRS compared to CRS due to a reduction in the mass flow rate of utilities. Jain et al. [195] have reported the highest exergy destruction among all three cases, as shown in Table 5.3; which is 63.28 % greater than SCRS and 37.31 % greater than CRS, respectively, due to higher compressor work and mass flow rate of utilities determined in [195].

It can be observed that there is a significant difference in the heat load of the thermal compressor of VARS between CRS, SCRS, and reference paper [195]. The mass flow rate of the weak solution, strong solution, and refrigerant in VARS changed from 0.27 kg/s to 0.04 kg/s, 0.23 kg/s to 0.04 kg/s, and 0.04 kg/s to 0.006 kg/s, respectively, for $CaCl_2$-LiBr-$LiNO_3$-H_2O due to less refrigeration load in the VARS section of SCRS. However, the mass flow rate of weak solution, strong solution, and VARS refrigerant for reference paper is determined as 0.31 kg/s, 0.28 kg/s, and 0.037 kg/s, respectively, which seems higher than CRS and SCRS cases. No significant difference was found in the circulation ratio, calculated as 6.8 and 6.6 for CRS and SCRS, respectively, for $CaCl_2$-LiBr-$LiNO_3$-H_2O; hence, the heat transfer in the solution heat exchanger is similar for both SCRS and CRS while for Jain et al.[195] it is reported as 9.06, 24.94 % higher than SCRS and 27.15 % higher than CRS. SCRS can be a better system than CRS based on the exergy analysis as it leads to lower BDT, heat load, and utility mass flow rate.

5.4.4. Economic analysis

Decreased heat load in SCRS significantly impacts the area of heat exchangers. Despite the inclusion of an additional condenser in SCRS, the lesser heat transfer area of other heat exchangers helps lower the total investment cost of the system, as seen in Figs. 5.3 (a-b). An increase in compressor work increases the penalty cost of the system. Reduction in heat load reduces the usage of cold utilities, resulting in lower CCU for SCRS. $CaCl_2$-LiBr-$LiNO_3$-H_2O combined with R290 showed the lowest total annual cost for both SCRS and CRS Figs. 5.3 (a-

TH-3395_176107002

b). Compared to CRS, SCRS reports a higher annual cost for all absorbent-refrigerant-refrigerant combinations, primarily due to higher penalty costs (Table 5.2).

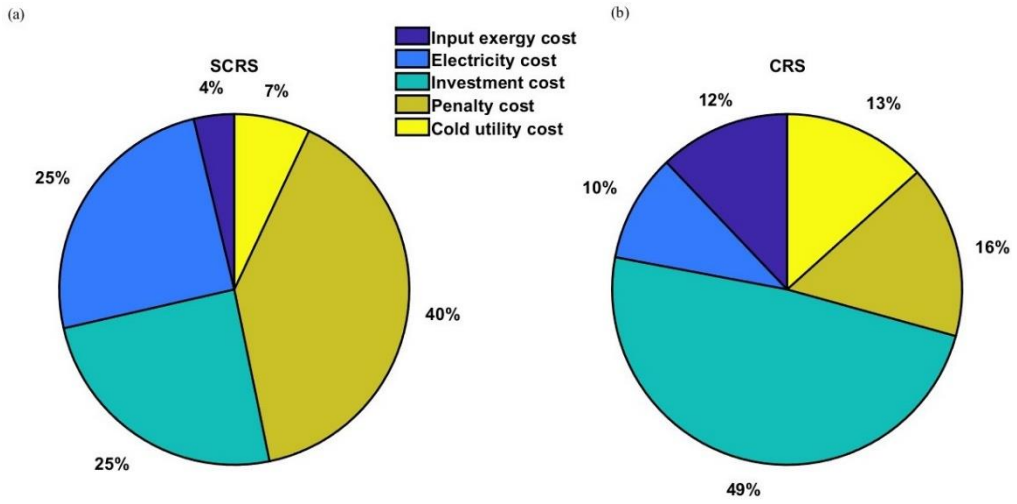

Fig. 5. 3 Cost break up for the best solution (a) SCRS and (b) CRS

5.4.4.1.Investment cost

In SCRS, the lower heat load on VARS exchangers is due to refrigerant subcooling in VCRS. The total area of heat exchangers is 27.87 m^2 and 54.6 m^2 for SCRS and CRS, respectively, for $CaCl_2$-LiBr-$LiNO_3$-H_2O-R290. Due to this, the estimated investment cost is 8198.94 US $/year and 9309.46 US $/year for SCRS and CRS, respectively (Table 5.2). R290 combined with all absorbent solution/solution mixture-water-refrigerant combinations showed the lowest investment cost.

5.4.4.2.Maintenance cost

The cost of energy is proportional to compressor work in VCRS. Due to the higher condenser temperature in SCRS, the compressor operates at higher pressure. This increases the energy demand and power costs. The compressor work is 12.75 kW and 4.37 kW, with the maintenance cost of 3828.7 US $/year and 1309.37 US $/year for SCRS and CRS, respectively, for $CaCl_2$-LiBr-$LiNO_3$-H_2O-R290 (Tables 5.2 and 5.4) while for reference paper [195] compressor work and maintenance cost are reported as 8.51 kW and 2553 US $/year which is greater than CRS but is lower than SCRS. The maintenance of a refrigeration system also includes the cost of exergy input. The cost of exergy is proportional to the total exergy destruction of the system. The total exergy destruction for reference paper [195], CRS, and SCRS is 21.87 kW, 13.41 kW, 8.03 kW, which results in 3194.3 US $/year, 1593.7 US $/year, and 575 US $/year, respectively (Table 5.3) indicating higher maintenance cost of 5746.3 US $/year for reference paper [195].

TH-3395_176107002

5.4.4.3.Penalty cost/Carbon tax

Condenser temperature affects the compressor work in both CRS and SCRS. Lower cascade condenser temperature requires lower compressor pressure and results in lesser compressor work for CRS, whereas higher cascade condenser temperature in SCRS requires higher compressor pressure and results in higher compressor work. Higher compressor work results in higher penalty costs. The penalty cost of the system increases (2096.73 US $/year to 6129.34 US $/year) with compressor work in SCRS for $CaCl_2$-LiBr-$LiNO_3$-H_2O-R290 as shown in Table 5.2 and Figs.5.3 (a-b).

5.4.4.4.Cost of cold utility (CCU)

The heat exchangers (condenser and absorber) considered here are water-cooled. As a result, the cost of cold water plays a vital role in the total annual cost in this analysis. Table 5.2 reveals that CRS reports a higher CCU than SCRS due to the higher heat load on exchangers. The additional condenser in SCRS might affect the CCU due to the lesser heat load on the absorber and condenser 1. $CaCl_2$-LiBr-$LiNO_3$-H_2O paired with all refrigerants shows the lowest CCU. The CCU is 1758.6 US $/year and 1081.1 US $/year for CRS and SCRS, respectively, for $CaCl_2$-LiBr-$LiNO_3$-H_2O-R290 (Table 5.2 and Figs. 5.3 (a-b)).

5.4.5. Environmental analysis

Incorporating the environmental effect of the refrigeration system is especially crucial given the growing environmental difficulties, particularly those related to global warming brought on by greenhouse gases. The impact of the refrigeration system on the environment is analyzed by its CO_2 emissions. The CO_2 emission amount is around 68.02 tons/year, and 23.31 tons/year for SCRS and CRS, respectively, in the case of (($CaCl_2$-LiBr-$LiNO_3$)-H_2O)-R290. Less pressure on the compressor eventually leads to less electricity consumption, which significantly reduces CO_2 emission in the case of CRS. The penalty cost for CO_2 emission for CRS is $ 2096.72 and $ 6121.86 for SCRS, respectively. The penalty cost of CO_2 emission varies from country to country. The current study determines the cost of each heat exchanger and system component in US dollars. Therefore, the environmental cost of CRS and SCRS is estimated using the Iranian-considered penalty cost of US $90/ton of CO_2. Based on the CO_2 emissions, CRS is a more promising decarbonizing cooling technology than SCRS.

5.5. Convergence analysis

This section discusses how each algorithm converges across all runs while identifying the optimal cost for each refrigerant-absorbent solution pair. Based on these convergence curves,

TH-3395_176107002

one may conclude which algorithm converged swiftly with the lowest annual cost. Figs. 5.4 (a-c) shows the convergence of all algorithms for all absorbent solution/solution mixture-water-refrigerant combinations of SCRS. The convergence is demonstrated by considering the best-run values over the maximum function evaluations corresponding to each metaheuristic technique.

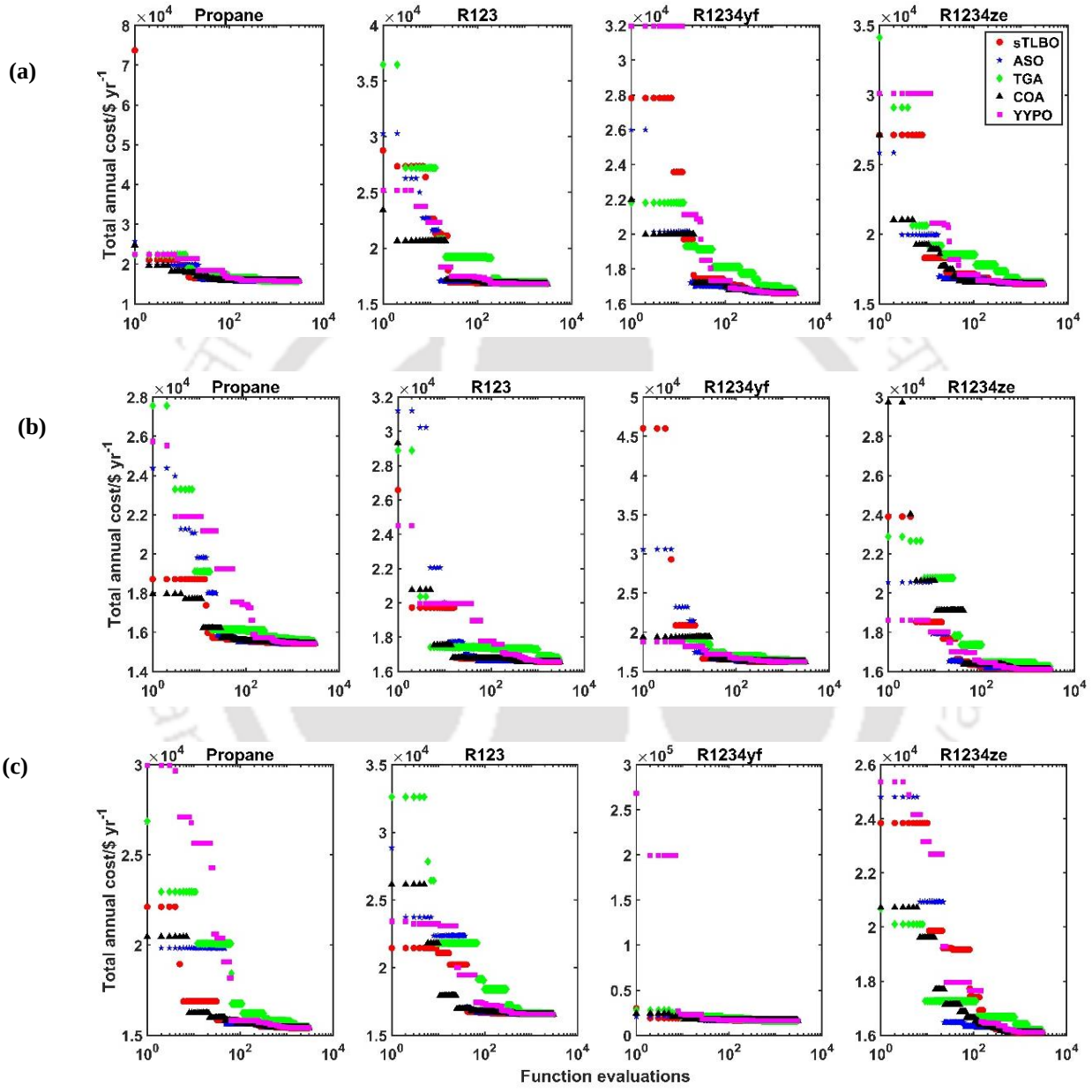

Fig. 5. 4 SCRS convergence profile for the best solution corresponding to absorbent combinations with (a) LiBr (b) LiCl and (c) $CaCl_2$-LiBr-$LiNO_3$

ASO and YYPO converge to the final objective value by utilizing approximately 47% of the functional evaluations. In all the refrigerant combinations with LiBr-H_2O, except R1234ze, TGA used the maximum number of function evaluations among all metaheuristic techniques

TH-3395_176107002

to converge to the final value. In the case of the LiBr-H_2O-R1234ze combination, COA provided a poorer convergence than other metaheuristic techniques. In all the refrigerant combinations with LiBr-H_2O, sTLBO has converged to the best objective value by utilizing approximately 66 % of the maximum function evaluations (Figs. 5.2 (a) and 5.4 (a)).

TGA provided a poor convergence in LiCl-H_2O-R290 and LiCl-H_2O-R123 by utilizing more than 95% of the function evaluations to reach the final objective value. In the case of LiCl-H_2O-R1234yf and LiCl-H_2O-R1234ze, sTLBO shows a poor convergence by utilizing more than 74% of the functional evaluations. Although COA used 64% of the maximum function evaluations to reach the final objective value, it has determined the best solution in all the LiCl-H_2O-refrigerant combinations (Figs. 5.2 (a) and 5.4(b)).

Among all the algorithms, sTLBO utilizes the highest (approximately 77%) functional evaluations to reach the final objective function for the $CaCl_2$-LiBr-$LiNO_3$-H_2O-refrigerant combinations except for R1234ze. In the $CaCl_2$-LiBr-$LiNO_3$-R1234ze combination, TGA is used in more than 88% of the maximum functional evaluations to reach the final objective value. YYPO shows a quick convergence in $CaCl_2$-LiBr-$LiNO_3$-H_2O-refrigerant combinations except for R1234yf, where ASO has converged to the final objective value faster than other metaheuristic techniques (Figs. 5.2 (a) and 5.4 (c)).

5.5.1. Statistical Analysis

Table 5.6 shows the best, mean, and standard deviation for overall runs of each algorithm in all twelve optimization scenarios for SCRS. The best value found by each algorithm for each absorbent solution/solution mixture-water-refrigerant combination indicates the minimum total annual cost computed across all runs. The mean value indicates the mean of the total annual cost for each absorbent solution/solution mixture-water-refrigerant combination, while the standard deviation suggests the overall annual cost difference from the mean, calculated by the respective algorithm across all runs. sTLBO identified optimal parameters for the best total annual cost for all refrigerants paired with LiBr-H_2O, whereas COA identified the best total annual cost for all refrigerants paired with LiCl-H_2O in SCRS.

Both sTLBO and COA identified the best total annual cost for all refrigerants paired with $CaCl_2$-LiBr-$LiNO_3$-H_2O. sTLBO provided the best mean and lowest standard deviation among all algorithms except for R123-LiBr-H_2O in all absorbent solution/solution mixture-water-refrigerant combinations (Table 5.6). The standard deviations from ASO and TGA were significantly larger than those from the other algorithms, demonstrating their inefficiency in selecting better solutions.

TH-3395_176107002

Table 5. 6 Statistical Analysis for SCRS

		Best					Mean					Standard Deviation				
Absorbent	Refrigerant	sTLBO	ASO	TGA	COA	YYPO	sTLBO	ASO	TGA	COA	YYPO	sTLBO	ASO	TGA	COA	YYPO
LiBr	R290	**15731.11**	15796.13	15818.21	15731.21	15744.30	**15731.41**	16098.37	15877.21	15733.40	15767.16	**0.35**	1124.37	30.50	5.16	13.85
	R123	**16785.10**	16819.04	16899.58	16785.11	16798.87	16788.75	16913.02	16951.57	**16787.28**	16832.95	13.61	58.32	39.46	**2.95**	27.03
	R1234yf	**16606.67**	16668.52	16728.01	16606.77	16619.23	**16607.63**	17060.51	16814.81	16609.17	16652.86	**2.46**	1261.93	51.17	3.45	22.64
	R1234ze	**16427.08**	16486.54	16549.55	16427.12	16438.48	**16428.48**	16862.66	16606.65	16429.31	16477.51	**3.24**	1252.22	42.71	3.97	26.12
LiCl	R290	15421.54	15457.98	15518.17	**15421.52**	15436.06	**15421.79**	15516.93	15619.28	15424.41	15474.19	**0.48**	37.17	42.34	14.09	28.91
	R123	16552.09	16582.46	16681.01	**16552.08**	16567.76	**16553.20**	16626.20	16755.96	16558.06	16615.10	**2.61**	36.02	61.19	10.57	32.28
	R1234yf	16238.32	16257.45	16328.57	**16238.29**	16250.12	**16239.43**	16353.12	16500.37	16241.01	16304.80	**3.03**	47.60	77.37	4.83	36.25
	R1234ze	**16106.26**	16153.62	16254.96	**16106.26**	16114.50	**16107.18**	16200.84	16341.16	16111.35	16160.45	**2.70**	41.10	61.12	15.18	28.16
$CaCl_2$-LiBr-$LiNO_3$	R290	**15401.91**	15477.93	15476.90	**15402.00**	15419.17	**15402.21**	15589.23	15575.18	15404.69	15447.63	**0.31**	55.42	64.25	10.50	22.33
	R123	16537.37	16585.32	16611.59	**16537.33**	16561.16	**16538.88**	16680.08	16732.18	16540.36	16599.21	**3.01**	50.86	73.13	3.70	32.14
	R1234yf	16215.02	16295.82	16331.70	**16214.93**	16232.76	**16216.35**	16438.73	16477.20	16218.02	16286.30	**3.07**	52.60	82.96	4.78	38.23
	R1234ze	**16086.00**	16173.27	16182.56	16086.01	16107.40	**16087.67**	16288.26	16305.23	16089.47	16146.88	**4.65**	37.23	63.92	5.64	30.67

TH-3395_176107002

5.6. Closure

A comparative study of thermoeconomic optimization of a subcooler compression-absorption cascaded refrigeration system (SCRS) with a cascaded refrigeration system (CRS) is presented in the current work. Refrigerants with low ODP and GWP, such as R290, R123, R1234yf, and R1234ze in VCRS and absorbent-refrigerant pairs of LiBr-H_2O, LiCl-H_2O, and ($CaCl_2$-LiBr-$LiNO_3$)-H_2O in VARS are used in both cases. A nonlinear objective function is optimized to minimize the total annual cost. Five metaheuristic techniques, namely STLBO, ASO, TGA, COA, and YYPO, are used in the optimization study. The following are the major conclusions from the comparison analysis:

- Adding a sub-cooler in the standalone cascaded refrigeration system improves COP by ~250% compared to CRS for $CaCl_2$-LiBr-$LiNO_3$-H_2O-R290 and reduces the exergy destruction by ~ 40%.
- The lowest total annual cost for SCRS and CRS (13164.8 US $/year and 15401.91 US $/year) is reported for ($CaCl_2$-LiBr-$LiNO_3$)-$H_2O$-R290 whereas the highest cost is observed for LiBr-H_2O-R290. When paired with all absorbent solutions, R123 in SCRS and R1234yf in CRS predicted higher total annual costs.
- Due to higher compressor pressure, the CO_2 emission of SCRS is higher than CRS resulting in higher penalty cost and thus increased total annual cost of SCRS.
- Based on the energy and exergy of the SCRS proves to be a more efficient refrigeration system, while according to economic analysis and environmental analysis, CRS can be interpreted as a better system.
- Increased generator heat load is observed to reduce COP_{VARS} of CRS and SCRS. sTLBO and COA obtain the optimal total annual cost for most VCRS-VARS absorbent solution/solution mixture-water-refrigerant combinations, whereas YYPO and ASO acquire optimal total annual cost quite a few times but lesser than COA and sTLBO and higher than TGA. TGA performs worst among all algorithms.
- Among all algorithms, COA identifies the optimal total annual cost for all LiCl-H_2O combinations, whereas sTLBO gives the optimal total annual cost for all LiBr-H_2O and ($CaCl_2$-LiBr-$LiNO_3$)-H_2O combinations in SCRS. sTLBO reported the lowest standard deviation except for R123-LiBr-H_2O, and TGA recorded the highest standard deviation in SCRS.

TH-3395_176107002

- COA determines the minimum total annual cost, mean, and lowest standard deviation for all combinations. ASO reports the highest value of standard deviation, followed by TGA in CRS, indicating the poor performance of the algorithm.

TH-3395_176107002

CHAPTER 6

Multi-objective thermoeconomic optimization of vapor recompression-absorption refrigeration system

6.1. Introduction

Despite all these advantages, cascaded refrigeration systems are more expensive and more complicated to build when compared to a single refrigeration system. Along with the cascaded refrigeration of compression and absorption refrigeration, researchers have put forward the absorption-recompression model, which removes the condenser and utilizes rejected heat to superheat the refrigerant in the generator. Riffat and Wong [153] introduced a gas-driven absorption-compression single refrigeration system driven by waste heat. Razmi et al. [156] proposed a hybrid combination of absorption and recompression refrigeration systems. The proposed system COP determined was 4.4 at a generator temperature of 60 °C. In this vapor recompression absorption refrigeration system (VRARS), instead of the condenser in the VARS a compact generator-condenser and a compressor between the generator and the condenser coil. The heat released from the condensation of the superheated refrigerant from the compressor is utilized for the separation of the refrigerant from the absorbent-refrigerant mixture in the generator by heating.

A system with high exergy efficiency is not always the best option because the total cost of the system may also be high; likewise, a system with lower cost may not be efficient because of significant irreversible losses and low exergy efficiency. Therefore, an optimization study is required to determine the minimum total annual cost along with maximum exergy efficiency. The literature shows that no multi-objective thermoeconomic optimization study has been conducted using a absorbent mixture solution, i.e., ($CaCl_2$-LiBr-$LiNO_3$)-H_2O as an absorbent-refrigerant working pair of the VRARS. Furthermore, while calculating the total annual cost, most literature does not consider the cost of coolant and the penalty cost for CO_2 emission, and also, no literature considered the absorber coolant mass flow rate, effectiveness of the solution heat exchanger in thermal compressor and compression ratio as decision variables for optimization of VRARS. The coolant mass flow rate is a key variable that influences the exergy destruction, which has a substantial effect on the exergy efficiency and total annual cost of the system. A compression ratio has an impact on the performance of the refrigeration system as it influences the optimal operating pressure of the generator-condenser for VRARS. Selection of the optimal compression ratio will aid in enhancing the energy efficiency and overall performance of the system.

TH-3395_176107002

The penalty cost or carbon tax is imposed for the emission of CO_2 in the atmosphere due to the compressor work. The calculation of compressor work for VRARS relies on the condenser temperature and the compressor ratio; thus, optimizing these two parameters will result in optimal penalty cost. The absorber and evaporator temperature determines the absorber heat load. Considering these two temperatures as decision variables for the system optimization also has an impact on the absorber heat load which also affects the absorber coolant required to remove the heat load from the absorbent solution to the maintain desired temperature. Studying coolant costs can assist to discover cost-effective choices, such as using a less expensive coolant or optimizing coolant flow rate and temperature. Overall, the coolant cost is an essential component in thermoeconomic analysis since it influences the operating cost of a system and may assist in finding the potential for cost reductions. However, as per the literature survey, penalty and absorber coolant costs have not been considered for the current system (VRARS).

According to the literature review, LiBr-H_2O is commonly used as a working fluid for the VRARS, despite having crystallization problems. It has been observed that the mixture of salts helps to overcome the crystallization problem; however, studies with refrigeration systems using this mixture are scarce. Comparative studies considering LiBr-H_2O and $CaCl_2$-LiBr-$LiNO_3$-H_2O using the current system remain to be conducted. This chapter presents multi-objective thermoeconomic optimization of the vapor recompression-absorption refrigeration system employing metaheuristic techniques with different absorbent solutions, i.e., LiBr and $CaCl_2$-LiBr-$LiNO_3$, in the absorption section. Environmental issues such as global warming are associated with higher ODP and GWP refrigerants; therefore, low ODP and GWP refrigerants are selected for this refrigeration system. The outlet temperature of the evaporator, generator-condenser, absorber, compression ratio, and the effectiveness of the solution heat exchanger are selected decision variables for Case 1; however, in Case 2, the absorber coolant mass flow rate is also taken into account in addition to Case 1 decision variables. A comparison between the results obtained from each metaheuristic technique to identify the most efficient technique and absorbent solution in terms of exergy and cost (including the absorber coolant cost) is made.

Hence, the presented work comprises a multi-objective thermoeconomic optimization of vapor recompression-absorption refrigeration system study with low ODP and GWP refrigerant and different absorbent solutions in the absorption section, including the absorber coolant cost while determining total annual cost and a Pareto front that comprises non-dominated optimal solutions of the system is determined for all algorithms. Nonlinear objective

TH-3395_176107002

functions are formulated that primarily consist of energy, exergy, and economic parameters to minimize the total annual cost and maximize the exergy efficiency of the present system. The no-free lunch theorem [24] suggests implementing multiple metaheuristic techniques because a single algorithm cannot effectively handle all optimization problems. Hence, various metaheuristic algorithms, such as the MOGA [31], MOPSO [32], and MOsTLBO [33] are tested to optimize the vapor recompression-absorption refrigeration system. The effect of decision variables, i.e., outlet temperatures of the heat exchanger, such as the evaporator, generator-condenser, and absorber, compression ratio, effectiveness of the solution heat exchanger, and mass flow rate of absorber coolant on total annual cost and the exergy efficiency of the system.

6.2. Thermodynamic modelling of VRARS

6.2.1. System description

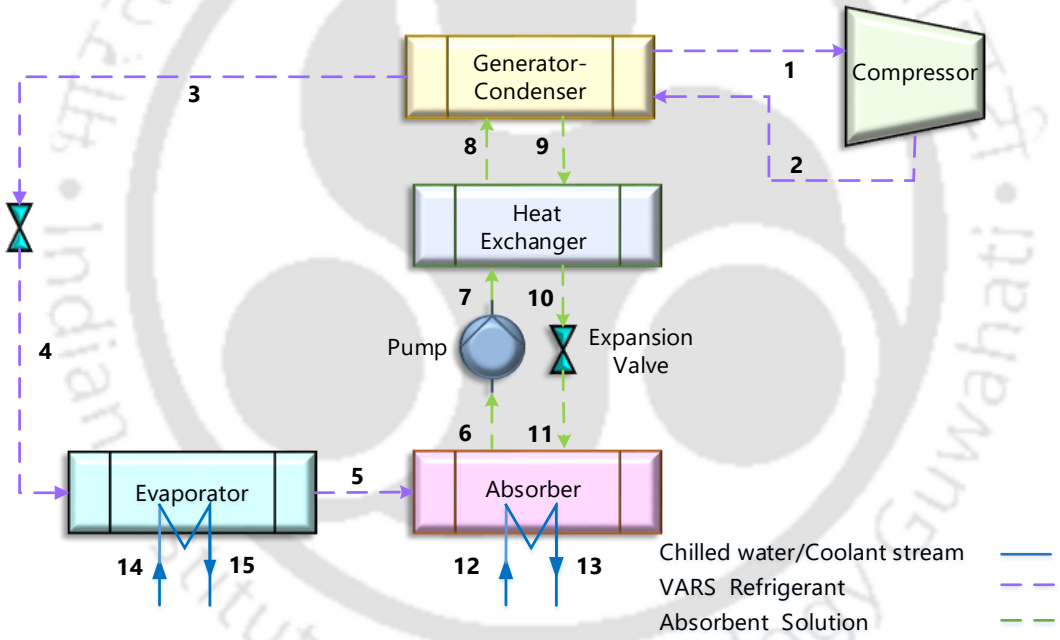

Fig. 6. 1 Vapor recompression-absorption refrigeration system (VRARS) [237]

Fig. 6.1 shows the schematic of the vapor recompression-absorption refrigeration system. This system uses two absorbent-refrigerant mixture solutions, i.e., LiBr-H_2O and $CaCl_2$-LiBr-$LiNO_3$-H_2O. Refrigeration heat load is transferred from chilled water (streams 14-15) to the refrigerant, which is converted to saturated vapor (stream 5). In the absorber, saturated vapor from the evaporator mixes with absorbent solution forming a weak solution (stream 6), and is pumped to the generator-condenser through the solution heat exchanger. Simultaneously, the extra heat from the absorber is dissipated using cooling water (streams 12-13). The absorbent-refrigerant solution mixture temperature is elevated in the generator, where the refrigerant

TH-3395_176107002

separates from the solution owing to its lower boiling temperature and enters into the compressor (stream 1). Through the expansion valves, the strong solution from the generator is redirected to the absorber. (streams 9-11). Superheated refrigerant with high pressure and temperature (stream 2) enters the condenser, transfers heat to the solution in the compacted generator-condenser, and converts the refrigerant to a saturated liquid. The cycle is completed when the saturated liquid refrigerant inflows through the expansion valve and reaches the evaporator (stream 4)[237].

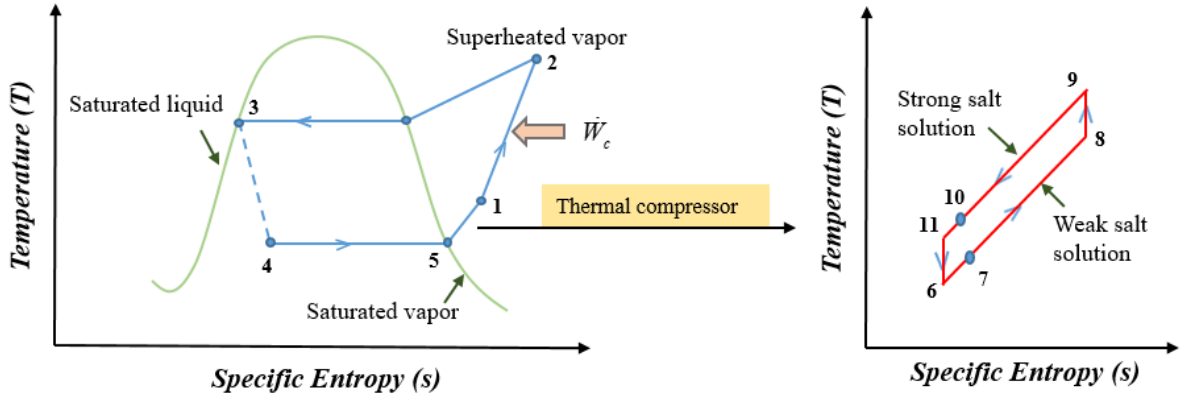

Fig. 6. 2 T-S diagram for Vapor recompression-absorption refrigeration system

Fig. 6.2. illustrates the temperature and entropy of the absorbent and refrigerant streams throughout the cycle. Points 4-5 (pure refrigerant stream) indicate the conversion of liquid-vapor refrigerant into saturated vapor, characterized by constant temperature, pressure, and increasing entropy. Points 5-1 (absorbent-refrigerant solution streams) represent the thermal compressor operation. Within the thermal compressor, temperatures, pressure and entropies are increased for the weak absorber-refrigerant solution, while the strong absorber-refrigerant solution experiences a decrease in those parameters. Point 9 (absorbent-refrigerant solution stream) and Point 1 (pure refrigerant stream) are at the same temperature since both are the outlet streams of the generator. From Points 1-2, the refrigerant vapor is compressed and exits the compressor as high-pressure, high-temperature superheated vapor. Points 2-3 depict the condensation process where the temperature is reduced until a certain point as only the vapor superheat is removed and later it remains constant since the vapor is converted to liquid in the condenser. The throttling process is denoted by Points 3-4, where both the temperature and entropy for the refrigerant decrease.

- **Model Assumptions**

For the energy and exergy analysis following assumptions are considered [182], [195]:

TH-3395_176107002

- The presented exploration does not consider potential and kinetic energies and is executed at a steady state. For exergy calculation, reference pressure and temperature are 101.3 kPa and 25˚C, respectively.
- Between the system and its surroundings, there is no heat exchange.
- Temperature variation within the system components is disregarded.
- To prevent crystallization of the salt solution, the temperature differential between the strong solution temperature entering the expansion valve and the crystallization temperature of the absorbent is always maintained at or above 5˚C. The maximum concentration of absorbent solutions is restricted to 65%.
- Absorbent solutions exiting the generator and the absorber are in equilibrium with regard to their specific conditions.
- The absorbent solution leaving the generator and the absorber, as well as the refrigerant leaving the evaporator and condenser, are assumed to be in their saturated states.
- Expansion/ Throttling valves are assumed as isenthalpic. Heat and pressure losses in the system components are not considered.
- The evaporator load is considered to be 150 kW. Compressor and pump efficiency is regarded as 88% and 85 %, respectively.

6.2.2. Thermodynamic model of VRARS

The main thermodynamic equations employed in system modelling are listed below Eqs. (6.1) - (6.6), with Fig. 6.1 serving as the state point. The enthalpy of the refrigerant and utility thermophysical properties are calculated using REFPROP software while the enthalpies of the thermal compressor streams are calculated using concentration, mass flow rate, and temperatures in Eqs. (A.4-A.5) for LiBr and in Eqs. (A.14-A.16) for $CaCl_2$-LiBr-$LiNO_3$ given in Appendix-A.

$$\dot{Q}_{Evp} = \dot{m}_4 \left(H_5 - H_4 \right) = \dot{m}_{14} \left(H_{14} - H_{15} \right) \tag{6.1}$$

$$\dot{Q}_{Abs} = \dot{m}_5 H_5 + \dot{m}_{11} H_{11} - \dot{m}_6 H_6 = \dot{m}_{12} \left(H_{13} - H_{12} \right) \tag{6.2}$$

$$\dot{Q}_{Shx} = \dot{m}_{11} \left(H_9 - H_{10} \right) = \dot{m}_6 \left(H_8 - H_7 \right) \tag{6.3}$$

$$\dot{Q}_{Gen-Cond} = \dot{m}_1 H_1 + \dot{m}_{11} H_9 - \dot{m}_6 H_8 = \dot{m}_3 \left(H_1 - H_3 \right) \tag{6.4}$$

$$\dot{m}_6 \left(X_9 - X_6 \right) = \dot{m}_5 X_9 \tag{6.5}$$

$$\dot{m}_9 \left(X_9 - X_6 \right) = \dot{m}_5 X_6 \tag{6.6}$$

TH-3395_176107002

Absorbent solution temperatures can be determined using the effectiveness (ε) of the solution heat exchanger using Eqs.(6.7)-(6.8).

$$\varepsilon = \frac{\left(\dot{m}C_p\right)_9}{\left(\dot{m}C_p\right)_{min}} \frac{T_9 - T_{10}}{T_9 - T_6} \tag{6.7}$$

$$\varepsilon = \frac{\left(\dot{m}C_p\right)_6}{\left(\dot{m}C_p\right)_{min}} \frac{T_8 - T_6}{T_9 - T_6} \tag{6.8}$$

Eqs.(6.9)-(6.12) show the calculation of the compressor actual enthalpy and the work done by the compressor and pump.

$$H_{2r} = H_1 + \frac{\left(H_{2isen} - H_1\right)}{\eta_C} \tag{6.9}$$

$$\dot{W}_C = \dot{m}_1 \left(H_{2r} - H_1\right) \tag{6.10}$$

$$\rho_{mix} = X_6 \rho_{salt} + \left(1 - X_6\right) \rho_{water} \tag{6.11}$$

$$\dot{W}_P = \frac{\dot{m}_6 \left(P_1 - P_5\right)}{\rho_{mix} \eta_P} \tag{6.12}$$

To determine the input exergy cost, it is necessary to estimate the input exergy $\left(B_{in}\right)$, as given in Eqs. (6.13)-(6.14) [182], [195].

$$\dot{B}_{D,T} = \sum_{\substack{All\ heat \\ Exchangers}} \dot{B}_D + \left(\dot{W}_C + \dot{W}_P\right) \tag{6.13}$$

$$\dot{B}_{in} = \dot{B}_{D,T} + \left(\dot{B}_{14} - \dot{B}_{15}\right) \tag{6.14}$$

Exergy is the maximum amount of work that can be extracted from a system. Energy losses not considered in the first law of thermodynamics can easily be determined using exergy analysis. Exergy efficiency $\left(\eta_{ex}\right)$ is the ratio of the minimum available energy needed to the actual energy consumed and depicts the quality of the energy throughout the system (Eq.(6.15)) [237].

$$\eta_{ex} = 1 - \frac{B_{D,T}}{\dot{W}_C + \dot{W}_P} \tag{6.15}$$

6.2.3. Economic model of VRARS

As the name implies, the thermoeconomic model of a refrigeration system connects the thermodynamic parameters to the cost of the system. The objective function for the minimization of the total annual cost (C_T) of the present system is formulated as Eq.(6.16),

TH-3395_176107002

$$min\ C_T(x) = topC_{exer}\dot{B}_{in} + topC_{el}\left(\dot{W}_C + \dot{W}_P\right) + a^c Z_T + C_{Env} + CCU\left(\dot{Q}_{Abs}\right) \quad (6.16)$$

The first term in Eq.(6.16) indicates the input exergy fuel cost, while the second and third terms denote the electrical energy consumption cost by pump and compressor and the heat exchangers investment cost and payback period, respectively. The fourth and fifth terms in Eq. (6.16) are penalty and absorber coolant cost. The absorber coolant cost (*CCU*) is considered as 10 $/kW [247]. Total component cost (Z_T), such as heat exchangers, compressor, pump, and expansion valves, mainly contributes to the annual cost of the system. It is calculated using the cost index ratio. In Eq.(6.17), Z_0 and A_0 represent the cost and area reference values, respectively [182] and are given in Table A4 (Appendix-I) [237].

$$Z_k = Z_0\left(\frac{A_k}{A_0}\right)^{0.6} \quad \forall k, k = Evp, Abs, Gen-Cond, Shx \quad (6.17)$$

The compressor cost (Z_C) is determined using the refrigerant mass flow rate $\left(\dot{m}_1\right)$, compressor efficiency (η_C), and input and output pressure ratio (C_r) (Eq.(6.18)), while the pump cost (Z_p) is evaluated using the pump work $\left(\dot{W}_P\right)$ and pump efficiency (η_P), as shown in Eq. (6.18)[237].

$$Z_C = 44.71 m_1\left(\frac{1}{0.95-\eta_C}\right)C_r \ln\left(C_r\right) \quad (6.18)$$

$$Z_P = 2100\left(\frac{\dot{W}_P}{100}\right)^{0.26}\left(\frac{1-\eta_P}{\eta_P}\right) \quad (6.19)$$

The cost of the expansion valve (Z_{valve}) is computed using the mass flow rate of the refrigerant/ absorbent flowing through the valve (Eq. (6.20)) [237].

$$Z_{valve} = 114.5\left(\dot{m}_i\right) \quad \forall i = 3,10 \quad (6.20)$$

The total investment cost (Z_T) is the summation of the expenses of all heat exchangers, compressor, pump, and expansion valves, as shown in Eq. (6.21).

$$Z_T = \sum Z_k + Z_C + Z_p + Z_{valve} \quad \forall k, k = Evp, Abs, Gen-Cond, Shx \quad (6.21)$$

The capital recovery factor (a^c) in Eq. (6.16) is determined using Eq. (3.16) in Chapter 3. The term C_{Env} in Eq. (4.15) represents a penalty cost for CO_2 emission. Generally, a compressor works on the electricity produced from burning fossil fuels which emit CO_2 into the

TH-3395_176107002

atmosphere. CO_2 is a greenhouse gas that contributes to global warming and climate change. The rise in the emission of CO_2 increases global warming. Goetzler et al. [248] report that direct and indirect emission of CO_2 from stationary air conditioning systems is 700 million metric tons per year. Penalty costs or carbon tax associated with CO_2 emissions are factored in here due to rising concern for the environment. Carbon taxation is imposed here as a penalty for releasing CO_2 into the atmosphere using fossil fuels for steam and electricity generation and is calculated using Eqs. (4.32-4.33) in Chapter 4.

6.2.4. Optimization model formulation for the proposed system

For an ideal refrigeration system, maximum exergy efficiency for a better quality of energy and a lower total annual cost is required; however, higher exergy efficiency (η_{ex}) entails higher costs. Thus, in the current work, two conflicting objective functions are considered for the multi-objective thermoeconomic optimization, i.e., (i) Minimization of total annual cost (C_T) and (ii) Maximization of exergy efficiency (η_{ex}). The objective functions of the proposed model are presented in Eq. (6.22).

$$\begin{aligned} &Min\ C_T = top\ C_{exer}\dot{B}_{in} + top\ C_{el}\left(\dot{W}_C + \dot{W}_P\right) + a^c\ Z_T + C_{Env} + CCU\left(\dot{Q}_{Abs}\right) \\ &Max\ \eta_{ex} = 1 - \frac{B_{D,T}}{\dot{W}_C + \dot{W}_P} \end{aligned} \tag{6.22}$$

Subject to

$$\begin{aligned} &T_{11} - T_{Cr} > 5;\ X_9 - X_6 > 2 \\ &60 \le T_{Gen} \le 80;\ 60 \le T_{Cond} \le 80;\ 5 \le T_{Evp} \le 10; \\ &32 \le T_{Abs} \le 38;\ 0.6 \le \varepsilon \le 0.9;\ 5 \le CR \le 25; \\ &5 \le \dot{m}_{12} \le 10 \end{aligned} \tag{6.23}$$

The first constraint in Eq. (6.23) ensures that the strong solution temperature (T_{11}) inflowing the absorber will always be higher than the crystallization temperature (T_{Cr}) to avoid crystallization, while the second constraint maintains the concentration difference between the strong (X_9) and weak (X_6) concentration solution needs to be kept by two units for the realistic depiction as shown in Eq. (6.23). Upper (*UB*) and lower bounds (*LB*) for the decision variables are also given. *UB*, *LB*, and constraints chosen for the proposed work are based on the absorbent-refrigerant combinations used.

The proposed optimization work is solved using three meta-heuristic multi-objective algorithms, i.e., MOGA, MOPSO, and (MOsTLBO). The maximum generations and population considered for all algorithms are set as 200 and 100, respectively. The termination

TH-3395_176107002

criteria for the algorithms is maximum generations. MATLAB 2021a platform is utilized to perform the simulations. Decision variables (x) are forwarded to the thermoeconomic model, where objective functions (C_T, η_{ex}) are calculated and returned to the metaheuristic algorithm. Fig. 6.3 displays the flowchart for fitness function calculation.

6.3. Model validation

Table 6. 1 Model validation of VRARS

Parameters	**Energy and Exergy model validation**		
	Razmi et al. [237]	Present work	Error %
Generator temperature (T_1 /°C)	65	65	-
Condenser temperature (T_3 /°C)	70	70	-
Evaporator temperature (T_5/ °C)	10	10	-
Absorber temperature (T_6 /°C)	35	35	-
Effectiveness (ε)	0.9	0.9	-
Compression ratio (CR)	7.52	7.52	-
$\dot{Q}_{Evp}$ (kW)	150	150	-
$\dot{Q}_{Abs}$ (kW)	181	180.67	0.18
$\dot{Q}_{Gen-Cond}$ (kW)	188	187.97	0.016
$\dot{Q}_{SHX}$ (kW)	47.2	46.58	1.31
$\dot{W}_C$ (kW)	31.05	31.05	0
BDT (kW)	20.23	20.25	0.09
COP	4.83	4.83	0
η_{ex} (%)	34.84	34.77	0.2
Refrigerant mass flow rate (kg/s)	0.067	0.067	0
Weak solution concentration (X_6 /%)	52.2	51.89	0.59
Strong solution concentration (X_9/%)	56.3	56.04	0.46

Table 6.1 compares the simulation findings between the present VRARS and the data reported by Razmi et al. [236]. The model can be regarded as valid since it can be observed that there is a minor difference (error in the range of 0.016 % - 1.33 %) between both current work and Razmi et al. [236].

TH-3395_176107002

6.4. Results and discussions

A multi-objective thermoeconomic optimization of a VRARS is presented in this article. The main objective is to maximize the exergy efficiency and minimize the total annual cost (TAC) of the present system using two different absorbent-refrigerant combinations. The decision variables considered in Case 1 are outlet temperatures of the generator (T_1), condenser (T_3), evaporator (T_5), absorber (T_6), compression ratio (CR), and effectiveness of the solution heat exchanger (ε), while in Case 2, the mass flow rate of the absorber coolant ($\dot{m}_{12}$) is also considered as a decision variable along with the other decision variables considered in Case 1. The effect of the mass flow rate of the absorber coolant used is also studied here.

6.4.1. Case 1

A refrigeration system with minimum TAC and maximum exergy efficiency is always preferred; hence, to optimize TAC and exergy efficiency, the temperature of the generator-condenser, evaporator, absorber, and compression ratio, effectiveness of the solution heat exchanger are considered as the decision variables in this case. MOGA, MOPSO, and MOsTLBO algorithms are implemented to solve this multi-objective problem for the individual working pair, i.e., LiBr-H_2O and $CaCl_2$-LiBr-$LiNO_3$-H_2O. The corner points obtained from each algorithm are reported in Tables 6.2 and 6.3 for LiBr-H_2O and $CaCl_2$-LiBr-$LiNO_3$-H_2O, respectively, with their corresponding objective functions. The minimum TAC and maximum exergy efficiency reported by each algorithm are highlighted in **boldface font** in Tables 6.2 and 6.3. MOsTLBO determines the maximum exergy efficiency with the corresponding maximum TAC, while MOPSO reports the minimum exergy efficiency and the associated minimum TAC (Table 6.2).

Table 6. 2 Corner Points for LiBr-H_2O (Case 1)

	T_1 (°C)	T_3 (°C)	T_5 (°C)	T_6 (°C)	ε	CR	TAC ($/year)	Exergy Efficiency
MOGA	70.607	66.175	5.841	34.543	0.601	5.001	20341.39	**0.522**
	69.221	60.019	7.560	37.701	0.601	5.001	**19610.62**	0.491
MOPSO	63.276	60.130	5.000	32.000	0.600	5.000	20577.87	**0.523**
	70.003	60.000	7.665	37.827	0.600	5.000	**19601.74**	0.487
MOsTLBO	63.139	60.000	5.000	32.000	0.600	5.000	20578.39	**0.524**
	69.744	60.000	7.736	38.000	0.600	5.000	**19602.25**	0.488

TH-3395_176107002

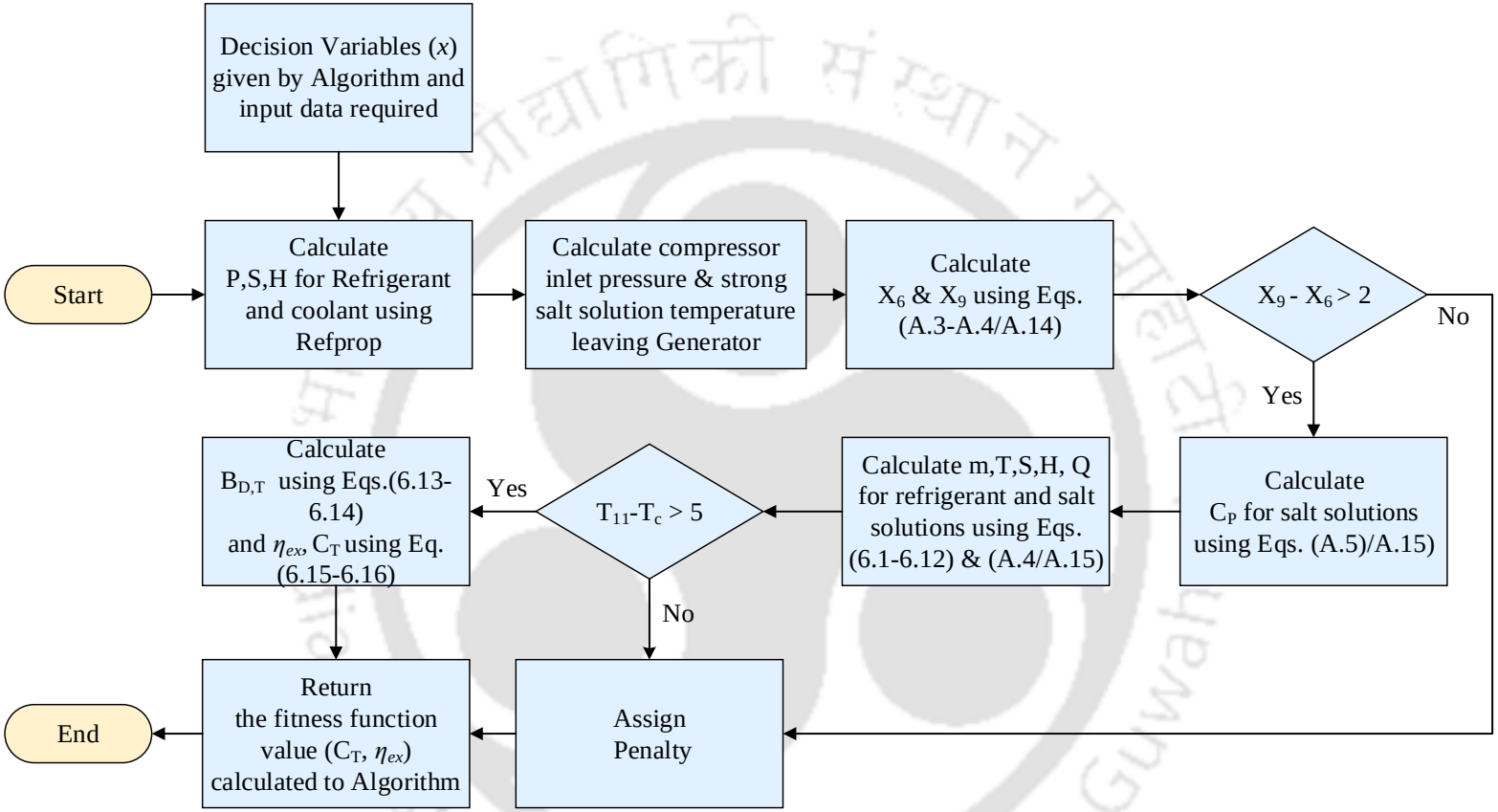

Fig. 6. 3 Flowchart for the fitness calculation

TH-3395_176107002

The maximum exergy efficiency (0.524) reported by MOsTLBO is ~8% higher than the minimum exergy efficiency (0.487) obtained by MOPSO. The minimum TAC reported (19601.74 $/year) by MOPSO is ~5% lesser than the maximum TAC (20578.39 $/year) determined by MOsTLBO for LiBr-H_2O, as shown in Table 6.2.Table 6.3 shows that MOPSO reports both the maximum exergy efficiency and minimum TAC. The maximum exergy efficiency (0.484) obtained is ~12% higher than the minimum one (0.427) while the minimum TAC (19063.136 $/year) determined is ~10% lower than the maximum TAC (19063.136 $/year).

Table 6. 3 Corner Points for $CaCl_2$-LiBr-$LiNO_3$ -H_2O (Case 1)

	T_1 (°C)	T_3 (°C)	T_5 (°C)	T_6 (°C)	ε	*CR*	TAC ($/year)	Exergy Efficiency
MOGA	60.000	60.107	5.017	32.005	0.600	5.000	20348.086	**0.482**
	68.288	60.027	6.765	37.871	0.601	5.000	**19070.862**	0.429
MOPSO	71.263	74.468	6.022	32.000	0.605	5.002	20940.696	**0.484**
	69.461	60.000	6.276	38.000	0.600	5.000	**19063.136**	0.427
MOsTLBO	60.000	60.090	5.000	32.000	0.600	5.000	20348.973	**0.482**
	68.937	60.011	6.263	38.000	0.600	5.000	**19065.643**	0.429

The total exergy destruction (*BDT*), heat load ($\dot{Q}$), total area (A_{total}), weak (X_6) and strong (X_9) solutions concentration, the mass flow rate of absorber coolant ($\dot{m}_{12}$), and compressor work ($\dot{W}_C$) obtained for the respective corner points reported by each algorithm is given in Table 6.4. Tables 6.2 and 6.3 show that high evaporator (T_5), absorber (T_6), and low condenser (T_3) temperatures determine the minimum TAC and exergy efficiency. In contrast, slightly higher condenser, lower evaporator, and absorber temperatures lead to higher exergy efficiency and maximum TAC. For both working pairs, the optimal effectiveness and compression ratio reported by all algorithms tend to be at the lower bound. Evaporator (T_5), absorber (T_6), generator (T_1), and condenser pressure determined using T_3 affect the weak and strong solution concentration. As an example, the decision variables set given by MOsTLBO are discussed further.

TAC comprises the investment cost, maintenance cost, penalty cost, and absorbent coolant cost (CCU), where investment cost includes equipment cost, and maintenance cost is the operational cost, including electricity cost and exergy input cost. In the case of minimum TAC, high evaporator and absorber temperature results in a high concentration of the weak solution,

TH-3395_176107002

while lower condenser (T_3) and higher generator temperature (T_1) leads to a higher concentration of the strong solution and vice versa.

Table 6. 4 Exergy destruction, heat load, total area, and solution concentration for corner points (Case 1)

	BDT (kW)	$\dot{Q}_{Gen-Cond}$ (kW)	$\dot{Q}_{Abs}$ (kW)	$\dot{Q}_{SHX}$ (kW)	A_{total} (m^2)	X_6 (%)	X_9 (%)	$\dot{m}_{12}$ (kg/s)	$\dot{W}_C$ (kW)
LiBr-H_2O									
MOGA	11.383	181.908	230.066	80.318	69.596	54.386	56.388	5.505	23.804
	11.927	**181.047**	**201.589**	**38.351**	**56.596**	**55.059**	**58.611**	**4.823**	**23.412**
MOPSO	10.994	180.278	219.288	68.127	111.017	53.471	55.483	5.247	23.062
	12.037	**181.178**	**199.658**	**34.911**	**55.618**	**55.062**	**59.014**	**4.777**	**23.459**
MOsTLBO	10.980	180.243	219.242	68.147	111.643	53.471	55.474	5.246	23.045
	11.993	**181.117**	**200.431**	**36.214**	**55.810**	**55.114**	**58.883**	**4.796**	**23.440**
$CaCl_2$-LiBr-$LiNO_3$ -H_2O									
MOGA	11.838	179.639	186.865	72.658	114.281	54.640	56.640	4.471	22.837
	13.333	**180.980**	**157.290**	**28.348**	**47.568**	**57.841**	**63.416**	**3.763**	**23.362**
MOPSO	12.488	182.474	208.966	104.651	88.262	53.819	55.857	5.000	24.210
	13.445	**181.277**	**156.522**	**26.945**	**45.487**	**58.364**	**64.423**	**3.745**	**23.449**
MOsTLBO	11.838	179.641	186.842	72.627	114.379	54.651	56.652	4.471	22.836
	13.372	**181.178**	**157.687**	**28.806**	**46.007**	**58.375**	**63.973**	**3.773**	**23.414**

The difference in the concentration of the weak and strong solution affects the respective mass flow rate of the solution streams. The higher concentration difference leads to a lower mass flow rate, and a lower concentration difference results in an increased mass flow rate of weak and strong solutions. The parameters related to minimum TAC are **shown in boldface font** in Table 6.4 for both working pairs and report a higher difference in the concentration of the weak and strong solution, which determines the lower value of the corresponding mass flow rates of absorbent solution and refrigerant. In the case of decision variables corresponding to minimum TAC, higher generator, and absorber temperature leads to a higher temperature of thermal compressor streams; however, the reduction in mass flow rate results in a lower heat load for the solution heat exchanger and absorber in the thermal compressor, consecutively affecting the area and TAC (Table 6.4). Lower heat load leads to a smaller area and, hence lower system capital cost. Changes in the condenser and generator temperature affect the penalty cost of the system. Lower condenser and higher generator temperature result in slightly

TH-3395_176107002

lesser compressor work and, therefore, low penalty cost. As the heat load rejected by the condenser is utilized for the separating refrigerant from the absorbent-refrigerant mixture; hence, the coolant is not required for the condenser. Therefore, only the coolant cost of the absorber is considered; a decrease in the heat load reduces CCU. This cost reduction in investment, penalty, and CCU results in lower TAC.

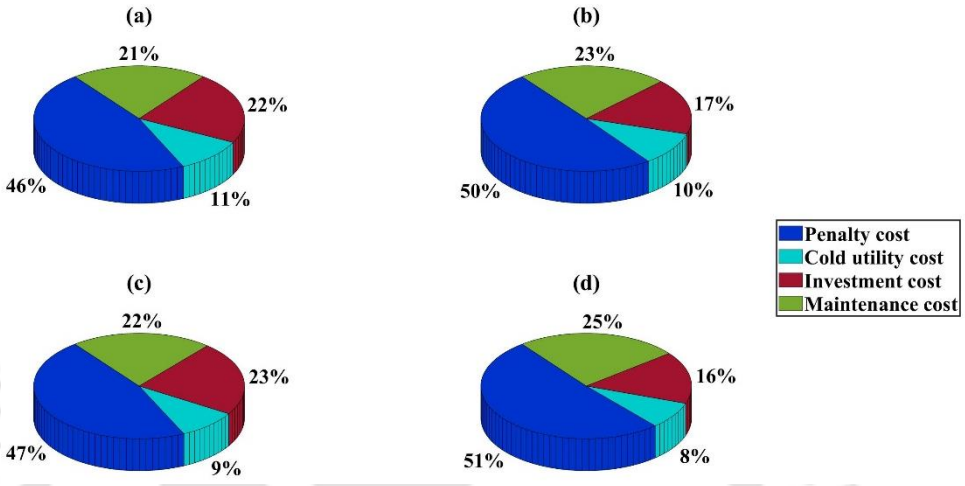

Fig. 6. 4 Case 1- Maximum TAC break up of LiBr- H_2O (a) and $CaCl_2$-LiBr-$LiNO_3$-H_2O (c) and minimum TAC break up of LiBr- H_2O (b) and $CaCl_2$-LiBr-$LiNO_3$-H_2O (d)

Fig. 6.4 demonstrates the distribution of the TAC obtained by MOsTLBO for both working pairs. Almost ~50% of the TAC is contributed by penalty cost for all cases, as depicted in Fig. 6.4 since the compressor work is nearly the same. Following penalty cost, maintenance, and investment costs have a significant impact on TAC for both working pairs. The set of decision variables associated with the maximum TAC shows a higher area leading to higher equipment cost. Therefore, the maximum TAC of LiBr-H_2O and $CaCl_2$-LiBr-$LiNO_3$-H_2O shows a higher contribution (22% -23%) of investment cost, as presented in Fig. 6.4 (a, c) than the minimum TAC (Fig 6.4. (b, d)). The difference in the impacts of absorber coolant cost on the TAC is due to variations in the absorber heat load reported for the maximum and minimum TAC. The heat load on the absorber is lesser for $CaCl_2$-LiBr-$LiNO_3$-H_2O than LiBr-H_2O mainly due to the thermophysical properties calculated using solution concentration, temperature, and mass flow rates of the system. Therefore, the impact of CCU on TAC for $CaCl_2$-LiBr-$LiNO_3$-H_2O is lower (8%-9%) than LiBr-H_2O (10%-11%), as shown in Fig. 6.4 due to variation in the absorber heat load and its corresponding coolant mass flow rate.

It can be observed that higher exergy efficiency is accompanied by lower exergy destruction (Table 6.4). The maximum exergy efficiency (0.484) and minimum TAC (19063.136 $/year) reported by $CaCl_2$-LiBr-$LiNO_3$-H_2O is found to be lesser than LiBr-H_2O by ~9% and ~3%,

TH-3395_176107002

respectively. The set of decision variables associated with a minimum TAC of both working pairs given by MOPSO, $CaCl_2$-LiBr-$LiNO_3$ reports higher exergy destruction of ~12% than LiBr-H_2O which is mainly due to the mass flow rate of the absorber coolant. The thermophysical properties of absorbent solutions, the mass flow rate of the thermal compressor streams and coolant affects the absorber, solution heat exchanger, and generator-condenser heat loads, leading to variation in the heat loads of the absorber. MOPSO and MOsTLBO determine nearly the same minimum TAC for both working pairs, as reported in Tables 6.2 and 6.3. Among these two working pairs, if exergy efficiency is the priority of the user, LiBr-H_2O can be selected, whereas $CaCl_2$-LiBr-$LiNO_3$-H_2O can be chosen for minimum TAC.

6.4.1.1. Pareto and Global Pareto Fronts for Case 1

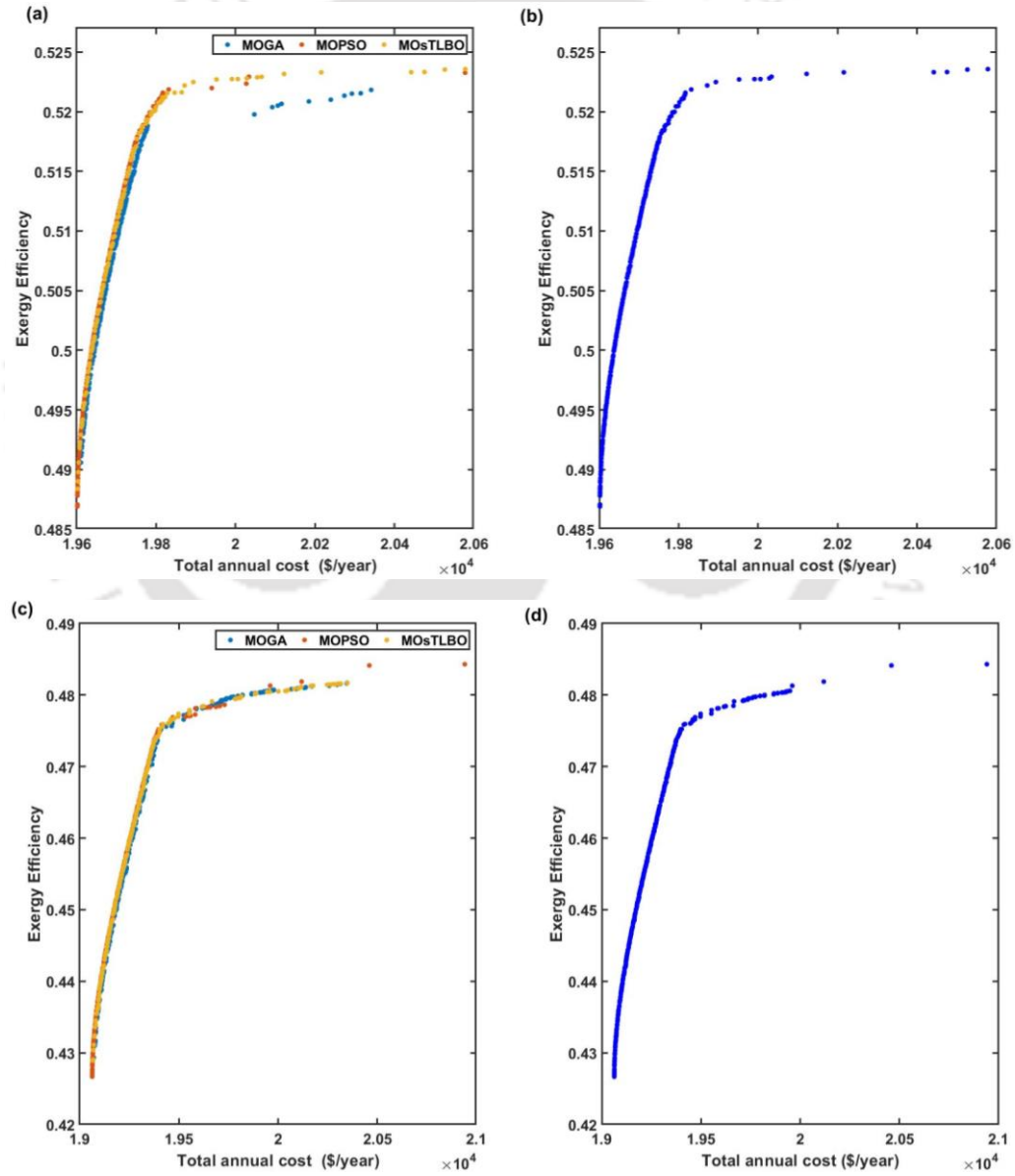

Fig. 6. 5 Pareto fronts of LiBr-H_2O (a) and $CaCl_2$-LiBr-$LiNO_3$-H_2O (c) obtained by all algorithms and Global Pareto front of LiBr-H_2O (b) and $CaCl_2$-LiBr-$LiNO_3$-H_2O (d)

TH-3395_176107002

Fig. 6.5 (a, c) shows the Pareto fronts obtained by each algorithm for the individual working pair, whereas the Global Pareto Fronts (GPF) generated after applying the non-dominated sorting method to all the non-dominated points across all runs and algorithms are illustrated in Fig. 6.5 (b, d). It is evident that there are fewer non-dominated solutions from all the algorithms in the domain of maximum exergy efficiency (and maximum TAC) for both the working pairs; as a result, fewer options are available to a user interested in finding solutions with the maximum exergy efficiency as it is directly proportional to maximum TAC (Fig. 6.5 (a, c)). When compared to MOPSO, MOsTLBO, and MOGA obtain considerable non-dominated points in the region of maximum exergy efficiency in the case of LiBr-H_2O; however, for $CaCl_2$-LiBr-$LiNO_3$-H_2O, the non-dominated solutions determined by MOsTLBO and MOGA are very fewer than MOPSO. MOPSO has contributed more points on the GPF, followed by MOGA and MOsTLBO in the case of $CaCl_2$-LiBr-$LiNO_3$ (Fig. 6.5 (c, d)); however, the scarcity of points in the Pareto front does not imply that the points are of poor quality. In the GPF of LiBr-H_2O (Fig. 6.5 (b)), MOGA did not provide any point; however, the contributions of MOPSO and MOsTLBO are 81.85% and 18.15% of the total points, respectively. For Fig. 6.5 (d), the contribution of MOGA, MOPSO, and MOsTLBO is 12.92%, 65.16%, and 21.91%, respectively.

6.4.1.2. Inverted general distance for Case 1

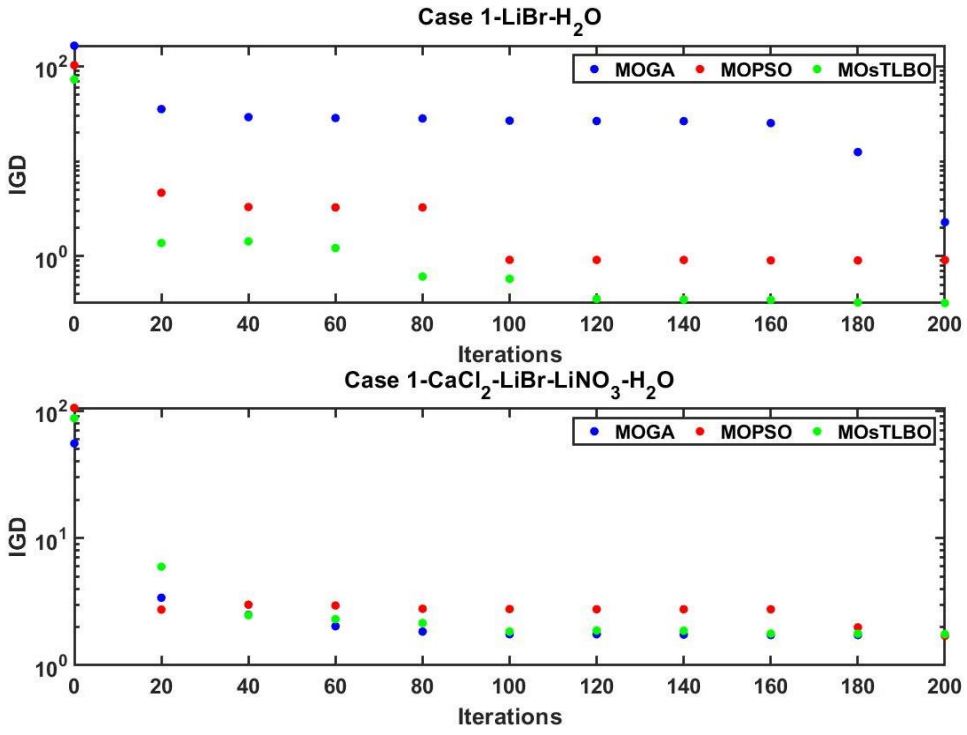

Fig. 6. 6 Best run IGD determined by MOGA, MOPSO, and MOsTLBO for LiBr-H_2O and $CaCl_2$-LiBr-$LiNO_3$-H_2O

TH-3395_176107002

IGD calculated using Eq. (3.17) in Chapter 3 is regarded as a performance metric to determine better performance of the multi-objective algorithms. The global Pareto front is considered as the true Pareto for calculating the IGD obtained from each algorithm. In this case, Fig. 6.5 (b, d) are the true Pareto. The run with the least IGD is assumed as the best run. The best run IGD versus iteration of an algorithm is depicted in Fig. 6.6. At the end of 200 iterations, MOsTLBO reports the minimum IGD compared to MOGA and MOPSO for both working pairs. It indicates that the Pareto front of MOsTLBO obtained in the best run contains better-converged solutions for LiBr-H_2O, while for $CaCl_2$-LiBr-$LiNO_3$-H_2O, all algorithms determine almost the same IGD.

6.4.2. Case 2

Along with heat exchanger outlet temperatures, effectiveness, and compression ratio, the mass flow rate of the absorber coolant is also considered as one of the decision variables in Case 2. Coolant mass flow rate is also an essential parameter of the refrigeration system since it affects the exergy destruction of the system, ultimately impacting exergy efficiency and TAC. Tables 6.5 and 6.6 present the corner points determined by each algorithm and their objective function for LiBr-H_2O and $CaCl_2$-LiBr-$LiNO_3$-H_2O, respectively. The minimum TAC and maximum exergy efficiency reported by each algorithm are shown in **boldface font** in Tables 6.5 and 6.6.

Table 6. 5 Corner Points for LiBr –H_2O (Case 2)

	T_1 (°C)	T_3 (°C)	T_5 (°C)	T_6 (°C)	ε	CR	$\dot{m}_{12}$ (kg/s)	TAC ($/year)	Exergy Efficiency
MOGA	61.345	60.137	9.805	35.593	0.602	5.000	10.000	18831.827	**0.814**
	69.296	60.004	8.529	37.621	0.602	5.000	10.000	**18441.223**	0.795
MOPSO	60.000	60.000	10.000	32.000	0.600	5.000	10.000	19410.254	**0.818**
	69.696	60.000	8.239	37.624	0.600	5.000	10.000	**18435.280**	0.794
MOsTLBO	60.000	60.000	10.000	32.000	0.600	5.000	10.000	19410.254	**0.818**
	69.497	60.000	8.199	37.450	0.600	5.000	10.000	**18435.737**	0.794

MOPSO and MOsTLBO, followed by MOGA, show the maximum exergy efficiency and minimum TAC (in **boldface fonts)** for both working pairs. It can be observed that the decision variables determined by MOPSO and MOsTLBO are similar (Tables 6.5-6.6) and hence, both the algorithms reported the same objective functions, indicating that the obtained solution is robust. MOPSO and MOsTLBO report the maximum exergy efficiency as 0.818, with the corresponding maximum TAC as 19410.254 $/year. The minimum TAC reported by MOPSO

TH-3395_176107002

and MOsTLBO is 18435.280 $/year and 18435.737 $/year, respectively, which is ~6% lower than the maximum TAC, with a corresponding exergy efficiency of 0.794. The maximum exergy efficiency (0.818) obtained is ~3% higher than the minimum one (0.794) for LiBr-H_2O, as shown in Table 6.5.

Table 6. 6 Corner Points for $CaCl_2$-LiBr-$LiNO_3$-H_2O (Case 2)

	T_1 (°C)	T_3 (°C)	T_5 (°C)	T_6 (°C)	ε	CR	$\dot{m}_{12}$ (kg/s)	TAC ($/year)	Exergy Efficiency
MOGA	60.009	60.018	9.941	35.067	0.626	5.001	10.000	18150.114	**0.817**
	68.396	60.002	7.146	37.747	0.601	5.000	10.000	**17665.946**	0.796
MOPSO	60.000	60.000	10.000	32.000	0.600	5.000	10.000	18652.098	**0.818**
	69.941	60.000	6.645	38.000	0.600	5.000	10.000	**17653.599**	0.792
MOsTLBO	60.000	60.000	10.000	32.000	0.600	5.000	10.000	18652.098	**0.818**
	69.710	60.000	6.586	37.570	0.600	5.000	10.000	**17656.504**	0.793

MOPSO determines the minimum TAC as 17653.599 $/year, which is ~6% lower than the maximum TAC (18652.098 $/year) reported by MOPSO and MOsTLBO and the maximum exergy efficiency as 0.818 (Table 6.6) for $CaCl_2$-LiBr-$LiNO_3$-H_2O. Though the maximum exergy efficiency determined is the same for all algorithms, the maximum TAC reported for MOGA is less by ~3% than MOPSO and MOsTLBO (Table 6.6). The minimum exergy efficiency (0.792) determined is ~4 % lower than the maximum exergy efficiency (0.818) as reported in Table 6.6. For both working pairs, the optimal values of effectiveness, compression ratio, and condenser temperature are obtained at their lower bound, whereas the absorber coolant mass flow rate optimal values are at the upper bound (Tables 6.5 -6.6). The minimum TAC determined by $CaCl_2$-LiBr-$LiNO_3$-H_2O is ~5% lesser than LiBr-H_2O.

BDT, $\dot{Q}$, *A*, X_6 and X_9 obtained for the corner points reported by each algorithm are listed in Table 6.7. Tables 6.5 and 6.6 show that a higher generator (T_1), absorber temperature (T_6), and lower evaporator temperature (T_5) determine the minimum TAC, while a higher evaporator (T_5) and lower absorber (T_6) and generator temperature (T_1) need to be maintained to obtain the maximum exergy efficiency. The evaporator, absorber, generator, and condenser temperature affect the weak and strong absorbent solution concentration; A higher evaporator temperature leads to a lower X_6 compared to Case 1, which can be observed from Tables 6.4 and 6.7. The mass flow rate of weak and strong solution streams is reduced in Case 2 due to a

TH-3395_176107002

decrease in the weak solution concentration, leading to lower absorber, solution heat exchanger, and generator-condenser heat loads, as shown in Tables 6.4 and 6.7.

Table 6. 7 Exergy destruction, heat load, total area, and solution concentration for corner points (Case 2)

	BDT (kW)	$\dot{Q}_{Gen-Cond}$ (kW)	$\dot{Q}_{Abs}$ (kW)	$\dot{Q}_{SHX}$ (kW)	A_{total} (m^2)	X_6 (%)	X_9 (%)	$\dot{W}_C$ (kW)
LiBr-H_2O								
MOGA	4.251	179.207	206.736	53.651	84.046	52.370	54.459	22.842
	4.803	**180.916**	**196.511**	**31.607**	**58.776**	**54.378**	**58.654**	**23.396**
MOPSO	4.148	178.912	191.147	31.831	129.281	50.130	53.808	22.741
	4.835	**181.034**	**197.134**	**31.839**	**57.486**	**54.569**	**58.858**	**23.428**
MOsTLBO	4.148	178.912	191.147	31.831	129.281	50.130	53.808	22.741
	4.823	**181.002**	**197.165**	**32.031**	**57.872**	**54.497**	**58.758**	**23.415**
$CaCl_2$-LiBr-$LiNO_3$-H_2O								
MOGA	4.153	178.926	159.636	35.319	80.356	53.014	56.710	22.746
	4.772	**180.947**	**155.689**	**25.817**	**48.222**	**57.416**	**63.528**	**23.364**
MOPSO	4.148	178.912	154.041	22.184	110.789	50.667	56.713	22.741
	4.882	**181.315**	**154.765**	**24.215**	**45.623**	**58.048**	**64.829**	**23.474**
MOsTLBO	4.148	178.912	154.041	22.184	110.789	50.667	56.713	22.741
	4.867	**181.279**	**154.637**	**23.915**	**46.255**	**57.751**	**64.634**	**23.460**

Due to minor change in the temperature difference of the streams, heat exchangers, results in a slight increase in the total area of the system in Case 2; however, significant reduction in the exergy destruction in Case 2 aids in determining a minimum TAC than in Case 1. The reduced exergy destruction helps to determine better exergy efficiency than Case 1. The parameters associated with minimum TAC and exergy efficiency are shown in **boldface fonts** in Table 6.7.

A significant portion of the TAC is covered by penalty cost (49%-55%) for both working pairs in Case 2, similar to Case 1, as illustrated in Fig. 6.7. The lower exergy destruction reduces the cost of exergy input, which also decreases the impact of maintenance cost on the TAC unlike Case 1. The maintenance cost in Case 2 contributes to TAC in the range of 16%-19%, while in Case 1, the contribution is in the range of 21%-25%. Similar to Case 1, in the case of maximum TAC of both working pairs, investment cost contributes more due to a higher area of the heat exchanger (Fig. 6.7 (a, c)). The CCU impact on the LiBr-H_2O is higher (10%-11%)

TH-3395_176107002

than $CaCl_2$-LiBr-$LiNO_3$-H_2O (8%-9%) due to the absorber heat load variation, as depicted in Fig. 6.7.

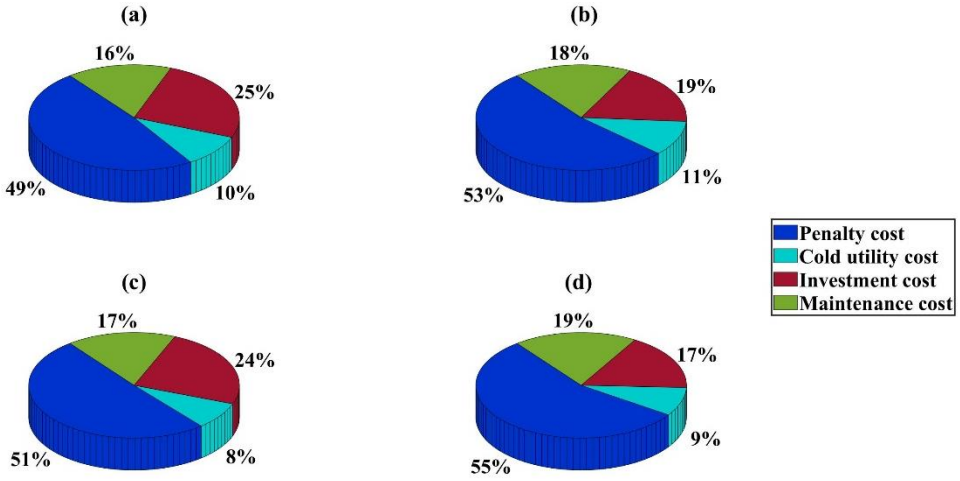

Fig. 6. 7 Case 2- Maximum TAC break up of LiBr-H_2O (a) and $CaCl_2$-LiBr-$LiNO_3$-H_2O (c) and minimum TAC break up of LiBr-H_2O (b) and $CaCl_2$-LiBr-$LiNO_3$-H_2O (d)

6.4.2.1. Pareto and Global Pareto Fronts for Case 2

Fig. 6.8 (a, c) shows the Pareto fronts obtained by each algorithm for the individual working pair while, Fig. 9 (b, d) displays the GPF generated by all algorithms across all the runs, with all the non-dominated points. MOGA provides fewer non-dominated points than the other two algorithms in the region of maximum exergy efficiency for both working pairs. It can be observed that further increment in the exergy efficiency after 0.815 for both working pairs is negligible; however, this minor increment in exergy efficiency causes a considerable increase in the TAC as it increases to 19410 $/year from 18947.5 $/year for LiBr-$H_2O$ (Fig. 6.8 (b)) and from 18072.4 $/year to 18652.1 $/year for $CaCl_2$-LiBr-$LiNO_3$-H_2O (Fig. 6.8 (d)) respectively. MOGA, MOPSO, and MOsTLBO contribute 10.70%, 20.03%, and 69.34%, respectively, for the GPF of LiBr-H_2O (Fig. 6.8 (b)), whereas the percentage of contribution is 7.47%, 20.35%, and 72.25% respectively, for $CaCl_2$-LiBr-$LiNO_3$-H_2O (Fig. 6.8 (d)).

In the region of maximum exergy efficiency, the non-dominated points provided by MOPSO and MOsTLBO algorithms is significant than MOGA for both working pairs, unlike Case 1 (Fig. 6.5). The minimum exergy efficiency (0.794) reported in Case 2 is ~39% enhanced than Case 1 (0.487), while maximum exergy efficiency in Case 2 (0.818) is ~36% improved than Case 1 (0.524) for LiBr-H_2O. The maximum (0.818) and minimum exergy efficiency (0.792) determined in Case 2 for $CaCl_2$-LiBr-$LiNO_3$-H_2O are ~41% and ~46% enhanced than Case 1 respectively. The minimum (19601.74 $/year) and maximum TAC (20578.39 $/year) obtained in Case 1 is ~7% and ~6% higher than Case 2 for LiBr-H_2O, whereas for $CaCl_2$-LiBr-

TH-3395_176107002

$LiNO_3$-H_2O, the maximum TAC (20940.696 $/year) reported is ~13% and minimum TAC (19063.136 $/year) is ~8% higher in Case 1 than Case 2.

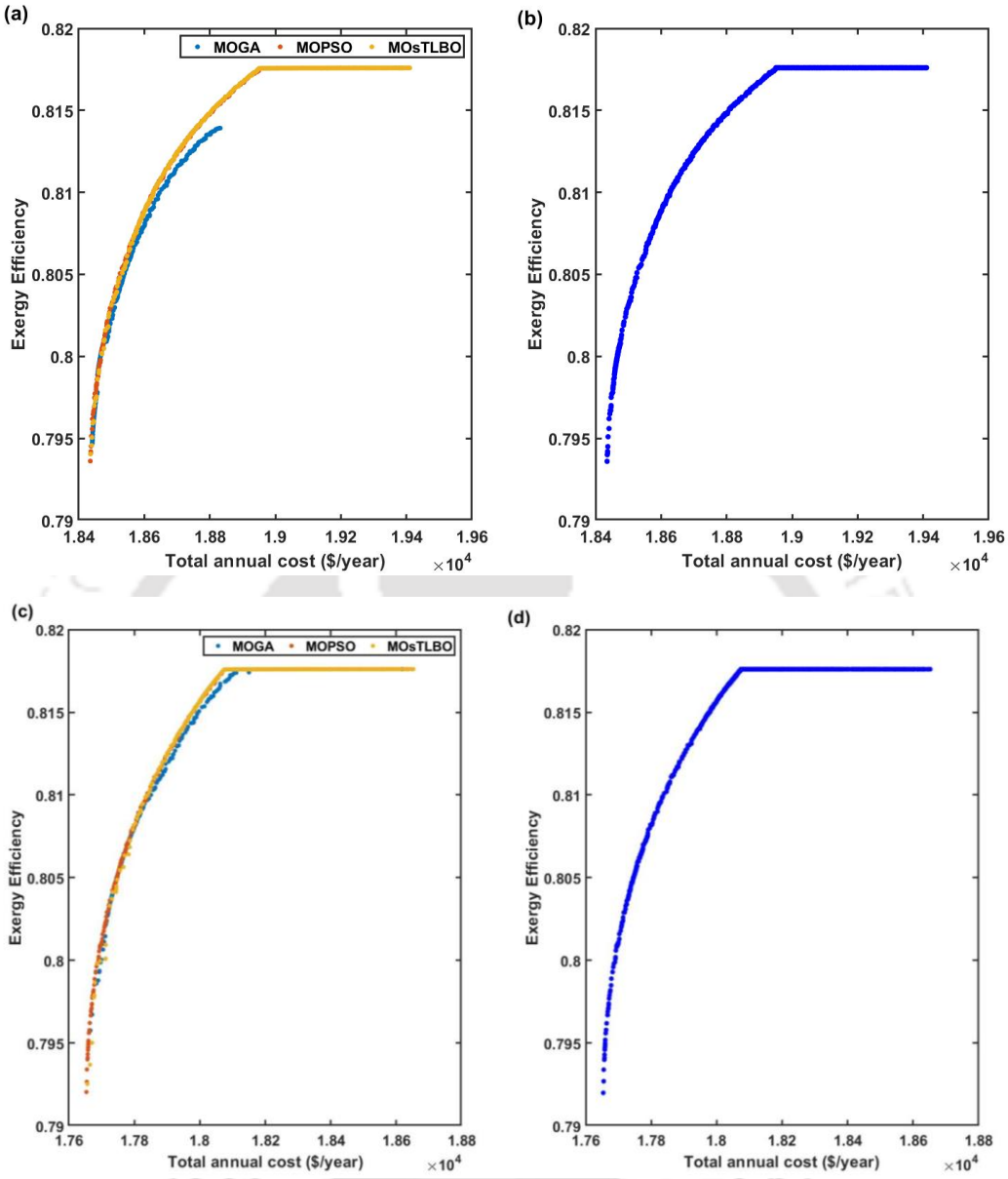

Fig. 6. 8 Pareto fronts of LiBr-H_2O (a) and $CaCl_2$-LiBr-$LiNO_3$-H_2O (c) obtained by all algorithms and Global Pareto front of LiBr-H_2O (b) and $CaCl_2$-LiBr-$LiNO_3$-H_2O (d)

6.4.2.2. Inverted generational distance for Case 2

The IGD of the best run versus the iterations determined for Case 2 is provided in Fig. 6.9. Indicating that the final Pareto of all algorithms has a wider variety of solutions than prior iterations, the final IGD reported by all algorithms has the lowest of all iterations. All algorithms in the initial iteration reported higher IGD, indicating that the non-dominated solutions discovered in the initial iteration had poor convergence and variance. However, as the iteration increases, the IGD starts to decrease. Though the difference between the final

TH-3395_176107002

IGDs at the end of 200 iterations is quite low; however, MOsTLBO reports the lowest IGD indicating that the non-dominated solutions obtained by MOsTLBO are nearer to the true Pareto for both working pairs.

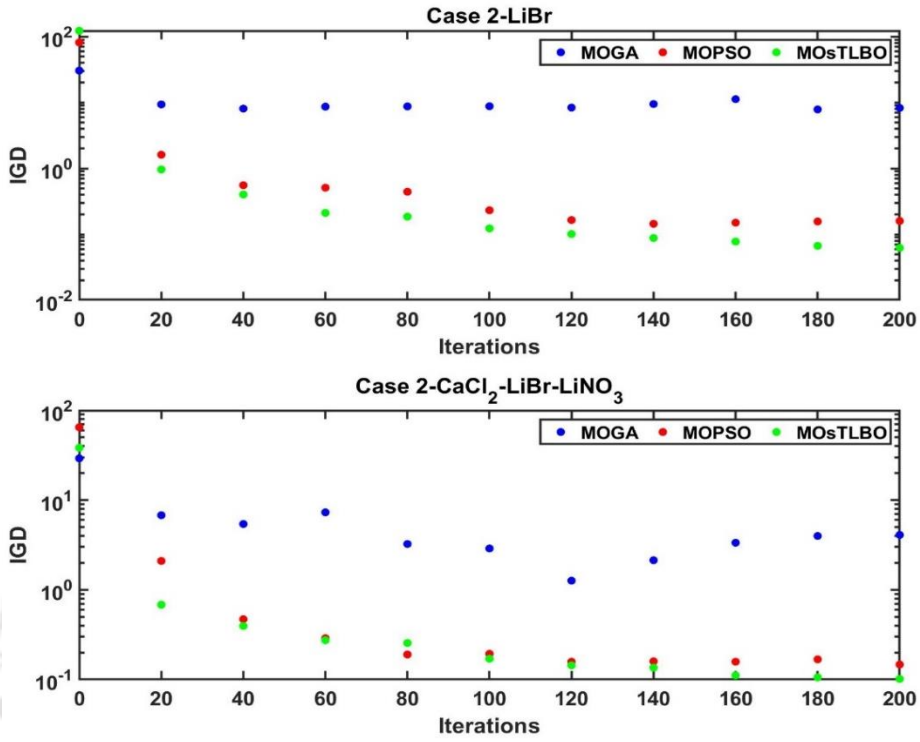

Fig. 6. 9 Best IGD determined for best run of MOGA, MOPSO, and MOsTLBO for LiBr-H_2O and $CaCl_2$-LiBr-$LiNO_3$-H_2O

6.4.3. Comparison between Case 1 and Case 2

Except for evaporator temperature, the decision variables obtained for Case 1 and Case 2 are almost similar for both working pairs; however, the minimum TACs obtained are different in all cases due to the change in the exergy destruction. The enthalpies, entropies, and mass flow rates of absorber coolant, mass flow rate of chilled water, and compressor work affect the exergy destruction. Compressor work for both cases has a negligible difference as the generator and condenser temperatures given by all algorithms are similar; however, the absorber coolant mass flow rate has a significant change. Due to this, the exergy destruction also varies drastically. The exergy destruction determined for the maximum exergy efficiency in Case 2 is decreased by ~165% for LiBr-H_2O and ~202% reduced for $CaCl_2$-LiBr-$LiNO_3$-H_2O than Case 1. Hence, the maximum exergy efficiency obtained for LiBr-H_2O and $CaCl_2$-LiBr-$LiNO_3$-H_2O in Case 2 is improved by ~36% and ~41% than in Case 1.

Considering absorber coolant mass flow rate as a decision variable has an impact on the other decision variables as well. The evaporator temperature determined for maximum exergy

TH-3395_176107002

efficiency in Case 1 is lower than in Case 2. This leads to a higher weak solution concentration for Case 1, resulting in a higher mass flow rate of weak and strong solution streams and ultimately higher absorber heat load than Case 2. Thus, increasing the absorber coolant cost due to an increment in the absorber heat load for Case 1. Lower absorber coolant cost also aids in reducing the TAC of the system in Case 2, ~ 7% and ~8% lower than Case 1 for LiBr-H_2O and $CaCl_2$-LiBr-$LiNO_3$-H_2O, respectively. Because of these reasons, it can be concluded that Case 2 is better than Case 1.

The base case [237] has considered evaporator, absorber, and generator temperature as decision variables to determine maximum COP, maximum exergy efficiency, and minimum payback period; however, in the present work, the authors have considered condenser temperature, compression ratio, and effectiveness of solution heat exchanger along with base case variables in Case 1 and additional mass flow rate of the absorber in Case 2 as decision variables. Compared to the base case [237], the exergy efficiency obtained in Case 1 (0.524) and Case 2 (0.818) for LiBr-H_2O is ~29%, and ~55% improved than optimal exergy efficiency (0.374) reported in [237]. The highest COP determined for Case 1 and Case 2 are 6.509 and 6.595, i.e., ~26% more enhanced than the optimal COP (4.88) given in [237].

6.4.4. Impact of evaporator heat loads on exergy efficiency, exergy destruction, and total annual cost

The influence of different evaporator heat loads on the exergy efficiency, BDT, and TAC has been studied, as shown in Fig. 6.10, for a better understanding of the importance of absorber coolant mass flow rate as one of the decision variables. For the study, the optimal decision variables obtained for the maximum exergy efficiency are considered here for both cases. It can be observed that the BDT and TAC increase as the evaporator load increases for Case 1-LiBr-H_2O; however, the exergy efficiency is constant for all heat loads (Fig. 6.10). An increase in the evaporator heat load increases the thermal compressor heat load, compressor work, and mass flow rates of the refrigerant, weak solution, strong solution, coolant, and chilled water. The mass flow rate of absorber coolant and chilled water impacts the exergy destruction determination and, ultimately, the TAC. Thus, an increment in their mass flow rate increases the BDT and TAC (Fig. 6.10). Exergy efficiency is calculated using exergy destruction and compressor work ratio as shown in Eq. 6.15. Though these two are increasing, their ratio is maintained constant due to an increase in both the chilled water and absorber coolant mass flow rate with respect to the increasing evaporator heat load. Due to this constant ratio, the exergy efficiency is also the same.

TH-3395_176107002

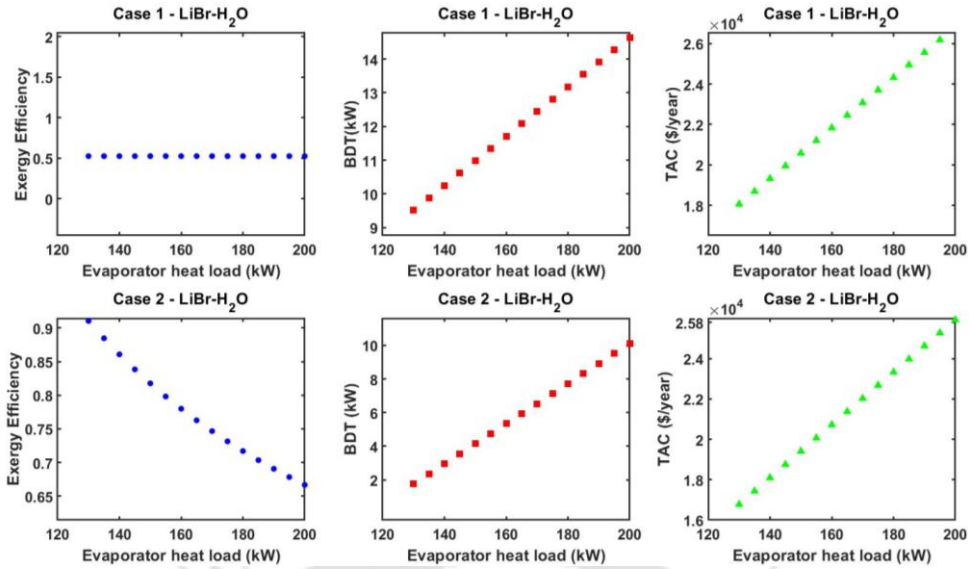

Fig. 6. 10 Effect of different evaporator loads on exergy efficiency, BDT, and TAC: Case-1 & Case-2

The mass flow rate of the absorber coolant is considered one of the decision variables in Case 2. So for this study, the optimal decision variable set for the maximum exergy efficiency of LiBr-H_2O has been considered for all evaporator heat loads. Here, the absorber coolant mass flow rate is fixed to the optimal value determined. Due to this, the exergy efficiency is observed to be decreasing with the increase in evaporator heat load, unlike Case 1, as shown in Fig. 6.10. Similar to Case 1, BDT and TAC increase with the increase in evaporator load; however, these values for Case 2 are smaller than the Case 1. This indicates that assigning absorber coolant mass flow rate as a decision variable can be beneficial as it increases exergy efficiency and reduces BDT and TAC as well. The same trend has been observed for Case 1 and Case 2 of $CaCl_2$-LiBr-$LiNO_3$-H_2O.

6.5. Closure

The current study investigates multi-objective thermoeconomic optimization of a vapor recompression-absorption refrigeration system (VRARS). LiBr-H_2O and $CaCl_2$-LiBr-$LiNO_3$-H_2O are absorbent-refrigerant combinations for the proposed system. The present system targets to minimize the total annual cost and maximize the exergy efficiency of the system using a nonlinear objective function developed. The total annual cost calculation comprises investment, carbon tax/penalty, and absorber coolant costs. The MOGA, MOPSO, and MOsTLBO metaheuristic techniques are used for the optimization analysis. The outlet temperatures of the evaporator, absorber, generator-condenser, absorber, compression ratio, and the effectiveness of the solution heat exchanger are the selected decision variables for Case 1; however, in Case 2, the absorber coolant mass flow rate is also considered in addition to the

TH-3395_176107002

Case 1 decision variables. The present work investigates the impact of decision variables on the economic, energy, and exergy analysis of the system. Results from the multi-objective optimization are presented in the Pareto front obtained from the non-dominated solutions of each algorithm. The following list includes the key findings from the analysis:

Case 1:

- LiBr-H_2O determines maximum exergy efficiency (0.524), while $CaCl_2$-LiBr-$LiNO_3$-H_2O reports the minimum TAC (19063.136 $/year). LiBr-$H_2O$ solution determines the exergy efficiency improved by ~8%, while $CaCl_2$-LiBr-$LiNO_3$-H_2O reports a lower TAC by ~3% than the corresponding other absorbent solution for MOPSO.
- Higher generator, evaporator, absorber temperature, and lower condenser temperatures aid in determining the minimum TAC of the system in this case and vice versa.
- ($CaCl_2$-LiBr-$LiNO_3$)-H_2O can be selected for minimum TAC, while for maximum exergy efficiency, LiBr-H_2O can be chosen.

Case 2:

- LiBr-H_2O and $CaCl_2$-LiBr-$LiNO_3$-H_2O solution determine the maximum exergy efficiency as 0. 818. The minimum TAC determined by $CaCl_2$-LiBr-$LiNO_3$-H_2O is ~5% lesser than LiBr-H_2O. For Case 2, $CaCl_2$-LiBr-$LiNO_3$-H_2O can be chosen due to its lower TAC than LiBr-H_2O.
- Lower evaporator temperature and higher generator, and absorber temperatures help to determine the minimum TAC of the system and vice versa.

Overall:

- The maximum exergy efficiency obtained for Case 2 is ~36 % and ~41% enhanced than in Case 1 for LiBr-H_2O and ($CaCl_2$-LiBr-$LiNO_3$)-H_2O, respectively. The minimum TAC achieved in Case 1 is higher by ~7 % and ~8% than in Case 2 for LiBr-H_2O and ($CaCl_2$-LiBr-$LiNO_3$)-H_2O, respectively. The exergy destruction determined in Case 1 is ~165% and ~202% higher than in Case 2, respectively, for LiBr-H_2O and ($CaCl_2$-LiBr-$LiNO_3$)-H_2O. Among Case 1 and Case 2, Case 2 can be a better choice considering the maximum exergy efficiency and minimum TAC.
- Based on the IGD obtained for each algorithm, MOsTLBO outperforms other algorithms for both cases.

TH-3395_176107002

CHAPTER 7

Conclusions and future scope

This chapter covers the key findings from the single and multi-objective thermoeconomic optimization study using metaheuristic techniques. Further, the future scopes of the current work have also been discussed.

7.1. Multi-objective thermoeconomic optimization of the VARS and MVARS

A detailed study of the VARS and MVARS has been conducted by employing multi-objective metaheuristic techniques such as MOGA, MOPSO, and MOsTLBO. Minimizing the total annual cost and minimizing the exergy destruction are considered objectives. Two separate coolant streams are used for the absorber and condenser in VARS, while MVARS uses the outlet coolant stream of the absorber as an inlet coolant stream to the condenser. Outlet temperatures and the effectiveness of the solution heat exchanger are decision variables for VARS, and in addition, temperatures and the absorber coolant mass flow rate are the decision variables for MVARS. The significant observations from this optimization study are as follows:

- Higher effectiveness, evaporator, and absorber temperature while lower condenser and generator temperature lead to lower exergy destruction and higher system cost for both cases.
- An increase in the generator and condenser temperature leads to the lower strong and weak solution concentration, which increases the mass flow rate of refrigerant, absorbent solution & coolant and eventually raises the exergy destruction, while their higher heat load aids in determining lower area and hence the lower cost.
- MOGA reports the lowest total annual cost for both cases, while MOPSO determines the lowest exergy destruction for VARS & MVARS.
- Between VARS & MVARS, exergy destruction determined for MVARS is ~17% lesser, and the total annual cost is ~0.9% higher than conventional VARS.
- IGD for MOPSO is lesser than MOGA and MOsTLBO, implying that the Pareto front solutions obtained by MOPSO are better converged.
- MOsTLBO reports the minimum annual cost of plant operation for the given minimum exergy destruction for both VARS and MVARS.

TH-3395_176107002

7.2. Themoeconomic optimization of the cascaded refrigeration system

A single-objective thermoeconomic optimization study of vapor compression-absorption cascaded refrigeration system (CRS) to determine the minimum total annual cost. The metaheuristic techniques such as sTLBO, COA, TGA, YYPO, and ASO have been used. Different absorbent-refrigerant combinations have been utilized for this current system as working pairs. In VCRS, low ODP and GWP refrigerants like R290, R123, R1234yf, and R1234ze are refrigerants, while in VARS LiBr-H_2O, LiCl-H_2O and $CaCl_2$-LiBr-$LiNO_3$-H_2O are the absorbent solutions. Impact of decision variables on the various parameters of the refrigeration systems such as COP, exergy destruction, total area, and total annual cost. Important results obtained are summarized here:

- Among all refrigerants of VCRS, R290 determines the lowest total annual cost, while R1234yf obtains the highest annual cost irrespective of the absorbent pair in VARS.
- The highest total annual cost is reported by the LiBr-H_2O-R1234yf combination, which is ~15% higher than the lowest total annual cost determined by the $CaCl_2$-LiBr-$LiNO_3$-H_2O-R290 combination.
- It has been observed that generator temperature, condenser temperature, and overlap temperature predominantly influence the operation of CRS.
- The COP of VARS obtained for the $CaCl_2$-LiBr-$LiNO_3$-H_2O pair is ~24% and ~18% improved than LiBr-H_2O and LiCl-H_2O, respectively, due to the enthalpy difference calculated for the thermal compressor streams for each absorbent.
- The COP of the CRS reported for the $CaCl_2$-LiBr-$LiNO_3$-H_2O pair is ~22% and ~17% enhanced than LiBr-H_2O and LiCl-H_2O, respectively. Higher evaporator temperature and lower cascade condenser temperature for VCRS result in less compressor work and an increased COP of CRS.
- In the case of minimum total annual cost, the exergy destruction obtained for LiBr-H_2O and LiCl-H_2O is ~23% and ~17% higher than the $CaCl_2$-LiBr-$LiNO_3$-H_2O. This is due to the difference in the utility mass flow rate for the thermal compressor section. The heat load of the generator and absorber changes as a result of variations in the enthalpies of the streams, which also affects the mass flow rate.
- Among all the algorithms, COA determined solutions with the least total cost for all combinations except LiBr-H_2O-R1234ze. The best and mean values reported by

TH-3395_176107002

sTLBO and COA have negligible differences.

- The worst performance is shown by ASO, followed by TGA and YYPO based on the standard deviation determined for all combinations.

7.3. A comparative study of the thermoeconomic optimization of the CRS and SCRS

An extensive comparison between a subcooler-assisted vapor compression absorption cascaded refrigeration system (SCRS) and an independent cascaded refrigeration system (CRS) is carried out to determine the efficient refrigeration system. The study relies on the energy, exergy, economic, and environmental performance of both systems. R290, R123, R1234yf, and R1234ze are refrigerants in VCRS, while LiBr-H_2O, LiCl-H_2O, and $CaCl_2$-LiBr-$LiNO_3$-H_2O have been employed as working absorbent-refrigerant pair for both systems. To perform an optimization study, sTLBO, ASO, TGA, YYPO, and COA have been used. The comparison reported here is made for $CaCl_2$-LiBr-$LiNO_3$-H_2O-R290 in both systems, as only this pair determines higher COP, lower exergy destruction, and lower total annual cost. The following are the main outcomes from the comparison analysis:

- The COP of SCRS is observed to be ~250% enhanced than CRS due to the subcooler addition to the CRS, resulting in a lower heat load supply to VARS as a cooling load. The cooling load supplied to VARS in CRS is ~84% higher than SCRS.
- The COP of the VCRS for SCRS is ~192% higher than CRS due to an increase in the compressor work. Adding a subcooler to VCRS elevates the condenser pressure, leading to a higher compressor load than CRS.
- The exergy destruction reported by CRS is ~ 40% higher than the SCRS, caused due to the lower heat load of the VARS that results in a lower mass flow rate of utility (hot and cold) streams and hence reduced exergy destruction.
- Higher condenser pressure leads to higher compressor work. The compressor work reported by SCRS is ~66% higher, resulting in a higher penalty cost.
- Due to the higher utility mass flow rate in CRS, the cost of cold utility calculated for CRS is ~39% more than SCRS, indicating that SCRS has better thermodynamic performance than CRS.
- The total annual cost reported for SCRS is ~15% minimum than the CRS, implying economically better performance than CRS.

TH-3395_176107002

- The standard deviation reported for sTLBO is lesser, followed by COA compared to other algorithms indicating that sTLBO is the best performer for both systems.

7.4. A multi-objective thermoeconomic optimization of the vapor recompression absorption refrigeration system

A vapor recompression absorption system accommodates the compressor between the condenser and generator recovers the condensation heat rejected to heat the refrigerant-absorbent solution in the generator. A detailed multi-objective thermoeconomic optimization of this system is conducted with two cases based on the decision variables. In the first case, the temperatures of heat exchangers, the effectiveness of the solution heat exchanger, and the compressor ratio are the decision variables while the second case includes the mass flow rate of the absorber coolant along with the first case. LiBr-H_2O and $CaCl_2$-LiBr-$LiNO_3$-H_2O are the working fluids and the multi objective study is carried out by employing MOGA, MOPSO, and MOsTLBO algorithms. For an ideal refrigeration system, maximum exergy efficiency and minimum total annual cost is required; however, these two are conflicting in nature. Therefore, maximization of exergy efficiency and minimization of the total annual cost of the system are considered as objective functions. The following are the key findings from this study:

- Case 1 report that LiBr-H_2O has higher exergy efficiency (0.524) ~8% higher than ($CaCl_2$-LiBr-$LiNO_3$)-H_2O while ($CaCl_2$-LiBr-$LiNO_3$)-H_2O obtains the lowest total annual cost (19063.136 $/year) ~ 3% lesser than LiBr-H_2O for MOPSO.
- The exergy efficiency determined by both the absorbent solutions for Case 2 is the same (0.818), whereas the total annual cost obtained by ($CaCl_2$-LiBr-$LiNO_3$)-H_2O is less than LiBr-H_2O by ~5%.
- The exergy efficiency of LiBr-H_2O and ($CaCl_2$-LiBr-$LiNO_3$)-H_2O in Case 2 is improved by ~36 % and ~41 %, respectively, whereas the minimum total annual cost reported for both absorbents is reduced by ~7 % and ~8% respectively, compared to Case 1.
- MOsTLBO achieves better results than MOGA and MOPSO based on the inverted generational distance for both cases.

Among all systems studied in this thesis, VARS and VRARS operated using low-grade heat can be employed if cooling is required above 4°C when water is used as the refrigerant. This is particularly because, at temperatures below this threshold, water reaches its freezing point. The implementation of VARS can offer significant benefits, primarily in food processing

TH-3395_176107002

industries, textile industries, refineries, and petrochemical industries. For instance, approximately 75% of the moisture is released into the atmosphere through the chimney in the form of water vapor in the potato fryer industry. The hot water vapor or CO_2 obtained as a byproduct in refineries or from textile industries can be utilized to operate VARS. CRS and SCRS can be operated using both low-grade and high-grade energy sources. In terms of energy and exergy analysis, CRS and SCRS outperform conventional VCRS and VARS. Both CRS and SCRS can be effectively utilized for achieving low-temperature refrigeration. The energy and exergy efficiency of VRARS surpasses that of VARS. Therefore, implementing VRARS is a beneficial choice.

All the systems investigated in this study are variations of either traditional VARS or VARS integrated with other systems or modified VARS. One challenge that may arise is the crystallization problem of lithium salts and associated pressure drops. For VCRS, refrigerant leakage is a potential issue to contend with.

7.5. Scope of the future work

In this present work, it is assumed that the refrigeration systems utilized are smoothly working using a low-grade heat system. However, real-life low-grade energy systems such as solar energy, biomass energy, or hot flue gas from the industry can be integrated with present refrigeration systems, and detailed analysis and optimization of such systems can be presented. Though the number of publications on liquid desiccant has been enormous, liquid desiccant air dehumidification practical uses in real buildings are still limited. Therefore, publications related to the engineering case studies and practical operations should be encouraged. A few relevant areas of the liquid desiccant system have been identified, and further investigation is needed on them. Listed below are the recommended topics for research in the near future:

- Experimental analysis of the proposed system with various absorbent-refrigerant combinations
- Integration and optimization of vapor adsorption refrigeration system with VCRS and VARS
- Design and optimization for mixed renewable energy-based VARS and CRS
- Integration of optimized refrigeration system with existing incumbent real-time control system for better operation

TH-3395_176107002

- Optimization of chilled water configurations and HVAC systems to provide conditioned space with the required cooling capacities and minimal energy consumption and cost
- Design and optimization of a small-scale poly-generation energy system in different climate zones in India

TH-3395_176107002

References

[1] "World energy consumption - Transportation, Industry, Residential." https://www.nuclear-power.com/how-much-energy-does-the-world-consume/world-energy-consumption-transportation-industry-residential/ (accessed Feb. 15, 2023).

[2] "Sustainability With Wide Bandgap Technologies." https://www.electronicsforu.com/technology-trends/interviews/sustainability-with-wide-bandgap-technologies (accessed Feb. 18, 2023).

[3] T. Peters, "A Cool World: Defining the Energy Conundrum of Cooling for All Contributors," 2018.

[4] "Keeping homes cool on a warming planet." https://www.dw.com/en/climate-emergency-keeping-homes-cool-on-a-warming-planet/a-59933154 (accessed Mar. 01, 2023).

[5] N. Kaja, "An Overview of Energy Sector in India," *Int. J. Sci. Res.*, vol. 6, pp. 2319–7064, 2015.

[6] S. B. Singh, H. Kumar, I. Chowdhury Roy, and P. Ram, "Energy statistical India-2023," 2023.

[7] "Electricity generation in India 2023: Share of different sources." https://groundreport.in/electricity-generation-in-india-2023-share-of-different-sources/ (accessed May 25, 2023).

[8] "Global Temperature Report for 2022 - Berkeley Earth." https://berkeleyearth.org/global-temperature-report-for-2022 (accessed Apr. 05, 2023).

[9] "The future of Air Conditioning World Demand & Warming Temperature Increases." https://www.enerdata.net/publications/executive-briefing/the-future-air-conditioning-global-demand.html (accessed Mar. 18, 2023).

[10] "The Cooling Imperative - Economist Intelligence Unit." https://www.eiu.com/n/the-cooling-imperative/ (accessed May 16, 2023).

[11] Y. Wang, H. Lin, W. Wang, Y. Liu, R. Wennersten, and Q. Sun, "Impacts of climate change on the cooling loads of residential buildings differences between occupants with different age," *Energy Procedia*, vol. 142, pp. 2677–2682, Dec. 2017, doi:

TH-3395_176107002

10.1016/J.EGYPRO.2017.12.210.

[12] "Latest Cooling News: the G20, air conditioners, cities, green procurement and philanthropy - Integrate." https://www.renewableenergy.ox.ac.uk/latest-cooling-news-the-g20-air-conditioners-cities-green-procurement-and-philanthropy/ (accessed Apr. 23, 2023).

[13] "Chart: Air Conditioning Biggest Factor in Growing Electricity Demand | Statista." https://www.statista.com/chart/14401/growing-demand-for-air-conditioning-and-energy/ (accessed Mar. 17, 2023).

[14] "India Cooling Action Plan," 2019.

[15] A. Teke and O. Timur, "Assessing the energy efficiency improvement potentials of HVAC systems considering economic and environmental aspects at the hospitals," *Renew. Sustain. Energy Rev.*, vol. 33, pp. 224–235, May 2014, doi: 10.1016/J.RSER.2014.02.002.

[16] I. Dincer and M. Kanoglu, *Refrigeration Systems And Applications*, Second. John Wiley & Sons, Ltd, 2010.

[17] N. Cherrad, A. Benchabane, L. Sedira, and A. Rouag, "Transient numerical model for predicting operating temperatures of solar adsorption refrigeration cycle," *Appl. Therm. Eng.*, vol. 130, pp. 1163–1174, 2018, doi: 10.1016/j.applthermaleng.2017.11.059.

[18] H. Soualmi and R. Khelfaoui, "Modeling and Simulation Study of a Solar Adsorption Refrigeration System to Highlight Its Performance under the Desert Climate Conditions," *Appl. Sol. Energy*, vol. 57, no. 3, pp. 205–215, May 2021, doi: 10.3103/S0003701X21030075/FIGURES/10.

[19] N. A. Mezaal, K. V Osintsev, and T. B. Zhirgalova, "Review of magnetic refrigeration system as alternative to conventional refrigeration system," in *IOP Conf. Series: Earth and Environmental Science*, 2017, pp. 1–7, doi: 10.1088/1755-1315/87/3/032024.

[20] S. Bandaru and K. Deb, *Metaheuristic Techniques*. Taylor & Francis Group, 2016.

[21] Y. Cui, Z. Geng, Q. Zhu, and Y. Han, "Review: Multi-objective optimization methods and application in energy saving," *Energy*, vol. 125, pp. 681–704, 2017, doi: 10.1016/J.ENERGY.2017.02.174.

TH-3395_176107002

[22] R. Ahmed *et al.*, "4E analysis of a two-stage refrigeration system through surrogate models based on response surface methods and hybrid grey wolf optimizer," *PLoS One*, vol. 18, no. 2 February, 2023, doi: 10.1371/journal.pone.0272160.

[23] R. Ahmed, S. Mahadzir, N. Erniza B Rozali, K. Biswas, F. Matovu, and K. Ahmed, "Artificial intelligence techniques in refrigeration system modelling and optimization: A multi-disciplinary review," *Sustain. Energy Technol. Assessments*, vol. 47, p. 101488, Oct. 2021, doi: 10.1016/J.SETA.2021.101488.

[24] D. H. Wolpert and W. G. Macready, "No free lunch theorems for optimization," *IEEE Trans. Evol. Comput.*, vol. 1, no. 1, pp. 67–82, 1997, doi: 10.1109/4235.585893.

[25] R. V. Rao, V. J. Savsani, and D. P. Vakharia, "Teaching–learning-based optimization: A novel method for constrained mechanical design optimization problems," *Comput. Des.*, vol. 43, no. 3, pp. 303–315, Mar. 2011, doi: 10.1016/J.CAD.2010.12.015.

[26] R. Kommadath and K. Prakash, "Sanitized teaching-learning based optimization," *Tech. Report, Indian Inst. Technol. Guwahati*, 2016.

[27] W. Zhao, L. Wang, and Z. Zhang, "Atom search optimization and its application to solve a hydrogeologic parameter estimation problem," *Knowledge-Based Syst.*, vol. 163, pp. 283–304, Jan. 2019, doi: 10.1016/j.knosys.2018.08.030.

[28] J. Pierezan and L. Dos Santos Coelho, "Coyote Optimization Algorithm: A New Metaheuristic for Global Optimization Problems," in *2018 IEEE Congress on Evolutionary Computation (CEC)*, Sep. 2018, pp. 1–8, doi: 10.1109/CEC.2018.8477769.

[29] A. Cheraghalipour, M. Hajiaghaei-Keshteli, and M. M. Paydar, "Tree Growth Algorithm (TGA): A novel approach for solving optimization problems," *Eng. Appl. Artif. Intell.*, vol. 72, pp. 393–414, Jun. 2018, doi: 10.1016/j.engappai.2018.04.021.

[30] V. Punnathanam and P. Kotecha, "Yin-Yang-pair Optimization: A novel lightweight optimization algorithm," *Eng. Appl. Artif. Intell.*, vol. 54, pp. 62–79, Sep. 2016, doi: 10.1016/J.ENGAPPAI.2016.04.004.

[31] K. Deb, *Mutliobjective Optimization using Evolutionary Algorithms*, vol. 44, no. 8. John Wiley & Sons, Ltd, 2001.

[32] C. A. Coello Coello, G. T. Pulido, and M. S. Lechuga, "Handling multiple objectives

TH-3395_176107002

with particle swarm optimization," *IEEE Trans. Evol. Comput.*, vol. 8, no. 3, pp. 256–279, Jun. 2004, doi: 10.1109/TEVC.2004.826067.

[33] R. Kommadath and P. Kotecha, "Multi objective sanitized teaching learning based optimization.pdf," *Tech. Report, Indian Inst. Technol. Guwahati*, 2016.

[34] P. Dhankhar, "A Study on Refrigeration," *Int. J. Sci. Res. ISSN*, vol. 3, no. 5, pp. 1212–1220, 2012.

[35] H. Pedersen, "Low GWP Alternatives to HFCs in Refrigeration," 2012.

[36] I. Dincer, "Refrigerants," in *Comprehensive Energy Systems*, I. B. T.-C. E. S. Dincer, Ed. Oxford: Elsevier, 2018, pp. 435–474.

[37] J. T. McMullan, "Refrigeration and the environment - Issues and strategies for the future," *Int. J. Refrig.*, vol. 25, no. 1, pp. 89–99, 2002, doi: 10.1016/S0140-7007(01)00007-X.

[38] A. Reizian, Y. Dat, S. Rault, and M. Robba, "Mass spectral study of chlorofluorocarbons (CFCs) and potential alternatives (HCFCs and HFCs)," *Ecotoxicol. Environ. Saf.*, vol. 29, no. 1, pp. 47–60, Oct. 1994, doi: 10.1016/0147-6513(94)90029-9.

[39] S. A. M. Said, Y. M. Suleiman, and B. Ismail, "Theoretical performance of HCFC123 as an alternative to CFC11," *Energy*, vol. 20, no. 3, pp. 205–208, 1995, doi: 10.1016/0360-5442(94)00072-B.

[40] D.-W. Sun and I. W. Eames, "Performance characteristics of HCFC-123 ejector refrigeration cycles," *Int. J. Energy Res.*, vol. 20, no. 10, pp. 871–885, Oct. 1996, doi: https://doi.org/10.1002/(SICI)1099-114X(199610)20:10<871::AID-ER201>3.0.CO;2-4.

[41] P. Midgley, "HCFCs and HFCs: Halocarbon replacements for CFCs," *Atmos. Environ.*, vol. 31, no. 7, pp. 1095–1096, 1997, doi: 10.1016/S1352-2310(96)00293-2.

[42] D. Jung, C. B. Kim, S. Cho, and K. Song, "Condensation heat transfer coefficients of enhanced tubes with alternative refrigerants for CFC11 and CFC12," *Int. J. Refrig.*, vol. 22, no. 7, pp. 548–557, 1999, doi: 10.1016/S0140-7007(99)00020-1.

[43] A. Arora, B. B. Arora, B. D. Pathak, and H. L. Sachdev, "Exergy analysis of a Vapour

TH-3395_176107002

Compression Refrigeration system with R-22, R-407C and R-410A," *Int. J. Exergy*, vol. 4, no. 4, pp. 441–454, 2007, doi: 10.1504/IJEX.2007.015083.

[44] E. Clark, "HCFC Phase-out:A Comparative Assessment of the Proposed Adjustments," 2007.

[45] "Govt of India committed to phase out Hydrochlorofluorocarbons by 2030," 2017.

[46] "Phaseout of Class II Ozone-Depleting Substances | US EPA." https://www.epa.gov/ods-phaseout/phaseout-class-ii-ozone-depleting-substances (accessed Jun. 06, 2023).

[47] G. Lorentzen, "The use of natural refrigerants: a complete solution to the CFC/HCFC predicament," *Int. J. Refrig.*, vol. 18, no. 3, pp. 190–197, 1995, doi: 10.1016/0140-7007(94)00001-E.

[48] M. A. Alsaad and M. A. Hammad, "The application of propane/butane mixture for domestic refrigerators," *Appl. Therm. Eng.*, vol. 18, no. 9–10, pp. 911–918, 1998, doi: 10.1016/s1359-4311(97)00113-0.

[49] B. A. Akash and S. A. Said, "Assessment of LPG as a possible alternative to R-12 in domestic refrigerators," *Energy Convers. Manag.*, vol. 44, no. 3, pp. 381–388, Feb. 2003, doi: 10.1016/S0196-8904(02)00065-1.

[50] H. O. Spauschus, "HFC 134a as a substitute refrigerant for CFC 12," *Int. J. Refrig.*, vol. 11, no. 6, pp. 389–392, Nov. 1988, doi: 10.1016/0140-7007(88)90063-1.

[51] M. Padilla, R. Revellin, and J. Bonjour, "Exergy analysis of R413A as replacement of R12 in a domestic refrigeration system," *Energy Convers. Manag.*, vol. 51, no. 11, pp. 2195–2201, Nov. 2010, doi: 10.1016/J.ENCONMAN.2010.03.013.

[52] A. Kilicarslan and M. Hosoz, "Energy and irreversibility analysis of a cascade refrigeration system for various refrigerant couples," *Energy Convers. Manag.*, vol. 51, no. 12, pp. 2947–2954, Dec. 2010, doi: 10.1016/J.ENCONMAN.2010.06.037.

[53] "Lower GWP blends in Bitzer compressors - Cooling Post." https://www.coolingpost.com/world-news/lower-gwp-blends-in-bitzer-compressors/ (accessed Jun. 15, 2023).

[54] "IPCC Includes GWP for Hydrocarbons in New Report."

TH-3395_176107002

https://hydrocarbons21.com/ipcc-includes-gwps-for-hydrocarbons-in-new-report/ (accessed May 14, 2023).

[55] "Ammonia As a Refrigerant: Pros and Cons | Just Venting." https://www.goodway.com/hvac-blog/2009/08/ammonia-as-a-refrigerant-pros-and-cons/ (accessed Jun. 28, 2023).

[56] A. Kabul, Ö. Kizilkan, and A. K. Yakut, "Performance and exergetic analysis of vapor compression refrigeration system with an internal heat exchanger using a hydrocarbon, isobutane (R600a)," *Int. J. Energy Res.*, vol. 32, no. 9, pp. 824–836, 2008, doi: 10.1002/ER.1396.

[57] H. C. Bayrakçi and A. E. Özgür, "Energy and exergy analysis of vapor compression refrigeration system using pure hydrocarbon refrigerants," *Int. J. Energy Res.*, vol. 33, no. 12, pp. 1070–1075, 2009, doi: 10.1002/ER.1538.

[58] M. Rasti, S. Aghamiri, and M. S. Hatamipour, "Energy efficiency enhancement of a domestic refrigerator using R436A and R600a as alternative refrigerants to R134a," *Int. J. Therm. Sci.*, vol. 74, pp. 86–94, Dec. 2013, doi: 10.1016/J.IJTHERMALSCI.2013.07.009.

[59] J. A. Shilliday, S. A. Tassou, and N. Shilliday, "Comparative energy and exergy analysis of R744, R404A and R290 refrigeration cycles," *Int. J. Low-Carbon Technol.*, vol. 4, no. 2, pp. 104–111, 2009, doi: 10.1093/ijlct/ctp014.

[60] C. C. Yu and T. P. Teng, "Retrofit assessment of refrigerator using hydrocarbon refrigerants," *Appl. Therm. Eng.*, vol. 66, no. 1–2, pp. 507–518, May 2014, doi: 10.1016/J.APPLTHERMALENG.2014.02.050.

[61] "Natural Refrigerants | Secop — Sustainable Cooling Solutions." https://www.secop.com/solutions/natural-refrigerants (accessed Apr. 10, 2023).

[62] A. Yataganbaba, A. Kilicarslan, I. ˙ Rfan, and K. Kurtbas¸, "Exergy analysis of R1234yf and R1234ze as R134a replacements in a two evaporator vapour compression refrigeration system," *Int. J. Refrig.*, vol. 60, pp. 26–37, 2015, doi: 10.1016/j.ijrefrig.2015.08.010.

[63] R. Ben Jemaa, R. Mansouri, I. Boukholda, and A. Bellagi, "Energy and exergy investigation of R1234ze as R134a replacement in vapor compression chillers," *Int. J.*

TH-3395_176107002

Hydrogen Energy, vol. 42, no. 17, pp. 12877–12887, Apr. 2017, doi: 10.1016/J.IJHYDENE.2016.12.010.

[64] Z. Sun, Q. Wang, Z. Xie, S. Liu, D. Su, and Q. Cui, "Energy and exergy analysis of low GWP refrigerants in cascade refrigeration system," *Energy*, vol. 170, pp. 1170–1180, Mar. 2019, doi: 10.1016/J.ENERGY.2018.12.055.

[65] Z. Yang *et al.*, "Analysis of lower GWP and flammable alternative refrigerants," *Int. J. Refrig.*, vol. 126, no. January, pp. 12–22, 2021, doi: 10.1016/j.ijrefrig.2021.01.022.

[66] R. Llopis, R. Cabello, D. Sánchez, and E. Torrella, "Energy improvements of CO2 transcritical refrigeration cycles using dedicated mechanical subcooling," *Int. J. Refrig.*, vol. 55, pp. 129–141, Jul. 2015, doi: 10.1016/J.IJREFRIG.2015.03.016.

[67] M. H. Yang and R. H. Yeh, "Performance and exergy destruction analyses of optimal subcooling for vapor-compression refrigeration systems," *Int. J. Heat Mass Transf.*, vol. 87, pp. 1–10, Aug. 2015, doi: 10.1016/J.IJHEATMASSTRANSFER.2015.03.085.

[68] Q. Chen, J. Yu, and G. Yan, "Performance analysis of a modified zeotropic mixture (R290/R600) refrigeration cycle with internal subcooler for freezer applications," *Appl. Therm. Eng.*, vol. 108, pp. 172–180, Sep. 2016, doi: 10.1016/J.APPLTHERMALENG.2016.07.132.

[69] Z. Li, E. Chen, Y. Jing, and S. Lv, "Thermodynamic relationship of subcooling power and increase of cooling output in vapour compression chiller," *Energy Convers. Manag.*, vol. 149, pp. 254–262, Oct. 2017, doi: 10.1016/J.ENCONMAN.2017.07.030.

[70] T. S. Mogaji, A. Awolala, O. Z. Ayodeji, P. B. Mogaji, and D. E. Philip, "COP enhancement of vapour compression refrigeration system using dedicated mechanical subcooling cycle," *Niger. J. Technol.*, vol. 39, no. 3, pp. 776–784, Sep. 2020, doi: 10.4314/njt.v39i3.17.

[71] R. Roy, A. J. Bhowal, and B. K. Mandal, "Thermoeconomic analysis of vapor compression refrigeration system with dedicated subcooler for high-Temperature lift applications," *J. Therm. Sci. Eng. Appl.*, vol. 13, no. 6, pp. 1–12, 2021, doi: 10.1115/1.4050481.

[72] O. Rezayan and A. Behbahaninia, "Thermoeconomic optimization and exergy analysis of CO2/NH3 cascade refrigeration systems," *Energy*, vol. 36, no. 2, pp. 888–895, Feb.

TH-3395_176107002

2011, doi: 10.1016/J.ENERGY.2010.12.022.

[73] S. Bhattacharyya, S. Mukhopadhyay, A. Kumar, R. K. Khurana, and J. Sarkar, "Optimization of a CO2-C3H8 cascade system for refrigeration and heating," *Int. J. Refrig.*, vol. 28, no. 8, pp. 1284–1292, 2005, doi: 10.1016/j.ijrefrig.2005.08.010.

[74] T. S. Lee, C. H. Liu, and T. W. Chen, "Thermodynamic analysis of optimal condensing temperature of cascade-condenser in CO2/NH3 cascade refrigeration systems," *Int. J. Refrig.*, vol. 29, no. 7, pp. 1100–1108, 2006, doi: 10.1016/j.ijrefrig.2006.03.003.

[75] A. Da Silva, E. P. Bandarra Filho, and A. H. P. Antunes, "Comparison of a R744 cascade refrigeration system with R404A and R22 conventional systems for supermarkets," *Appl. Therm. Eng.*, vol. 41, pp. 30–35, 2012, doi: 10.1016/j.applthermaleng.2011.12.019.

[76] Z. Sun *et al.*, "Comparative analysis of thermodynamic performance of a cascade refrigeration system for refrigerant couples R41/R404A and R23/R404A," *Appl. Energy*, vol. 184, pp. 19–25, 2016, doi: 10.1016/j.apenergy.2016.10.014.

[77] M. W. Faruque, M. R. Uddin, S. Salehin, and M. M. Ehsan, "A Comprehensive Thermodynamic Assessment of Cascade Refrigeration System Utilizing Low GWP Hydrocarbon Refrigerants," *Int. J. Thermofluids*, vol. 15, no. July, p. 100177, 2022, doi: 10.1016/j.ijft.2022.100177.

[78] J. Fernández-Seara and M. Vázquez, "Study and control of the optimal generation temperature in NH3–H2O absorption refrigeration systems," *Appl. Therm. Eng.*, vol. 21, no. 3, pp. 343–357, Feb. 2001, doi: 10.1016/S1359-4311(00)00047-8.

[79] S. A. Adewusi and S. M. Zubair, "Second law based thermodynamic analysis of ammonia-water absorption systems," *Energy Convers. Manag.*, vol. 45, no. 15–16, pp. 2355–2369, Sep. 2004, doi: 10.1016/J.ENCONMAN.2003.11.020.

[80] F. Boudéhenn, H. Demasles, J. Wyttenbach, X. Jobard, D. Chèze, and P. Papillon, "Development of a 5 kW cooling capacity ammonia-water absorption chiller for solar cooling applications," *Energy Procedia*, vol. 30, pp. 35–43, 2012, doi: 10.1016/J.EGYPRO.2012.11.006.

[81] S. Du, R. Z. Wang, P. Lin, Z. Z. Xu, Q. W. Pan, and S. C. Xu, "Experimental studies

TH-3395_176107002

on an air-cooled two-stage NH3-H2O solar absorption air-conditioning prototype," *Energy*, vol. 45, no. 1, pp. 581–587, 2012, doi: 10.1016/J.ENERGY.2012.07.041.

[82] J. Aman, D. S. K. Ting, and P. Henshaw, "Residential solar air conditioning: Energy and exergy analyses of an ammonia–water absorption cooling system," *Appl. Therm. Eng.*, vol. 62, no. 2, pp. 424–432, Jan. 2014, doi: 10.1016/J.APPLTHERMALENG.2013.10.006.

[83] R. Ramesh, S. N. Murugesan, C. Narendran, and R. Saravanan, "Experimental investigations on shell and helical coil solution heat exchanger in NH3-H2O vapour absorption refrigeration system (VAR)," *Int. Commun. Heat Mass Transf.*, vol. 87, pp. 6–13, Oct. 2017, doi: 10.1016/J.ICHEATMASSTRANSFER.2017.06.010.

[84] O. Kaynakli and M. Kilic, "Theoretical study on the effect of operating conditions on performance of absorption refrigeration system," *Energy Convers. Manag.*, vol. 48, no. 2, pp. 599–607, Feb. 2007, doi: 10.1016/j.enconman.2006.06.005.

[85] S. Aphornratana and T. Sriveerakul, "Experimental studies of a single-effect absorption refrigerator using aqueous lithium–bromide: Effect of operating condition to system performance," *Exp. Therm. Fluid Sci.*, vol. 32, no. 2, pp. 658–669, Nov. 2007, doi: 10.1016/J.EXPTHERMFLUSCI.2007.08.003.

[86] A. Arora and S. C. Kaushik, "Theoretical analysis of LiBr/H2O absorption refrigeration systems," *Int. J. Energy Res.*, vol. 33, no. 15, pp. 1321–1340, 2009, doi: 10.1002/ER.1542.

[87] C. M. Lamine and Z. Said, "Energy analysis of single effect absorption chiller (LiBr/H2O) in an industrial manufacturing of detergent," *Energy Procedia*, vol. 50, pp. 105–112, 2014, doi: 10.1016/j.egypro.2014.06.013.

[88] E. D. Kerme, A. Chafidz, O. P. Agboola, J. Orfi, A. H. Fakeeha, and A. S. Al-Fatesh, "Energetic and exergetic analysis of solar-powered lithium bromide-water absorption cooling system," *J. Clean. Prod.*, vol. 151, pp. 60–73, 2017, doi: 10.1016/j.jclepro.2017.03.060.

[89] A. A. V. Ochoa, J. C. C. Dutra, J. R. G. Henríquez, and C. A. C. Dos Santos, "Dynamic study of a single effect absorption chiller using the pair LiBr/H2O," *Energy Convers. Manag.*, vol. 108, pp. 30–42, 2016, doi: 10.1016/j.enconman.2015.11.009.

TH-3395_176107002

[90] S. Arivazhagan, S. N. Murugesan, R. Saravanan, and S. Renganarayanan, "Simulation studies on R134a-DMAC based half effect absorption cold storage systems," *Energy Convers. Manag.*, vol. 46, no. 11–12, pp. 1703–1713, Jul. 2005, doi: 10.1016/J.ENCONMAN.2004.10.006.

[91] S. Roy and M. P. Maiya, "Analysis of R134a–DMAC vapour absorption refrigeration system with add-on components," *Int. J. Sustain. Built Environ.*, vol. 1, no. 1, pp. 26–35, 2012, doi: 10.1016/J.IJSBE.2012.04.001.

[92] L. G. Farshi, C. A. Infante Ferreira, S. M. S. Mahmoudi, and M. A. Rosen, "First and second law analysis of ammonia/salt absorption refrigeration systems," *Int. J. Refrig.*, vol. 40, pp. 111–121, 2014, doi: 10.1016/j.ijrefrig.2013.11.006.

[93] J. Patel, B. Pandya, and A. Mudgal, "Exergy Based Analysis of LiCl-H2O Absorption Cooling System," *Energy Procedia*, vol. 109, pp. 261–269, Mar. 2017, doi: 10.1016/J.EGYPRO.2017.03.061.

[94] N. Li, C. Luo, and Q. Su, "A working pair of CaCl2–LiBr–LiNO3/H2O and its application in a single-stage solar-driven absorption refrigeration cycle," *Int. J. Refrig.*, vol. 86, pp. 1–13, Feb. 2018, doi: 10.1016/j.ijrefrig.2017.11.004.

[95] L. Garousi Farshi and S. Asadi, "Ammonia lithium nitrate and ammonia sodium thiocyanate double effect absorption refrigeration systems: Thermodynamic analysis," *Appl. Therm. Eng.*, vol. 138, pp. 374–385, Jun. 2018, doi: 10.1016/J.APPLTHERMALENG.2018.04.079.

[96] Z. Zhang, S. M. Alelyani, N. Zhang, C. Zeng, Y. Yuan, and P. E. Phelan, "Thermodynamic analysis of a novel sodium hydroxide-water solution absorption refrigeration, heating and power system for low-temperature heat sources," *Appl. Energy*, vol. 222, pp. 1–12, Jul. 2018, doi: 10.1016/J.APENERGY.2018.04.008.

[97] Á. Martín and M. D. Bermejo, "Thermodynamic analysis of absorption refrigeration cycles using ionic liquid + supercritical CO2 pairs," *J. Supercrit. Fluids*, vol. 55, no. 2, pp. 852–859, Dec. 2010, doi: 10.1016/J.SUPFLU.2010.10.012.

[98] Y. J. Kim, S. Kim, Y. K. Joshi, A. G. Fedorov, and P. A. Kohl, "Thermodynamic analysis of an absorption refrigeration system with ionic-liquid/refrigerant mixture as a working fluid," *Energy*, vol. 44, no. 1, pp. 1005–1016, Aug. 2012, doi:

TH-3395_176107002

10.1016/J.ENERGY.2012.04.048.

[99] G. D. Takalkar, R. R. Bhosale, N. A. Mali, and S. S. Bhagwat, "Thermodynamic analysis of EMISE–Water as a working pair for absorption refrigeration system," *Appl. Therm. Eng.*, vol. 148, pp. 787–795, Feb. 2019, doi: 10.1016/J.APPLTHERMALENG.2018.11.092.

[100] J. M. Asensio-Delgado, S. Asensio-Delgado, G. Zarca, and A. Urtiaga, "Analysis of hybrid compression absorption refrigeration using low-GWP HFC or HFO/ionic liquid working pairs," *Int. J. Refrig.*, vol. 134, pp. 232–241, Feb. 2022, doi: 10.1016/J.IJREFRIG.2021.11.013.

[101] Y. Chen, T. Zhou, T. Zhao, and Y. He, "Thermodynamic analysis of H2O − 3-aminopropyl tributyl phosphonium glycinate as a working pair for absorption refrigeration system," *Appl. Therm. Eng.*, vol. 213, p. 118658, Aug. 2022, doi: 10.1016/J.APPLTHERMALENG.2022.118658.

[102] Z. Qian, C. Xu, and J. Ren, "Thermal Analysis of a Novel Single-Effect Absorption Refrigeration System Using Water/Ionic Liquid As Working Fluids," *Therm. Sci.*, vol. 26, no. 4, pp. 3107–3118, 2022, doi: 10.2298/TSCI201026038Q.

[103] P. Kalinowski, Y. Hwang, R. Radermacher, S. Al Hashimi, and P. Rodgers, "Application of waste heat powered absorption refrigeration system to the LNG recovery process," *Int. J. Refrig.*, vol. 32, no. 4, pp. 687–694, Jun. 2009, doi: 10.1016/J.IJREFRIG.2009.01.029.

[104] W. Salmi, J. Vanttola, M. Elg, M. Kuosa, and R. Lahdelma, "Using waste heat of ship as energy source for an absorption refrigeration system," *Appl. Therm. Eng.*, vol. 115, pp. 501–516, Mar. 2017, doi: 10.1016/J.APPLTHERMALENG.2016.12.131.

[105] A. T. Rêgo, S. M. Hanriot, A. F. Oliveira, P. Brito, and T. F. U. Rêgo, "Automotive exhaust gas flow control for an ammonia–water absorption refrigeration system," *Appl. Therm. Eng.*, vol. 64, no. 1–2, pp. 101–107, Mar. 2014, doi: 10.1016/J.APPLTHERMALENG.2013.12.018.

[106] J. Stalin, Barath, and G. Manikandan, "Air Conditioning Using Waste Heat and Solar Energy with Phase Change Materials," *Energy Procedia*, vol. 52, pp. 579–587, Jan. 2014, doi: 10.1016/J.EGYPRO.2014.07.113.

TH-3395_176107002

[107] T. Cao, H. Lee, Y. Hwang, R. Radermacher, and H. H. Chun, "Performance investigation of engine waste heat powered absorption cycle cooling system for shipboard applications," *Appl. Therm. Eng.*, vol. 90, pp. 820–830, 2015, doi: 10.1016/j.applthermaleng.2015.07.070.

[108] K. Ebrahimi, G. F. Jones, and A. S. Fleischer, "Thermo-economic analysis of steady state waste heat recovery in data centers using absorption refrigeration," *Appl. Energy*, vol. 139, pp. 384–397, Feb. 2015, doi: 10.1016/J.APENERGY.2014.10.067.

[109] Y. Lu, A. P. Roskilly, and C. Ma, "A techno-economic case study using heat driven absorption refrigeration technology in UK industry," *Energy Procedia*, vol. 123, pp. 173–179, Sep. 2017, doi: 10.1016/J.EGYPRO.2017.07.254.

[110] Y. A. Chaboki, A. Khoshgard, G. Salehi, and F. Fazelpour, "Energy, exergy, and environmental analysis of meeting cooling demand of a ship with waste heat recovery," *Energy Effic.*, vol. 14, no. 2, 2021, doi: 10.1007/s12053-020-09911-2.

[111] S. Zhou, G. He, Y. Li, X. Liang, Q. Pang, and D. Cai, "Comprehensive experimental evaluation of an exhaust-heat-driven absorption refrigeration cycle system using NH3-NaSCN as working pair," *Int. J. Refrig.*, vol. 126, pp. 168–180, Jun. 2021, doi: 10.1016/J.IJREFRIG.2021.01.013.

[112] B. H. Gebreslassie, M. Medrano, and D. Boer, "Exergy analysis of multi-effect water-LiBr absorption systems: From half to triple effect," *Renew. Energy*, vol. 35, no. 8, pp. 1773–1782, Aug. 2010, doi: 10.1016/J.RENENE.2010.01.009.

[113] O. Kaynakli, K. Saka, and F. Kaynakli, "Energy and exergy analysis of a double effect absorption refrigeration system based on different heat sources," *Energy Convers. Manag.*, vol. 106, pp. 21–30, Dec. 2015, doi: 10.1016/J.ENCONMAN.2015.09.010.

[114] A. M. Abed, M. A. Alghoul, K. Sopian, H. S. Majdi, A. N. Al-Shamani, and A. F. Muftah, "Enhancement aspects of single stage absorption cooling cycle: A detailed review," *Renew. Sustain. Energy Rev.*, vol. 77, pp. 1010–1045, Sep. 2017, doi: 10.1016/J.RSER.2016.11.231.

[115] S. A. Kholghi and S. M. S. Mahmoudi, "Energy and exergy analysis of a modified absorption cycle: A comparative study," *Sustain. Energy Technol. Assessments*, vol. 32, pp. 19–28, Apr. 2019, doi: 10.1016/J.SETA.2019.01.002.

TH-3395_176107002

[116] B. S. Bagheri, R. Shirmohammadi, S. M. S. Mahmoudi, and M. A. Rosen, "Optimization and comprehensive exergy-based analyses of a parallel flow double-effect water-lithium bromide absorption refrigeration system," *Appl. Therm. Eng.*, vol. 152, pp. 643–653, Apr. 2019, doi: 10.1016/J.APPLTHERMALENG.2019.02.105.

[117] K. Mohammadi, M. S. Efati Khaledi, and K. Powell, "A novel hybrid dual-temperature absorption refrigeration system: Thermodynamic, economic, and environmental analysis," *J. Clean. Prod.*, vol. 233, pp. 1075–1087, Oct. 2019, doi: 10.1016/J.JCLEPRO.2019.06.130.

[118] J. Fernández-Seara, J. Sieres, and M. Vázquez, "Compression-absorption cascade refrigeration system," *Appl. Therm. Eng.*, vol. 26, no. 5–6, pp. 502–512, Apr. 2006, doi: 10.1016/J.APPLTHERMALENG.2005.07.015.

[119] V. H. Oza and N. M. Bhatt, "Optimization of Ammonia-Water Absorption Refrigeration System using Taguchi Method of Design of Experiment," *Int. J. Mech. Solids*, vol. 13, no. 2, pp. 111–126, 2018.

[120] S. Garimella, A. M. Brown, and A. K. Nagavarapu, "Waste heat driven absorption/vapor-compression cascade refrigeration system for megawatt scale, high-flux, low-temperature cooling," *Int. J. Refrig.*, vol. 34, no. 8, pp. 1776–1785, Dec. 2011, doi: 10.1016/J.IJREFRIG.2011.05.017.

[121] L. Wang, A. Ma, Y. Tan, X. Cui, and H. Cui, "Study on solar-assisted cascade refrigeration system," *Energy Procedia*, vol. 16, no. PART C, pp. 1503–1509, 2012, doi: 10.1016/j.egypro.2012.01.236.

[122] S. Anand, A. Gupta, and S. K. Tyagi, "Comparative thermodynamic analysis of a hybrid refrigeration system for promotion of cleaner technologies," *J. Therm. Anal. Calorim.*, vol. 117, no. 3, pp. 1453–1468, 2014, doi: 10.1007/s10973-014-3889-x.

[123] S. M. Hojjat Mohammadi and M. Ameri, "Energy and exergy comparison of a cascade air conditioning system using different cooling strategies," *Int. J. Refrig.*, vol. 41, pp. 14–26, 2014, doi: 10.1016/j.ijrefrig.2013.06.015.

[124] L. Kairouani and E. Nehdi, "Cooling performance and energy saving of a compression–absorption refrigeration system assisted by geothermal energy," *Appl. Therm. Eng.*, vol. 26, no. 2–3, pp. 288–294, Feb. 2006, doi:

TH-3395_176107002

10.1016/J.APPLTHERMALENG.2005.05.001.

[125] Z. G. Sun and K. H. Guo, "Cooling performance and energy saving of a compression-absorption refrigeration system driven by a gas engine," *Int. J. Energy Res.*, vol. 30, no. 13, pp. 1109–1116, Oct. 2006, doi: 10.1002/ER.1205.

[126] Z. Seyfouri and M. Ameri, "Analysis of integrated compression-absorption refrigeration systems powered by a microturbine," *Int. J. Refrig.*, vol. 35, no. 6, pp. 1639–1646, Sep. 2012, doi: 10.1016/J.IJREFRIG.2012.04.010.

[127] C. Cimsit and I. T. Ozturk, "Analysis of compression–absorption cascade refrigeration cycles," *Appl. Therm. Eng.*, vol. 40, pp. 311–317, Jul. 2012, doi: 10.1016/J.APPLTHERMALENG.2012.02.035.

[128] D. Colorado and V. M. Velázquez, "Exergy analysis of a compression–absorption cascade system for refrigeration," *Int. J. Energy Res.*, vol. 37, no. 14, pp. 1851–1865, Nov. 2013, doi: 10.1002/ER.3012.

[129] V. Jain, S. S. Kachhwaha, and G. Sachdeva, "Thermodynamic performance analysis of a vapor compression–absorption cascaded refrigeration system," *Energy Convers. Manag.*, vol. 75, pp. 685–700, Nov. 2013, doi: 10.1016/J.ENCONMAN.2013.08.024.

[130] C. Cimsit, I. Tekin OZTURK, and M. Hosoz, "Second Law Based Thermodynamic Analysis of Compression-Absorption Cascade Refrigeration Cycles," *J. Therm. Sci. Technol.*, vol. 34, pp. 9–18, 2014.

[131] D. Colorado and W. Rivera, "Performance comparison between a conventional vapor compression and compression-absorption single-stage and double-stage systems used for refrigeration," *Appl. Therm. Eng.*, vol. 87, pp. 273–285, Aug. 2015, doi: 10.1016/J.APPLTHERMALENG.2015.05.029.

[132] V. Jain, G. Sachdeva, and S. S. Kachhwaha, "Thermodynamic modelling and parametric study of a low temperature vapour compression-absorption system based on modified Gouy-Stodola equation," *Energy*, vol. 79, no. C, pp. 407–418, Jan. 2015, doi: 10.1016/J.ENERGY.2014.11.027.

[133] M. Dixit, S. C. Kaushik, and A. Arora, "Energy And Exergy Analysis Of Absorption-Compression Cascade Refrigeration System," *J. Therm. Eng.*, vol. 2, no. 6, pp. 995–1006, 2016.

TH-3395_176107002

[134] Y. Chen, W. Han, and H. Jin, "Analysis of an absorption/absorption-compression refrigeration system for heat sources with large temperature change," *Energy Convers. Manag.*, vol. 113, pp. 153–164, 2016, doi: 10.1016/j.enconman.2016.01.063.

[135] B. Patel, S. S. Kachhwaha, and B. Modi, "Thermodynamic Modelling and Parametric Study of a Two Stage Compression-Absorption Refrigeration System for Ice Cream Hardening Plant," *Energy Procedia*, vol. 109, pp. 190–202, Mar. 2017, doi: 10.1016/J.EGYPRO.2017.03.091.

[136] K. Salhi, M. Korichi, and K. M. Ramadan, "Thermodynamic and thermo-economic analysis of compression–absorption cascade refrigeration system using low-GWP HFO refrigerant powered by geothermal energy," *Int. J. Refrig.*, vol. 94, pp. 214–229, Oct. 2018, doi: 10.1016/J.IJREFRIG.2018.03.017.

[137] H. Lijuan, S. Wang, L. Suxia, and W. Xuan, "Numerical and experimental evaluation of the performance of a coupled vapour absorption-compression refrigeration configuration," *Int. J. Refrig.*, vol. 99, pp. 429–439, Mar. 2019, doi: 10.1016/J.IJREFRIG.2018.11.023.

[138] H. He, L. Wang, J. Yuan, Z. Wang, W. Fu, and K. Liang, "Performance evaluation of solar absorption-compression cascade refrigeration system with an integrated air-cooled compression cycle," *Energy Convers. Manag.*, vol. 201, p. 112153, Dec. 2019, doi: 10.1016/j.enconman.2019.112153.

[139] W. Chen, Z. Li, Q. Sun, and B. Zhang, "Energy and exergy analysis of proposed compression-absorption refrigeration assisted by a heat-driven turbine at low evaporating temperature," *Energy Convers. Manag.*, vol. 191, pp. 55–70, Jul. 2019, doi: 10.1016/J.ENCONMAN.2019.04.024.

[140] L. Jianbo, L. Kai, H. Xiaolong, Z. Chen, C. Fulin, and K. Xiangqiang, "A novel absorption–compression combined refrigeration cycle activated by engine waste heat," *Energy Convers. Manag.*, vol. 205, p. 112420, Feb. 2020, doi: 10.1016/j.enconman.2019.112420.

[141] S. Agarwal, A. Arora, and B. B. Arora, "Energy and exergy analysis of vapor compression–triple effect absorption cascade refrigeration system," *Eng. Sci. Technol. an Int. J.*, vol. 23, no. 3, pp. 625–641, Jun. 2020, doi: 10.1016/J.JESTCH.2019.08.001.

TH-3395_176107002

[142] V. Jain and D. Colorado, "Thermoeconomic and feasibility analysis of novel transcritical vapor compression-absorption integrated refrigeration system," *Energy Convers. Manag.*, vol. 224, p. 113344, Nov. 2020, doi: 10.1016/J.ENCONMAN.2020.113344.

[143] Y. Xu, N. Jiang, Q. Wang, and G. Chen, "Comparative study on the energy performance of two different absorption-compression refrigeration cycles driven by low-grade heat," *Appl. Therm. Eng.*, vol. 106, pp. 33–41, Aug. 2016, doi: 10.1016/j.applthermaleng.2016.05.169.

[144] J. Wang, B. Wang, W. Wu, X. Li, and W. Shi, "Performance analysis of an absorption-compression hybrid refrigeration system recovering condensation heat for generation," *Appl. Therm. Eng.*, vol. 108, pp. 54–65, Sep. 2016, doi: 10.1016/J.APPLTHERMALENG.2016.07.100.

[145] Y. Xu, N. Jiang, F. Pan, Q. Wang, Z. Gao, and G. Chen, "Comparative study on two low-grade heat driven absorption-compression refrigeration cycles based on energy, exergy, economic and environmental (4E) analyses," *Energy Convers. Manag.*, vol. 133, pp. 535–547, 2017, doi: 10.1016/j.enconman.2016.10.073.

[146] Y. Jing, Z. Li, L. Liu, S. Lu, and S. Lv, "Exergoeconomic-optimized design of a solar absorption-subcooled compression hybrid cooling system for use in low-rise buildings," *Energy Convers. Manag.*, vol. 165, pp. 465–476, Jun. 2018, doi: 10.1016/j.enconman.2018.03.083.

[147] V. Jain, G. Sachdeva, and S. S. Kachhwaha, "Comparative performance study and advanced exergy analysis of novel vapor compression-absorption integrated refrigeration system," *Energy Convers. Manag.*, vol. 172, no. May, pp. 81–97, 2018, doi: 10.1016/j.enconman.2018.06.116.

[148] X. Ye, L. Liu, and Z. Li, "Performance analysis of solar absorption-subcooled compression hybrid refrigeration system in subtropical city," *Front. Energy*, vol. 13, no. 1, pp. 185–192, Mar. 2019, doi: 10.1007/s11708-017-0452-z.

[149] X. Liu, Z. Ye, L. Bai, and M. He, "Performance comparison of two absorption-compression hybrid refrigeration systems using R1234yf/ionic liquid as working pair," *Energy Convers. Manag.*, vol. 181, pp. 319–330, Feb. 2019, doi: 10.1016/J.ENCONMAN.2018.12.030.

TH-3395_176107002

[150] F. N. Carvalho and P. E. L. Barbieri, "Thermoeconomic Simulation of Cascaded and Integrated Vapor Compression-Absorption Refrigeration Systems," *Therm. Eng.*, vol. 20, no. 1, pp. 93–99, Apr. 2020, doi: 10.26678/abcm.encit2020.cit20-0224.

[151] E. Chen, J. Chen, T. Jia, Y. Zhao, and Y. Dai, "A solar-assisted hybrid air-cooled adiabatic absorption and vapor compression air conditioning system," *Energy Convers. Manag.*, vol. 250, p. 114926, Dec. 2021, doi: 10.1016/J.ENCONMAN.2021.114926.

[152] J. Herrera-Romero and D. Colorado-Garrido, "Comparative Study of a Compression–Absorption Cascade System Operating with NH3-LiNO3, NH3-NaSCN, NH3-H2O, and R134a as Working Fluids," *Processes*, vol. 8, no. 7, pp. 1–15, 2020, doi: 10.3390/pr8070816.

[153] S. B. Riffat and C. W. Wong, "Gas-driven absorption/recompression system," *Heat Recover. Syst. CHP*, vol. 14, no. 2, pp. 165–171, 1994, doi: 10.1016/0890-4332(94)90007-8.

[154] J. Kim *et al.*, "Experimental study of operating characteristics of compression/absorption high-temperature hybrid heat pump using waste heat," *Renew. Energy*, vol. 54, pp. 13–19, Jun. 2013, doi: 10.1016/J.RENENE.2012.09.032.

[155] A. Razmi, M. Soltani, C. Aghanajafi, and M. Torabi, "Thermodynamic and economic investigation of a novel integration of the absorption-recompression refrigeration system with compressed air energy storage (CAES)," *Energy Convers. Manag.*, vol. 187, pp. 262–273, May 2019, doi: 10.1016/J.ENCONMAN.2019.03.010.

[156] A. Razmi, M. Soltani, F. M. Kashkooli, and L. Garousi Farshi, "Energy and exergy analysis of an environmentally-friendly hybrid absorption/recompression refrigeration system," *Energy Convers. Manag.*, vol. 164, pp. 59–69, May 2018, doi: 10.1016/J.ENCONMAN.2018.02.084.

[157] S. A. Mousavi and M. Mehrpooya, "A comprehensive exergy-based evaluation on cascade absorption-compression refrigeration system for low temperature applications - exergy, exergoeconomic, and exergoenvironmental assessments," *J. Clean. Prod.*, vol. 246, p. 119005, Feb. 2020, doi: 10.1016/J.JCLEPRO.2019.119005.

[158] A. Ustaoglu, "Parametric study of absorption refrigeration with vapor compression refrigeration cycle using wet, isentropic and azeotropic working fluids: Conventional

TH-3395_176107002

and advanced exergy approach," *Energy*, vol. 201, p. 117491, Jun. 2020, doi: 10.1016/J.ENERGY.2020.117491.

[159] I. Baniasad Askari, H. Ghazizade-Ahsaee, and A. Kasaeian, "Investigation of an ejector-cascaded vapor compression–absorption refrigeration cycle powered by linear fresnel and organic rankine cycle," *Environ. Dev. Sustain.*, pp. 1–46, Jun. 2022, doi: 10.1007/S10668-022-02442-Z/TABLES/9.

[160] M. G. Gado, T. F. Megahed, S. Ookawara, S. Nada, and I. I. El-Sharkawy, "Potential application of cascade adsorption-vapor compression refrigeration system powered by photovoltaic/thermal collectors," *Appl. Therm. Eng.*, vol. 207, p. 118075, May 2022, doi: 10.1016/J.APPLTHERMALENG.2022.118075.

[161] M. Higa, C. de Souza Pereira, T. M. O. A. Cunha, and L. Maximiano, "Performance analysis of a hybrid compression-assisted absorption system using heat recovery ammonia generator," *Appl. Therm. Eng.*, vol. 211, p. 118437, Jul. 2022, doi: 10.1016/J.APPLTHERMALENG.2022.118437.

[162] S. T. Kadam *et al.*, "Thermo-economic and environmental assessment of hybrid vapor compression-absorption refrigeration systems for district cooling," *Energy*, vol. 243, p. 122991, 2022, doi: 10.1016/j.energy.2021.122991.

[163] E. Brendeng and K. Aflekt, "Economic optimization of refrigeration plants Optimisation," *Int. J. Refrig.*, vol. 3, no. 5, pp. 289–294, 1980, doi: 10.1016/0140-7007(80)90034-1.

[164] M. D. D'Accadia and F. De Rossi, "Thermoeconomic optimization of a refrigeration plant," *Int. J. Refrig.*, vol. 21, no. 1, pp. 42–54, Jan. 1998, doi: 10.1016/S0140-7007(97)00071-6.

[165] N. Usta and A. Ileri, "Computerized economic optimization of refrigeration system design," *Energy Convers. Manag.*, vol. 40, no. 10, pp. 1089–1109, 1999, doi: 10.1016/S0196-8904(99)00004-7.

[166] L. Grosu, R. Benelmir, and M. Feidt, "Technico-economic simulation and optimization of a compression refrigerating machine," *Energy Convers. Manag.*, vol. 40, no. 15–16, pp. 1651–1660, Oct. 1999, doi: 10.1016/S0196-8904(99)00058-8.

[167] S. Sanaye and H. R. Malekmohammadi, "Thermal and economical optimization of air

TH-3395_176107002

conditioning units with vapor compression refrigeration system," *Appl. Therm. Eng.*, vol. 24, no. 13, pp. 1807–1825, Sep. 2004, doi: 10.1016/J.APPLTHERMALENG.2003.12.017.

[168] D. A. Al-Otaibi, I. Dincer, and M. Kalyon, "Thermoeconomic optimization of vapor-compression refrigeration systems," *Int. Commun. Heat Mass Transf.*, vol. 31, no. 1, pp. 95–107, Jan. 2004, doi: 10.1016/S0735-1933(03)00205-7.

[169] M. Hosoz and H. M. Ertunc, "Modelling of a cascade refrigeration system using artificial neural network," *Int. J. Energy Res.*, vol. 30, no. 14, pp. 1200–1215, Nov. 2006, doi: 10.1002/ER.1218.

[170] R. Selbaş, Ö. Kizilkan, and A. Şencan, "Thermoeconomic optimization of subcooled and superheated vapor compression refrigeration cycle," *Energy*, vol. 31, no. 12, pp. 2108–2128, Sep. 2006, doi: 10.1016/J.ENERGY.2005.10.015.

[171] M. Özkaymak, H. Kurt, and Z. Recebli, "Thermo-economic optimization of superheating and sub-cooling heat exchangers in vapor-compressed refrigeration system," *Int. J. Energy Res.*, vol. 32, no. 7, pp. 634–647, 2008, doi: 10.1002/ER.1381.

[172] L. Zhao, W. Cai, X. Ding, and W. Chang, "Model-based optimization for vapor compression refrigeration cycle," *Energy*, vol. 55, pp. 392–402, Jun. 2013, doi: 10.1016/J.ENERGY.2013.02.071.

[173] S. S. Baakeem, J. Orfi, and A. Alabdulkarem, "Optimization of a multistage vapor-compression refrigeration system for various refrigerants," *Appl. Therm. Eng.*, vol. 136, pp. 84–96, May 2018, doi: 10.1016/J.APPLTHERMALENG.2018.02.071.

[174] C. H. de Paula, W. M. Duarte, T. T. M. Rocha, R. N. de Oliveira, and A. A. T. Maia, "Optimal design and environmental, energy and exergy analysis of a vapor compression refrigeration system using R290, R1234yf, and R744 as alternatives to replace R134a," *Int. J. Refrig.*, vol. 113, pp. 10–20, May 2020, doi: 10.1016/J.IJREFRIG.2020.01.012.

[175] R. D. Misra, P. K. Sahoo, and A. Gupta, "Application of the exergetic cost theory to the LiBr/H2O vapour absorption system," *Energy*, vol. 27, no. 11, pp. 1009–1025, Nov. 2002, doi: 10.1016/S0360-5442(02)00065-8.

[176] R. D. Misra, P. K. Sahoo, S. Sahoo, and A. Gupta, "Thermoeconomic optimization of

TH-3395_176107002

a single effect water/LiBr vapour absorption refrigeration system," *Int. J. Refrig.*, vol. 26, no. 2, pp. 158–169, Mar. 2003, doi: 10.1016/S0140-7007(02)00086-5.

[177] R. D. Misra, P. K. Sahoo, and A. Gupta, "Thermoeconomic evaluation and optimization of an aqua-ammonia vapour-absorption refrigeration system," *Int. J. Refrig.*, vol. 29, no. 1, pp. 47–59, Jan. 2006, doi: 10.1016/J.IJREFRIG.2005.05.015.

[178] R. D. Misra, P. K. Sahoo, and A. Gupta, "Thermoeconomic evaluation and optimization of a double-effect H2O/LiBr vapour-absorption refrigeration system," *Int. J. Refrig.*, vol. 28, no. 3, pp. 331–343, May 2005, doi: 10.1016/J.IJREFRIG.2004.09.006.

[179] R. D. Misra, P. K. Sahoo, and A. Gupta, "Thermoeconomic Optimization of a LiBr/H 2 O Absorption Chiller Using Structural Method," *J. Energy Resour. Technol.*, vol. 127, no. 2, pp. 119–124, 2005, doi: 10.1115/1.1830049.

[180] D. Zebbar, S. Kherris, S. Zebbar, and K. Mostefa, "Thermodynamic optimization of an absorption heat transformer," *Int. J. Refrig.*, vol. 35, no. 5, pp. 1393–1401, Aug. 2012, doi: 10.1016/J.IJREFRIG.2012.04.007.

[181] Ö. Kizilkan, A. Şencan, and S. A. Kalogirou, "Thermoeconomic optimization of a LiBr absorption refrigeration system," *Chem. Eng. Process. Process Intensif.*, vol. 46, no. 12, pp. 1376–1384, Dec. 2007, doi: 10.1016/j.cep.2006.11.007.

[182] C. Rubio-Maya, J. J. Pacheco-Ibarra, J. M. Belman-Flores, S. R. Galván-González, and C. Mendoza-Covarrubias, "NLP model of a LiBr–H2O absorption refrigeration system for the minimization of the annual operating cost," *Appl. Therm. Eng.*, vol. 37, pp. 10–18, May 2012, doi: 10.1016/J.APPLTHERMALENG.2011.12.035.

[183] M. S. Mazzei, M. C. Mussati, and S. F. Mussati, "NLP model-based optimal design of LiBr-H2O absorption refrigeration systems," *Int. J. Refrig.*, vol. 38, no. 1, pp. 58–70, 2014, doi: 10.1016/j.ijrefrig.2013.10.012.

[184] S. F. Mussati, K. V. Gernaey, T. Morosuk, and M. C. Mussati, "NLP modeling for the optimization of LiBr-H2O absorption refrigeration systems with exergy loss rate, heat transfer area, and cost as single objective functions," *Energy Convers. Manag.*, vol. 127, pp. 526–544, Nov. 2016, doi: 10.1016/J.ENCONMAN.2016.09.021.

[185] M. Azhar and M. A. Siddiqui, "Optimization of operating temperatures in the gas

TH-3395_176107002

operated single to triple effect vapour absorption refrigeration cycles," *Int. J. Refrig.*, vol. 82, pp. 401–425, Oct. 2017, doi: 10.1016/J.IJREFRIG.2017.06.033.

[186] T. Zhao, X. Chen, and Q. Chen, "Heat current method-based modeling and optimization of the single effect lithium bromide absorption chiller," *Appl. Therm. Eng.*, vol. 175, p. 115345, Jul. 2020, doi: 10.1016/J.APPLTHERMALENG.2020.115345.

[187] S. F. Mussati, T. Morosuk, and M. C. Mussati, "Superstructure-based optimization of vapor compression-absorption cascade refrigeration systems," *Entropy*, vol. 22, no. 4, pp. 1–21, 2020, doi: 10.3390/E22040428.

[188] A. Myat, K. Thu, Y. D. Kim, A. Chakraborty, W. G. Chun, and K. C. Ng, "A second law analysis and entropy generation minimization of an absorption chiller," *Appl. Therm. Eng.*, vol. 31, no. 14–15, pp. 2405–2413, 2011, doi: 10.1016/j.applthermaleng.2011.04.004.

[189] K. Mohammadi, Y. Jiang, S. Borjian, and K. Powell, "Thermo-economic assessment and optimization of a hybrid triple effect absorption chiller and compressor," *Sustain. Energy Technol. Assessments*, vol. 38, p. 100652, Apr. 2020, doi: 10.1016/J.SETA.2020.100652.

[190] Y. Xu, Z. Li, H. Chen, and S. Lv, "Assessment and optimization of solar absorption-subcooled compression hybrid cooling system for cold storage," *Appl. Therm. Eng.*, vol. 180, p. 115886, Nov. 2020, doi: 10.1016/j.applthermaleng.2020.115886.

[191] L. María Chávez-Islas, C. L. Heard, and I. E. Grossmann, "Synthesis and Optimization of an Ammonia-Water Absorption Refrigeration Cycle Considering Different Types of Heat Exchangers by Application of Mixed-Integer Nonlinear Programming," *Ind. Eng. Chem. Res.*, vol. 48, no. 6, pp. 2972–2990, 2009, doi: 10.1021/ie801309h.

[192] A. Beghi, L. Cecchinato, G. Cosi, and M. Rampazzo, "A PSO-based algorithm for optimal multiple chiller systems operation," *Appl. Therm. Eng.*, vol. 32, no. 1, pp. 31–40, Jan. 2012, doi: 10.1016/J.APPLTHERMALENG.2011.08.008.

[193] B. Ghorbani, M. Mafi, R. Shirmohammadi, M. H. Hamedi, and M. Amidpour, "Optimization of operation parameters of refrigeration cycle using particle swarm and NLP techniques," *J. Nat. Gas Sci. Eng.*, vol. 21, pp. 779–790, Nov. 2014, doi:

TH-3395_176107002

10.1016/j.jngse.2014.10.007.

[194] C. Cimsit, I. T. Ozturk, and O. Kincay, "Thermoeconomic optimization of LiBr/H2O-R134a compression-absorption cascade refrigeration cycle," *Appl. Therm. Eng.*, vol. 76, pp. 105–115, Feb. 2015, doi: 10.1016/J.APPLTHERMALENG.2014.10.094.

[195] V. Jain, G. Sachdeva, and S. S. Kachhwaha, "NLP model based thermoeconomic optimization of vapor compression-absorption cascaded refrigeration system," *Energy Convers. Manag.*, vol. 93, pp. 49–62, Mar. 2015, doi: 10.1016/j.enconman.2014.12.095.

[196] V. Jain, G. Sachdeva, and S. S. Kachhwaha, "Energy, exergy, economic and environmental (4E) analyses based comparative performance study and optimization of vapor compression-absorption integrated refrigeration system," *Energy*, vol. 91, pp. 816–832, Nov. 2015, doi: 10.1016/J.ENERGY.2015.08.041.

[197] M. U. Ghani, M. Zaman, and I. Khan, "Thermodynamic modeling and optimization of double effect series flow LiBr-H2O vapor absorption chiller," in *2016 International Conference on Emerging Technologies (ICET)*, 2016, pp. 1–6, doi: 10.1109/ICET.2016.7813266.

[198] Z. Li, L. Liu, and Y. Jing, "Exergoeconomic analysis of solar absorption-subcooled compression hybrid cooling system," *Energy Convers. Manag.*, vol. 144, pp. 205–216, Jul. 2017, doi: 10.1016/j.enconman.2017.04.052.

[199] M. Dixit, A. Arora, and • S C Kaushik, "Energy, exergy, environment and economic analyses and optimization of two-stage absorption-compression combined refrigeration system," *Clean Technol. Environ. Policy*, vol. 19, pp. 2215–2229, 2017, doi: 10.1007/s10098-017-1404-3.

[200] S. Mohtaram, W. Chen, and J. Lin, "Investigation on the combined Rankine-absorption power and refrigeration cycles using the parametric analysis and genetic algorithm," *Energy Convers. Manag.*, vol. 150, pp. 754–762, Oct. 2017, doi: 10.1016/J.ENCONMAN.2017.08.011.

[201] B. Patel, N. B. Desai, and S. S. Kachhwaha, "Optimization of waste heat based organic Rankine cycle powered cascaded vapor compression-absorption refrigeration system," *Energy Convers. Manag.*, vol. 154, pp. 576–590, Dec. 2017, doi:

TH-3395_176107002

10.1016/J.ENCONMAN.2017.11.045.

[202] S. F. Mussati, S. Cignitti, S. S. Mansouri, K. V. Gernaey, T. Morosuk, and M. C. Mussati, "Configuration optimization of series flow double-effect water-lithium bromide absorption refrigeration systems by cost minimization," *Energy Convers. Manag.*, vol. 158, pp. 359–372, Feb. 2018, doi: 10.1016/J.ENCONMAN.2017.12.079.

[203] Y. Jing, Z. Li, L. Liu, and S. Lu, "Exergoeconomic assessment of solar absorption and absorption-compression hybrid refrigeration in building cooling," *Entropy*, vol. 20, no. 2, pp. 1–22, 2018, doi: 10.3390/e20020130.

[204] L. Ren and Y. Peng, "Optimization of Ammonia-water Absorption Refrigeration System for Ocean-going Fishing Vessels Based on PSO-GA Algorithm; Optimization of Ammonia-water Absorption Refrigeration System for Ocean-going Fishing Vessels Based on PSO-GA Algorithm," in *14th International Conference on Natural Computation, Fuzzy Systems and Knowledge Discovery (ICNC-FSKD)*, 2018, vol. 294, pp. 1–4.

[205] R. Shirmohammadi, M. Soltanieh, and L. M. Romeo, "Thermoeconomic analysis and optimization of post-combustion CO2 recovery unit utilizing absorption refrigeration system for a natural-gas-fired power plant," *Environ. Prog. Sustain. Energy*, vol. 37, no. 3, pp. 1075–1084, May 2018, doi: 10.1002/EP.12866.

[206] M. U. Arshad, M. U. Ghani, A. Ullah, A. Güngör, and M. Zaman, "Thermodynamic analysis and optimization of double effect absorption refrigeration system using genetic algorithm," *Energy Convers. Manag.*, vol. 192, pp. 292–307, Jul. 2019, doi: 10.1016/J.ENCONMAN.2019.03.083.

[207] M. Tavakoli *et al.*, "Thermodynamic and Thermoeconomic Optimization of an Absorption Refrigeration System integrated with Refinery Crude Oil Furnace," *Gas Process. J.*, vol. 7, no. 1, pp. 1–14, 2019, doi: 10.22108/gpj.2019.113570.1043.

[208] D. Kong, X. Yin, X. Ding, N. Fang, and P. Duan, "Global optimization of a vapor compression refrigeration system with a self-adaptive differential evolution algorithm," *Appl. Therm. Eng.*, vol. 197, p. 117427, Oct. 2021, doi: 10.1016/J.APPLTHERMALENG.2021.117427.

[209] M. U. Arshad, M. Zaman, M. Rizwan, and A. Elkamel, "Economic optimization of

TH-3395_176107002

parallel and series configurations of the double effect absorption refrigeration system," *Energy Convers. Manag.*, vol. 210, p. 112661, Apr. 2020, doi: 10.1016/J.ENCONMAN.2020.112661.

[210] J. H. Cho, Y. Wang, I. R. Chen, K. S. Chan, and A. Swami, "A Survey on Modeling and Optimizing Multi-Objective Systems," *IEEE Commun. Surv. Tutorials*, vol. 19, no. 3, pp. 1867–1901, 2017, doi: 10.1109/COMST.2017.2698366.

[211] H. Sayyaadi and M. Nejatolahi, "Multi-objective optimization of a cooling tower assisted vapor compression refrigeration system," *Int. J. Refrig.*, vol. 34, no. 1, pp. 243–256, Jan. 2011, doi: 10.1016/J.IJREFRIG.2010.07.026.

[212] M. Aminyavari, B. Najafi, A. Shirazi, and F. Rinaldi, "Exergetic, economic and environmental (3E) analyses, and multi-objective optimization of a CO2/NH3 cascade refrigeration system," *Appl. Therm. Eng.*, vol. 65, no. 1–2, pp. 42–50, 2014, doi: 10.1016/J.APPLTHERMALENG.2013.12.075.

[213] S. Eini, H. Shahhosseini, N. Delgarm, M. Lee, and A. Bahadori, "Multi-objective optimization of a cascade refrigeration system: Exergetic, economic, environmental, and inherent safety analysis," *Appl. Therm. Eng.*, vol. 107, pp. 804–817, 2016, doi: 10.1016/j.applthermaleng.2016.07.013.

[214] M. M. Keshtkar and P. Talebizadeh, "Multi-objective optimization of cooling water package based on 3E analysis: A case study," *Energy*, vol. 134, pp. 840–849, 2017, doi: 10.1016/j.energy.2017.06.085.

[215] S. Asgari, A. R. Noorpoor, and F. A. Boyaghchi, "Parametric assessment and multi-objective optimization of an internal auto-cascade refrigeration cycle based on advanced exergy and exergoeconomic concepts," *Energy*, vol. 125, pp. 576–590, Apr. 2017, doi: 10.1016/J.ENERGY.2017.02.158.

[216] R. Roy and B. K. Mandal, "Thermo-economic assessment and multi-objective optimization of vapour compression refrigeration system using Low GWP refrigerants," in *2019 8th International Conference on Modeling Simulation and Applied Optimization, ICMSAO 2019*, 2019, pp. 0–4, doi: 10.1109/ICMSAO.2019.8880390.

[217] A. Zendehboudi, A. Mota-Babiloni, P. Makhnatch, R. Saidur, and S. M. Sait,

TH-3395_176107002

"Modeling and multi-objective optimization of an R450A vapor compression refrigeration system," *Int. J. Refrig.*, vol. 100, pp. 141–155, Apr. 2019, doi: 10.1016/J.IJREFRIG.2019.01.008.

[218] R. Roy, A. J. Bhowal, and B. Kumar Mandal, "Exergy and Cost Optimization of a Two-Stage Refrigeration System Using Refrigerant R32 and R410A," *J. Therm. Sci. Eng. Appl.*, vol. 12, pp. 031024-(1-13), 2020, doi: 10.1115/1.4046253.

[219] V. Patel, D. Panchal, A. Prajapati, A. Mudgal, and P. Davies, "An efficient optimization and comparative analysis of cascade refrigeration system using NH3/CO2 and C3H8/CO2 refrigerant pairs," *Int. J. Refrig.*, vol. 102, pp. 62–76, Jun. 2019, doi: 10.1016/J.IJREFRIG.2019.03.001.

[220] R. Roy and B. K. Mandal, "Thermo-economic analysis and multi-objective optimization of vapour cascade refrigeration system using different refrigerant combinations: A comparative study," *J. Therm. Anal. Calorim.*, vol. 139, no. 5, pp. 3247–3261, 2020, doi: 10.1007/s10973-019-08710-x.

[221] A. Iranmanesh and M. A. Mehrabian, "Optimization of a lithium bromide–water solar absorption cooling system with evacuated tube collectors using the genetic algorithm," *Energy Build.*, vol. 85, pp. 427–435, Dec. 2014, doi: 10.1016/J.ENBUILD.2014.09.047.

[222] B. H. Gebreslassie, E. A. Groll, and S. V. Garimella, "Multi-objective optimization of sustainable single-effect water/Lithium Bromide absorption cycle," *Renew. Energy*, vol. 46, pp. 100–110, Oct. 2012, doi: 10.1016/J.RENENE.2012.03.023.

[223] V. Jain and G. Sachdeva, "Energy, exergy, economic (3E) analyses and multi-objective optimization of vapor absorption heat transformer using NSGA-II technique," *Energy Convers. Manag.*, vol. 148, pp. 1096–1113, Sep. 2017, doi: 10.1016/J.ENCONMAN.2017.06.055.

[224] F. Panahizadeh, M. Hamzehei, M. Farzaneh-Gord, and A. Ochoa, "Energy, exergy, economic analysis and optimization of single-effect absorption chiller network," *J. Therm. Anal. Calorim.*, vol. 145, pp. 669–699, 2020, doi: 10.1007/s10973-020-09966-4.

[225] M. H. Ahmadi and M. A. Ahmadi, "Multi objective optimization of performance of

TH-3395_176107002

three-heat-source irreversible refrigerators based algorithm NSGAII," *Renew. Sustain. Energy Rev.*, vol. 60, pp. 784–794, Jul. 2016, doi: 10.1016/J.RSER.2015.12.181.

[226] R. Venkata Rao and V. Patel, "Multi-objective optimization of two stage thermoelectric cooler using a modified teaching–learning-based optimization algorithm," *Eng. Appl. Artif. Intell.*, vol. 26, no. 1, pp. 430–445, Jan. 2013, doi: 10.1016/J.ENGAPPAI.2012.02.016.

[227] P. Cui, M. Yu, Z. Liu, Z. Zhu, and S. Yang, "Energy, exergy, and economic (3E) analyses and multi-objective optimization of a cascade absorption refrigeration system for low-grade waste heat recovery," *Energy Convers. Manag.*, vol. 184, pp. 249–261, Mar. 2019, doi: 10.1016/J.ENCONMAN.2019.01.047.

[228] M. H. Ahmadi, M. A. Ahmadi, M. Mehrpooya, H. Hosseinzade, and M. Feidt, "Thermodynamic and thermo-economic analysis and optimization of performance of irreversible four-temperature-level absorption refrigeration," *Energy Convers. Manag.*, vol. 88, pp. 1051–1059, Dec. 2014, doi: 10.1016/J.ENCONMAN.2014.09.041.

[229] A. Shirazi, R. A. Taylor, G. L. Morrison, and S. D. White, "A comprehensive, multi-objective optimization of solar-powered absorption chiller systems for air-conditioning applications," *Energy Convers. Manag.*, vol. 132, pp. 281–306, Jan. 2017, doi: 10.1016/J.ENCONMAN.2016.11.039.

[230] F. A. Boyaghchi, M. Mahmoodnezhad, and V. Sabeti, "Exergoeconomic analysis and optimization of a solar driven dual-evaporator vapor compression-absorption cascade refrigeration system using water/CuO nanofluid," *J. Clean. Prod.*, vol. 139, pp. 970–985, Dec. 2016, doi: 10.1016/J.JCLEPRO.2016.08.125.

[231] M. S. Turgut and O. E. Turgut, "Comparative investigation and multi objective design optimization of a cascaded vapor compression absorption refrigeration system operating with different refrigerants in the vapor compression cycle," *Heat Mass Transf.*, vol. 55, no. 2, pp. 467–488, 2019, doi: 10.1007/s00231-018-2430-3.

[232] V. Jain, N. Sharma, G. Sachdeva, and S. Kachhwaha, "Performance analysis and multi-objective optimization of cooling tower assisted vapor compression-absorptioin cascaded and hybrid refrigeration systems," *Int. J. Green Energy*, vol. 16, no. 13, pp. 1024–1045, 2019.

TH-3395_176107002

[233] V. Jain, G. Sachdeva, S. S. Kachhwaha, and B. Patel, "Thermo-economic and environmental analyses based multi-objective optimization of vapor compression-absorption cascaded refrigeration system using NSGA-II technique," *Energy Convers. Manag.*, vol. 113, pp. 230–242, Apr. 2016, doi: 10.1016/J.ENCONMAN.2016.01.056.

[234] X. Sun, Y. Zhuang, L. Liu, Y. Dong, L. Zhang, and J. Du, "Multi-objective optimization of heat exchange network and thermodynamic cycles integrated system for cooling and power cogeneration," *Appl. Energy*, vol. 321, p. 119366, Sep. 2022, doi: 10.1016/J.APENERGY.2022.119366.

[235] M. S. Salim and M. H. Kim, "Multi-objective thermo-economic optimization of a combined organic Rankine cycle and vapour compression refrigeration cycle," *Energy Convers. Manag.*, vol. 199, p. 112054, Nov. 2019, doi: 10.1016/J.ENCONMAN.2019.112054.

[236] C. Wu, X. Xu, Q. Li, J. Li, S. Wang, and C. Liu, "Proposal and assessment of a combined cooling and power system based on the regenerative supercritical carbon dioxide Brayton cycle integrated with an absorption refrigeration cycle for engine waste heat recovery," *Energy Convers. Manag.*, vol. 207, Mar. 2020, doi: 10.1016/J.ENCONMAN.2020.112527.

[237] A. R. Razmi, A. Arabkoohsar, and H. Nami, "Thermoeconomic analysis and multi-objective optimization of a novel hybrid absorption/recompression refrigeration system," *Energy*, vol. 210, p. 118559, Nov. 2020, doi: 10.1016/J.ENERGY.2020.118559.

[238] H. Ghaebi, T. Parikhani, H. Rostamzadeh, and B. Farhang, "Thermodynamic and thermoeconomic analysis and optimization of a novel combined cooling and power (CCP) cycle by integrating of ejector refrigeration and Kalina cycles," *Energy*, vol. 139, pp. 262–276, Nov. 2017, doi: 10.1016/J.ENERGY.2017.07.154.

[239] H. Rashidi and J. Khorshidi, "Exergoeconomic analysis and optimization of a solar based multigeneration system using multiobjective differential evolution algorithm," *J. Clean. Prod.*, vol. 170, pp. 978–990, Jan. 2018, doi: 10.1016/J.JCLEPRO.2017.09.201.

[240] B. Azizimehr, E. Assareh, and R. Moltames, "Thermoeconomic analysis and optimization of a solar micro CCHP by using TLBO algorithm for domestic

TH-3395_176107002

application," *Energy Sources, Part A Recover. Util. Environ. Eff.*, vol. 42, no. 14, pp. 1747–1761, Jul. 2020, doi: 10.1080/15567036.2019.1604883.

[241] S. Wang *et al.*, "Techno-economic-environmental evaluation of a combined cooling heating and power system for gas turbine waste heat recovery," *Energy*, vol. 231, p. 120956, 2021, doi: 10.1016/j.energy.2021.120956.

[242] P. Yang, M. Yuan, Z. Liu, N. Xie, Y. Liu, and S. Yang, "Multi- objective optimization and life cycle assessment of a cascade system integrating LiBr/H2O absorption refrigeration with transcritical CO2 power cycle," *Energy Convers. Manag.*, vol. 244, p. 114453, Sep. 2021, doi: 10.1016/J.ENCONMAN.2021.114453.

[243] F. Musharavati, S. Khanmohammadi, and R. Tariq, "Comparative exergy, multi-objective optimization, and extended environmental assessment of geothermal combined power and refrigeration systems," *Process Saf. Environ. Prot.*, vol. 156, pp. 438–456, Dec. 2021, doi: 10.1016/J.PSEP.2021.10.018.

[244] A. Mahmoudan, P. Samadof, S. Hosseinzadeh, and D. A. Garcia, "A multigeneration cascade system using ground-source energy with cold recovery: 3E analyses and multi-objective optimization," *Energy*, vol. 233, p. 121185, Oct. 2021, doi: 10.1016/J.ENERGY.2021.121185.

[245] V. Davoodi, P. Kazemiani-Najafabadi, and E. Amiri Rad, "Presenting a power and cascade cooling cycle driven using solar energy and natural gas," *Renew. Energy*, vol. 186, pp. 802–813, Mar. 2022, doi: 10.1016/J.RENENE.2022.01.031.

[246] S. I. U. H. Gilani and M. S. M. S. Ahmed, "Solution Crystallization Detection for Double-effect LiBr-H2O Steam Absorption Chiller," *Energy Procedia*, vol. 75, pp. 1522–1528, Aug. 2015, doi: 10.1016/J.EGYPRO.2015.07.304.

[247] S. Ahmad, B. Linnhoff, and R. Smith, "Cost optimum heat exchanger networks-2. targets and design for detailed capital cost models," *Comput. Chem. Eng.*, vol. 14, no. 7, pp. 751–767, Jul. 1990, doi: 10.1016/0098-1354(90)87084-3.

[248] W. Goetzler, M. Guernsey, J. Young, J. Fuhrman, and O. Abdelaziz, "The Future of Air Conditioning for Buildings," 2016.

[249] F. L. Lansing, "Computer modeling of a single-stage lithium bromide/water absorption refrigeration unit," *PL Deep Sp. Netw. Prog. Rep.*, pp. 247–257, 1976.

TH-3395_176107002

[250] Y. Kaita, “Thermodynamic properties of lithium bromide-water solutions at high temperatures,” *Int. J. Refrig.*, vol. 24, no. 5, pp. 374–390, Aug. 2001, doi: 10.1016/S0140-7007(00)00039-6.

[251] M. M. Talbi and B. Agnew, “Exergy analysis: an absorption refrigerator using lithium bromide and water as the working fluids,” *Appl. Therm. Eng.*, vol. 20, no. 7, pp. 619–630, May 2000, doi: 10.1016/S1359-4311(99)00052-6.

[252] G. S. Grover, M. A. R. Eisa, and F. A. Holland, “Thermodynamic design data for absorption heat pump systems operating on water-lithium chloride—Part one. Cooling,” *Heat Recover. Syst. CHP*, vol. 8, no. 1, pp. 33–41, Jan. 1988, doi: 10.1016/0890-4332(88)90039-7.

[253] M. R. Conde, “Properties of aqueous solutions of lithium and calcium chlorides: formulations for use in air conditioning equipment design,” *Int. J. Therm. Sci.*, vol. 43, no. 4, pp. 367–382, Apr. 2004, doi: 10.1016/J.IJTHERMALSCI.2003.09.003.

[254] Y. Yao and S. Liu, “Appendix A: Basic Equations for Properties of Common Liquid Desiccants,” *Ultrason. Technol. Desiccant Regen.*, no. LiCl, pp. 293–306, 2014, doi: 10.1002/9781118921616.app1.

[255] S. K. Chaudhari and K. R. Patil, “Thermodynamic properties of aqueous solutions of lithium chloride,” *Phys. Chem. Liq.*, vol. 40, no. 3, pp. 317–325, 2002, doi: 10.1080/0031910021000004883.

TH-3395_176107002

Appendix-A

Thermophysical properties calculation for absorbent-refrigerant mixtures

Thermo-physical properties of absorbent-refrigerant (VARS) working pairs (LiBr-H_2O, LiCl-H_2O, and ($CaCl_2$-LiBr-$LiNO_3$)-H_2O) used in this study are calculated using the below equations.

A1. LiBr-H_2O

The concentration, enthalpy, and specific heat of LiBr solution are calculated as follows [249]:

$$X_{ws} = \frac{49.04 + 1.125\,T_S - T_R}{134.65 + 0.47\,T_S} \tag{A. 1}$$

$$X_{ss} = \frac{49.04 + 1.125\,T_S - T_R}{134.65 + 0.47\,T_S} \tag{A. 2}$$

where X_{ws} and X_{ss} (in %) are the concentrations of LiBr in weak solution and strong solution, respectively. T_S and T_R indicate the temperature of the absorbent-refrigerant mixture and refrigerant, respectively. Enthalpy and specific heat for the streams consisting of LiBr-H_2O is given as [250], [251]: Constant values used in Eqs. A.3, A.5 and Eq. A.4 are given in Table A1 and A2 respectively.

$$H_i = (a_0 + a_1 X_i)\,T_i + 0.5(b_0 + b_1 X_i)\,T_i^2 + (d_0 + d_1 X_i + d_2 X_i^{\,2} + d_3 X_i^{\,3}) \tag{A. 3}$$

$$\begin{aligned} Y_1 &= A_{11} + A_{12}\cdot X_i + A_{13}\cdot X_i^2 + A_{14}\cdot X_i^3 + A_{15}\cdot X_i^4 \\ Y_2 &= A_{21} + A_{22}\cdot X_i + A_{23}\cdot X_i^2 + A_{24}\cdot X_i^3 + A_{25}\cdot X_i^4 \\ Y_3 &= A_{31} + A_{32}\cdot X_i + A_{33}\cdot X_i^2 + A_{34}\cdot X_i^3 + A_{35}\cdot X_i^4 \\ H_i &= Y_1 + Y_2\cdot T_i + Y_3\cdot T_i^2 \\ \forall i &= 6,7,8,9,10,11 \end{aligned} \tag{A. 4}$$

$$C_{p_i} = a_0 + a_1 X_i + (b_0 + b_1 X_i)\,T_i \tag{A. 5}$$

A2.LiCl-H_2O

The concentration and specific heat capacity of LiCl-H_2O are calculated as follows [252]–[254]:

$$X = (A_1 + A_2 T_S) + (B_1 + B_2 T_S)\,T_R \tag{A. 6}$$

In Eq. (A.5), the temperature is in ˚C, the concentration is in %, and the constant values are given in Table A1.

TH-3395_176107002

$$\theta_i = \left(\frac{T_i}{228}\right) - 1 \tag{A. 7}$$

$$C_{p_i,water} = A_1 + B_1\theta_i^{0.02} + C_1\theta_i^{0.04} + D_1\theta_i^{0.06} + E_1\theta_i^{1.8} + F_1\theta_i^{8} \tag{A. 8}$$

$$f_1(T) = a_1\,\theta_i^{0.02} + b_1\,\theta_i^{0.04} + c_1\,\theta_i^{0.06} \tag{A. 9}$$

$$f_2(\xi) = \begin{cases} d_1X_i + e_1X_i^2 + f_1X_i^3 & if\ X_i \le 0.31 \\ g_1 + h_1X_i & if\ X_i > 0.31 \end{cases} \tag{A. 10}$$

$$C_{p_i,LiCl} = C_{p_i,water}\left(1 - f_1(T)\ f_2(\xi)\right) \tag{A. 11}$$

where T is in K; ζ is the mass fraction of the absorbent in the solution. The parameters used in Eqs. A. 8-A. 10 are listed in Table A2. The enthalpy equation for LiCl-H_2O is given by Chaudhari and Patil [255] for the concentration range of 0-50% of LiCl.

$$\begin{aligned} A &= A_1 + A_2\,X_i + A_3\,X_i^2 + A_4\,X_i^3 + A_5X_i^4 \\ B &= B_1 + B_2\,X_i + B_3\,X_i^2 + B_4\,X_i^3 + B_5X_i^4 \\ C &= C_1 + C_2\,X_i + C_3\,X_i^2 + C_4\,X_i^3 + C_5X_i^4 \end{aligned} \tag{A. 12}$$

$$H_{i,LiCl} = A + BT_i + CT_i^2 \tag{A. 13}$$

where T is in ˚C and X is in %. The coefficient values of Eqs. A. 12-A. 13 are given in Table A1.

A3. $CaCl_2$-LiBr-$LiNO_3$/H_2O:

Thermo-physical property expressions for specific heat capacity, vapor pressure, and specific enthalpy are obtained from the literature[94]. The equation for vapor pressure is given as:

$$log\ P = \sum_{i=0}^{2}\left[A_i + B_i/(T - C_i)\right](100w)^i \tag{A. 14}$$

The coefficient values of Eq. A. 13 are given in Table A1. The specific heat capacity and enthalpy of the combination are given in Eqs. A.15-A.16:

$$C_p = \sum_{i=0}^{2}\left[\left(A_i + B_iT + C_iT^2\right)w^i\right] \tag{A. 15}$$

$$H = \sum_{i=0}^{2}\left[\left(A_i + B_iw + C_iw^2\right)T^i\right] \tag{A. 16}$$

where P is in kPa, T is in ˚C, and w is in %. The coefficient values of Eqs. A.15-A.16 are mentioned in Table A1.

TH-3395_176107002

Table A1 Constants for LiBr-H_2O/ LiCl-H_2O/$CaCl_2$ –LiBr-$LINO_3$-H_2O thermo-physical properties calculation

	Index	**a**	**b**	**d**
LiBr-H_2O Specific heat capacity and enthalpy Eqs. (A.3-A.4) [250]	0	3.46E+00	1.35E-03	1.63E+02
	1	-2.68E-02	-6.55E-06	-6.04E+00
	2	-	-	4.53E-03
	3	-	-	1.21E-03
LiCl-H_2O Concentration calculation Eq. (A.6) [252]	**Index**	**A**	**B**	
	1	6.95E+00	-7.29E-01	-
	2	1.01E+00	-2.52E-03	-
LiCl-H_2O Enthalpy Eqs. (A.12-A13) [255]	**Index**	**A**	**B**	**C**
	1	-6.62E+01	4.58E+00	-8.10E-04
	2	1.13E+01	-1.47E-01	2.18E-04
	3	-7.99E-01	6.31E-03	-1.36E-05
	4	2.15E-02	-1.38E-04	3.21E-07
	5	-1.66E-04	1.07E-06	-2.64E-09
$CaCl_2$-LiBr-$LiNO_3$-H_2O Vapor pressure Eq. (A.14) [94]	**Index**	**A**	**B**	**C**
	0	6.04E+00	-1.38E+03	-3.23E+02
	1	3.58E-02	-1.73E+01	-1.89E+02
	2	-5.88E-03	4.95E+01	-8.30E+03
$CaCl_2$-LiBr-$LiNO_3$-H_2O Specific heat capacity Eq. (A.15) [94]	**Index**	**A**	**B**	**C**
	0	3.84E+00	3.03E-02	-2.53E-04
	1	-3.19E-02	-9.98E-04	8.62E-06
	2	2.24E-05	8.34E-06	-7.22E-08
$CaCl_2$-LiBr-$LiNO_3$- H_2O Enthalpy Eq. (A.16) [94]	**Index**	**A**	**B**	**C**
	0	3.20E+02	-1.96E+00	1.10E-02
	1	4.13E+00	-4.62E-02	1.87E-04
	2	2.39E-03	2.07E-05	-2.75E-07

Table A2 Constants for LiBr-H_2O Enthalpy calculation (Eq. A.4) [251]

j	**Aj_1**	**Aj_2**	**Aj_3**	**Aj_4**	**Aj_5**
1	-2024.19	163.30	-4.88	6.30E-02	-2.91E-04
2	18.28	-1.17	3.25E-02	-4.03E-04	1.85E-06
3	-3.70 E-02	2.89E-03	-8.13E-05	9.91E-07	-4.44E-09

TH-3395_176107002

Table A3 Constants for LiCl- H_2O specific heat capacity Eqs. (A.7-A.11) [254]

A_1	B_1	C_1	D_1	E_1	F_1		
88.7891	-120.1958	-16.9264	52.4654	0.10826	0.46988		
a_1	b_1	c_1	d_1	e_1	f_1	g_1	h_1
58.5225	-105.6343	47.7948	1.43980	-1.24317	-0.12070	0.12825	0.62934

Table A4 Cost and area references values (Eq.6.16) [237] (Chapter 6)

Components	Evaporator	Absorber	Heat Exchanger	Generator-Condenser
Z_0 ($)	16000	16500	12000	25500
A_0 (m^2)	100	100	100	100

Table A5 Thermodynamic properties of VCRS refrigerants

Refrigerant	**Molar mass (g/mol)**	**Critical pressure (MPa)**	**Critical temperature (K)**	**Normal boiling point (K)**
R290	44.09	4.301	369.9	231.8
R123	152.9	3.66	456.8	300.97
R1234yf	114.0	3.38	367.9	243.15
R1234ze	114.0	3.64	382.5	254.15

Table A6 Thermodynamic properties of absorbents

Absorbent combination	**Molar mass (g/mol)**	**Component % Li**	**Normal boiling point (°C)**
LiBr	86.85	[Li: 7.99, Br: 92.01]	1265
LiCl	42.39	[Li: 16.37, Cl:83.62]	1382
$CaCl_2$-LiBr-$LiNO_3$	166.40	[$CaCl_2$: 80, LiBr:10, $LiNO_3$:10]	1734

TH-3395_176107002

Appendix-B

Input parameter values

Table B1 Values for coolant, hot streams and economic parameters (Chapter 3)

Variable/Parameter [195], [196]	**Value**
Absorber coolant inlet temperature (T_{15} in ˚C)	27
Condenser coolant outlet temperature (T_{12} in ˚C)	33
Evaporator chilled water inlet temperature (T_{13} in ˚C)	20
Evaporator chilled water outlet temperature (T_{14} in ˚C)	12
Generator heating inlet stream temperature (T_{17} in ˚C)	100
Generator heating outlet stream temperature (T_{18} in ˚C)	100
Interest rate (i_r in %)	15
Repayment Period (N_y in years)	10
Time of operation per year (*top* in hours)	5000
Unit cost of input exergy (C_{exer} in $/kW h)	0.03785

Table B2 Values for coolant, hot streams and economic parameters (Chapters 4-5)

Variable/Parameter [195], [196]	**Value**
Absorber coolant inlet temperature (T_{19} in ˚C)	30
Absorber coolant outlet temperature (T_{20} in ˚C)	35
Condenser coolant inlet temperature (T_{15} in ˚C)	30
Condenser coolant outlet temperature (T_{16} in ˚C)	35
Cost charged for CO_2 (US $/ton)	90
Cost for cold utility (*CCU* in $ /kW h)	10
Emission conversion factor (λ in kg/kW h)	0.968
Evaporator chilled water inlet temperature (T_{21} in ˚C)	10
Evaporator chilled water outlet temperature (T_{22} in ˚C)	5
Generator heating inlet stream temperature (T_{17} in ˚C)	100
Generator heating outlet stream temperature (T_{18} in ˚C)	90
Interest rate (i_r in %)	15
Maintenance factor (m_f)	1.06

TH-3395_176107002

Pump efficiency (η_P)	0.9
Repayment Period (N_y in years)	10
Time of operation per year (*top* in hours)	5000
Unit cost of Electricity (C_{el} in \$/kW h)	0.06
Unit cost of input exergy (C_{exer} in \$/kW h)	0.03785

Table B3 Values for coolant and economic parameters (Chapter 6)

Variable/Parameter [195], [196], [237], [247]	**Value**
The entering temperature of the coolant (Absorber) (T_{12} in˚C)	28
The exit temperature of the coolant (Absorber) (T_{13} in˚C)	33
Pressure ratio (C_r)	7.52
Cost charged for CO_2 (US \$/ton)	90
Cost for cold utility (*CCU* in \$/kW)	10
Emission conversion factor (λ in kg/kW h)	0.968
The entering temperature of chilled water (Evaporator) (T_{14} in˚C)	18
The exit temperature of chilled water (Evaporator) (T_{15} in ˚C)	13
Interest rate (i_r in %)	15
Maintenance factor (m_f)	1.06
Pump efficiency (η_P)	0.85
Compressor efficiency (η_C)	0.88
Repayment Period (N_y in years)	20
Operation time per year (*top* in hours)	4320
Electricity unit cost (C_{el} in \$/kW h)	0.033
Input exergy unit cost (C_{exer} in \$/kW h)	0.03785

TH-3395_176107002

List of Publications

Journal Publications

1. **M. S. Nagraj**, R. Kommadath, P. Kotecha, and R. Anandalakshmi. 2022. "Multi-Objective Optimization of Vapor Absorption Refrigeration System for the Minimization of Annual Operating Cost and Exergy Destruction." *Journal of Building Engineering* 49 (September 2021): 103925. https://doi.org/10.1016/j.jobe.2021.103925
2. **M. S. Nagraj,** D. Maharana, P. Kotecha, and R. Anandalakshmi. 2022. "Thermoeconomic Optimization of Cascade Refrigeration System Using Computational Intelligence Techniques." *Journal of Thermal Analysis and Calorimetry* 147(23): 13805–27. https://doi.org/10.1007/s10973-022-11516-z
3. **M. S. Nagraj,** D. Maharana, P. Kotecha, and R. Anandalakshmi. 2023. "Thermo-economic and environmental analyses based single objective optimization of subcooled compression-absorption cascaded refrigeration system using evolutionary techniques." *Energy Sources, Part A: Recovery, Utilization, and Environmental Effects* 45 (4) 10764–10788. https://doi.org/10.1080/15567036.2023.2244909
4. **M. S. Nagraj,** P. Kotecha, and R. Anandalakshmi. 2023. "Multi-Objective Thermoeconomic Optimization of Vapor Recompression-Absorption Refrigeration System Using Metaheuristic Techniques." (Under review)

Conference Proceedings

1. **M. S. Nagraj,** P. Kotecha, and R. Anandalakshmi. 2023 "Comparative multi-objective thermoeconomic optimization assessment of different refrigeration systems.", *2nd International Conference on Innovations in Clean Energy Technologies (ICET 2023)*, Bhopal, India, April 8-April 10, 2023. Springer Proceedings in Energy.
2. R. Kommadath, B. Ramchandani, **M. S. Nagraj,** and P. Kotecha. 2022. "Performance Evaluation of Recently Proposed Metaheuristics Algorithms on Solving Job Shop Scheduling Problem." In *International Conference on Automation, Computing and Renewable Systems*, 1052–60.
3. R. Kommadath, **M. S. Nagraj**, D. Maharana, and P. Kotecha. 2023." Efficient bounding strategy for CEC 2020 winner algorithms in solving production planning problems ", *Proceedings in International Conference on Smart Trends in Computing and Communications*, SmartCom 2023.

TH-3395_176107002